Fragment-Oriented Design of Catalysts
A Theoretical Study on Bond Activation

Dissertation

zur

Erlangung des Doktorgrades
der Naturwissenschaften
(Dr. rer. nat.)

dem Fachbereich Chemie
der Philipps-Universität Marburg

vorgelegt von

Axel Diefenbach

aus Ludwigshafen

Marburg/Lahn, 7.12.2000

Vom Fachbereich Chemie der Philipps-Universität Marburg als Dissertation angenommen am _____.

Erstgutachter: Prof. Dr. Gernot Frenking

Zweitgutachter: Univ.-Doz. Dr. F. Matthias Bickelhaupt

Datum der Promotion: 20.12.2000.

Credo ut intelligam

The time necessary to create a dissertation is both a time of scientific work and personal development. I would like to thank those persons who have accompanied me during this period.

My scientific progress is primarily due to F. Matthias Bickelhaupt who initialized this work and provided several useful ideas. Furthermore, he taught me to concentrate on those things which are most important for a scientific *understanding*. Scientifically important impulses came also from Gernot Frenking, whom I would like to thank for his collaboration.

Great impact on my personal development had Jochen Röpke to whom I am very grateful for suggesting a fundament on which a whole branch of thoughts, aims and attitudes have grown. The latter were significantly influenced by Frank Kuhnecke.

Contents

List of Abbreviations

ADF	Amsterdam Density Functional
ATS	Activation strain-Transition State interaction model of chemical reactivity
B88	Becke-88 nonlocal exchange energy functional
BDE	Bond Dissociation Energy
CDA	Charge Decomposition Analysis
DFT	Density Functional Theory
DZP	Double–ζ basis set with one Polarization function
ETS	Extended Transition State method
GGA	Generalized Gradient Approximation
KS	Kohn–Sham
LDA	Local Density Approximation
MEP	Minimum Energy Path
MO	Molecular Orbital
P86	Perdew-86 nonlocal correction energy functional
QR	Quasirelativistic
SCF	Self-Consistent Field
STO	Slater-Type Orbital
TS	Transition State
TZP	Triple–ζ basis set with one polarization function
TZ2P	Triple–ζ basis set with two polarization functions
TZ(2)P	Triple–ζ basis set with two polarization functions on H, C, O, Cl, I and one polarization function on Pd
VWN	Local correlation energy functional based on the Vosko–Wilk–Nusair parameterization
ZORA	Zeroth-Order Regular Approximation

Fragment-Oriented Design of Catalysts
A Theoretical Study on Bond Activation

Dissertation

zur

Erlangung des Doktorgrades
der Naturwissenschaften
(Dr. rer. nat.)

dem Fachbereich Chemie
der Philipps-Universität Marburg

vorgelegt von

Axel Diefenbach

aus Ludwigshafen

Marburg/Lahn, 7.12.2000

Vom Fachbereich Chemie der Philipps-Universität Marburg als Dissertation angenommen am _____.

Erstgutachter: Prof. Dr. Gernot Frenking

Zweitgutachter: Univ.-Doz. Dr. F. Matthias Bickelhaupt

Datum der Promotion: 20.12.2000.

Credo ut intelligam

The time necessary to create a dissertation is both a time of scientific work and personal development. I would like to thank those persons who have accompanied me during this period.

My scientific progress is primarily due to F. Matthias Bickelhaupt who initialized this work and provided several useful ideas. Furthermore, he taught me to concentrate on those things which are most important for a scientific *understanding*. Scientifically important impulses came also from Gernot Frenking, whom I would like to thank for his collaboration.

Great impact on my personal development had Jochen Röpke to whom I am very grateful for suggesting a fundament on which a whole branch of thoughts, aims and attitudes have grown. The latter were significantly influenced by Frank Kuhnecke.

Contents

List of Abbreviations

ADF	Amsterdam Density Functional
ATS	Activation strain-Transition State interaction model of chemical reactivity
B88	Becke-88 nonlocal exchange energy functional
BDE	Bond Dissociation Energy
CDA	Charge Decomposition Analysis
DFT	Density Functional Theory
DZP	Double–ζ basis set with one Polarization function
ETS	Extended Transition State method
GGA	Generalized Gradient Approximation
KS	Kohn–Sham
LDA	Local Density Approximation
MEP	Minimum Energy Path
MO	Molecular Orbital
P86	Perdew-86 nonlocal correction energy functional
QR	Quasirelativistic
SCF	Self-Consistent Field
STO	Slater-Type Orbital
TS	Transition State
TZP	Triple–ζ basis set with one polarization function
TZ2P	Triple–ζ basis set with two polarization functions
TZ(2)P	Triple–ζ basis set with two polarization functions on H, C, O, Cl, I and one polarization function on Pd
VWN	Local correlation energy functional based on the Vosko–Wilk–Nusair parameterization
ZORA	Zeroth-Order Regular Approximation

1 Introduction

1.1 Culture, Chemistry and Catalysis

Chemistry lays at the very heart of human culture.[1] Already in ancient times, chemistry provided a basis on which the development of higher culture could be founded. Preserving food, dyeing clothes, and medical treatment are only a few of the many early applications of chemistry.[2] Over the centuries, chemical techniques and chemical knowledge steadily increased. The first known theories of matter were developed by presocratic philosophers like Empedokles (450 BC) and Demokrit (160 BC).[3,4] There are two complementary principles at the core of chemistry: the act of combining, creation or synthesis, and the act of separation, destruction or analysis.[2] These techniques were continuously refined and, as a result, chemistry became more manifold and powerful. In spite of the long history of the use of chemical methods, the *science* of chemistry was born only a few centuries ago. The transition from alchemy to modern chemistry was brought about, amongst others, by R. Boyle (*1627, †1691), A.-L. de Lavoisier (*1743, †1794) and F. Wöhler (*1800, †1882). It is based on an approach in which hypotheses and theories must be quantitatively verified through carefully designed experiments.[4] In a relatively short time, this new orientation lead to the formulation of chemical theories that were both more general and more detailed; chemistry began to develop rapidly. Outstanding milestones in the development of chemistry are the formulation of the periodic table of the elements in 1869 by D. Mendelejew (*1834, †1907) and L. Meyer (*1830, †1895), the theory of atomic structure by E. Rutherford (*1871, †1937) in 1911, and the model of the hydrogen atom by N. Bohr (*1885, †1962) in 1913.

A new era was heralded in the beginning of the 20th century when quantum mechanics, a mathematical formalism for describing systems of microscopic scale, was developed by M. Planck (*1858, †1947), A. Einstein (*1879, †1955), W. Heisenberg (*1901, †1976), E. P. Jordan (*1902, †1980), M. Born (*1882, †1970), P. A. M. Dirac (*1902, †1984), E. Schrödinger (*1887, †1961) and others.[5] One of the successes of

this new theory was the accurate description and sound microscopic understanding of chemical phenomena that could now be achieved.[6] However, only with the advent of powerful modern computers and software, more than half a century later, it became feasible to tackle more complex and computationally demanding problems relevant to synthetic and industrial chemistry such as homogeneous catalysis, the subject of the present thesis.[7]

The effect of introducing a catalyst is a reduction of the activation energy of the chemical reaction that one wishes to accomplish, say, the transformation of A + B into C + D; the reaction energy is however not affected. This is schematically shown in Figure 1. In the process, the catalyst interacts with the reaction system but it is not consumed. After completion of the reaction, an intact catalytically active species is recovered which can assist, repeatedly, many elementary conversions of A + B into C + D. The development of active and selective catalysts is important for many reasons. Catalysis leads, for example, to more moderate reaction conditions and higher yields of the desired compound. This helps saving both energy and feedstock and is therefore of direct importance for economy and environment. Also, it can open synthetic routes to substances that otherwise would not have been accessible at all.

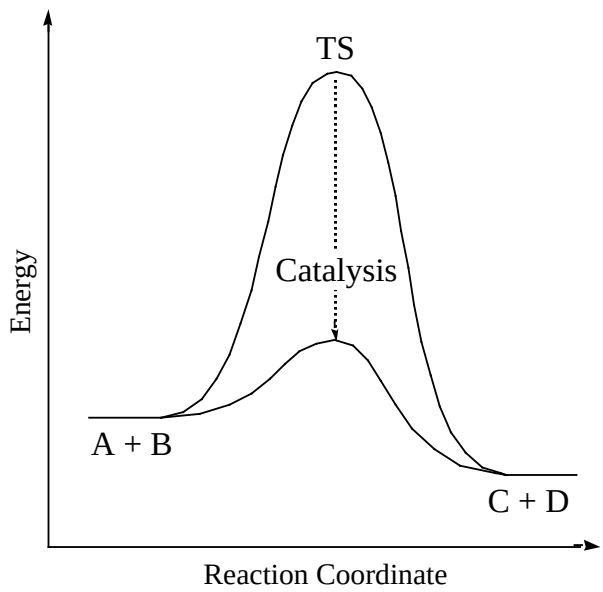

Figure 1. Schematic illustration of the effect of a catalyst on the transformation of A + B into C + D.

1.2 Fragment-Oriented Design of Catalysts

The objective of the work presented in this thesis is the development of a method for rationally designing efficient and selective catalysts based on quantum chemical analyses that is designated Fragment-oriented Design of Catalysts (FDC). In the focus is the process of C–X bond activation. This process involves the elementary organometallic reactions of oxidative addition and reductive elimination (the reverse process) which occur in nearly all homogeneous, catalytic processes (eq 1).[8]

$$ML_n + R{-}X \underset{\text{Reductive Elimination}}{\overset{\text{Oxidative Addition}}{\rightleftharpoons}} R{-}ML_n{-}X \qquad (1)$$

Here, ML_n is a catalytically active complex of a transition metal M with ligands L and R–X represents a substrate in which, for example, a functional group is to be introduced through activation of the R–X bond.

The basic idea of FDC is to build up the catalyst stepwise from its functional fragments, that is, the transition metal center M and the ligands L (see Figure 2). In a first step, the intrinsic reactivity of the bare, uncoordinated transition metal atom is investigated. This provides insight into the nature of the interactions between the metal and the substrate in the absence of ligands. But more importantly, it is now possible to reveal directly the overall effect of introducing, in a second stage, one or more ligands. Knowing how the metal behaves in a certain way in the absence of ligands and why particular ligands change this behavior in a particular manner enables one to design and tune the catalytic activity in a rational manner. Eventually, in a third stage, one can also introduce the solvent molecules from the inner solvation shell. Efforts to tackle this final step are under way. This is however beyond the scope of this thesis.

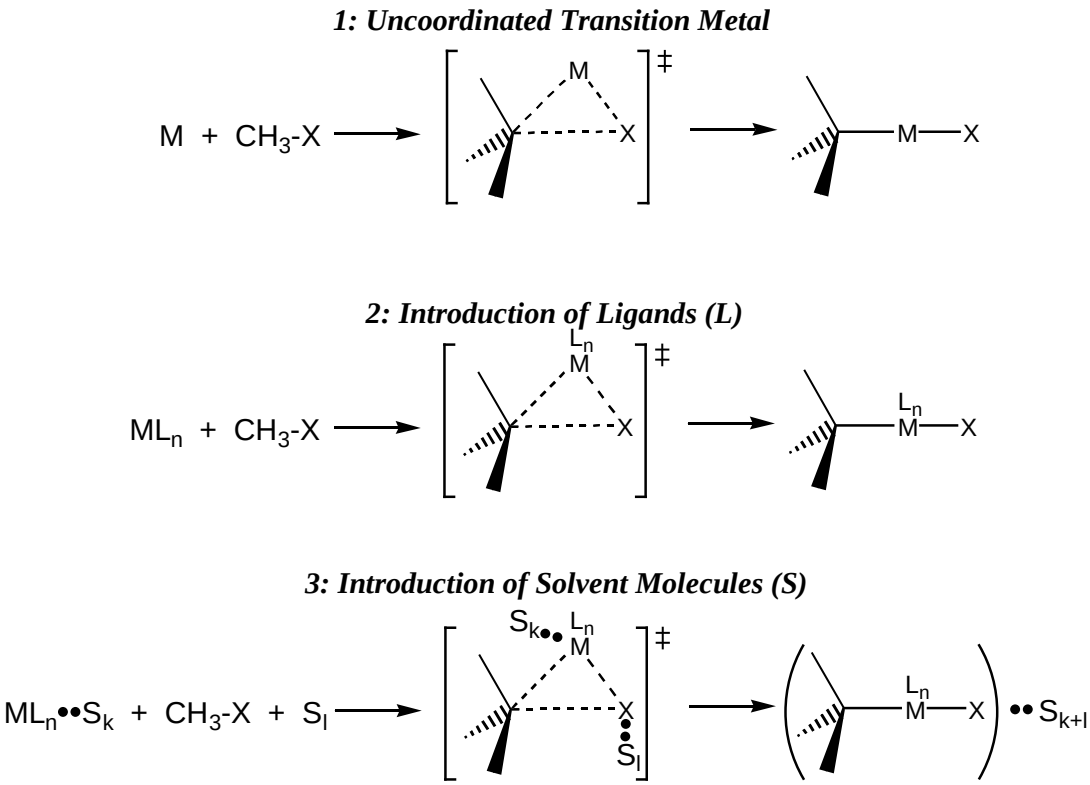

Figure 2. Fragment-oriented Design of Catalysts (FDC) for C–X bond activation. The catalyst is build up stepwise from its functional fragments.

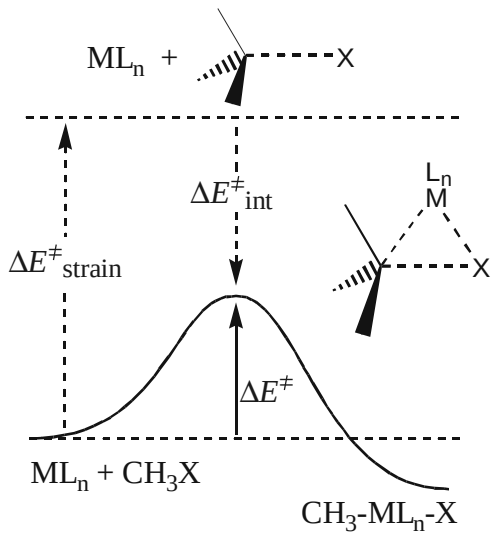

Figure 3. The Activation strain-TS interaction (ATS) model of chemical reactivity. The activation energy $\Delta E^{\neq}$ is decomposed (eq 2) into and interpreted in terms of the activation strain $\Delta E^{\neq}_{\text{strain}}$ of and the TS interaction $\Delta E^{\neq}_{\text{int}}$ between the deformed reactants (e.g. substrate and catalyst) in the activated complex.

The purpose of FDC is lowering the activation energy selectively for the desired pathway by appropriately tuning the catalyst–substrate interaction in the transition state of the bond activation process. This is achieved by making use of the Activation strain-TS interaction (ATS) model (Figure 3), introduced originally for understanding and steering the competition of elementary organic reactions.[7] The ATS model is simply a fragment approach to analyzing transition states in terms of reactants. Thus, the activation energy $\Delta E^{\neq}$ is decomposed into the activation strain $\Delta E^{\neq}_{\text{strain}}$, associated with deforming the reactants from their equilibrium structure to the geometry they adopt in the activated complex, and the TS interaction $\Delta E^{\neq}_{\text{int}}$ between these deformed reactants in the transition state (eq 2).

$$\Delta E^{\neq} = \Delta E^{\neq}_{\text{strain}} + \Delta E^{\neq}_{\text{int}} \tag{2}$$

Note that this can be done independently of both the quantum chemical method and the electronic structure and bonding model employed. In this work, the ATS model together with nonlocal density functional theory (DFT)[9] and the Kohn–Sham molecular orbital model[10] of electronic structure (see Chapter 2) is used. In particular, the TS interaction $\Delta E^{\neq}_{\text{int}}$ is further decomposed using the Extended Transition State (ETS) method developed by Ziegler and Rauk.[10,11] Interestingly, both the activation strain and the TS interaction adopt values that are characteristic for a particular type of reaction. For example, it was shown previously[7] that the activation strain is high for base-induced E2 elimination and low for the competing S_N2 substitution. Here, it is anticipated that the same holds true for various competing C–X bond activation processes. As it will be shown, this can be employed to direct activity and selectivity of a catalyst.

1.3 Outline

After the introduction of this chapter and a brief overview in chapter 2 of theoretical methods used, a detailed analysis of the nature of the transition metal–carbonyl bond in a series of neutral and ionic hexacarbonyl complexes is presented in chapter 3. This serves a better understanding of how the workhorse of coordination chemistry, the CO ligand, interacts with and affects the electronic structure at a metal center, an issue raised later on. Note that the form of chapter 3 is like it was published in the Journal of American Chemical Society. Thereafter, the approach of Fragment-oriented Design of Catalysts (FDC) is introduced and developed.

The focus of these investigations is on the activation of the prototypical H–H, C–H, C–C, C–Cl and C–I bonds by the Pd^0 atom as well as by complexes of Pd^0 and Pd^{II} with Cl^-, I^- and CO. Palladium has the advantage that the uncoordinated metal atom has a stable d^{10} ground state which facilitates comparison with the closed-shell configuration of both Pd^0 and Pd^{II} complexes. In addition, palladium is widely used in catalytic processes[12] such as, for example, the oxidation of alkenes by $PdCl_2/CuCl_2$ (Wacker process)[13] or the activation of aryl–halogen bonds for C–C coupling reactions (Heck reaction).[14]

Chapter 4 presents the results of a thorough investigation on how, that is, how strongly and through which mechanism, relativity affects the DFT calculations and how the latter compare with previous experimental and *ab initio* studies. In chapter 5, the intrinsic reactivity of Pd^0 toward molecular hydrogen, methane, ethane and chloromethane is studied using the Activation strain-TS interaction (ATS) model of chemical reactivity. The competition between the different C–X oxidative addition processes is discussed. In particular, the competition between two alternative mechanisms for oxidative addition, namely, direct oxidative insertion (OxIn) and nucleophilic substitution (S_N2), is examined. Next, in chapter 6, as a first step toward more complex catalysts, the reactivity of $PdCl^-$ is examined. In this way, it is possible to infer the effect of anion assistance which is known to speed up the rate-determining step in various catalytic processes such as, e.g., the famous Monsanto process.[15]

Finally, in chapter 7, more realistic model catalysts are investigated by introducing additional ligands. Here, the CO and I^- ligands, which are ubiquitous in coordination chemistry, are used. Thus, the oxidative addition of the model catalyst *cis*-$Pd(CO)_2I_2$ into C–H, C–C and C–I bonds is studied. Also, an extension of the ATS model is introduced which considers explicitly how the catalyst and the substrate calibrate to the transition state of the particular bond activation process. The thesis ends with a summary of the findings and an evaluation of problems that remain to be tackled.

1.4 References

(1) Hoffmann, R. *The Same and Not the Same*, Columbia University Press, New York, 1995.

(2) Janich, P.: *Kleine Weltgeschichte der Naturwissenschaften*, München, 1997, p. 153.

(3) Diels, H.; Kranz, W. (ed.): *Die Fragmente der Vorsokratiker, I-III*, Berlin, 1903, [17]1989.

(4) Ströker, E.: *Denkwege der Chemie. Elemente ihrer Wissenschaftstheorie*, Freiburg / München, 1967.

(5) (a) Dirac, P. A. M.: *The Principles of Quantum Mechanics*, Oxford, [4]1958. (b) Merzbacher, E.: *Quantum Mechanics*, Wiley, New York, [2]1970. (c) Landau, R. H.: *Quantum Mechanics II. A Second Course in Quantum Theory*, Wiley, New York, [2]1996. (d) Scherz, U.: *Quantenmechanik. Eine Einführung mit Anwendungen auf Atome, Moleküle und Festkörper*, Teubner, Leipzig, 1999.

(6) (a) Szabo, A.; Ostlund, N. S.: *Modern Quantum Chemistry. Introduction to Advances Electronic Structure Theory*, New York: Dover Publications, 1996. (b) Levine, I. N.: *Quantum Chemistry*, Prentice Hall, London, [4]1991. (c) Reinhold, J.: *Quantentheorie der Moleküle*, Stuttgart: Teubner, 1994. (d) Jensen, F.: *Introduction to Computational Chemistry*, Wiley, New York, 1999. (e) Leach, A. R.: *Molecular Modeling. Principles and applications*, Longman, Singapore, 1996.

(7) (a) Bickelhaupt, F. M. *J. Comput. Chem.* **1999**, *20*, 114. See also: (b) Bickelhaupt, F. M.; Ziegler, T.; von Ragué Schleyer, P. *Organometallics* **1995**, *14*, 2288.

(8) (a) Collman, J. P.; Hegedus, L. S.; Norton, J. R.; Finke, R. G. *Principles and Applications of Organotransition Metal Chemistry*; University Science Books:

Mill Valley, CA, 1987. (b) Elschenbroich, Ch.; Salzer, A. *Organometallics. A Concise Indroduction*, 2nd ed.; VCH, Weinheim, Germany 1992. (c) Parshall, G. W.; Ittel, S. D. *Homogeneous Catalysis*, 2nd ed.; Wiley, New York, 1992.

(9) (a) Dreizler, R. M.; Gross, E. K. U. *Density Functional Theory. An approach to the Quantum Many-Body Problem*; Springer, Berlin, 1990. (b) Parr, R. G.; Yang, W. *Density-Functional Theory of Atoms and Molecules*; Oxford University Press, New York, 1989.

(10) Bickelhaupt, F. M.; Baerends, E. J. In: Rev. Comput. Chem.; Lipkowitz, K. B. and Boyd, D. B., Eds.; Wiley-VCH: New York, **2000**, Vol. 15, 1-86.

(11) (a) Ziegler, T.; Rauk, A. *Inorg. Chem.* **1979**, *18*, 1558. (b) Ziegler, T.; Rauk, A. *Inorg. Chem.* **1979**, *18*, 1755. (c) Ziegler, T.; Rauk, A. *Inorg. Chem.* **1977**, *46*, 1.

(12) (a) Basile, A.; Fasson, S.; Vitulli, G.; Drioli, E. *Stud. Surf. Sci. Catal.* **1998**, *119*, 453. (b) Malleron, J.-L.; Fiaud, J.-C.; Legros, J.-Y. *Handbook of Palladium Catalyzed Organic Reactions*; Academic Press, 1997. (c) Cornils, R.; Herrmann, W. A. *Applied Homogenous Catalysis with Organometallic Compounds. Vol. 1;* VCH: Weinheim, 1996, p394. (d) Carey, F. A.; Sundberg, R. J. *Advanced Organic Chemistry, 3rd ed.*, Plenum Press, New York, 1993.

(13) (a) Pauley, D.; Anderson, F.; Hudlicky, T. *Org. Synth.* **1988**, *67*, 12. (b) Januszkiewicz, K.; Smith, D. J. H. *Tetrahedron Lett.* **1985**, *26*, 2263. (c) Tsuji, J.; Nagashima, H.; Nemoto, H. *Org. Synth.* **1984**, *62*, 9. (d) Januszkiewicz, K.; Alper, H. *Tetrahedron Lett.* **1983**, *24*, 5159. (e) Tsuji, J.; Shimizu, I.; Yamamoto, K. *Tetrahedron Lett.* **1976**, 2975.

(14) (a) Schmalz, H.-G. *Nachr. Chem. Tech. Lab.* **1994**, *42*, 270. (b) Kim, J. I.; Patel, B. A.; Heck, R. F. *J. Org. Chem.* **1981**, *46*, 1067. (c) Patel, B. A.; Kim, J. I.; Bender, D. D.; Kao, L. C.; Heck, R. F. *J. Org. Chem.* **1981**, *46*, 1061. (d) Heck, R. F. *Acc. Chem. Res.* **1979**, *12*, 146. (e) Patel, B. A.; Heck, R. F. *J. Org. Chem.* **1978**, *43*, 3898. (f) Dieck, H. A.; Heck, R. F. *J. Am. Chem. Soc.* **1974**, *96*, 1133.

(15) (a) Forster, D. *Advances in Organometallic Chemistry, Vol. 17.* **1979**, *255*. (b) Houminer, V.; Kao, J.; Seeman, J. I. *J. Chem. Soc., Chem. Commun.* **1984**, 1605. (c) Forster, D. *J. Am. Chem. Soc.* **1975**, *97*, 952.

2 Methods

2.1 Density Functional Theory[1]

The work presented in this thesis is based on density functional calculations, all of which have been carried out with the Amsterdam Density Functional (ADF) program.[2] The history of density functional theory[1] (DFT) begins in the 1920s with the notion by Thomas[3a] and Fermi[3,c] that the ground state energy of a system of electrons moving in the external potential $v(\boldsymbol{r})$ of a nuclear frame, may be expressed directly and alone in terms of the electron density. It took however until 1964, before Hohenberg and Kohn[4] provided a solid foundation with their fundamental first theorem, expressing that indeed the ground state energy E is uniquely determined by the corresponding electron density $\rho(\boldsymbol{r})$ (eq 1).

$$E = E[\rho(\boldsymbol{r})] \tag{1}$$

The second Hohenberg-Kohn theorem, furthermore, provides the energy variational principle for DFT. It states that for a well-behaved trial density, ρ_{trial}, the energy functional yields an energy which is higher than or equal to that belonging to the exact ground state density ρ (eq 2).

$$E[\rho_{trial}] \geq E[\rho]. \tag{2}$$

Thus, the exact ground state electronic energy and density can be calculated without recourse to the Schrödinger equation. At least *in principle*, that is, because the first Hohenberg-Kohn theorem merely proves the *existence* of such a functional relationship between E and ρ; it does not give any prescription how to systematically construct or find $E[\rho]$. For a prove of both Hohenberg–Kohn theorems I refer to ref. 5.

The introduction in 1965 by Kohn and Sham[6] of a practical computational scheme may, therefore, be considered as the next major milestone in the development of

formal DFT. The essential ingredient in this approach is the postulation of a reference system of *N noninteracting* electrons, moving in an effective external potential $v_s(\boldsymbol{r})$, the so-called Kohn-Sham potential, instead of the electrostatic potential $v(\boldsymbol{r})$ of the nuclei (eq 3).

$$[-\frac{1}{2}\nabla^2 + v_s(\boldsymbol{r})]\ \phi_i = \varepsilon_i\ \phi_i \tag{3}$$

The first term in brackets is the usual kinetic energy operator. This noninteracting reference system has the property that its one-determinantal wavefunction of the lowest N orbitals yields the exact density of the interacting system with external potential $v(\boldsymbol{r})$ as a sum over densities of the occupied orbitals, i.e.,

$$\rho(\boldsymbol{r}) = \sum |\phi_i|^2, \tag{4}$$

and the corresponding exact energy $E[\rho(\boldsymbol{r})]$. The Kohn-Sham potential should account for all effects stemming from the electron–nuclear and electron–electron interactions. Not only does it contain the attractive potential $v(\boldsymbol{r})$ of the nuclei (the so-called "external potential") and the classical Coulomb repulsion $V_{Coul}(\boldsymbol{r})$ within the electron density $\rho(\boldsymbol{r})$, but it also accounts for all exchange and correlation effects, which have so-to-say been “folded into” a local potential $v_{xc}(\boldsymbol{r})$ (see eq 5).

$$v_s(\boldsymbol{r}) = v(\boldsymbol{r}) + V_{Coul}(\boldsymbol{r}) + v_{xc}(\boldsymbol{r}) \tag{5}$$

The energy can accordingly be written as

$$E[\rho(\boldsymbol{r})] = T_s[\rho(\boldsymbol{r})] + V[\rho(\boldsymbol{r})] + V_C[\rho(\boldsymbol{r})] + E_{xc}[\rho(\boldsymbol{r})] \tag{6}$$

where $T_s[\rho(\boldsymbol{r})]$ represents the kinetic energy of the electrons of the noninteracting reference system, $V[\rho(\boldsymbol{r})]$ the attraction between the electron density $\rho(\boldsymbol{r})$ and external

potential $v(\boldsymbol{r})$, and $V_{Coul}[\rho(\boldsymbol{r})]$ the Coulomb repulsion within $\rho(\boldsymbol{r})$. $E_{xc}[\rho(\boldsymbol{r})]$ is the so-called exchange-correlation energy which accounts for exchange and Coulomb correlation between electrons and it also includes a correction $\Delta T = T - T_s$ for the fact that $T_s[\rho(\boldsymbol{r})]$ differs from the exact kinetic energy $T[\rho(\boldsymbol{r})]$. Note that the definition of E_{xc} in DFT differs from the one in traditional *ab initio* theory, where the exchange-correlation energy does not contain such a kinetic energy correction ΔT. This leaves us with an effective one-electron formulation of the quantum many-body problem which is used in essence by all current implementations of DFT.

However, the exact exchange-correlation potential $v_{xc}(\boldsymbol{r})$ and energy functional $E_{xc}[\rho(\boldsymbol{r})]$ are not known as some analytical expression in the density $\rho(\boldsymbol{r})$. Thus, approximations have been developed such as the local density approximation (LDA, in which E depends on ρ only) or generalized gradient approximations (GGA or nonlocal DFT, in which E depends on ρ and, e.g., gradients of ρ), whose quality determines the level of density functional theory applied. All calculations have been carried out using the Becke-88 functional for exchange[7] and the Perdew-86 functional for correlation.[8]

2.2 Relativity

Relativity can be considered as arising from the speed of light c being finite.[9] Relativistic effects on the electronic energy of atomic systems roughly scale with Z^2, with Z the nuclear charge. For heavier elements like second- and third-row transition metals, they are in general substantial and can not be neglected. One of the well-known effects[10a] of relativity is the relativistic mass increase of fast moving electrons according to

$$m = m_0 / (1-(v/c))^{1/2}, \tag{7}$$

which together with the effective Bohr radius,

$$a_0 = (4\pi\varepsilon_0)(\hbar^2 / m\, c^2), \tag{8}$$

is the origin of the orbital contraction (v is the velocity of the electron, m_0 the rest mass).[9] For s electrons, this contraction is strongest, because they have a great amplitude at the nucleus where they achieve high velocities. Since outer electrons must be orthogonal to all inner electrons, the contraction also applies to valence electrons.[10b] The greater mass and the contracted orbital result in an energetic stabilization. On the other hand, due to the effect on the s electrons, the d orbitals experience an increase in the screening of nucleus, and hence expand and rise in energy.

A further effect is the bond contraction,[9,11] which has been shown to be primarily due to a lowering of the repulsive kinetic energy of the electrons which results in shorter equilibrium distances between the atoms.

The master equation in relativistic quantum mechanics is the Dirac equation[12] (eq 9).

$$(c\,\boldsymbol{\alpha}\cdot\mathbf{p} + \beta\, m\, c^2 + V)\,|\Psi\rangle = i\,\frac{\partial}{\partial t}\,|\Psi\rangle \tag{9}$$

Here, $\mathbf{p}$ is the momentum operator, m the mass, V the external potential, and $\boldsymbol{\alpha}$ and β are constant 4×4 matrices.[13] Hence, the state function $|\Psi\rangle$ is a 4-spinor,

$$|\Psi\rangle = \begin{pmatrix} \Psi_{L\alpha} \\ \Psi_{L\beta} \\ \Psi_{S\alpha} \\ \Psi_{S\beta} \end{pmatrix} = \begin{pmatrix} \Psi_L \\ \Psi_S \end{pmatrix}, \tag{10}$$

which can be divided into two components, $|\Psi_L\rangle$ and $|\Psi_S\rangle$, called the “large” and the “small” components, respectively. For systems of chemical interest, the Dirac equation can not be solved exactly and it is thus necessary to device adequate approximations. In this work, relativistic effects are treated using two different approaches: (i) the quasirelativistic (QR) formalism,[14,15] and (ii) the zeroth-order regular approximation (ZORA).[16] The quasirelativistic (QR) formalism[14] proceeds from a first-order perturbation approach based on the Pauli Hamiltonian H^{Pauli} (eq 11, in atomic units).[14] The latter is obtained from the Dirac Hamiltonian by the procedure of elimination of the small components, followed by an expansion, up to first order, of the resulting operator in $(E - V)/2c^2$ and some manipulations.

$$H^{Pauli} = V + \frac{p^2}{2} - \frac{p^4}{8c^2} + \frac{\Delta V}{8c^2} + \frac{1}{4c^2}\vec{\sigma}\cdot(\vec{\nabla}V \times \vec{p}) \tag{11}$$

The first two terms of H^{Pauli} (the potential V and kinetic energy operator $p^2/2$) represent the nonrelativistic Hamiltonian and, in fact, correspond to an expansion up to only zeroth order. The last three terms can be conceived as a first-order relativistic perturbation, consisting of the so-called mass-velocity term $p^4/8c^2$ (a correction to the kinetic energy associated with the relativistic increase of the electron's mass), the Darwin term $\Delta V/8c^2$ (a correction to the effective potential associated with the so-called *Zitterbewegung* of the electron), and the spin-orbit operator (which couples electron spin and orbital momenta). In the present study, only scalar relativistic effects are considered, i.e., the spin-orbit term is not included. In the QR approach, the relativistic energy correction is obtained through diagonalizing the first-order relativistic operator (i.e., the relativistic terms in H^{Pauli}) in the space of zeroth-order solutions (i.e., the nonrelativistic MOs). This turns out to improve results significantly over a simple first-order perturbation treatment. Nevertheless, the QR treatment suffers from a series of problems (see Ref. 17). For example, the expansion used to obtain the Pauli Hamiltonian is invalid for particles in Coulomb potentials because the corresponding (nonrelativistic) eigenstates have components of high momentum near the nuclei, as a result of which the condition $(E - V)/2c^2 << 1$ is not satisfied). Another serious problem is that H^{Pauli} is unbound from below which, in principal, implies a core-collapse of the valence MOs. In practice, this collapse is in most but not all cases prevented merely by the absence of the highly compact components in the valence basis set that would be necessary for describing the corresponding solutions, i.e., the collapsed MOs.

Most of the problems associated with the Pauli Hamiltonian and the QR approach can be solved[16,17] if the Hamiltonian resulting from elimination of the small components is expanded in $1/(2c^2 - V)$ instead of $(E - V)/2c^2$. To zeroth order, this leads to the ZORA Hamiltonian (eq 12, in atomic units).

$$H^{ZORA} = \vec{\sigma} \cdot \vec{p} \frac{c^2}{2c^2 - V} \vec{\sigma} \cdot \vec{p} + V \tag{12}$$

In chapter 4, the performance of the QR and the more reliable ZORA approaches are compared with each other and with the nonrelativistic DFT results. The work in the chapters thereafter is entirely based on the ZORA approach.

2.3 Bond Analysis

As pointed out above, Kohn–Sham DFT provides us with an effective one-electron formulation of the quantum many-body problem.[18] For some time, an interpretative connection between physical reality and the Kohn-Sham orbitals has been denied. They were merely conceived as an instrument to conveniently construct the exact density, which could then be substituted into (a good approximation to) the Hohenberg-Kohn density functional to provide, in turn, the exact (or an accurate) total energy: $E = E[\rho(\boldsymbol{r})]$. However, it has been pointed out that Kohn-Sham orbitals do have a physical interpretation, that they are perfectly suited for the use in orbital theories of chemistry, and that they even have certain advantages over Hartree-Fock orbitals.[18,19]

In the framework of Kohn-Sham MO theory, one can decompose an accurate bond energy between mono- and/or polyatomic fragments of a molecular system (say, a catalyst and a substrate for C–X bond activation) into the contributions associated with the various orbital interactions (Figure 1). In addition, electrostatic interactions are also part of this quantitative MO model (Figure 1).

First, the overall bond energy ΔE is divided into two major components (eq 13): (i) the preparation energy ΔE_{prep} corresponding to the amount of energy required to deform the separated fragments, A and B say, from their equilibrium structure to the geometry they acquire in the overall molecule ($\Delta E_{\text{prep,geo}}$) and to excite them to the their valence electronic configuration ($\Delta E_{\text{prep,el}}$), and (ii) the actual interaction energy ΔE_{int} between the prepared fragments.

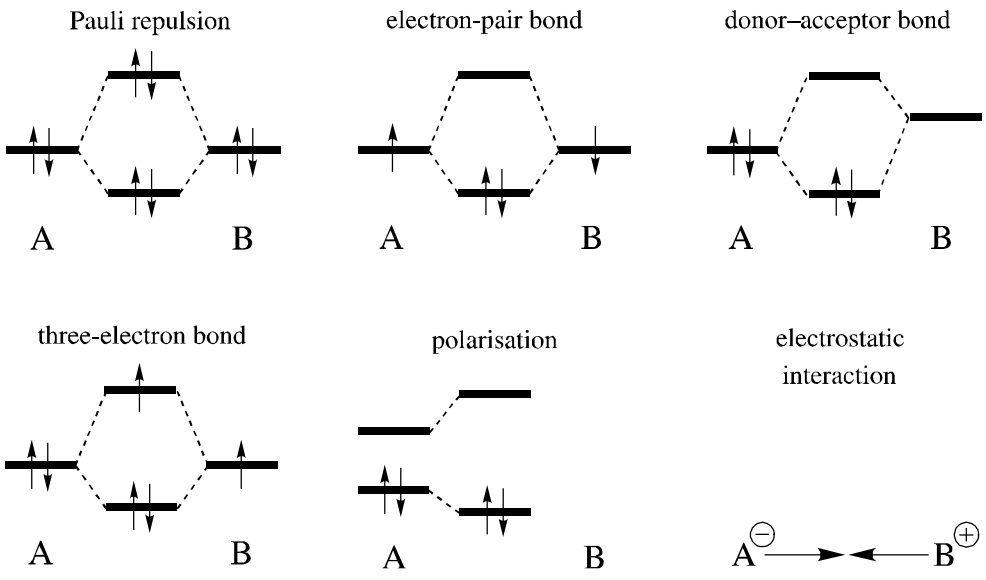

Figure 1. Schematic representation of a number of elementary types of interaction between fragments A and B in the Kohn–Sham MO model.

$$\Delta E \;=\; \Delta E_{\text{prep}} + \Delta E_{\text{int}} \;=\; \Delta E_{\text{prep,geo}} + \Delta E_{\text{prep,el}} + \Delta E_{\text{int}} \tag{13}$$

For further decomposing the interaction energy ΔE_{int}, the extended transition state (ETS) method developed by Ziegler and Rauk[20] is followed (for related analyses in various MO approaches, see Ref. 21). This yields three different physically meaningful terms (eq 14).4,11

$$\Delta E_{\text{int}} \;=\; \Delta V_{\text{elst}} + \Delta E_{\text{Pauli}} + \sum_{\Gamma} \Delta E_{\text{oi},\Gamma} \tag{14}$$

The term ΔV_{elst} corresponds to the classical electrostatic interaction between the unperturbed charge distributions of the prepared fragments as they are brought together

at their final positions, giving rise to an overall density which is simply a superposition of fragment densities $\rho_A + \rho_B$. For neutral fragments, ΔV_{elst} is usually attractive.[18] The Pauli repulsion ΔE_{Pauli} arises then as the energy change associated with going from $\rho_A + \rho_B$ to the wavefunction $\Psi^0 = N\,\hat{A}\,[\Psi_A\,\Psi_B]$ that properly obeys the Pauli principle through explicit antisymmetrization ($\hat{A}$ operator) and renormalization (N constant) of the product of fragment wavefunctions. It comprises the four-electron destabilizing interactions between occupied orbitals and is responsible for any steric repulsion. Finally, the wavefunction is allowed to relax from Ψ^0 to the fully converged wavefunction Ψ. The associated orbital interactions ΔE_{oi} account for electron-pair bonding, charge transfer (e.g. HOMO–LUMO interactions) and polarization (empty/occupied orbital mixing on one fragment due to the presence of another fragment). They can be further decomposed into the contributions from each irreducible representation Γ of the interacting system (eq 14). In systems with a clear σ/π separation, this symmetry partitioning proves to be most informative. In the present study, these fragments are, e.g., a catalyst and a substrate or a metal center and ligands. But they could also be the two $CH_3^{\bullet}$ fragments of C_2H_6. Together with the information that the analyses provide about the orbital electronic structure (frontier orbital interactions) and the electron density distribution, the quantitative decomposition of the interaction energy provides powerful complementary tools for understanding and, thus, directing chemical bonding and reactivity.

2.4 References

(1) Parr, R. G.; Yang, W.: *Density-Functional Theory of Atoms and molecules*, New York: Oxford University Press, 1989.

(2) (a) te Velde, G.; Bickelhaupt, F. M.; Baerends, E. J.; van Gisbergen, S. J. A.; Fonseca Guerra, C.; Snijders, J. G.; Ziegler, T. *J. Comput. Chem.*, accepted. (b) Fonseca-Guerra, C.; Snijders, J. G.; te Velde, G.; Baerends, E. J. *Theor. Chem. Acc.* **1998**, *99*, 391. (c) Baerends, E. J.; Ellis, D. E.; Ros, P. *Chem. Phys.* **1973**, *2*, 41.

(3) (a) Thomas, L. H. *Proc. Camb. Phil. Soc.* **1927**, *23*, 542. (b) Fermi, E. *Rend. Accad., Lincei* **1927**, *6*, 602. (c) Fermi, E. *Z. Phys.* **1928**, *48***,** 73.

(4) Hohenberg, P.; Kohn, W. *Phys. Rev. B* **1964**, *136*, 864.

(5) (a) Scherz, U.: *Quantenmechanik. Eine Einführung mit Anwendungen auf Atome, Moleküle und Festkörper*, Teubner, Stuttgart, 1999. (b) Jensen, F.: *Introduction to Computational Chemistry*, Wiley, Chichester, 1999.

(6) Kohn, W.; Sham, L. J. *Phys. Rev. A* **1965**, *140*, 1133.

(7) Becke, A. D. *Phys. Rev. B* **1988**, *38*, 3098.

(8) (a) Perdew, J. P. *Phys. Rev. B.* **1986**, *33*, 8822. (b) Perdew, J. P. *Phys. Rev. B.* **1986**, *34*, 7406.

(9) Pyykkö, P. *Chem. Rev.* **1988**, *88*, 563.

(10) (a) Pitzer, K. S. *Acc. Chem. Res.* **1979**, *12*(8), 271. (b) Christiansen, P. A.; Ermler, W. C.; Pitzer, K. S. *Ann. Rev. Phys. Chem.* **1985**, *36*, 407.

(11) (a) Ziegler, T.; Snijders, J. G.; Baerends, E. J. *J. Chem. Phys.* **1981**, *74*, 1273. (b) Pyykkö, P.; Scnijders, J. G.; Baerends, E. J. *Chem. Phys. Lett.* **1981**, *83*, 432. (c) Ziegler, T.; Snijders, J. G.; Baerends, E. J. . *Chem. Phys. Lett.* **1980**, *75*, 1. (d) Snijders, J. G.; Pyykkö, P. *Chem. Phys. Lett.* **1980**, *75*, 5.

(12) Landau, R. H.: Quantum Mechanics II, 2nd ed., Wiley, New York, 1996.

(13) Moss, R. E. Advanced *Molecular Quantum Mechanics*, Chapman and Hall, London, 1973.

(14) (a) Ziegler, T.; Tschinke, V.; Baerends, E. J.; Snijders, J. G.; Ravenek, W. *J. Phys. Chem.* **1989**, *93*, 3050.

(15) (a) Snijders, J. G.; Baerends, E. J.; Ros, P. *Mol. Phys.* **1979**, *38*(6), 1909. (b) Snijders, J. G.; Baerends, E. J. *Mol. Phys.* **1978**, *78*(6), 1789.

(16) (a) van Lenthe, E.; Baerends, E. J.; Snijders, J. G. *J. Chem. Phys.* **1993**, *99*, 4597. (b) (l) van Lenthe, E.; Baerends, E. J.; Snijders, J. G. *J. Chem. Phys.* **1994**, *101*, 9783. (c) van Lenthe, E.; Snijders, J.; Baerends, E. J. *J. Chem. Phys.* **1996**, *105*(15), 6505. (d) van Lenthe, E.; van Leeuwen, R.; Baerends, E. J.; Snijders, J.

G. *Int. J. Quantum Chem.* **1996**, *57*, 281. (e) Snijders, J. G.; Sadlej, A. J. *Chem. Phys. Lett.* **1996**, *252*, 51.

(17) (a) Foldy, L. L.; Wouthuysen, S. A. *Phys. Rev.* **1950**, *78*(1), 29. (b) Cowan, R. D.; Griffin, D. C. *J. Opt. Soc. Am.* **1976**, *66*(10), 1010. (c) Snijders, J. G.; Baerends, E. J. *Mol. Phys.* **1978**, *36*(6), 1789. (d) Snijders, J. G.; Baerends, E. J.; Ros, P. *Mol. Phys.* **1979**, *38*(6), 1909.

(18) Bickelhaupt, F.M.; Baerends, E.J. In: *Rev. Comput. Chem.*; Lipkowitz, K. B. and Boyd, D. B., Eds.; Wiley-VCH: New York, **2000**, Vol. 15, 1-86.

(19) E. J. Baerends and O. V. Gritsenko, J. Phys. Chem. A **1997**, *101*, 5383.

(20) (a) Ziegler, T.; Rauk, A. *Inorg. Chem.* **1977**, *46*, 1. (b) Ziegler, T.; Rauk, A. *Inorg. Chem.* **1979**, *18*, 1558. (c) Ziegler, T.; Rauk, A. *Inorg. Chem.* **1979**, *18*, 1755.

(21) (a) Morokuma, K. *J. Chem. Phys* **1971**, 55, 1236. (b) Kitaura, K.; Morokuma, K. *Int. J. Quantum. Chem.* **1976**, *10*, 325. (c) Stone, A. J.; Erskine,R. W. *J. Am. Chem. Soc.* **1980**, *102*, 7185. (d) Bernardi, F.; Bottoni, A.; Mangini, A.; Tonachini, G.; *J. Molec. Struct. (THEOCHEM)* **1981**, *86*, 163. (e) Post, D.; Baerends, E. J. *J. Chem. Phys.* **1983**, *78*, 5663. (f) Dapprich, S.; Frenking, G. *J. Phys. Chem.* **1995**, 99, 9352.

3 The Nature of the Transition Metal-Carbonyl Bond

This chapter has been published:

Axel Diefenbach, F. Matthias Bickelhaupt and Gernot Frenking: »The Nature of the Transition Metal–Carbonyl Bond and the Question about the Valence Orbitals of Transition Metals. A Bond-Energy Decomposition Analysis of $TM(CO)_6^q$ (TM^q = Hf^{2-}, Ta^-, W, Re^+, Os^{2+}, Ir^{3+})«, *J. Am. Chem. Soc.* **2000**, *122*, 6449.

Abstract

The equilibrium geometries and bond dissociation energies for loss of one CO and loss of six CO from $TM(CO)_6^q$ (TM^q = Hf^{2-}, Ta^-, W, Re^+, Os^{2+}, Ir^{3+}) have been calculated at the BP86 level using Slater-type basis sets. The bonding interactions between $TM(CO)_5$ and one CO and between TM^q in the t_{2g}^6 valence state and the ligand cage $(CO)_6$ were analyzed in the framework of Kohn-Sham MO theory with the use of the quantitative ETS energy partitioning scheme. The BDEs exhibit a U-shaped curve from $Hf(CO)_6^{2-}$ to $Ir(CO)_6^{3+}$ with $W(CO)_6$ having the lowest BDE for loss of one CO, while $Re(CO)_6^+$ has the lowest BDE for loss of 6 CO. The stabilizing orbital interaction term ΔE_{oi} and the electrostatic attraction term ΔV_{elst} have comparable contributions to the $(CO)_5TM^q$-CO bond strength. The largest orbital contributions relative to the electrostatic attraction are found for the highest charged complexes $Hf(CO)_6^{2-}$ and $Ir(CO)_6^{3+}$. The contribution of the $(CO)_5TM^q \leftarrow CO$ σ-donation continuously increases from $Hf(CO)_6^{2-}$ to $Ir(CO)_6^{3+}$ and eventually becomes the dominant orbital interaction term in the carbonyl cations, while the $(CO)_5TM^q \rightarrow CO$ π-backdonation decreases in the same direction. The breakdown of the contributions of the d, s and p valence orbitals of the metals to the energy and charge terms of the $TM^q \leftarrow (CO)_6$ donation shows for a single AO the order d >> s > p, but the contributions of the three p orbitals of TM^q are larger than the contribution of the s orbital.

3.1 Introduction

The nature of the chemical bond is at the very heart of chemical research. The lack of true insight into the inter-atomic interactions in molecules in the pre-quantum chemical period prior to 1925[1] forced chemists to use heuristic models that were developed by correlating experimental observations with plausible ad-hoc assumptions. Whereas these models proved to be very helpful as an ordering scheme for experimental observations and as a tool for the design of new experiments, they do not provide any information about the nature of the chemical bond. Only after sophisticated quantum chemical methods were developed and powerful computers were available, it became possible to accurately analyze the interatomic interactions of molecules and to understand the physical nature of the chemical bond. The progress in quantum chemistry also contributed to the development of bonding models, with molecular orbital (MO) theory being the most prominent example. MO theoretical models belong now to the standard curriculum of modern chemical textbooks.

The enormous success of MO theory, particularly in form of the frontier molecular orbital model,[2] led to its widespread use in organic and inorganic chemistry for explaining the structure and reactivity of molecules. There is a danger, however, in the uncritical use of the frontier orbital model for explaining chemical bonding, because other factors such as electrostatic interactions and Pauli repulsion may also play a significant role. A thorough analysis of the different factors which contribute to the strength of the interatomic interactions is seldom done, and the results of such studies often reveal that the nature of the chemical bond is more complicated than the simple bonding models which are commonly used. Nevertheless, it is fair to say that much progress has been made in the understanding of the chemical bond in the last decades.

Most quantum chemical analyses of the chemical bond focused in the beginning on the elements of the first row of the periodic system. The extension of the bonding concepts which were developed for the first octal row to the heavier main-group elements already proved to be more complicated than most chemists would have expected.[3] Nevertheless, quantum chemical calculations gave insight into the bonding

situation of the main-group elements beyond neon. A detailed analysis of the multiple bonds of light and heavy main-group elements, which led to some surprising results, gave an understanding for the different geometries and significantly lower stabilities of molecules with multiple bonds between heavier elements.[3,4] The long lasting controversy about the question whether the d orbitals of the heavier main group elements should be considered as true valence orbitals was finally solved with the help of sophisticated methods for analyzing the electronic structure in favor of the sp-valence bonding model.[5]

Theoretical analyses of the chemical bond of transition metal (TM) compounds which are based on accurate quantum chemical calculations could only be made in the more recent past, because the electronic structure of the TMs is more complicate. Previous studies based on approximate MO methods particularly by Hoffmann demonstrated that MO arguments are very helpful to explain the structures and geometries of transition metal (TM) compounds.[6] However, two detailed analyses of the Cr–CO interactions in $Cr(CO)_6$ by Davidson et al.[7a] and by Baerends and Rozendaal[7b] have shown that the nature of the chemical bond in chromium hexacarbonyl is much more complicated than it may be assumed by considering qualitative models such as the popular Dewar-Chatt-Duncanson (DCD) model[8] of TM←CO σ-donation and TM→CO π-backdonation (Figure 1).

Inspection of the different energy terms for the metal-ligand interactions which were identified with the Morokuma energy partitioning scheme[9] showed that the contribution of the Cr→CO π-backdonation to the total binding energy is larger than the energy term which comes from the Cr←CO σ-donation. This is in agreement with numerous earlier theoretical studies of metal-CO interactions.[10] However, analysis of the changes in the electronic structure by Davidson et al.[7] revealed that the driving force for the large π back-bonding is the electrostatic energy that arises from the penetration of the 5σ electrons, which are the carbon lone-pair electrons, into the chromium valence shell. The authors pointed out that electrostatic forces and the Pauli

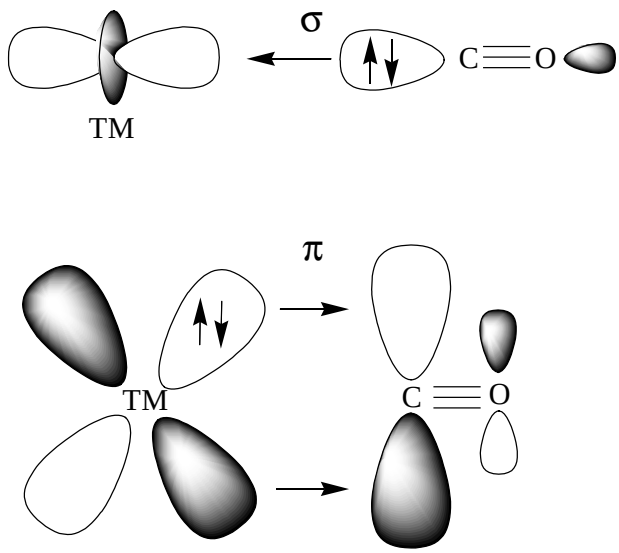

Figure 1. Schematic representation of the TM-CO orbital interactions in carbonyl complexes. TM←CO σ-donation (top) and TM→CO π-backdonation.

exclusion principle must be considered for a true understanding of the chemical bonding.

It is possible to maintain the conceptual power of the MO model and at the same time consider all energy components including correlation energy for the chemical bonding by using density functional theory (DFT). Davidson has already shown that the Morokuma energy partitioning of $Cr(CO)_6$ using Kohn-Sham (KS) orbitals leads to very similar results about the relative size of the Cr→CO π-backdonation and the Cr←CO σ-donation.[7] A closely related energy decomposition method as the Morokuma analysis[9] has been introduced for DFT methods by Ziegler and Rauk.[11] It is called extended transition state (ETS) method, and it has been used for analyzing the binding interactions in numerous TM compounds.[12,13] Details of the method are shortly described in the method section.

Most previous theoretical studies which analyzed the chemical bond in TM carbonyls focused on *neutral* complexes. However, TM carbonyls can also be negatively or positively charged. TM carbonyl complexes which carry a positive charge have been intensively investigated in recent years, both experimentally[14] and

theoretically.[15,16] The finding that some complexes $TM(CO)_n^{m+}$ may have C-O stretching frequencies which are higher than in free CO (2143 cm^{-1}) led Strauss suggest that they should be called "nonclassical" carbonyls, while carbonyl complexes with $\nu(CO) < 2143$ cm^{-1} are "classical".[17] A recent theoretical investigation by Szilagyi and Frenking (SF)[16] of the structure and bonding of the isoelectronic hexacarbonyls $TM(CO)_6^q$ (TM^q = Hf^{2-}, Ta^-, W, Re^+, Os^{2+}, Ir^{3+}) using the charge decomposition analysis (CDA)[18] showed that the $TM^q \rightarrow CO$ π-backdonation continuously decreases from Hf^{2-} to Ir^{3+}, which explains why the C-O stretching frequency increases in the same order in intervals of ~100 cm^{-1}.

A surprising result was found for the trend of the first CO bond dissociation energies (BDE) of the hexacarbonyls, which show a U-shaped curve from Hf^{2-} to Ir^{3+}. The lowest BDE was calculated for $W(CO)_6$. The bond energy increases slightly for $Ta(CO)_6^-$ and then for $Hf(CO)_6^{2-}$, and an even stronger increase in the BDE was calculated for the carbonyl cations. $Ir(CO)_6^{3+}$ has clearly the highest BDE of the six isoelectronic species.[16] This is surprising in the light of the results for neutral TM carbonyls, which all agree that the TM→CO π-backdonation contributes more to the metal-CO bond energy than TM←CO σ-donation.[7,10] A plausible explanation would be that either σ-donation becomes much more important in TM carbonyl cations, or that electrostatic interactions play a larger role in positively charged species. The higher BDE of the negatively charged carbonyls than $W(CO)_6$ might then be due to larger π-backdonation. Because the molecular charge changes from -2 to +3, it might be expected that electrostatic forces significantly influence the strength of the metal-carbonyl interactions.

The question about the change in the size of the energy contributions to the metal–CO interactions when the carbonyl complex is negatively or positively charged was one reason for carrying out this study. Which factors determine the U-shaped trend of the BDE in the metal hexacarbonyls? A second question which we want to address concerns a more fundamental aspect of TM bonding. There is at present a controversy

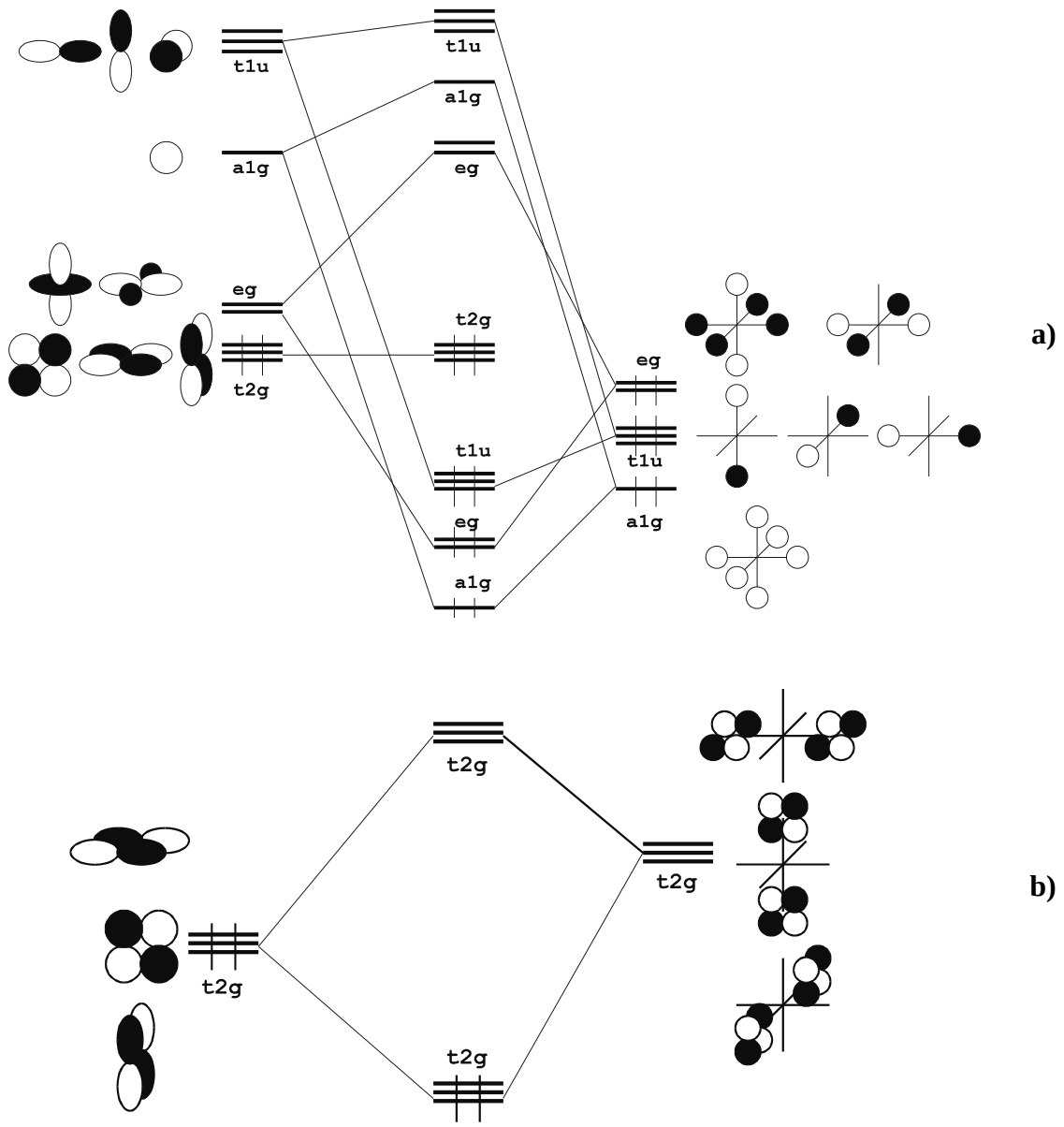

Figure 2. Orbital interaction diagram of the splitting of the d, s, p valence orbitals of a transition metal in an octahedral ligand field. (a) Interactions of the σ orbitals; (b) Interactions of the π orbitals.

about the question if the lowest lying empty p orbitals of the transition metals should be considered as valence orbitals, or if they are only polarization functions, like the d-functions of the main-group elements.[19,20] The common picture of TM-ligand orbital

interactions in an octahedral complex TML_6 where the ligands L have σ donor and π acceptor orbitals suggests that TM←L σ-donation involves the empty d(σ), p and s orbitals of the metal (Figure 2). A CDA analysis of $W(CO)_6$ has shown that the W←CO σ-donation involves mainly the d orbitals, while the s and p orbitals are less important.[18] But how important are the s and p orbitals energy wise, and how do the contributions to the bond energy change when the hexacarbonyl complex carries a positive charge? In the course of this work we found that the analysis of the interactions between the metal TM^q and the ligand cage $(CO)_6$ is an excellent probe to address this question. In order to answer the two questions we carried out a quantitative bonding analysis of the title compounds in the framework of the Kohn-Sham MO model. This was done with the help of an energy decomposition analysis at the gradient-corrected DFT level using the ETS method. Details are described in the method section.

The bonding analysis was carried out in two ways. One way was to look on the interactions between one CO and the $TM(CO)_5^q$ fragment. The results give insight into the factors which determine the first BDE. In the second approach we analyzed the interactions between the bare transition metal TM^q and the cage of $(CO)_6$ in octahedral symmetry. This is the approach that has been used by Davidson for his bonding analysis of $Cr(CO)_6$.[7] Because O_h symmetry is retained in the latter analysis, it is possible to identify the energy contributions of the d, s, and p orbitals of the metal to the TM^q←CO σ-donation. An energy analysis of the metal-carbonyl bonding in neutral and charged complexes has recently been reported by Ehlers et al.[12] The authors investigated only the σ- and π-orbital contributions to the first BDE and not the energy components which are due to Pauli repulsion and electrostatic interaction. The bonding between the metal and the ligand cage $(CO)_n$ and the contributions by the d, s and p orbitals of the metal were not studied.

3.2 Methods

The calculations have been performed at the non-local DFT level of theory using the exchange functional of Becke[21] and the correlation functional of Perdew[22] (BP86). Relativistic effects have been considered by the zeroth-order regular approximation (ZORA),[23] which is more reliable than the widely used Pauli formalism. Uncontracted Slater-type orbitals (STOs) have been used as basis functions for the SCF calculations.[24] Basis sets for all atoms have triple-ζ quality, augmented with a 6p function on the metal atoms, and two sets of polarization functions, 3d and 4f, on carbon and oxygen atoms. The $(1s)^2$ core electrons of oxygen and carbon and the $(1s2s2p3s3p3d4s4p4d)^{46}$ core electrons of the metals were treated by the frozen-core approximation.[25] An auxiliary set of s, p, d, f and g STOs was used to fit the molecular densities and to represent the Coulomb and exchange potentials accurately in each SCF cycle.[26] The optimized structures have been verified as minima on the potential energy surface by calculation of the vibrational frequencies. The atomic partial charges have been calculated with the Hirshfeld partitioning scheme.[27] All calculations were carried out with the program package ADF.[28]

The bonding interactions between the pentacarbonyl fragments $TM(CO)_5^q$ and CO and between the metal atom TM^q and the ligand cage $(CO)_6$ have been analyzed with the energy decomposition scheme ETS developed by Ziegler and Rauk.[11] Within this method, the bond dissociation energy ΔE between two fragments A and B is partitioned into several contributions which can be identified as physically meaningful entities. First, ΔE is separated into two major components ΔE_{prep} and ΔE_{int}:

$$\Delta E = \Delta E_{prep} + \Delta E_{int}$$

ΔE_{prep} is the energy which is necessary to promote the fragments A and B from their equilibrium geometry and electronic ground state to the geometry and valance electronic state which they have in the compound AB. ΔE_{int} is the instantaneous interaction energy between the two fragments in the molecule. The latter quantity will

be the focus of the present work. The interaction energy ΔE_{int} can be divided into three main components:[28b, 29]

$$\Delta E_{int} = \Delta V_{elst} + \Delta E_{Pauli} + \Delta E_{oi}$$

ΔV_{elst} gives the electrostatic interaction energy between the fragments which are calculated with a frozen electron density distribution in the geometry of the complex. ΔE_{Pauli} gives the repulsive interaction energy between the fragments which are caused by the fact that two electrons with the same spin can not occupy the same region in space. The term comprises the four-electron destabilizing interactions between occupied orbitals. The stabilizing orbital interaction term ΔE_{oi} is calculated in the final step of the ETS analysis when the Kohn-Sham orbitals relax to their optimal form. The reader should note that the relaxation energy of the Kohn-Sham orbitals includes the effect of electron correlation. The ΔE_{oi} term can be further partitioned into contributions by orbitals which belong to different irreducible representations of the interacting system.

3.3 Results and Discussion

The discussion of the results is organized in the following way. First, we summarize the calculated geometries, bond dissociation energies (BDE) and the atomic partial charges of the hexacarbonyls. This section is rather short because part of the data have been reported before.[16] In the following parts we discuss the results of the bonding analysis. The second section gives an account of the interactions between CO and the metal pentacarbonyl fragments. In the third section we present a bonding analysis of the interactions between the metal atom TM_q and the ligand cage $(CO)_6$. The final section contains an analysis of the contributions of the metal d, s, and p valence orbitals to the carbonyl bonds.

3.3.1 Geometries, Bond Energies and Charge Distribution

Table 1 shows two types of calculated bonding energies. First, we give the theoretically predicted bond dissociation energies (BDEs) D_e of the metal hexacarbonyls for loss of one CO ligand yielding $TM(CO)_5^q$ and CO in the relaxed geometries (Reaction 1a) and in the frozen geometries of the hexacarbonyls (Reaction 1b). The latter set gives the instantaneous interaction energies ΔE_{int} between the pentacarbonyl fragment and CO in the complex. The two sets of data from reactions 1a and 1b are not very different, because the geometry changes of the fragments are small. The D_e value of $W(CO)_6$ (49.63 kcal/mol) gives a ZPE corrected theoretically predicted BDE of $W(CO)_6$ D_o = 47.5 kcal/mol which is in excellent agreement with the experimental value $D_o = 46 \pm 2$ kcal/mol.[30] The theoretical D_e and ΔE_{int} values show the same U-shaped trend from $Hf(CO)_6^{2-}$ to $Ir(CO)_6^{3+}$ with $W(CO)_6$ being the lowest point in the curve as found in our previous study.[16]

$$TM(CO)_6^q \rightarrow TM(CO)_5^q + CO + BDE(CO) \quad (1a)$$

$$TM(CO)_6^q \rightarrow TM(CO)_5^q(fr) + CO(fr) + BDE(CO) \quad (1b)$$

$$TM(CO)_6^q \rightarrow (t_{2g}^6)TM^q + 6\ CO + BDE(6\ CO) \quad (2a)$$

$$TM(CO)_6^q \rightarrow (t_{2g}^6)TM^q + (CO)_6(fr) + BDE(CO)_6 \quad (2b)$$

fr = frozen geometry

The second set of bonding energies given in Table 1 refers to the dissociation of $TM(CO)_6^q$ into the metal cation in the t_{2g}^6 reference state, which is the valence state of the metal in the hexacarbonyl, and six CO (Reaction 2). Reaction 2a gives the calculated BDEs for the reactions yielding 6 CO with optimized bond lengths, while reaction 2b describes the dissociation yielding the metal and the ligand cage $(CO)_6$ in the frozen geometry of the hexacarbonyl. Both sets of BDEs exhibit a similar U-shaped curve like the BDEs for loss of one CO. However, the lowest BDEs of reactions 2a and 2b are predicted for $Re(CO)_6^+$ (Table 1). The highest bonding energies of reactions 1 and 2 are calculated for $Ir(CO)_6^{3+}$.

Table 1 shows that the calculated metal–CO bond lengths *r*(TM-C) are in excellent agreement with experimental values. Please note that the *r*(TM-C) values decrease regularly from $Hf(CO)_6^{2-}$ to $Os(CO)_6^{2+}$ before they become longer again in triply charged $Ir(CO)_6^{3+}$. The calculations predict that the C-O bond lengths decrease regularly from $Hf(CO)_6^{2-}$ to $Ir(CO)_6^{3+}$. The experimental values for *r*(C-O) agree with the theoretical trend, but the scattering of the measured values is rather high. The regular increase of the C–O stretching frequency from $Hf(CO)_6^{2-}$ to $Ir(CO)_6^{3+}$ with intervals of ~100 cm^{-1} which was found experimentally[31] and theoretically[16, 32] is in agreement with the trend toward shorter C-O interatomic distances.

The charge distribution given by the Hirshfeld partitioning scheme indicates a regular decrease of negative charge (increase of positive charge) for the three atom types TM, C, O from $Hf(CO)_6^{2-}$ to $Ir(CO)_6^{3+}$. This is a reasonable trend. The previous study of SF gave NBO partial charges, which show larger charge separations and a less regular trend of the charge distribution.[16]

Table 1. Calculated Bond Dissociation Energies (kcal/mol) and Interatomic Distances (Å) and Atomic Partial Charges (*e*) According to the Hirshfeld Partitioning Scheme.

		$Hf(CO)_6^{2-}$	$Ta(CO)_6^{-}$	$W(CO)_6$	$Re(CO)_6^{+}$	$Os(CO)_6^{2+}$	$Ir(CO)_6^{3+}$
reaction	no.			bonding energy			
$TM(CO)_5^q + CO$	1a	-50.84	-48.26	-45.98	-48.36	-56.92	-73.74
$TM(CO)_5^q{}_{(fr)} + CO_{(fr)}$	1b	-56.59	-51.31	-49.63	-52.74	-61.92	-78.90
$TM^q(t_{2g}^6) + 6CO$	2a	-511.10	-498.24	-448.37	-439.51	-517.25	-774.71
$TM^q(t_{2g}^6) + (CO)_{6\,(fr)}$	2b	-543.90	-525.56	-473.89	-456.57	-544.40	-801.58
bond				distances [a]			
TM–C		2.195	2.112	2.061	2.036	2.034	2.055
		(2.174-2.180)	(2.083)	(2.018-2.033)	(1.98-2.07)		(2.00-2.05)
C–O		1.185	1.169	1.153	1.139	1.129	1.129
		(1.165)	(1.149)	(1.130-1.158)	(1.14-1.19)		(1.07-1.12)
atom				Hirshfeld charges			
TM		-0.065	0.016	0.079	0.148	0.226	0.337
C		-0.055	0.017	0.089	0.157	0.222	0.282
O		-0.268	-0.187	-0.102	-0.015	0.074	0.162

[a] Experimental values are given in parenthesis.[31,38]

Table 2. Energy Decomposition and Bonding Analysis of $TM(CO)_5^q$ + CO.

	$Hf(CO)_6^{2-}$	$Ta(CO)_6^{-}$	$W(CO)_6$	$Re(CO)_6^{+}$	$Os(CO)_6^{2+}$	$Ir(CO)_6^{3+}$
energy decomposition / (kcal/mol)						
ΔE_{int}	-56.59	-51.31	-49.63	-52.74	-61.92	-78.90
ΔE_{Pauli}	76.63	100.74	118.31	126.86	125.44	115.94
ΔV_{elst}	-59.38	-76.56	-90.08	-97.69	-98.48	-93.08
ΔE_{oi}	-73.83	-75.48	-77.87	-81.92	-88.87	-101.76
A_1	-17.19	-25.79	-35.92	-47.34	-60.08	-75.39
A_2	0.00	0.00	0.00	0.00	0.00	0.00
B_1	0.05	0.02	-0.03	-0.07	-0.09	-0.10
B_2	-0.05	-0.07	-0.07	-0.07	-0.06	-0.05
E	-56.64	-49.64	-41.85	-34.44	-28.64	-26.22
orbital overlap $\langle TM(CO)_5^q \mid CO \rangle$						
$\langle 11a_1 \mid 5\sigma \rangle$	0.428	0.446	0.468	0.486	0.476	0.414
$\langle 10e \mid 2\pi \rangle$	0.194	0.197	0.192	0.179	0.155	0.108
orbital population / *e*						
— Σ —						
$TM(CO)_5^q$ $11a_1$	0.18	0.21	0.26	0.34	0.43	0.50
CO 5σ	1.72	1.70	1.68	1.64	1.60	1.52
— Π —						
$TM(CO)_5^q$ $10e$	1.67	1.75	1.81	1.87	1.91	1.96
CO 2π	0.35	0.28	0.21	0.15	0.11	0.07

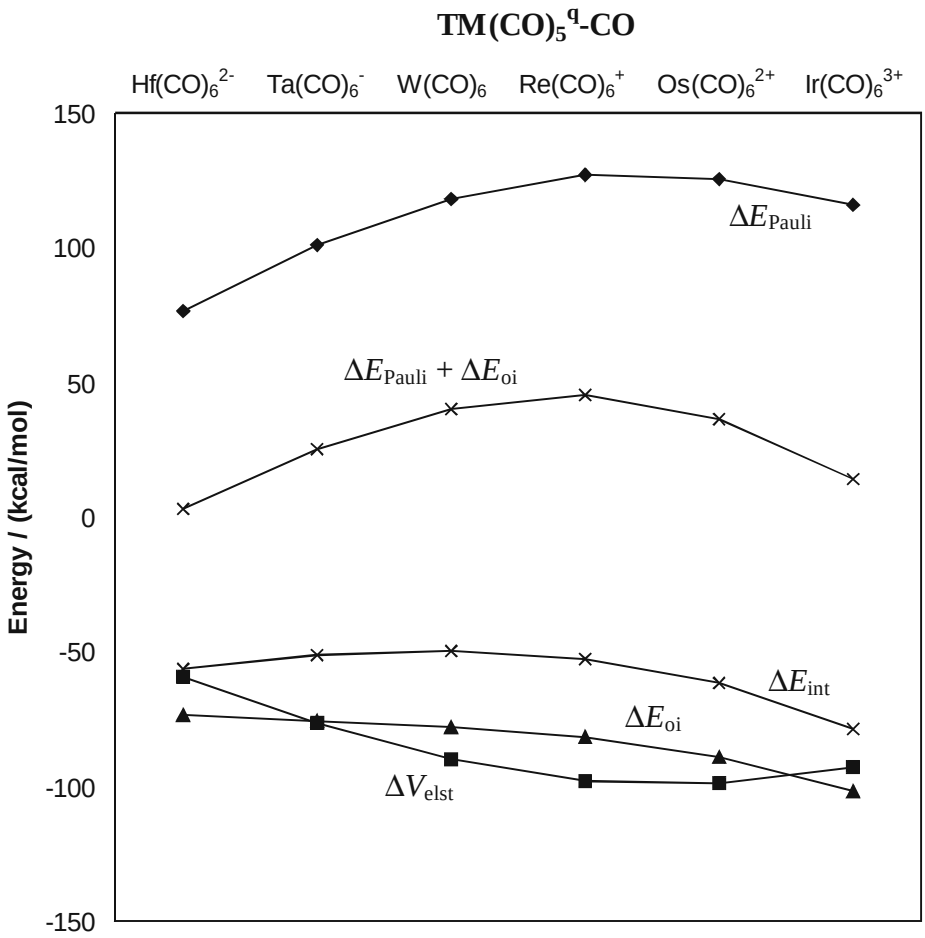

Figure 3. Trend of the energy contributions to the interaction energy between $TM(CO)_5^q$ and CO.

3.3.2 Energy Decomposition $TM(CO)_5^q$-CO

Table 2 shows the results of the partitioning of the interaction energies ΔE_{int}(CO) between $TM(CO)_5^q$ and CO into the three terms ΔE_{Pauli}, ΔV_{elst} and ΔE_{oi}. The trends of the different energy terms are displayed in Figure 3. One can see that the ΔE_{oi} values have indeed a similar trend as the total interaction energies ΔE_{int}, but the ΔE_{int} values increase from $W(CO)_6$ to $Hf(CO)_6^{2-}$ while the ΔE_{oi} values decrease (Table 2). The similar trends of ΔE_{int} and ΔE_{oi} exhibited in Figure 3 support the idea that the bond strength can be correlated with the orbital interactions, but the opposite behavior of the

two terms $W(CO)_6$ to $Hf(CO)_6^{2-}$ demonstrates that other factors can also be important. Figure 3 shows that the sum of ΔE_{Pauli} and ΔE_{oi} gives a trend which is in agreement with the increase of ΔE_{int} $W(CO)_6 < Ta(CO)_6^- < Hf(CO)_6^{2-}$, but the highest point of the curve is found for $Re(CO)_6^+$ and not for $W(CO)_6$.

An important point concerns the absolute values of the energy terms ΔE_{Pauli}, ΔV_{elst} and ΔE_{oi}. Table 2 shows that the calculated values of ΔV_{elst} and ΔE_{oi} are always higher than the bonding energy ΔE_{int}. An arbitrary consideration of only one attractive term would lead to the conclusion that the CO ligand either is only electrostatically bound or that it is only covalently bound. A reasonable consideration of all three terms leads to the conclusion that the ionic contribution and the covalent contribution to the $(CO)_5TM^q$-CO bonding interactions have a similar size, and that the Pauli repulsion leads to a net bonding which is $< 0.5(\Delta V_{elst} + \Delta E_{oi})$. Figure 3 shows that, for $Hf(CO)_6^{2-}$ and $Ir(CO)_6^{3+}$, the covalent bonding given by ΔE_{oi} is larger than the electrostatic bonding given by ΔV_{elst}, while for $W(CO)_6$, $Re(CO)_6^+$ and $Os(CO)_6^{2+}$ it holds that $\Delta E_{oi} < \Delta V_{elst}$. This is a counterintuitive result, because it means that *the highest charged complexes have the smallest degree of ionic character in the metal-CO bond.*

Table 2 shows that the values for ΔE_{Pauli} and ΔV_{elst} have a trend which follows the TM-CO bond lengths, i.e. the absolute values increase with the shortening of the bond from $Hf(CO)_6^{2-}$ to $Os(CO)_6^{2+}$ but decrease for $Ir(CO)_6^{3+}$. We want to point out that the ΔV_{elst} value of $Ir(CO)_6^{3+}$ is less than those of $Re(CO)_6^+$ and $Os(CO)_6^{2+}$. This means that the very high bonding energy of the iridium complex can not be explained with electrostatic forces.

Table 2 also gives the contributions of the stabilizing orbital interaction term ΔE_{oi} for the orbitals with different symmetry. Figure 4 shows a contour line diagram of the symmetry-allowed orbital interactions between the HOMO and LUMO of the fragments which can be expected to give the largest contributions to the ΔE_{oi} term. Table 2 shows that only the orbital interactions with a_1 and e symmetry significantly contribute to the ΔE_{oi} term. Although the stabilization arises from the sum of all orbital interactions with

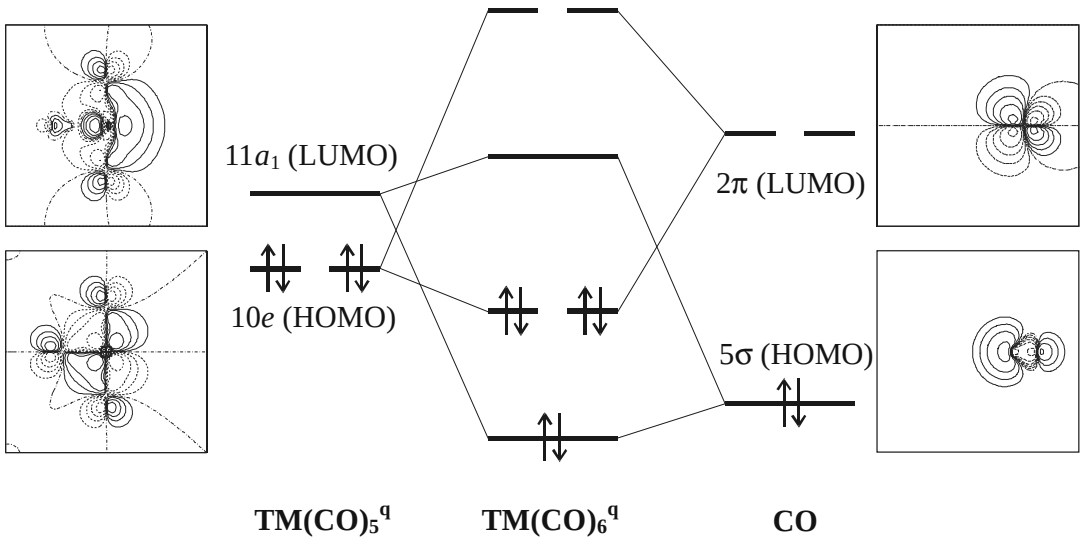

Figure 4. Orbital interaction diagram and plot of the HOMO and LUMO of $TM(CO)_5^q$ and CO.

a_1 and e symmetry, it can reasonably be argued that the dominant contributions come from the HOMO/LUMO interactions depicted in Figure 4. This is supported by the calculated orbital population given in Table 2, which shows that the HOMO and the LUMO exhibit a large change in the population along the series of molecules. It follows that the stabilizing orbital interactions are mainly given by $TM^q \leftarrow CO$ σ-donation (a_1 term) and the $TM^q \rightarrow CO$ π-backdonation (e term).

We want to comment on the *trend* of the energies given by the a_1 and e symmetric orbital interactions. Table 2 shows that the stabilization due to $TM^q \leftarrow CO$ σ-donation steadily increases from $Hf(CO)_6^{2-}$ to $Ir(CO)_6^{3+}$, while the $TM^q \rightarrow CO$ π-backdonation exhibits the opposite trend. The stabilization due to π-backdonation in $Hf(CO)_6^{2-}$, $Ta(CO)_6^-$ and $W(CO)_6$ is stronger than the σ-donation, while the positively charged hexacarbonyls have stronger σ-donation than π-backdonation. The trends can be explained with the lowering of the orbital energies of the 10e HOMO and 11a_1 LUMO of $TM(CO)_5^q$ from $Hf(CO)_6^{2-}$ to $Ir(CO)_6^{3+}$. Figure 5 shows that the energy levels of the frontier orbitals of $TM(CO)_5^q$ span a wide range from +5 eV to -25 eV. The very low

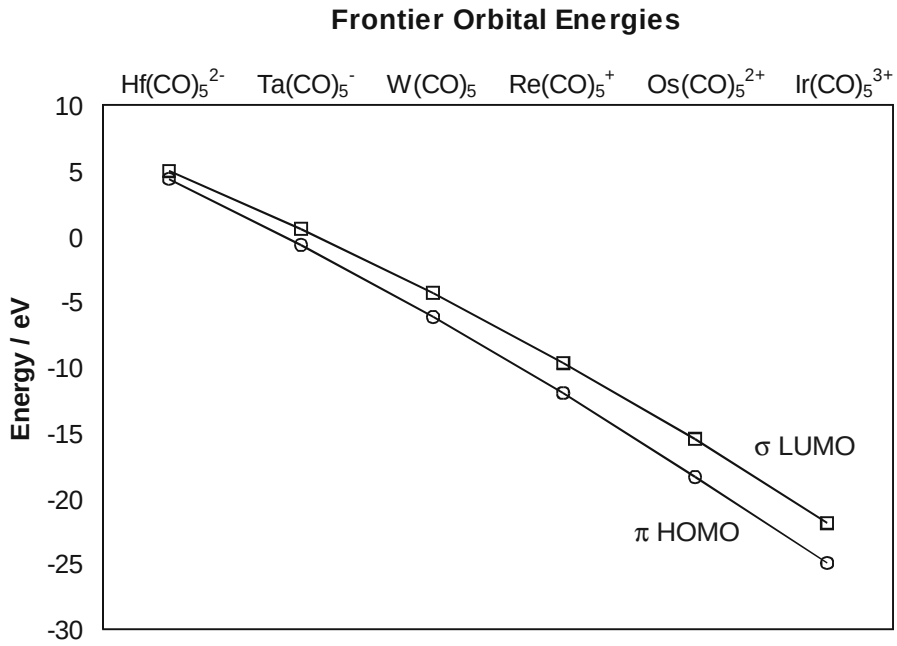

Figure 5. Trend of the frontier orbital energy levels of the pentacarbonyls.

lying σ LUMO of $Ir(CO)_5^{3+}$ and the very high lying π HOMO of $Hf(CO)_5^{2-}$ explain why the $TM^q \leftarrow CO$ σ-donation in the iridium complex and the $TM^q \rightarrow CO$ π-backdonation in the hafnium complex dominate the stabilizing orbital interactions in the compounds (Table 2). Table 2 shows also that the orbital overlap between the 5σ HOMO of CO and $11a_1$ LUMO of $TM(CO)_5^q$ does not change very much for the six interacting systems. Nor does the overlap between the 10e HOMO of $TM(CO)_5^q$ and the 2π LUMO of CO vary noticeably among the first four species listed in Table 2. Please note that $Ir(CO)_6^{3+}$, which has the strongest contribution by (a_1) σ-donation, has the smallest orbital overlap $\langle 11a_1|5\sigma\rangle$. It follows that orbital overlap is here overruled by the factor of matching orbital energies.

The calculated orbital population shows a steady increase of the $11a_1$ LUMO of the metal fragment and a decrease of the 2π LUMO population of CO from $Hf(CO)_6^{2-}$ to $Ir(CO)_6^{3+}$. The same trends have been found by SF in the CDA analysis of the compounds.[16] The change in the orbital population agrees with the trend of the orbital

interaction energies. The values in Table 2 demonstrate that the size of the orbital overlap between the bonded atoms does not correlate with the bond energy. The overlap of the σ orbital ⟨$11a_1$|5σ⟩ in $Hf(CO)_6^{2-}$, $Ta(CO)_6^-$ and $W(CO)_6$ is larger than the overlap of the π orbital ⟨11e|2π⟩ and yet, the π-bonding energy is higher than the σ-bonding. Also the trend of the orbital overlaps and the associated energy values do not agree with each other. The σ orbital overlap ⟨$11a_1$|5σ⟩ of $Ir(CO)_6^{3+}$ has the smallest value (0.414) of the carbonyl complexes, but the energy contribution is the largest of all compounds (Table 2). The change in the orbital overlap *population* of the σ and π orbitals, however, agrees with the relative contributions of the associated energies to ΔE_{oi}. The π orbital population of $Hf(CO)_6^{2-}$, $Ta(CO)_6^-$ and $W(CO)_6$ is larger than the σ population, while the opposite is found for the cations. Note that the values for the orbital overlap and for the orbital contribution given in Table 2 refer to only one component of the degenerate π orbital. They must be multiplied by two in order to get the total values.

Now we try to rationalize the U-shaped trend of the bonding energy ΔE_{int} in the light of the calculated values for the various terms of the ETS analysis. We use the results for $W(CO)_6$, which has the lowest ΔE_{int} value and the lowest BDE as reference point. It becomes obvious that the higher $TM(CO)_5^q$-CO interaction energies of the negatively charged complexes $Ta(CO)_6^-$ and $Hf(CO)_6^{2-}$ are *not* caused by the changes in the electrostatic attraction, which decreases for the anions, nor by the ΔE_{oi} term, which also becomes slightly smaller. The higher bonding energy is rather caused by the very large decrease in the repulsive ΔE_{Pauli} term (Table 2). Although the stabilizing $TM(CO)_5^q \rightarrow CO$ π-backdonation becomes larger in the anions, the increase is compensated by the larger decrease in the $TM(CO)_5^q \leftarrow CO$ σ-donation. The overall stabilization by the ΔE_{oi} term in $Ta(CO)_6^-$ and $Hf(CO)_6^{2-}$ is weaker than in $W(CO)_6$. A superficial consideration of the trend of the different terms could have attributed the higher BDEs of the anions to the increase in the π-backdonation.

A different explanation must be given for the higher bond energies of the positively charged systems. Table 2 shows that the increase of the ΔE_{int} values from $W(CO)_6$ to $Ir(CO)_6^{3+}$ runs parallel to the increase of the ΔE_{oi} values. This is because the

sum of the Pauli repulsion and electrostatic attraction is nearly constant for $W(CO)_6$, $Re(CO)_6^+$ and $Os(CO)_6^{2+}$ (Figure 3). Thus, it seems reasonable to conclude that the larger ΔE_{int} values of $Re(CO)_6^+$, $Os(CO)_6^{2+}$ and $Ir(CO)_6^{3+}$ are caused by the larger ΔE_{oi} values, which come from the stronger $TM(CO)_5^q \leftarrow CO$ σ-donation. However, the electrostatic attraction also increases from $W(CO)_6$ to $Os(CO)_6^{2+}$, and the further increase of the ΔE_{int} value for $Ir(CO)_6^{3+}$ may also be explained with the decrease of Pauli repulsion. It is arbitrary to state that the higher inter-action energies are *caused* by the ΔE_{oi} term. All one can say is that the increase of the ΔE_{int} values from $W(CO)_6$ to $Ir(CO)_6^{3+}$ can be *correlated* with the increase of the ΔE_{oi} term.

3.3.3 Energy Decomposition TM^q-$(CO)_6$

Table 3 gives the energy contributions ΔE_{Pauli}, ΔV_{elst} and ΔE_{oi} to the total interaction energy ΔE_{int} between the metal TM^q and the ligand cage $(CO)_6$. Figure 6 shows the trend of the energy terms from $Hf(CO)_6^{2-}$ to $Ir(CO)_6^{3+}$. It becomes obvious that the values of the orbital interaction term ΔE_{oi} are quite similar to the ΔE_{int} values and that the two curves exhibit a similar shape. The only qualitative difference between the two terms is found for $W(CO)_6$ and $Re(CO)_6^+$. The total interaction energy decreases from $W(CO)_6$ to $Re(CO)_6^+$ while the orbital interactions increase in this direction (Table 3). A similar trend as for ΔE_{oi} is found for the total orbital interactions $\Delta E_{oi} + \Delta E_{Pauli}$ (Figure 6). This is because the values of the Pauli repulsion and the electro-static interactions ΔV_{elst} change only little from $Hf(CO)_6^{2-}$ to $Ir(CO)_6^{3+}$, although the charge of the complexes varies from -2 to +3. We want to point out that the electrostatic attraction between Ir^{3+} and $(CO)_6$ is the smallest of the hexacarbonyls shown in Table 3, although the metal carries the largest charge and although $Ir(CO)_6^{3+}$ has the largest TM^q-$(CO)_6$ interaction energy. Thus the electrostatic interactions are not the reason for the large bonding energy in $Ir(CO)_6^{3+}$ and they do not play a role for the trend of the metal-CO interactions. Note that the trend of the ΔV_{elst} values given in Table 3 does not follow the pattern of the metal-CO distances, unlike the values which were calculated for the interactions between $TM(CO)_5^q$ and CO (Table 2).

Table 3. Energy Decomposition and Bonding Analysis of TM^q + $(CO)_6$.

	$Hf(CO)_6^{2-}$	**$Ta(CO)_6^{-}$**	**$W(CO)_6$**	**$Re(CO)_6^{+}$**	**$Os(CO)_6^{2+}$**	**$Ir(CO)_6^{3+}$**
energy decomposition / (kcal/mol)						
ΔE_{int}	-543.90	-525.56	-473.89	-456.57	-544.40	-801.58
ΔE_{Pauli}	367.40	413.38	438.80	454.51	451.33	420.93
ΔE_{elstat}	-358.62	-397.62	-396.24	-375.09	-353.44	-337.81
ΔE_{orb}	-552.68	-541.32	-516.44	-536.00	-642.27	-884.70
A_{1g}	-9.48	-10.49	-15.40	-27.42	-47.63	-78.78
A_{2g}	0.00	0.00	0.00	0.00	0.00	0.00
E_g	-83.36	-113.07	-159.08	-233.72	-348.84	-520.66
T_{1g}	-1.30	-0.98	-2.88	-8.91	-19.41	-33.92
T_{2g}	-437.42	-397.59	-308.18	-200.33	-101,14	-43.82
A_{1u}	-0.03	-0.04	-0.03	0.00	-0.02	-0.02
E_u	0.00	-0.00	0.00	0.00	0.00	0.00
T_{2u}	-2.74	-2.00	-4.35	-11.60	-23.86	-40.17
T_{1u}	-18.35	-17.15	-26.52	-54.00	-101.37	-167.33
T_{1u} (σ) [1)]	-12.97	-12.06	-18.65	-38.53	-73.98	-125.68
T_{1u} (π) [2)]	-5.38	-5.09	-7.87	-15.47	-27.39	-41.65
orbital overlap $\langle TM^q \mid (CO)_6 \rangle$						
$\langle 2a_{1g} \mid 3a_{1g} \rangle$	0.656	0.683	0.708	0.713	0.697	0.659
$\langle 1e_g \mid 3e_g \rangle$	0.620	0.619	0.573	0.495	0.412	0.329
$\langle 1t_{2g} \mid 2t_{2g} \rangle$	0.524	0.505	0.440	0.345	0.273	0.204
$\langle 3t_{1u} \mid 3t_{1u} \rangle$	0.261	0.274	0.281	0.275	0.257	0.226
$\langle 3t_{1u} \mid 4t_{1u} \rangle$	0.629	0.649	0.666	0.685	0.694	0.682
orbital population / *e*						
— **A_{1g}** —						
TM^q $2a_{1g}$	0.16	0.19	0.24	0.33	0.41	0.50
$(CO)_6$ $3a_{1g}$	1.76	1.76	1.76	1.72	1.66	1.56
— **E_g** —						
TM^q $1e_g$	0.41	0.55	0.66	0.73	0.83	0.91
$(CO)_6$ $3e_g$	1.55	1.46	1.37	1.28	1.18	1.05
— **T_{2g}** —						
TM^q $1t_{2g}$	0.60	0.99	1.29	1.46	1.61	1.75
$(CO)_6$ $2t_{2g}$	1.36	1.03	0.74	0.52	0.34	0.19
— **T_{1u}** —						
TM^q $3t_{1u}$	0.07	0.07	0.09	0.12	0.15	0.20
$(CO)_6$ $3t_{1u}$	1.97	1.96	1.95	1.94	1.93	1.93
$(CO)_6$ $4t_{1u}$	1.93	1.95	1.95	1.93	1.90	1.84

[1)] $E(T_{1u})\ (\sigma) = E(T_{1u}) \cdot \langle 3t_{1u} \mid 4t_{1u} \rangle / (\langle 3t_{1u} \mid 3t_{1u} \rangle + \langle 3t_{1u} \mid 4t_{1u} \rangle)$

[2)] $E(T_{1u})\ (\pi) = E(T_{1u}) \cdot \langle 3t_{1u} \mid 3t_{1u} \rangle / (\langle 3t_{1u} \mid 3t_{1u} \rangle + \langle 3t_{1u} \mid 4t_{1u} \rangle)$

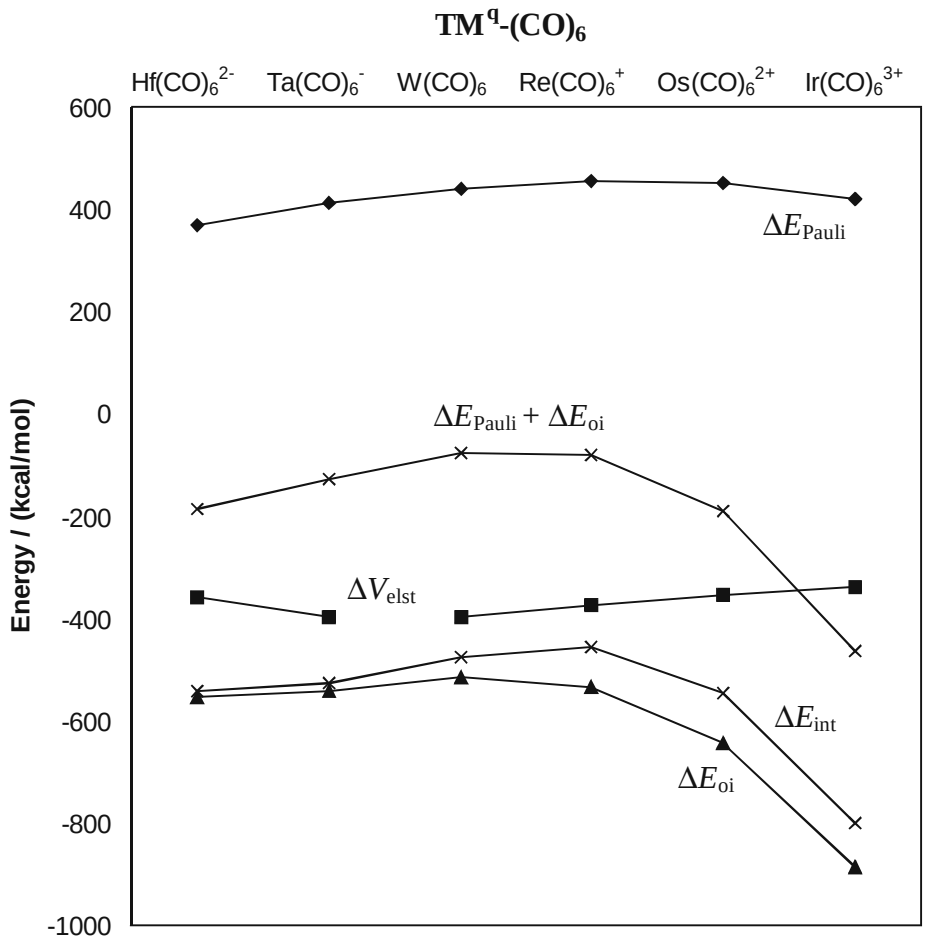

Figure 6. Trend of the energy contributions to the interaction energy between TM^q and $(CO)_6$.

The energy decomposition of the total binding energy of the hexacarbonyls $TM(CO)_6^q$ in terms of interactions between TM^q and $(CO)_6$ in the geometry of the complex retains O_h symmetry. This makes it possible to analyze the different orbital interactions of the metal valence orbitals having different symmetry and to estimate their contributions to the σ and π-type interactions with the ligand cage orbitals. Figure 2 suggests that σ interactions arise from orbitals with t_{1u}, e_g and a_{1g} symmetry, while the π interactions come from orbitals which have t_{2g} symmetry. Table 2 shows that the partitioning of the

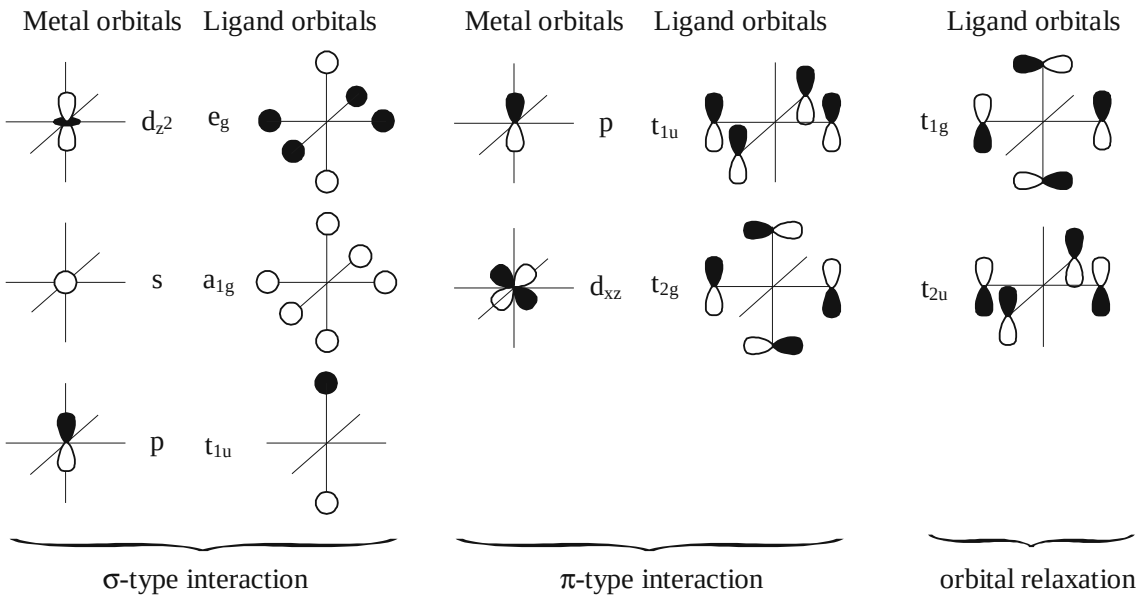

Figure 7. Schematic represenation of the orbitals with different symmetry which contribute to the ΔE_{oi} term according to the ETS analysis of TM^q-$(CO)_6$ (Table 3).

ΔE_{oi} term gives also contributions from orbitals which have t_{1g} and t_{2u} symmetry. Figure 7 shows a more detailed representation of the orbital interactions TM^q-$(CO)_6$ as given in Figure 2.

It becomes obvious that the metal valence orbitals which are engaged in σ-type interactions with $(CO)_6$ are the d_{z^2} and (not shown in Figure 7) the $d_{x^2-y^2}$ orbitals (e_g symmetry), the s orbital (a_{1g}) and the p orbitals (t_{1u}). The π-type interactions involve the d_{xz} and (not shown) d_{xy} and d_{yz} orbitals (t_{2g}), but also the p orbitals of the metal which can form a t_{1u} combination with the π-orbitals of $(CO)_6$. The latter stands for the donation of the occupied π-MOs of CO into empty p(π) AOs of the metal. The contribution of this interaction to the metal-CO π-bonding is not shown in Figure 2. It is often neglected, but a popular textbook of organometallic chemistry has pointed out that TM←CO π-donation may perhaps also be important.[33] Thus, the total t_{1u} contribution of the orbital interaction term ΔE_{oi} gives not only the stabilization due to TM←CO σ-

donation, but it contains also the stabilization due to TM←CO π-donation. In order to quantify the σ and π contributions to the t_{1u}-symmetric ΔE_{oi} term we used as a rough approximation the size of the overlaps of the metal p orbital with the $3t_{1u}$ and $4t_{1u}$ orbitals of $(CO)_6$, which consist primarily of π and σ CO orbitals, respectively.[34] Table 3 shows that the energy contribution of the TM←CO π-donation is always much less than the TM←CO σ-donation. We want to point out that the division of the t_{1u} orbital interactions into σ and π contributions is not very relevant for the other conclusions which are made in this paper.

The remaining contributions to the ΔE_{oi} term have t_{1g} and t_{2u} symmetry (Figure 7). The t_{1g} and t_{2u} contributions are not genuine orbital interaction terms. There are no metal orbitals which have t_{1g} or t_{2u} symmetry in an octahedral environment. The stabilization arises from the relaxation of the t_{1g} and t_{2u} ligand orbitals of $(CO)_6$ caused by the electrostatic attraction by the metal. The electric charge of the metal polarizes the electronic charge distribution of the carbonyl ligands. It has been suggested[35,36] that the charge distribution of CO, which is caused by a positive point charge, has a strong effect on the C-O bond length and stretching frequency. The electrostatic stabilization of the t_{1g} and t_{2u} ligand orbitals is quite small in the neutral and negatively charged carbonyls, but it becomes larger in the positively charged species. The size of the t_{1g} and t_{2u} terms in $Ir(CO)_6^{3+}$ becomes eventually comparable to the (t_{2g}) $Ir^{3+}\rightarrow(CO)_6$ π-backdonation (Table 3).

Figure 8 shows graphically the trend of the σ and π orbital interaction energies with different symmetry which contribute to the $TM^q\leftarrow(CO)_6$ donation (e_g, a_{1g}, t_{1u}, t_{1u}) and the $TM^q\rightarrow(CO)_6$ backdonation (t_{2g}). Note that the total π interaction includes the t_{1u} $TM^q\leftarrow(CO)_6$ π-backdonation. It becomes obvious that for the negatively charged and neutral species the π interactions are more important than the σ inter-actions, while the σ interactions dominate the ΔE_{oi} term for the positively charged metal carbonyls. The largest part of the π interactions comes from the t_{2g} term, while the largest contribution to the σ interactions comes from the e_g orbital.

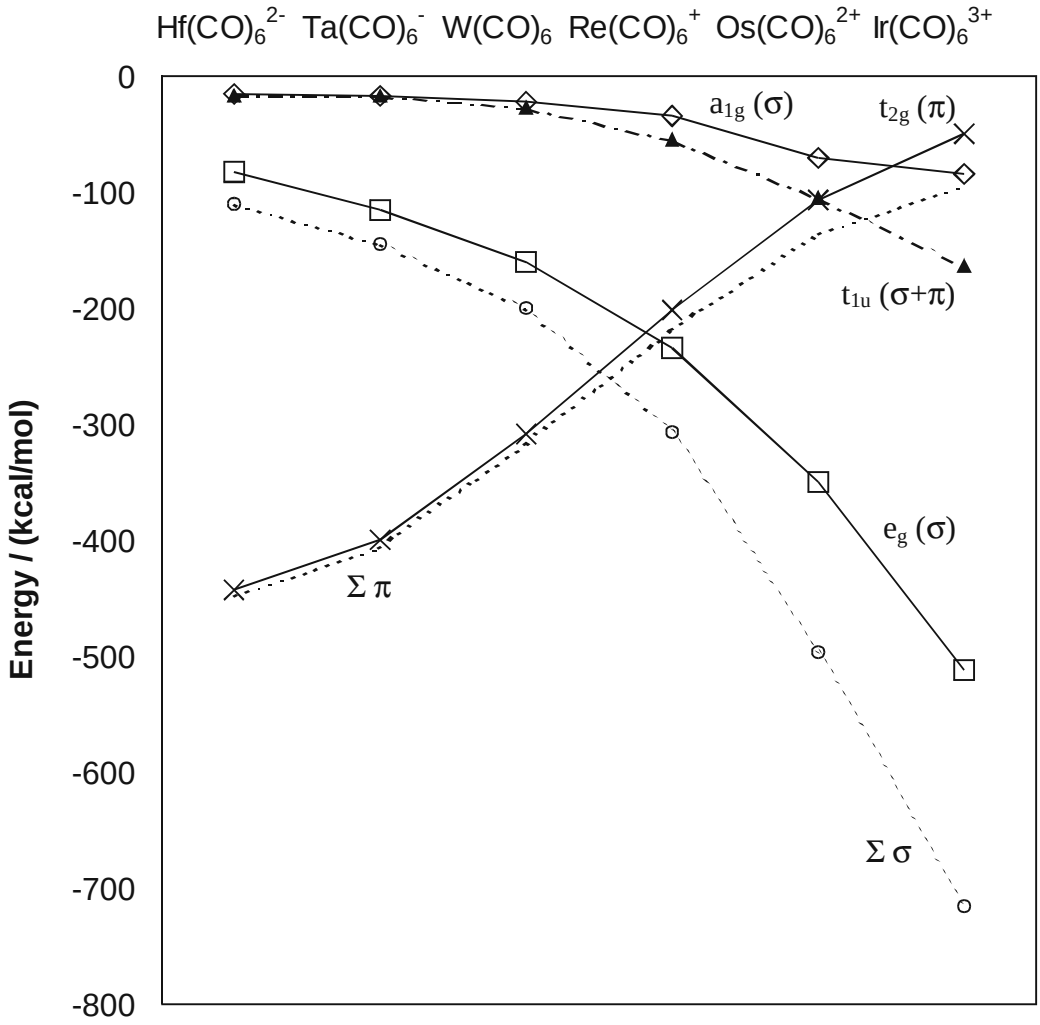

Figure 8. Trend of the contributions of the orbital interaction term ΔE_{oi} to the binding energy of TM^q-$(CO)_6$.

We also analyzed the changes in the electronic structure of the metal and the ligand cage by the bonding interactions. Table 3 shows that the calculated orbital overlaps $\langle TM^q|(CO)_6\rangle$ again do not correlate at all with the energy contributions. Thus, in the systems investigated here, the energy difference between the occupied and empty orbitals is much more important for the ΔE_{oi} value than the orbital overlap.

Table 4. Energy and Charge Contributions of a Single TM d, s, p Orbital to the OC→TM^q Donation[a]

		$Hf(CO)_6^{2-}$	$Ta(CO)_6^{-}$	$W(CO)_6$	$Re(CO)_6^{+}$	$Os(CO)_6^{2+}$	$Ir(CO)_6^{3+}$
Energy	d	-41.7	-56.5	-79.5	-116.9	-174.4	-260.3
Energy	s	-9.5	-10.5	-15.4	-27.4	-47.6	-78.8
Energy	p	-6.1	-5.7	-8.8	-18.0	-33.8	-55.8
Charge	d	0.41	0.55	0.66	0.73	0.83	0.91
Charge	s	0.16	0.19	0.24	0.33	0.41	0.50
Charge	p	0.07	0.07	0.09	0.12	0.15	0.20

[a] Energy values in kcal/mol, charge values in *e*.

3.3.4 Valence Orbitals of the Transition Metals

Figure 7 shows that the empty d(σ), s, and p valence orbitals of the metal receive electronic charge from the $(CO)_6$ ligand through orbitals having e_g, a_{1g} and t_{1u} symmetry. The respective energy terms may thus be used to estimate how important the metal orbitals are for the strength of the metal-ligand interactions.[37] The values given in Table 3 show for all metals the order $e_g >> t_{1u} > a_{1g}$. In order to relate this to the metal valence orbitals the degeneracy of the orbitals must be considered. There are two d orbitals, one s orbital and three p orbitals of the metal involved. This leads to the energy contributions by a single d, s, p metal orbital which are shown in Table 4. It becomes obvious that the relative importance of the TM valence orbitals is d >> s > p. The size of a single p orbital contribution to the ΔE_{oi} energy term is between 54% - 71% of the s orbital contribution. The metal d valence orbital is much more important energy wise than the s and p orbitals. However, the *total* contribution of the three p orbitals is larger than the contribution of the s orbital.

The valence orbital populations which are also shown in Table 3 indicate the charge exchange between the metal and the ligand cage. The orbital populations correlate nicely with the trend of the orbital interaction energies, similar as it was found before for the $(CO)_5TM^q$-CO systems. Table 4 also gives the contributions of the d(σ), s and p valence orbitals of the metals to the total $TM^q \leftarrow (CO)_6$ charge acceptance. The $2a_{1g}$ acceptor orbital of Hf^{2-}, which is the empty valence s orbital in the t_{2g}^6 state, receives only 0.16 electrons from $(CO)_6$ in $Hf(CO)_6^{2-}$, while 0.50 electrons are donated into the valence s orbital of Ir^{3+}. The $TM^q \leftarrow (CO)_6$ σ donation into the d(σ) orbitals of TM^q is significantly higher. The e_g donation in $Hf(CO)_6^{2-}$ is 0.41 electrons and it increases to 0.91 electrons in $Ir(CO)_6^{3+}$. Significantly smaller charge donations are found for the ligand donation into the metal p orbitals. The (t_{1u}) p orbital population of TM^q is between 0.07 electrons in $Hf(CO)_6^{2-}$ and 0.20 electrons in $Ir(CO)_6^{3+}$. However, these are the values for a single p orbital. The total $TM^q(p) \leftarrow (CO)_6$ donation into the three metal p orbitals is always larger than the $TM^q(s) \leftarrow (CO)_6$ donation. Thus, the breakdown of the charge and energy contributions of the d, s, p metal orbitals in $TM(CO)_6^q$ suggests that the p orbitals are as important as the s orbital and, therefore, should be considered as true valence orbitals.

3.4 Conclusions

The results of this chapter can be summarized as follows. The trend of the bond dissociation energies of $TM(CO)_6^q$ for loss of one CO follows a U-shaped curve from $Hf(CO)_6^{2-}$ to $Ir(CO)_6^{3+}$. The lowest BDE is calculated for $W(CO)_6$. The higher bond dissociation energies of the negatively charged hexacarbonyls $Hf(CO)_6^{2-}$ and $Ta(CO)_6^-$ compared with $W(CO)_6$ are caused by less Pauli repulsion and not by attractive orbital interactions. The increase of the $(CO)_5TM^q$-CO BDEs of the positively charged hexacarbonyls can be correlated with the stronger orbital interactions due to $TM^q \leftarrow CO$ σ-donation. There is a continuous decrease of the strength of the $(CO)_5TM^q \rightarrow CO$ π-backdonation and increase of the $(CO)_5TM^q \leftarrow CO$ σ-donation from $Hf(CO)_6^{2-}$ to

$Ir(CO)_6^{3+}$. The latter interaction dominates the orbital interaction term in the carbonyl cations. Electrostatic attraction and stabilizing orbital interaction have a similar strength in the $(CO)_5TM^q$-CO bonds. The calculated bond dissociation energies of $TM(CO)_6^q$ yielding TM^q in the t_{2g}^6 valence state and 6 CO also exhibit a U-shaped curve with $Re(CO)_6^+$ having the lowest BDE. The trend correlates with the calculated orbital interaction term ΔE_{oi}. Orbital interactions make the largest contributions to the bonding in the highly charged complex $Ir(CO)_6^{3+}$. This holds for the interactions between TM^q and $(CO)_6$ as well as for $(CO)_5TM^q$-CO. The breakdown of the ΔE_{oi} term into contributions by orbitals having different symmetry shows that the $TM^q \rightarrow (CO)_6$ π-donation is the most important contributor in $Hf(CO)_6^{2-}$, $Ta(CO)_6^-$ and $W(CO)_6$, while $TM^q \leftarrow (CO)_6$ σ-donation dominates the orbital interaction term in $Re(CO)_6^+$, $Os(CO)_6^{2+}$ and $Ir(CO)_6^{3+}$. The contribution of the three metal p orbitals to the energy terms and to the charge terms is slightly higher than the contribution of the s orbital. The metal p orbitals should thus be considered as valence orbitals for describing the bonding in the metal hexacarbonyls.

3.5 References

(1) Heitler, W.; London, F. *Z. Physik*, **1927**, *44*, 455.

(2) (a) Fukui, K. *Acc. Chem. Res.* **1971**, *4*, 57. (b) Fleming, I. *Frontier Orbitals and Organic Chemical Reactions*, Wiley, New York, 1976.

(3) Kutzelnigg, W. *Angew. Chem.* **1984**, *96*, 262; *Angew. Chem., Int. Ed. Engl.* **1984**, *23*, 272.

(4) (a) Schmidt, M.W.; Truong, P.N.; Gordon, M.S. *J. Am. Chem. Soc.* **1987**, *109*, 5217. (b) Jacobsen, H.; Ziegler, T. *J. Am. Chem. Soc.* **1994**, *116*, 3667.

(5) (a) Reed, A.; Schleyer, P.v.R. *J. Am. Chem. Soc.* **1990**, *112*, 1434. (b) Magnusson, E. *J. Am. Chem. Soc.* **1990**, *112*, 7940. (c) Cioslowski, J.; Mixon, S.T. *Inorg. Chem.* **1993**, *32*, 3209. (d) Cooper, D.L.; Cunningham, T.P.; Gerratt, J.; Karadakov, P.B.; Raimondi, M. *J. Am. Chem. Soc.* **1994**, *116*, 4414. (e) Häser, M.; *J. Am. Chem. Soc.* **1996**, *118*, 7311. (f) Dobado, J.A.; Martinez-Garcia, H.; Molina, J.M.; Sundberg, M.R. *J. Am. Chem. Soc.* **1998**, *120*, 8461.

(6) (a) Hoffmann, R.; Chen, M.M.L.; Thorn, D.L. *Inorg. Chem.* **1977**, *16*, 503. (b) Schilling, B.E.R.; Hoffmann, R. *J. Am. Chem. Soc.* **1979**, *101*, 3456. (c) Hoffmann, R. *Science* **1981**, *211*, 995. (d) Hoffmann, R.; Albright, T.A.; Thorn, D.L. *Pure Appl. Chem.* **1978**, *50*, 1. (e) Jean, Y.; Lledos, A.; Burdett, J.K.; Hoffmann, R. *J. Am. Chem. Soc.* **1988**, *110*, 4506. and further references cited therein.

(7) (a) Davidson, E.R.; Kunze, K.L.; Machado, F.B.C.; Chakravorty, S.J. *Acc. Chem. Res.* **1993**, *26*, 628. (b) Baerends, E.J.; Rozendaal, A. in *Quantum Chemistry: The Challenge of Transition Metals and Coordination Chemistry*, p. 159, Veillard A. (Ed), Proceedings of the NATO ASI, Reidel, Dordrecht, 1986.

(8) (a) Dewar, M.J.S.; *Bull. Soc. Chim. Fr.* **1951**, *18*, C79. (b) Chatt, J.; Duncanson, L.A. *J. Chem. Soc.* **1953**, 2929.

(9) Morokuma, K. *Acc. Chem. Res.* **1977**, *10*, 294.

(10) (a) Bauschlicher, C.W.; Bagus, P.S. *J. Chem. Phys.* **1984**, *81*, 5889. (b) Bauschlicher, C.W.; Petterson, L.G.M.; Siegbahn, P.E.M. *J. Chem. Phys.* **1987**, *87*, 2129. (c) Bauschlicher, C.W.; Langhoff, S.R.; Barnes, L.A. *Chem. Phys.* **1989**, *129*, 431. (d) Bauschlicher, C.W. *J. Chem. Phys.* **1986**, *84*, 260. (e) Bauschlicher, C.W.; Bagus, P.S.; Nelin, C.J.; Roos, B.O. *Chem. Phys.* **1986**, *85*, 354. (f) Barnes, L.A.; Rosi, M.; Bauschlicher, C.W. *J. Chem. Phys.* **1991**, *94*, 2031. (g) Barnes, L.A.; Rosi, M.; Bauschlicher, C.W. *J. Chem. Phys.* **1990,** *93*, 609. (h) Barnes, L.A.; Bauschlicher, C.W. *J. Chem. Phys.* **1989**, *91*, 314. (i) Blomberg, M.R.A.; Brandemark, U.B.; Siegbahn, P.E.M.; Wennerberg, J.; Bauschlicher, C.W. *J. Am. Chem. Soc.* **1988**, *110*, 6650. (j) Hall, M.B.; Fenske, R.F. *Inorg. Chem.* **1972**, *11*, 1620. (k) Sherwood, P.E.; Hall, M.B. *Inorg. Chem.* **1979**, *18*, 2325. (l) Sherwood, P.E.; Hall, M.B. *Inorg. Chem.* **1980**, *19*, 1805. (m)

Williamson, R.L.; Hall, M.B. *Int. J. Quantum Chem.* **1987**, *21S*, 503. (n) Hillier, I.H.; Saunders, V.R. *Mol. Phys.* **1971**, *23*, 1025. (o) Hillier; I.H.; Saunders, V.R. *J. Chem. Soc., Chem. Commun.* **1971**, 642. (p) Ford, P.C.; Hillier, I.H. *J. Chem. Phys.* **1984**, *80*, 5664. (q) Ford, P.C.; Hillier, I.H.; Pope, S.A.; Guest, M.F. *Chem. Phys. Lett.* **1983**, *102*, 555. (r) Cooper, G.; Green, J.C.; Payne, M.P.; Dobson, B.R.; Hillier, I. H. *Chem. Phys. Lett.* **1986**, *125*, 97. (s) Cooper, G.; Green, J.C.; Payne, M.P.; Dobson, B.R.; Hillier, I.H.; Vincent, M.; Rosi, M. *J. Chem. Soc., Chem. Commun.* **1986**, 438. (t) Moncrieff, D.; Ford, P.C.; Hillier, I.H.; Saunders, V.R. *J. Chem. Soc., Chem. Commun.* **1983**, 1108. (u) Smith, S.; Hillier, I.H.; von Niessen, W.; Guest, M.C. *Chem. Phys.* **1989**, *135*, 357. (v) Vanquickenborne, L.G.; Verhulst, J. *J. Am. Chem. Soc.* **1987**, *109*, 4825. (w) Pierfoot, K.; Verhulst, J.; Verbeke, P.; Vanquickenborne, L.G. *Inorg. Chem.* **1989**, *28*, 3059. (x) Yamamoto, S.; Kashiwagi, H. *Chem. Phys. Lett.* **1993**, *205*, 306. (y) Blomberg, M.R.A.; Siegbahn, P.E.M.; Lee, T. L.; Rendell, A.P.; Rice, J.E. *J. Chem. Phys.* **191**, *95*, 5898.

(11) (a) Ziegler, T.; Rauk, A. *Theor. Chim. Acta* **1977**, *46*, 1. (b) Ziegler, T.; Rauk, A. *Inorg. Chem.* **1979**, *18*, 1558. (c) Ziegler, T.; Rauk, A. *Inorg. Chem.* **1979**, *18*, 1755.

(12) Ehlers, A.W.; Ruiz-Molares, Y.; Baerends, E.J.; Ziegler, T. *Inorg. Chem.* **1997**, *36*, 5031.

(13) Selected examples: (a) Jacobsen, H.; Ziegler, T. *Organometallics* **1995**, *14*, 224. (b) Jacobsen, H.; Ziegler, T. *Inorg. Chem.* **1996**, *35*, 775. (c) Li, J.; Schreckenbach, G.; Ziegler, T. *J. Am. Chem. Soc.* **1995**, *117*, 486. (d) Ehlers, A.W.; Baerends, E.J.; Bickelhaupt, F.M.; Radius, U. *Chem. Eur. J.* **1998**, *4*, 210.

(14) (a) Strauss, S.H. *Chemtracts: Inorg. Chem.* **1997**, *10*, 77. (b) Willner, H.; Aubke, F. *Angew. Chem.* **1997**, *109*, 2506. *Angew. Chem., Int. Ed. Engl.* **1997**, 2402.

(15) (a) Mavridis, A.; Harrison, J.F.; Allison, J. *J. Am. Chem. Soc.* **1989**, *111*, 2482. (b) Allison, J.; Mavridis, A.; Harrison, J.F. *Polyhedron* **1988**, *7*, 1559. (c) Barnes, L.A.; Rosi, M.; Bauschlicher, C.W. *J. Chem. Phys.* **1990**, *93*, 609 (d) Bauschlicher, C.W.; Barnes, L.A. *Chem. Phys.* **1988**, 124, 383. (e) Büker, H.J.; Maitre, P.; Ohanessian, G. *J. Phys. Chem. A* **1997**, *101*, 3966. (f) Lupinetti, A.J.; Jonas, V.; Thiel, W.; Strauss, S.H.; Frenking, G. *Chem. Eur. J.*, in print. (g) Veldkamp, A.; Frenking, G. *Organometallics* **1993**, *12*, 4613. (h) Lupinetti, A.J.; Fau, S.; Frenking, G.; Strauss, S.H. *J. Phys. Chem. A* **1997**, *101*, 9551.

(16) Szilagyi, R.K.; Frenking, G. *Organometallics* **1997**, *16*, 4807.

(17) Lupinetti, A.J.; Frenking, G.; Strauss, S.H. *Angew. Chem.* **1998**, *110*, 2229; *Angew. Chem., Int. Ed. Engl.* **1998**, *37*, 2113.

(18) Dapprich, S.; Frenking, G. *J. Phys. Chem.* **1995**, *99*, 9352.

(19) (a) Landis, C.R.; Cleveland, T.; Firman, T.K. *J. Am. Chem. Soc.* **1995**, *117*, 1859. (b) Landis, C.R.; Firman, T.K.; Root, D.M.; Cleveland, T. *J. Am. Chem. Soc.* **1998**, *120*, 1842. (c) Landis, C.R.; Cleveland, T.; Firman, T.K. *J. Am. Chem. Soc.* **1998**, *120*, 2641. (d) Firman, T.K.; Landis, C.R. *J. Am. Chem. Soc.* **1998**, *120*, 12650.

(20) Bayse, C.A.; Hall, M.B. *J. Am. Chem. Soc.* **1999**, *121*, 1348.

(21) Becke, A.D. *Phys. Rev. A* **1988**, *38*, 3098.

(22) Perdew, J.P. *Phys. Rev. B* **1986**, *33*, 8822.

(23) (a) Chang, C.; Pelissier, M.; Durand, Ph. *Phys. Scr.* **1986**, *34*, 394. (b) Heully, J.-L.; Lindgren, I.; Lindroth, E.; Lundquist, S.; Martensson-Pendrill, A.-M. *J. Phys. B* **1986**, *19*, 2799. (c) van Lenthe, E.; Baerends, E.J.; Snijders, J.G. *J. Chem. Phys.* **1993**, *99*, 4597. (d) van Lenthe, E.; Baerends, E.J.; Snijders, J.G. *J. Chem. Phys.* **1996**, *105*, 6505. (c) van Lenthe, E.; van Leeuwen, R.; Baerends, E.J.; Snijders, J.G. *Int. J. Quantum Chem.* **1996**, *57*, 281.

(24) Snijders, J.G.; Baerends, E.J.; Vernooijs, P. *At. Nucl. Data Tables* **1982**, *26*, 483.7

(25) Baerends, E.J.; Ellis, D.E.; Ros, P. *Chem. Phys.* **1973**, *2*, 41.

(26) Krijn, J.; Baerends, E.J. *Fit Functions in the HFS-Method*, Internal Report (in dutch), Vrije Universiteit Amsterdam, The Netherlands, 1984.

(27) Hirshfeld, E.L. *Theor. Chim. Acta* **1977**, *44*, 129.

(28) (a) C. Fonseca Guerra, J. G. Snijders, G. te Velde, E. J. Baerends *Theor. Chem. Acc.* **1998**, *99*, 391. (b) Bickelhaupt, F.M.; Baerends, E.J. *Rev. Comput. Chem.*, Vol. 15, in print.

(29) It has become customary to add the values of ΔE_{Pauli} and ΔV_{elst} into a common term ΔE^0 (which is sometimes called steric term).[12,13] The bonding analysis is then often carried out in terms of the ΔE^0 and ΔE_{oi} values, which give a bonding model where the attractive orbital interaction term ΔE_{oi} and the ΔE^0 term are compared with the total interaction energy ΔE_{int}. Such a partitioning of the bonding energy often supports the common MO bonding model where the dominant contributions to the chemical bond arise from the interactions between particular orbitals such as the HOMO and LUMO.[2] However, the addition of ΔE_{Pauli} and ΔV_{elst} into a single term ΔE^0 is arbitrary and deceptive, because the contribution of the electrostatic forces to the bonding interactions is not obvious anymore. We decided to discuss the values for the three contributions ΔE_{Pauli}, ΔV_{elst} and ΔE_{oi} to the bond energy separately and to compare the trend of the three terms with the net bonding energies. This leads to an unbiased conclusion about the factors which are responsible for the U-shaped curves of the bonding energies. The separate presentation of the values of ΔV_{elst} and ΔE_{oi} makes it also possible to estimate the electrostatic and covalent contributions to the metal-CO bonding interactions.

(30) Lewis, K. E.; Golden, D. M.; Smith, G. P. *J. Am. Chem. Soc.* **1984**, *106*, 3905.

(31) (a) Ellis, J.E.; Chi, K.-M. *J. Am. Chem. Soc.* **1990**, *112*, 6022. (b) Siebert, H. *Anwendungen der Schwingungsspektroskopie in der anorganischen Chemie*, Springer, Berlin, 1966. (c) Jones, L.H.; McDowell, R.S.; Goldblatt, M. *Inorg. Chem.* **1969**, *8*, 2349. (d) Abel, E.W.; McLean, R.A.N.; Tyfield, S.P.; Braterman, P.S.; Walker, A.P.; Hendra, P.J. *J. Mol. Spectrosc.* **1969**, *30*, 29. (e) Wang, C.; Bley, B.; Balzer-Jöllenbeck, G.; Lewis, A.R.; Siu, S.C.; Willner, H.; Aubke, F. *J.*

Chem. Soc., Chem. Commun. **1995**, 2071. (f) Bach, C.; Willner, H.; Wang, C.; Rettig, S.J.; Trotter, J.; Aubke, F. *Angew. Chem.* **1996**, *108*, 2104; *Angew. Chem. Int Ed. Engl.* **1996**, *35*, 1974.

(32) Jonas, V.; Thiel, W. *Organometallics* **1998**, *17*, 353.

(33) Elschenbroich, Ch.; Salzer, A. *Organometallics*, Second Edition, VCH, Weinheim, 1992.

(34) We think that the approximation is justified, because we make a comparison within one system and for orbitals which have the same symmetry. The approximation yields an estimate of the π contribution via t_{1u} donation which is probably too high, because the $3t_{1u}(\pi)$ orbital is lower in energy (-11.684 eV) than the $4t_{1u}(\sigma)$ orbital of $(CO)_6$ (-9.060 eV). Thus, the calculated data can be considered as an upper bound for the TM←CO π-donation.

(35) Lupinetti, A.J.; Fau, S.; Frenking, G.; Strauss, S.H. *J. Phys. Chem. A* **1997**, *101*, 9551.

(36) Goldman, A.S.; Krogh-Jespersen, K. *J. Am. Chem. Soc.* **1996**, *118*, 12159.

(37) Please note that the orbital relaxation step gives the contributions by all s and p orbitals of the metal and not only the valence orbitals. However, the dominant contributions should come from the valence orbitals.

(38) (a) Arnesen, S.V.; Seip, H.M. *Acta Chem. Scand.* **1966**, *20*, 2711. (b) Calderazzo, F.; Englert, U.; Pampaloni, G.; Pelizzi, G.; Zamboni, R. *Inorg. Chem.* **1983**, *22*, 1865. (c) Bruce, D.M.; Holloway, J.H.; Russel, D.R.*; J. Chem. Soc., Dalton Trans.* **1978**, 1627. (d) Holloway, J.H.; Senior, J.B.; Szary, A.C. *J. Chem. Soc., Dalton Trans.* **1987**, 741.

4 Relativistic Effects in Metal-Catalyzed Bond Activation

This chapter will be published as:

Axel Diefenbach and F. Matthias Bickelhaupt: »Oxidative Addition of Pd to C–H, C–C and C–Cl Bonds. Importance of Relativistic Effects in DFT Calculations«

Abstract

To assess the importance of relativistic effects for the quantum chemical description of oxidative addition reactions of palladium to C–H, C–C and C–Cl bonds, we have carried out a systematic study of the corresponding reactions of CH_4, C_2H_6 and CH_3Cl with Pd-d^{10} using nonrelativistic (NR), quasirelativistic (QR), and zeroth-order regular approximated (ZORA) relativistic density functional theory (DFT) at the BP86/TZ(2)P level. Relativistic effects are important according to both QR and ZORA, the former yielding similar but somewhat more pronounced effects than the latter, more reliable method: activation barriers are reduced by 6 - 14 kcal/mol and reaction enthalpies become 15 - 20 kcal/mol more exothermic if one goes from NR to ZORA. This yields, for example, 298 K activation enthalpies $\Delta H^{\neq}_{298}$ of -5.0 (C–H), 9.6 (C–C) and -6.0 kcal/mol (C–Cl) at ZORA-BP86/TZ(2)P. In accordance with gas-phase experiments on reactions of Pd with alkanes, we find reaction profiles with pronounced potential wells for reactant complexes (collisionally stabilized and observed in experiments for alkanes larger than CH_4) at -11.4 (CH_4), -11.6 (C_2H_6) and -15.6 kcal/mol (CH_3Cl) relative to separated reactants (ZORA-BP86/TZ(2)P). Furthermore, we analyze the height of and the relativistic effects on the activation energies $\Delta E^{\neq}$ in terms of the activation strain $\Delta E^{\neq}_{strain}$ of and the transition-state interaction $\Delta E^{\neq}_{int}$ between the reactants in the activated complex, with $\Delta E^{\neq} = \Delta E^{\neq}_{strain} + \Delta E^{\neq}_{int}$.

4.1 Introduction

Oxidative addition and reductive elimination (eq 1) are ubiquitous in homogeneous catalysis[1] and have been the subject of many experimental[2-6] and theoretical[7-12] studies.

$$ML_n + R{-}X \underset{\text{Reductive Elimination}}{\overset{\text{Oxidative Addition}}{\rightleftharpoons}} R{-}ML_n{-}X \qquad (1)$$

These studies can basically be divided into two groups associated with two different approaches: (i) the experimental or theoretical investigation of particular transition metal complexes (with more or less realistic model systems in the latter case),[1-5,8,9] and (ii) the investigation of the intrinsic reactivity of metal ions or atoms in the absence of ligands or solvent molecules.[4-7,10,11] Experimentally, the latter is realized by mass spectrometric (metal ions)[3-5] and spectroscopic (neutral metal atoms)[6-7] techniques. Theoretical studies[10,11] play a key role in this approach because they allow for examining model reactions that are experimentally difficult to realize (or even inaccessible) and yet essential for unraveling a particular problem and achieving profound understanding.

We are interested in the prototypical processes of C–H, C–C and C–Cl bond activation. Whereas on the long term we aim at understanding and directing, on the basis of quantum chemical analyses, the factors that determine the catalytic activity of the corresponding transition metal *complexes*, our starting point is the investigation of the *intrinsic* reactivity of the transition metal *atom*. This enables us, in later stages, to precisely assess how ligands interfere with the metal electronic structure and how they exactly affect the activity and selectivity of the resulting homogeneous catalyst. Thus, recently, we have studied the oxidative addition of Pd + CH_3Cl using nonrelativistic density functional theory (DFT) at the BP86//LDA level.[10] It was shown that the palladium atom has an intrinsic preference for direct oxidative insertion into the C–Cl

bond (eq 2, OxIn), unlike transition metal complexes such as, e.g., $[Rh(CO)_2I_2]^-$ and $[Rh(CO)_2I_3]^{2-}$ that undergo oxidative addition to CH_3I via an S_N2 pathway.[2p-r] For palladium, this competing nucleophilic substitution mechanism (eq 2, S_N2) was found to have an activation energy that is 31 kcal/mol higher than direct oxidative insertion (eq 2, OxIn).

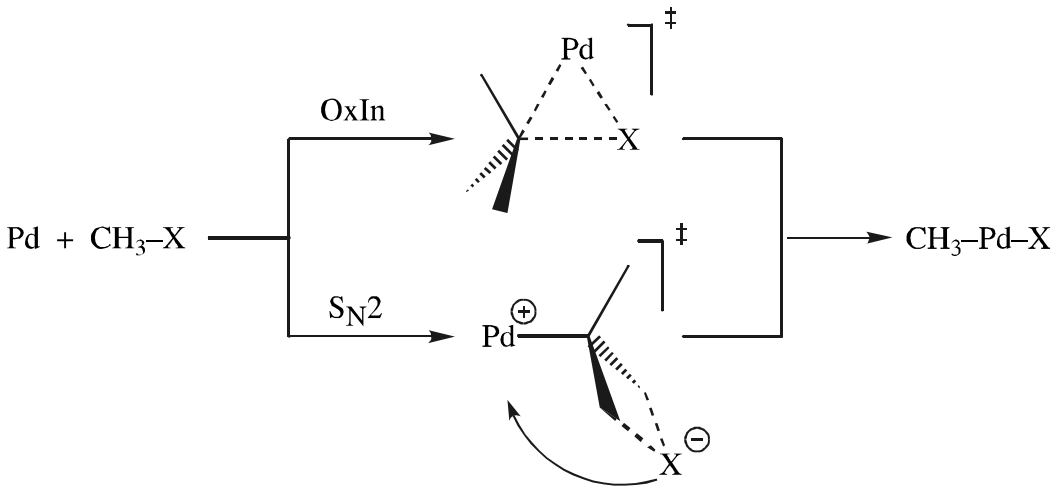

(2)

In the present paper, we extend our previous work in three ways: (i) relativistic effects are incorporated into the theoretical treatment, (ii) the DFT computations are brought to a higher level of theory, and (iii) the set of model substrates is extended to cover the processes of C–H and C–C in addition to C–Cl bond activation thus describing all three insertion reactions consistently at the same level of theory. The main purpose is to assess the importance of relativistic effects[12] in density functional theoretical (DFT)[13,14] studies on oxidative addition and to provide a sound basis for further theoretical studies on homogeneous catalysis.[15] Thus, we have carried out a systematic investigation on the oxidative insertion of Pd-d[10] into the C–H, C–C and C–Cl bonds of CH_4, C_2H_6 and CH_3Cl, respectively, using nonrelativistic (NR), quasirelativistic (QR), and zeroth-order regular approximated (ZORA) relativistic density functional theory (DFT) at the BP86/TZ(2)P level (see Section 2). The difference in activation energies $\Delta E^{\neq}$ between the different oxidative addition reactions is interpreted and discussed in terms of the activation strain $\Delta E^{\neq}_{strain}$ of and the transition-state interaction $\Delta E^{\neq}_{int}$ between the reactants in the activated complex, where $\Delta E^{\neq} = \Delta E^{\neq}_{strain} + \Delta E^{\neq}_{int}$ (cf.

Activation strain-TS interaction model[10a]). In particular, we discuss how relativity affects these barrier heights and the geometries of the corresponding transition states (see Section 3).

4.2 Methods

4.2.1 General procedure

All calculations were performed using the Amsterdam Density Functional (ADF) program.[16] The numerical integration was performed using the procedure developed by Boerrigter, te Velde, and Baerends.[16f,g] The MOs were expanded in a large uncontracted set of Slater type orbitals (STOs) containing diffuse functions: TZ(2)P.[16h] The TZ(2)P basis is of triple-ζ quality for all atoms and has been augmented with two sets of polarization functions on maingroup atoms (3d and 4f on C and Cl; 2p and 3d on H) and an extra set of 5p functions on palladium. The core shells of carbon (1s), chlorine (1s2s2p) and palladium (1s2s2p3s3p3d) were treated by the frozen-core (FC) approximation.[16b] An auxiliary set of s, p, d, f and g STOs was used to fit the molecular density and to represent the Coulomb and exchange potentials accurately in each SCF cycle.[16i]

Energies and geometries were calculated at the nonlocal BP86 level of theory: exchange is described by Slater's Xα potential[16j] with $\alpha = \frac{2}{3}$ with nonlocal corrections due to Becke[16k,l] and correlation is treated in the Vosko-Wilk-Nusair (VWN, formula V) parameterization[16m] with nonlocal corrections due to Perdew[16n] added self-consistently.[16o] Geometries were fully optimized using analytical gradient techniques.[16p] Frequencies[16q] were calculated by numerical differentiation of the analytical energy gradients. Transition state structures[16r] were optimized using Simons' algorithm[16s] in the implementation of Baker.[16t]

Bond enthalpies at 298.15 K and 1 atmosphere (ΔH_{298}) were calculated from 0 K electronic bond energies (ΔE) according to eq 3, assuming an ideal gas.[17]

$$\Delta H_{298} = \Delta E + \Delta E_{\text{trans},298} + \Delta E_{\text{rot},298} + \Delta E_{\text{vib},0} + \Delta(\Delta E_{\text{vib},0})_{298} + \Delta(pV) \quad (3)$$

Here, $\Delta E_{\text{trans},298}$, $\Delta E_{\text{rot},298}$ and $\Delta E_{\text{vib},0}$ are the differences between products and reactants in translational, rotational and zero point vibrational energy, respectively; $\Delta(\Delta E_{\text{vib}})_{298}$ is the change in the vibrational energy difference as one goes from 0 to 298.15 K. The vibrational energy corrections are based on our frequency calculations. The molar work term $\Delta(pV)$ is $(\Delta n)RT$; $\Delta n = -1$ for two reactants (Pd and CH_3X) combining to one species. Thermal corrections for the electronic energy are neglected.

4.2.2 Relativistic Effects

Relativistic effects were treated using two different approaches: (i) the quasirelativistic (QR) formalism,[18,19] and (ii) the zeroth-order regular approximation (ZORA).[20]

The quasirelativistic (QR) formalism[18] proceeds from a first-order perturbation approach based on the Pauli Hamiltonian H^{Pauli} (eq 4, in atomic units).[19] The latter is obtained from the Dirac Hamiltonian by the procedure of elimination of the small components, followed by an expansion, up to first order, of the resulting operator in $(E - V)/2c^2$ and some manipulations.

$$H^{Pauli} = V + \frac{p^2}{2} - \frac{p^4}{8c^2} + \frac{\Delta V}{8c^2} + \frac{1}{4c^2}\vec{\sigma}\cdot(\vec{\nabla}V \times \vec{p}) \quad (4)$$

The first two terms of H^{Pauli} (the potential V and kinetic energy operator $p^2/2$) represent the nonrelativistic Hamiltonian and, in fact, correspond to an expansion up to only zeroth-order. The last three terms can be conceived as a first-order relativistic perturbation, consisting of the so-called mass-velocity term $p^4/8c^2$(a correction to the kinetic energy associated with the relativistic increase of the electron's mass), the Darwin term $\Delta V/8c^2$ (a correction to the effective potential associated with the so-called *Zitterbewegung* of the electron), and the spin-orbit operator (which couples electron

spin and orbital momenta). In the present study, only scalar relativistic effects are considered, i.e., the spin-orbit term is not included. In the QR approach, the relativistic energy correction is obtained through diagonalizing the first-order relativistic operator (i.e., the relativistic terms in H^{Pauli}) in the space of zeroth-order solutions (i.e., the nonrelativistic MOs). This turns out to improve results significantly over a simple first-order perturbation treatment. Nevertheless, the QR treatment suffers from a series of problems (see Ref. 20). For example, the expansion used to obtain the Pauli Hamiltonian is invalid for particles in Coulomb potentials because the corresponding (nonrelativistic) eigenstates have components of high momentum near the nuclei, as a result of which the condition $(E - V)/2c^2 << 1$ is not satisfied). Another serious problem is that H^{Pauli} is unbound from below which, in principal, implies a core-collapse of the valence MOs. In practice, this collapse is in most but not all cases prevented merely by the absence of the highly compact components in the valence basis set that would be necessary for describing the corresponding solutions, i.e., the collapsed MOs.

Most of the problems associated with the Pauli Hamiltonian and the QR approach can be solved[20] if the Hamiltonian resulting from elimination of the small components is expanded in $1/(2c^2 - V)$ instead of $(E - V)/2c^2$. To zeroth-order, this leads to the ZORA Hamiltonian (eq 5, in atomic units).

$$H^{ZORA} = \vec{\sigma} \cdot \vec{p} \frac{c^2}{2c^2 - V} \vec{\sigma} \cdot \vec{p} + V \tag{5}$$

In the present study, the performance of the QR and the more reliable ZORA approaches are compared with each other and with the nonrelativistic (NR) DFT results.

4.2.3 Analysis of Activation Barriers

The bonding in transition states for oxidative insertion was analyzed in the conceptual framework provided by the Kohn-Sham molecular orbital (KS-MO) model[14] to gain insight into how the activation barriers of the different oxidative insertion reactions

arise and how they are influenced by relativity. This is done using the Activation-strain TS-interaction (ATS) model of chemical reactivity[10a] in which the activation energy $\Delta E^{\neq}$ is decomposed into the activation strain and the transition state interaction $\Delta E^{\neq}_{\text{int}}$ (eq 6):

$$\Delta E^{\neq} = \Delta E^{\neq}_{\text{strain}} + \Delta E^{\neq}_{\text{int}} \tag{6}$$

The activation strain $\Delta E^{\neq}_{\text{strain}}$ is the strain energy associated with deforming the reactants from their equilibrium geometry to the geometry they acquire in the activated complex. The TS-interaction $\Delta E^{\neq}_{\text{int}}$ is the actual interaction energy between the deformed reactants in the transition state. In the present study, one of the reactants is the Pd-d^{10} atom and the other reactant is one of the organic substrates CH_4, C_2H_6, and CH_3Cl.

Next, the extended transition state (ETS) method[21] developed by Ziegler and Rauk is used to further decompose the TS interaction $\Delta E^{\neq}_{\text{int}}$ between the strained reactants into three physically meaningful terms (eq 7).

$$\Delta E^{\neq}_{\text{int}} = \Delta V_{\text{elst}} + \Delta E_{\text{Pauli}} + \Delta E_{\text{oi}} \tag{7}$$

The term ΔV_{elst} corresponds to the classical electrostatic interaction between the unperturbed charge distributions of the deformed reactants and is usually attractive. The Pauli-repulsion ΔE_{Pauli} comprises the destabilizing interactions between occupied orbitals and is responsible for the steric repulsion. The orbital interaction ΔE_{oi} accounts for charge transfer (interaction between occupied orbitals on one moiety with unoccupied orbitals of the other, including the HOMO–LUMO interactions) and polarization (empty–occupied orbital mixing on one fragment due to the presence of another fragment).

4.3 Results and Discussion

4.3.1 Relativistic Effects on Potential Energy Surfaces and Structures

In this section, we examine the potential energy surfaces (PES) for the various oxidative insertion (OxIn) reactions of Pd + CH_3X using nonrelativistic (NR), quasirelativistic (QR) and ZORA relativistic DFT at the BP86/TZ(2)P level of theory (see Scheme 1, X = H, CH_3, C). Our results are summarized in Tables 1 (enthalpies) and 2 (energies), and in Figures 1 (geometries) and 2 (reaction profiles).

Each of the three oxidative addition reactions proceed from the reactants (R) by first forming a reactant complex (RC) which leads, via insertion of the metal atom into the C–X bond, to the transition state (TS) and, finally, the product (P; see Scheme 1 and Figure 1). The effect of relativity according to both the QR and ZORA approach is that stationary points along the reaction coordinate are stabilized with respect to the

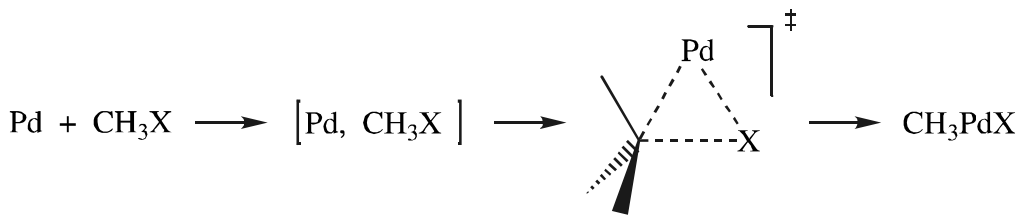

a	**b**	**c**	**d**
R	RC	TS	P
(reactants)	(reactant complex)		(product)

X =	H	**1a - 1d**
	CH_3	**2a - 2d**
	Cl	**3a - 3d**

Scheme 1. Model Systems and Nomenclature

Table 1. Reaction Profiles at BP86/TZ(2)P without and with Relativistic Effects for the Oxidative Insertion of Pd into the C–H, C–C, and C–Cl Bonds of CH_4, C_2H_6 and CH_3Cl, respectively: 298 K Enthalpies (in kcal/mol) Relative to Reactants and Geometry Parameters (in Å, degrees).[a]

	Pd + CH_4 (**1**)			Pd + C_2H_6 (**2**)			Pd + CH_3Cl (**3**)		
	RC	TS	P	RC	TS	P	RC	TS	P
Relative Enthalpies									
NR	-6.2	9.2	8.7	-6.1	20.6	5.7	-9.2	-0.4	-20.4
QR	-12.6	-7.6	-13.3	-12.5	7.4	-17.2	-15.5	-7.2	-38.2
ZORA	-11.4	-5.0	-9.7	-11.6	9.6	-14.1	-15.6	-6.0	-35.7
C–X									
NR	1.127	1.712	2.466	1.529	1.997	3.193	1.827	1.969	3.300
QR	1.146	1.484	2.530	1.528	1.879	3.197	1.838	1.919	3.367
ZORA	1.134	1.613	2.412	1.531	1.929	3.002	1.835	1.968	3.169
C–Pd									
NR	2.347	2.067	2.016	3.429	2.118	2.022	3.365	2.364	2.008
QR	2.194	2.055	1.976	3.307	2.085	1.981	3.251	2.573	1.974
ZORA	2.298	2.073	2.000	3.417	2.122	2.001	3.463	2.363	1.987
X–Pd									
NR	1.981	1.558	1.546	2.367	2.118	2.020	2.355	2.433	2.258
QR	1.875	1.552	1.517	2.210	2.085	1.980	2.242	2.314	2.211
ZORA	1.949	1.553	1.527	2.319	2.122	2.001	2.285	2.428	2.227
∠C-Pd-X									
NR	28.6	54.2	86.6	22.3	56.2	102.1	31.4	48.4	101.2
QR	31.5	46.0	91.8	22.7	53.6	107.6	33.1	45.9	107.0
ZORA	29.5	50.3	85.2	21.8	54.1	97.2	29.0	48.5	97.4
React. Coordinate[b]									
NR	0.02	0.45	1.00	0.00	0.28	1.00	0.01	0.11	1.00
QR	0.04	0.27	1.00	0.00	0.21	1.00	0.02	0.07	1.00
ZORA	0.03	0.39	1.00	0.00	0.27	1.00	0.02	0.12	1.00

[a] NR = nonrelativistic, QR = quasirelativistic, ZORA = zeroth-order regular approximation (Section 2.2). RC = reactant complex, TS = transition state, P = product (Scheme 1 and Figure 1).

[b] Reaction Coordinate = $[(C–X) – (C–X)_R] / [(C–X)_P – (C–X)_R]$ with (C–X), $(C–X)_R$ and $(C–X)_P$ the C–X bond length in a particular stationary point, in the reactants (i.e. isolated substrate) and in the product, respectively.

Table 2. Reaction Profiles Obtained with Different Methods for the Oxidative Insertion of Pd into the C–H, C–C, and C–Cl Bonds of CH_4, C_2H_6 and CH_3Cl, respectively: Zero-Kelvin Electronic Energies ΔE (in kcal/mol) Relative to Reactants (see also Figure 2) and ZPE-corrected Energies $\Delta E + \Delta ZPE$ in Parentheses.[a]

Reactants	Methods	RC		TS		P		Reference
Pd + CH_4	NR-BP86	–5.6	(–5.6)	12.6	(9.9)	11.3	(9.3)	this work
(**1**)	QR-BP86	–11.4	(–11.9)	–4.5	(–6.9)	–11.0	(–12.6)	this work
	ZORA-BP86	–10.5	(–10.8)	–1.6	(–4.2)	–7.1	(–9.1)	this work
	PCI-80//HF [b]		(–5.1)		(3.6)		(–2.3)	7b
	MCPF//HF [c]	–4		16		9		11j
	CCI+Q//CASSCF [d]	–		15.4		9.1		11l
	CCI+Q//CASSCF [e]	–		25.1		17.6		11l
	GVB-RCI [f]	–		30.5		20.1		11n,o
Pd + C_2H_6	NR-BP86	–5.4	(–5.7)	23.4	(21.1)	8.1	(5.6)	this work
(**2**)	QR-BP86	–11.3	(–12.0)	10.5	(8.2)	–15.0	(–17.2)	this work
	ZORA-BP86	–10.5	(–11.1)	12.5	(10.2)	–11.8	(–14.1)	this work
	PCI-80//HF [b]		(–6.6)		(19.5)		(–5.5)	7b
	CCI+Q//CASSCF [d]	–		31.5		7.5		11l
	CCI+Q//CASSCF [e]	–		39.2		19.7		11l
	GVB-RCI [f]	–		38.6		16.0		11n,o
Pd + CH_3Cl	NR-BP86	–9.5	(–9.2)	1.2	(0.1)	–19.4	(–20.3)	this work
(**3**)	QR-BP86	–15.8	(–15.2)	–6.1	(–6.7)	–37.2	(–38.0)	this work
	ZORA-BP86	–15.8	(–15.4)	–4.3	(–5.6)	–34.8	(–35.6)	this work
	BP86//LDA [g]	–9.9		1.7		–7.7		10b
	LDA [g]	–23.0		–16.1		–25.3		10b

[a] NR = nonrelativistic, QR = quasirelativistic, ZORA = zeroth-order regular approximation (Section 2.2). RC = reactant complex, TS = transition state, P = product (see Scheme 1 and Figure 1).

[b] ZPE corrections included. Scalar relativistic effects from first-order perturbation theory.

[c] Scalar relativistic effects from first-order perturbation theory.

[d] Scalar relativistic effects from first-order perturbation theory. CCI+Q refers to multireference externally contracted coupled cluster + Davidson correction.

[e] Same procedure as d, except for a smaller basis set.

[f] Relativistic ECPs.

[g] Nonrelativistic and with a smaller basis than in the present work.

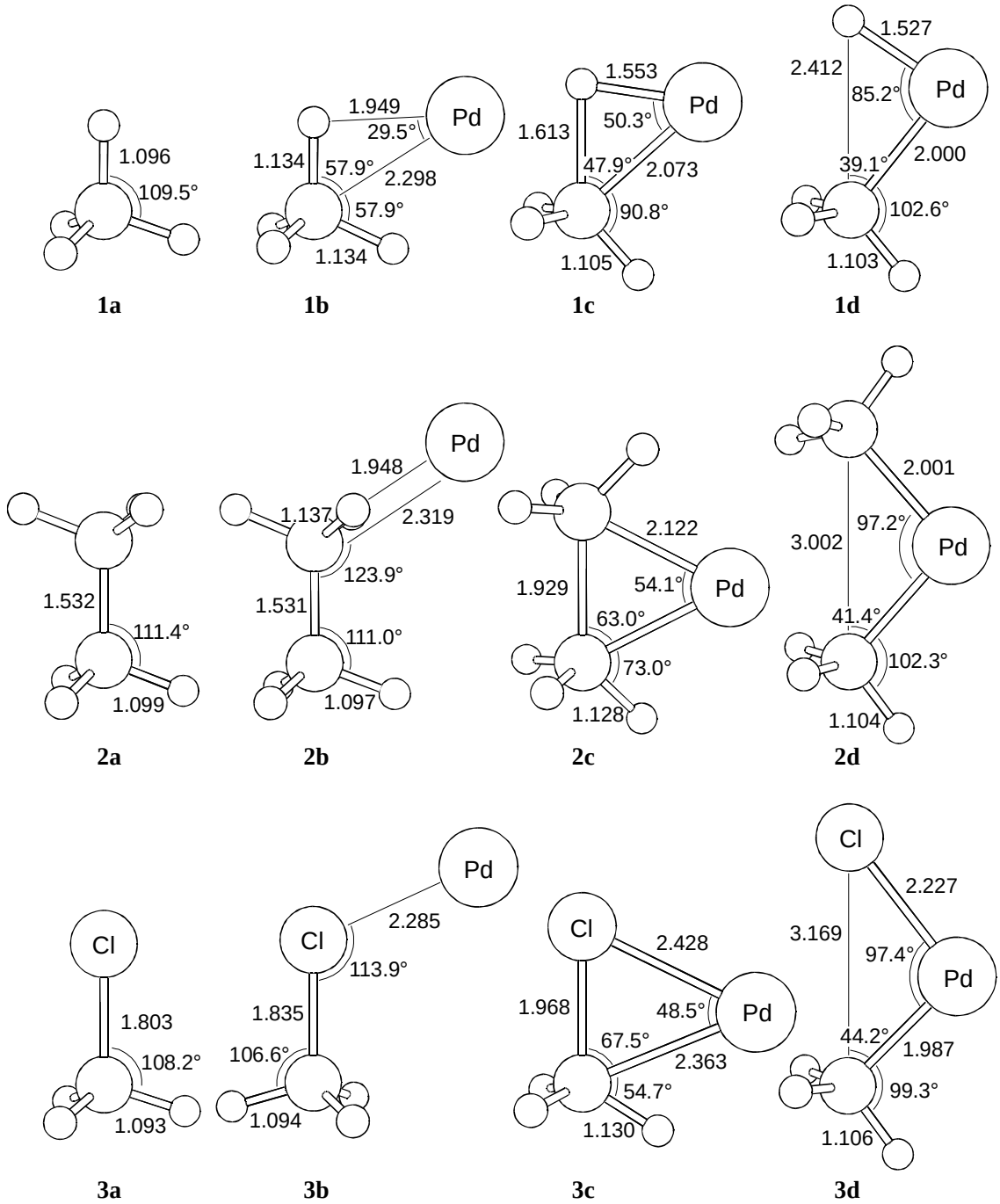

Figure 1. Geometries (in Å, degrees) of stationary points along the potential energy surface for oxidative insertion (OxIn) of Pd into the C–H, C–C and C–Cl bonds of CH_4 (**1a - 1d**), C_2H_6 (**2a - 2d**) and CH_3Cl (**3a - 3d**) at ZORA-BP86/TZ(2)P. See also Scheme 1.

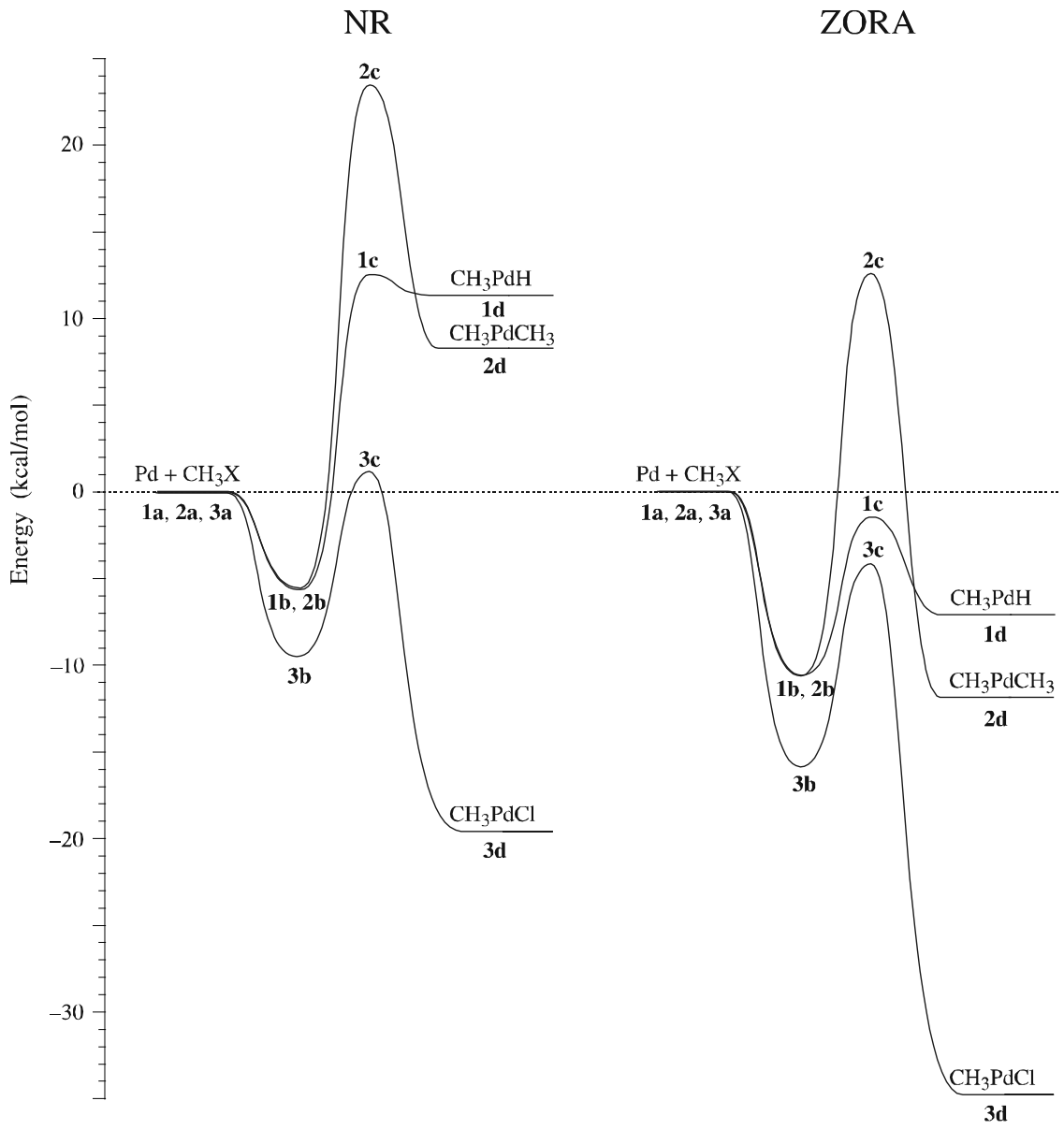

Figure 2. Relative zero-Kelvin electronic energies (in kcal/mol) of stationary points along the potential energy surface for oxidative insertion (OxIn) of Pd into the C–H, C–C and C–Cl bonds of CH_4 (**1**), C_2H_6 (**2**) and CH_3Cl (**3**) at nonrelativistic (NR, left) and ZORA relativistic (right) BP86/TZ(2)P (see Table 2). See also Scheme 1.

reactants, and that this stabilization becomes stronger as the reaction proceeds, i.e., in the order reactant complex (RC) < transition state (TS) < product (P). The effects are slightly less pronounced in ZORA than in QR. This picture emerges from the relative enthalpies in Table 1 as well as the electronic energies collected in Table 2. Note that only for the insertion of Pd into the C–Cl bond, the relativistic stabilizations of reactant complex and TS are essentially equal in magnitude, namely ca 6 kcal/mol. Let us, for example, take a closer look at the insertion of Pd into the C–H bond of methane. The nonrelativistic (NR) relative 298 K enthalpies of the stationary points along the reaction coordinate are 0.0 (R, **1a**), -6.2 (RC, **1b**), 9.2 (TS, **1c**) and 8.7 kcal/mol (P, **1d**; see Table 1). The corresponding quasirelativistic (QR) values are 0.0 (**1a**), -12.6 (**1b**), -7.6 (**1c**) and -13.3 kcal/mol (**1d**) and ZORA yields 0.0 (**1a**), -11.4 (**1b**), -5.0 (**1c**) and -9.7 kcal/mol (**1d**). Similar effects can be observed for insertion of palladium into the ethane C–C (**2a - 2d**) and chloromethane C–Cl bonds (**3a - 3d**; see Table 1). Thus, going from NR to ZORA, activation enthalpies are reduced by 6 (C–Cl) to 14 kcal/mol (C–H) and reaction enthalpies become more exothermic by 15 (C–Cl) to 20 kcal/mol (C–C). This yields 298 K activation enthalpies $\Delta H^{\neq}_{298}$ of -5.0 (C–H), 9.6 (C–C) and -6.0 kcal/mol (C–Cl) at ZORA-BP86. The corresponding reaction enthalpies $\Delta H_{r,298}$ are -9.7 (C–H), -14.1 (C–C) and -35.7 kcal/mol (C–Cl).

The relativistic stabilization of reactant complexes (RC), although weaker than that of transition states and products, is still substantial. This results in pronounced potential wells with complexation enthalpies of ca -11 kcal/mol for the alkanes (**1b** and **2b**) and ca -16 kcal/mol for chloromethane (**3b**) at ZORA-BP86. Figure 2 provides a graphical overview of the relativistic effects on potential energy surfaces by comparing the nonrelativistic (left) and ZORA relativistic (right) reaction profiles based on the energies in Table 2. Here, it can be clearly seen how relativity significantly reduces the activation barriers for insertion. Note, on the other hand, that the barriers for the reverse reactions, i.e. reductive elimination, become higher. This is of course simply due to the fact that the products (**1d - 3d**) are more strongly stabilized than the transition states (**1c**

- **3c**). Note also that relativistic effects, although sizeable, do not change the relative order of barrier heights and reaction energies or enthalpies (Figure 2).

How does this compare with the structural effects of relativity? In the first place, the relativistic stabilization of minimum energy structures is accompanied by a shortening of bonds that involve palladium, i.e. C–Pd and X–Pd, as can be seen in Table 1 for reactant complexes (RC) and products (P). This is in line with general experience.[12b] The relativistic C–Pd and X–Pd bond contractions are somewhat less pronounced for ZORA then for QR. We take again the reaction of Pd + CH_4 as an example. In the reactant complex **1b**, Pd has short contacts to both C and X (= H). If we go from NR to ZORA, the C–Pd bond length decreases from 2.347 to 2.298 Å in the reactant complex (**1b**) and from 2.016 to 2.000 Å in the product **1d**. Likewise, the H–Pd bond shrinks from 1.981 to 1.949 Å in **1b** and from 1.546 to 1.527 Å in **1d**. Similar effects occur for insertion of palladium into the ethane C–C (**2b** and **2d**) and chloromethane C–Cl bonds (**3b** and **3d**; see Table 1). Note, that the metal–substrate interaction in the reactant complexes **2b** and **3b** differs from that in **1b** (see Figure 1 and Table 1). In **2b**, Pd binds to ethane via two C–H bonds of a methyl group instead of forming direct C–Pd and X–Pd bonds (X = C). In **3b**, Pd binds to the substrate predominantly via X (= Cl) and not via C. Thus, the primary effect of relativity is Cl–Pd contraction while there is no pronounced trend for the C–Pd distance. In fact, the latter contracts for QR (from 3.365 to 3.251 Å) and expands for ZORA (from 3.365 to 3.463 Å; see Table 1).

Another striking effect is the relativistic *contraction* of the activated C–X bond in the transition states (see Table 1). It is strongest for the TS of C–H insertion (**1c**) and becomes less pronounced for the transition states of C–C (**2c**) and C–Cl (**3c**) insertion. For example, going from NR to ZORA, the C–X distance decreases by 0.1 Å in **1c** (from 1.712 to 1.613 Å), by 0.07 Å in **2c** (from 1.997 to 1.929 Å) and by only 0.001 Å in **3c** (from 1.969 to 1.968 Å). To enable a more straightforward comparison of the effect in the different reactions, we define a reaction coordinate R based on the C–X bond length (eq 8).

$$R = [(C–X) – (C–X)_R] / [(C–X)_P – (C–X)_R] \quad (8)$$

Here, (C–X) is the C–X bond length in a particular stationary point and $(C–X)_R$ and $(C–X)_P$ are the C–X bond length in the reactants (i.e. isolated substrate) and in the product, respectively. Thus, R = 0 at the beginning of the reaction (i.e. for the reactants) and R = 1 when the reaction has been completed (i.e. for the products). As can be seen in Table 1 (e.g. for ZORA-BP86), the extent of C–X bond elongation in the TS is highest for the most endothermic reaction, that is, insertion of Pd into the C–H bond (**1c**: R = 0.45), and lowest for the most exothermic reaction, that is, insertion of Pd into the C–Cl bond (**3c**: R = 0.12). This fits in nicely with the Hammond postulate[22] for transition states of homologous reaction systems (compare Table 1 and Figure 2). Note that the relativistic *contraction* of the C–X bond in the TS corresponds to a shift in character of the latter toward the educt. Note also that this occurs together with a relativistic increase in the reaction exothermicity. This is again reminiscent of the Hammond postulate. We return to this point in Section 3.3.

In conclusion, in our BP86/TZ(2)P calculations on the insertion of Pd into C–X bonds, relativity leads to more pronounced potential wells for the reactant complexes, lower activation barriers and more educt-like transition states, as well as more exothermic overall reaction enthalpies.

4.3.2 Comparison with Experiments and other Computations

In this section, we compare our results with those of previous experimental and theoretical investigations. Our findings are consistent with gas-phase experiments of Weisshaar and coworkers[6e,f,7b,e] who studied the reactions of neutral transition metal atoms with alkanes in He buffer gas using spectroscopic techniques. They found that Pd-d^{10} atoms insert neither into the C–H nor the C–C bonds of methane and ethane. No reaction at all is observed for Pd + CH_4 whereas Pd + C_2H_6 leads to the formation of a collisionally stabilized [Pd, C_2H_6] complex with an effective bimolecular rate constant

of 0.16(2) • 10^{-12} $cm^3molecule^{-1}s^{-1}$ (refined value from Ref. 7b).[6f,7b,e] The exponential decay of the Pd signal *versus* alkane pressure furthermore suggested a complexation energy of at least 8 kcal/mol for Pd–alkane complexes.[6f] This lower bound agrees well with our relativistic complexation energies (Table 2, ZORA: -10.5 kcal/mol, QR: -11.4 and -11.3 kcal/mol for CH_4 and C_2H_6). On the other hand, our nonrelativistic (NR: -5.6 and -5.4 kcal/mol) but also the PCI-80 complexation energies of Carroll et al.[7b] (-5.1 and -6.6 kcal/mol) are slightly too weak compared to experiment. The absence of a complex of Pd and methane in the experiments has been ascribed to a lifetime of the internally hot $[Pd, CH_4]^*$ encounter complex that is too short to allow for collisional cooling.[6f] The larger alkanes, starting with ethane, have more internal degrees of freedom and they more efficiently dissipate the internal energy. Thus, lifetimes of the $[Pd, alkane]^*$ encounter complex become long enough to benefit from termolecular cooling.

The fact that no products of C–H or C–C oxidative addition are observed can be understood if both the energy barrier and the entropy or statistical bottleneck are taken into account. In the case of Pd + CH_4, the internally hot $[Pd, CH_4]^*$ encounter complex dissociates back to the separate reactants rather than proceeding via the TS for C–H insertion, even though the latter has essentially the same energy as the former ($\Delta E^{\neq}$ = -1.6 kcal/mol at ZORA-BP86 and 3.6 kcal/mol at PCI-80, see Table 2). This can be ascribed to the high density of states of the unbound reactants and the low density of states of the tight TS for insertion as suggested by the negative activation entropy $\Delta S^{\neq}$ of -22.5 cal/mol K relative to reactants (298 K; at ZORA-BP86; not shown in the Tables). Such statistical barriers are well-known and often play a key role in gas-phase ion–molecule reactions.[23] In the case of Pd + C_2H_6, insertion into the C–C bond is prevented by an even less favorable entropy bottleneck associated with a negative activation entropy of -26.1 cal/mol K relative to reactants (298 K; at ZORA-BP86; not shown in the Tables) and, in addition, a rather high activation energy of 12.5 kcal/mol at ZORA-BP86 (Table 2).

Blomberg, Siegbahn and coworkers[7b,11b,j] have studied the oxidative addition of Pd (and other metal atoms) into the C–H and C–C bonds of methane and ethane (but not chloromethane) at PCI-80 in which relativistic effects are accounted for by first-order perturbation theory. With an estimated accuracy of some 3 kcal/mol,[7b] PCI-80 may be considered the best *ab initio* benchmark at present. In the first place, we note a remarkably strong dependence of the computed kinetic and thermodynamic parameters on the level of theory. For example, since the early GVB-RCI calculations of Low and Goddard,[11n,o] the value for the activation energy of Pd insertion into the methane C–H bond has decreased from 30.5 (no ZPE correction) to 3.6 kcal/mol (ZPE-corrected) at PCI-80, i.e. by approximately 27 (!) kcal/mol. Even the more recent MCPF value of 16 kcal/mol (no ZPE correction)[11j] is still some 12 kcal/mol above the PCI-80 barrier of 3.6 kcal/mol (ZPE-corrected). Now, the qualitative trends for potential energy surfaces of Pd + CH_4 and Pd + C_2H_6 are similar for our NR-, QR- and ZORA-BP86 as well as the PCI-80 computations (Table 2): C–H insertion has a lower barrier and is (slightly) more exothermic than C–C insertion. The best overall agreement with PCI-80 is achieved using the relativistic ZORA approach. Our ZPE-corrected ZORA-BP86 activation energies are 8 - 9 kcal/mol below the PCI-80 values, in line with the general tendency of present-day gradient-corrected DFT to underestimate reaction barriers.[13c] The absence of relativistic corrections in the NR-BP86 approach masks this deficiency and yields instead activation energies that are 2 - 6 kcal/mol *higher* than those of PCI-80. We wish to point out that the PCI-80 activation barriers were computed using two approximations: (i) the final scaled MCPF energies of the PCI-80 study were not computed at the MCPF but instead the HF optimum geometry;[7b,11a] (ii) the TS optimization[11a,j] for Pd + CH_4 was carried using the C–Pd and H–Pd distances obtained by Low and Goddard[11n] at HF. This may also contribute to the discrepancies with our ZORA-BP86 results. Furthermore, our ZPE-corrected reaction energies at ZORA-BP86 are 7 - 9 kcal/mol more exothermic than those obtained at PCI-80. Finally, we wish to emphasize that whereas the quasirelativistic approach to relativity is known to fail in a few cases due to the core-collapse mentioned in Section 2.2, such a complete

failure apparently does not occur, here. Deviations between QR-BP86 and PCI-80 relative energies are only 1 - 4 kcal/mol larger than those between ZORA-BP86 and PCI-80.

Previously, Bickelhaupt *et al.*[10b] have studied the insertion of Pd into the chloromethane C–Cl bond at the BP86//LDA level of DFT without relativistic corrections. As can be seen in Table 2, the older BP86//LDA relative energies agree well with those of the present nonrelativistic NR-BP86 computations for the reactant complex (RC, **1b**) and the transition state (TS, **1c**) but they differ significantly for the product (P, **1d**) which is at too high energy in case of BP86//LDA. The discrepancy is caused by the use in the latter[10b] of a smaller basis set (DZP instead of TZ2P for C and H) and LDA instead of BP86 for geometry optimization.

In conclusion, we achieve the best overall agreement with PCI-80 benchmark values using the ZORA-BP86 approach which also yields pronounced potential wells for reactant complexes that are consistent with relatively strongly bound, collisionally stabilized Pd–alkane reactant complexes observed in gas-phase experiments.

4.3.3 Analysis of Activation Energies and TS Structures

To shed light on *how* the relativistic stabilization of transition states for oxidative insertion is brought about, we analyze the NR, QR and ZORA activation energies $\Delta E^{\neq}$ in terms of the activation strain $\Delta E^{\neq}_{\text{strain}}$ of and the TS-interaction $\Delta E^{\neq}_{\text{int}}$ between the deformed reactants in the activated complexes (see eq 6 and Section 2.3). The results of these analyses are collected in Table 3. Two trends can be recognized: (i) relativity increases the TS interaction $\Delta E^{\neq}_{\text{int}}$ (except for QR in **1c**, *vide infra*), and (ii) it lowers the activation strain $\Delta E^{\neq}_{\text{strain}}$ (except for ZORA in **3c**). Let's for example take the Pd + CH_4 reaction (**1**): if we go from NR to ZORA, the TS interaction increases from -50.2 to -55.1 kcal/mol and the activation strain decreases from 62.8 to 53.5 kcal/mol. Both, the trend in TS interaction and activation strain can be understood quite straightforwardly as a consequence of the well-known relativistic effects[12] on the frontier d and s AOs of

Table 3. Analysis of the Metal–Substrate Interaction in the Transition State for the Oxidative Insertion of Pd with CH_4, C_2H_6 and CH_3Cl , without and with Relativistic Effects. [a]

		Pd + CH_4 (**1**)			Pd + C_2H_6 (**2**)			Pd + CH_3Cl (**3**)		
		NR	QR	ZORA	NR	QR	ZORA	NR	QR	ZORA
activation energy analysis (kcal/mol)										
ΔV_{elst}		–177.4	–166.1	–170.4	–139.7	–153.6	–139.5	–74.5	–81.2	–76.7
ΔE_{Pauli}		220.7	213.3	211.1	196.4	218.1	192.6	110.9	114.5	112.3
ΔE_{oi}		–93.5	–90.9	–95.8	–76.4	–87.2	–79.9	–43.7	–42.8	–48.7
$\Delta E^{\neq}_{int}$		–50.2	–43.7	–55.1	–19.7	–22.7	–26.8	–7.3	–9.5	–13.1
$\Delta E^{\neq}_{strain}$		62.8	39.2	53.5	43.1	33.2	39.3	8.5	3.4	8.8
$\Delta E^{\neq}$		12.6	–4.5	–1.6	23.4	10.5	12.5	1.2	–6.1	–4.3
fragment orbital overlaps ⟨ Pd | substrate ⟩										
⟨4d | LUMO⟩		0.331	0.297	0.327	0.134	0.131	0.129	0.086	0.044	0.082
⟨5s | HOMO⟩		0.400	0.368	0.401	0.197	0.185	0.213	0.136	0.148	0.144
fragment orbital populations (electrons)										
Pd:	4d	9.34	9.33	9.32	9.54	9.36	9.42	9.60	9.61	9.59
	5s	0.27	0.35	0.38	0.09	0.17	0.22	0.11	0.25	0.18
substrate:	HOMO	1.76	1.75	1.71	1.88	1.87	1.83	1.94	1.93	1.91
	LUMO	0.39	0.27	0.36	0.27	0.22	0.25	0.16	0.09	0.17
fragment orbital energies (eV)										
Pd:	4d	–4.241	–4.186	–4.193	–4.241	–4.186	–4.193	–4.241	–4.186	–4.193
	5s	–2.941	–3.504	–3.423	–2.941	–3.504	–3.423	–2.941	–3.504	–3.423
substrate:	HOMO	–7.234	–7.685	–7.435	–7.114	–7.532	–7.142	–7.107	–7.073	–7.303
	LUMO	–2.111	–0.878	–1.625	–0.713	–0.041	–0.306	–2.052	–1.538	–2.066

[a] At BP86/TZ(2)P. See Section 2.3. NR = nonrelativistic, QR = quasirelativistic, ZORA = zeroth-order regular approximation (Section 2.2). All analyses have been carried out using the same method for relativistic effects as in the geometry optimization.

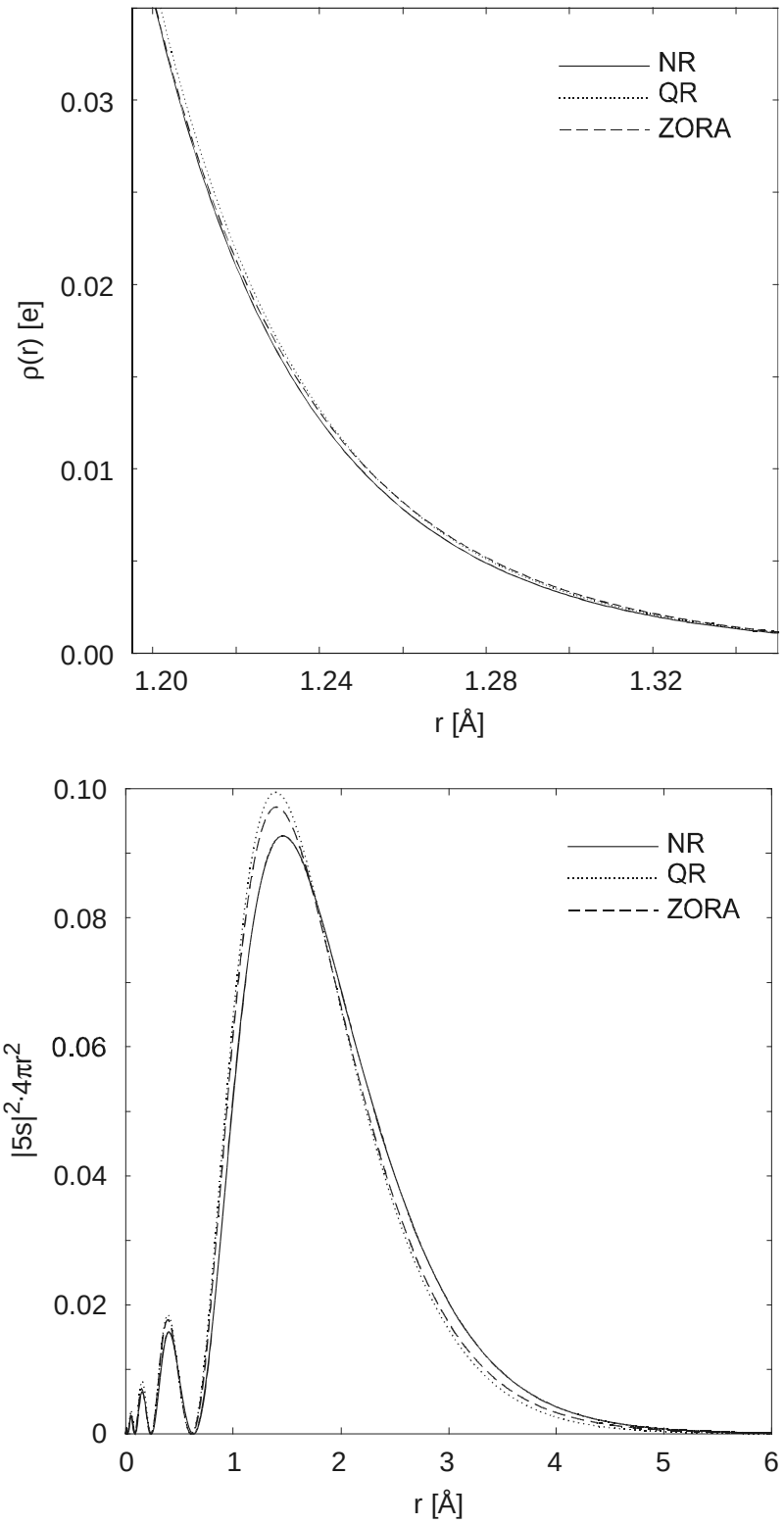

Figure 3. Electron density of Pd (top) and radial distribution function of the Pd 5s AO (bottom) at nonrelativistic (NR), quasirelativistic (QR) and ZORA relativistic BP86/TZ(2)P.

the Pd atom: going from NR to ZORA, the 4d HOMO is slightly *destabilized* (from -4.24 to -4.19 eV) and expanded, leading to a slight expansion of the overall Pd density, whereas the 5s LUMO is substantially *stabilized* (from -2.9 to -3.4 eV) and contracted (see Table 3 and Figure 3). This leads to smaller energy gaps between the Pd 4d HOMO and the substrate LUMO (e.g. the $\sigma^*_{C\text{-}H}$ of CH_4) as well as between the Pd 5s LUMO and the substrate HOMO (e.g. the $\sigma_{C\text{-}H}$ of CH_4) and, therefore, to a stronger Pd–substrate bonding through increased σ donation and π backdonation, respectively (see Figure 4 for relevant frontier orbital interactions).

The primary changes due to relativity in the Pd–substrate interaction are hidden to some extent by the structural changes they cause. Therefore, we have also analyzed the changes in TS interaction $\Delta E^{\neq}_{int}$ along NR, QR and ZORA using the optimum geometry of ZORA in all three cases. Table 4 shows the results for the transition state of the Pd + CH_4 insertion (**1c**). Now, it becomes much more clear than in Table 3 that the main effect of relativity on the TS interaction is generated in the orbital interaction term ΔE_{oi}. If we go from NR to ZORA, the latter increases by 8.3 kcal/mol (from -87.5 to -95.8 kcal/mol) which accounts for about two third of the relativistic strengthening of the TS interaction $\Delta E^{\neq}_{int}$. This correlates nicely with the reduced energy gaps between Pd and CH_4 frontier orbitals and it shows up in a decrease and increase of HOMO and LUMO populations, respectively (Table 4). The changes in the corresponding orbital overlaps are only marginal. Furthermore, the contributions of ΔV_{elst} and ΔE_{Pauli} to the trend in $\Delta E^{\neq}_{int}$, although not unimportant, are much smaller. Note that, in the analyses of Table 4, the trend in activation energy $\Delta E^{\neq}$ (e.g. the lowering by -13.7 kcal/mol if we go from NR to ZORA), is caused entirely by the trend in $\Delta E^{\neq}_{int}$ because the geometry is kept frozen (to the ZORA optimum) making the activation strain $\Delta E^{\neq}_{strain}$ essentially constant.

Next, the constraint of a frozen geometry is released as we go back to the analyses of Table 3. One might at first expect that the stronger Pd–substrate interaction causes the Pd atom to be further inserted into the C–X bond in the TS. However, the opposite happens, i.e. relativity leads to a contraction of the C–X bond in a more educt-like TS. In fact, this is easily understood if we consider the schematic reaction profile in Figure 5

which is based on quantitative analyses of all stationary points along the reaction coordinate (Tables 3 and 4 only show the results for the TS). Here, the nonrelativistic energy ΔE of the reaction system is decomposed into the strain energy ΔE_{strain} of and interaction energy ΔE_{int} between the reactants (see Section 2.3). Along the reaction coordinate, ΔE_{strain} increases because the C–X bond of the substrate is stretched while the Pd–substrate interaction ΔE_{int} becomes more stabilizing due to the decreasing HOMO–LUMO gap of the substrate. The net result is the reaction profile of $\Delta E^{\neq}$ with the transition state indicated by an asterisk. Now, if relativistic effects are switched on, the curve of the strain energy ΔE_{strain} as function of the reaction coordinate (or C–X bond stretching) is not much affected but the Pd–substrate interaction increases in all points along the reaction coordinate. This strengthening, indicated by vertical arrows in Figure 5, becomes larger as the reaction proceeds simply because the inherent strength of Pd–substrate interaction also increases along this direction (*vide supra*). Thus, all stationary points on the relativistic PES, the dashed line in Figure 5, are stabilized and the maximum shifts to the left, i.e. the TS becomes more reactant-like. This also accounts for the trend mentioned earlier (in Section 3.1) that the relativistic stabilization of stationary points relative to separate reactants increases in the order RC < TS < P. Finally, as can be seen in Table 3, the relativistic shift of the TS toward the reactant side is accompanied by a reduction in activation strain $\Delta E^{\neq}_{\text{strain}}$, in line with the smaller degree of C–X stretching (cf "Reaction coordinate" or scaled C–X distance in Table 1).

Table 4. Analysis of the Pd–CH_4 Interaction in the Transition State for Oxidative Insertion (**1c**), without and with Relativistic Effects. [a]

		NR//ZORA	QR//ZORA	ZORA//ZORA
activation energy analysis (kcal/mol)				
ΔV_{elst}		–68.6	–170.8	–170.4
ΔE_{Pauli}		214.8	210.5	211.1
ΔE_{oi}		–87.5	–97.5	–95.8
$\Delta E^{\neq}_{int}$		–41.3	–57.8	–55.1
$\Delta E^{\neq}_{strain}$		53.4	53.4	53.5
$\Delta E^{\neq}$		12.1	–4.4	–1.6
fragment orbital overlaps ⟨ Pd | CH_4 ⟩				
⟨4d | LUMO⟩		0.322	0.327	0.327
⟨5s | HOMO⟩		0.380	0.398	0.401
fragment orbital populations (electrons)				
Pd:	4d	9.37	9.31	9.32
	5s	0.24	0.37	0.38
CH_4:	HOMO	1.79	1.71	1.71
	LUMO	0.33	0.36	0.36
fragment orbital energies (eV)				
Pd:	4d	–4.241	–4.186	–4.193
	5s	–2.941	–3.504	–3.423
CH_4:	HOMO	–7.436	–7.436	–7.435
	LUMO	–1.624	–1.626	–1.625

[a] At BP86/TZ(2)P. NR = nonrelativistic, QR = quasirelativistic, ZORA = zeroth-order regular approximation (Section 2.2). Note that all analyses have been carried out using the ZORA geometry.

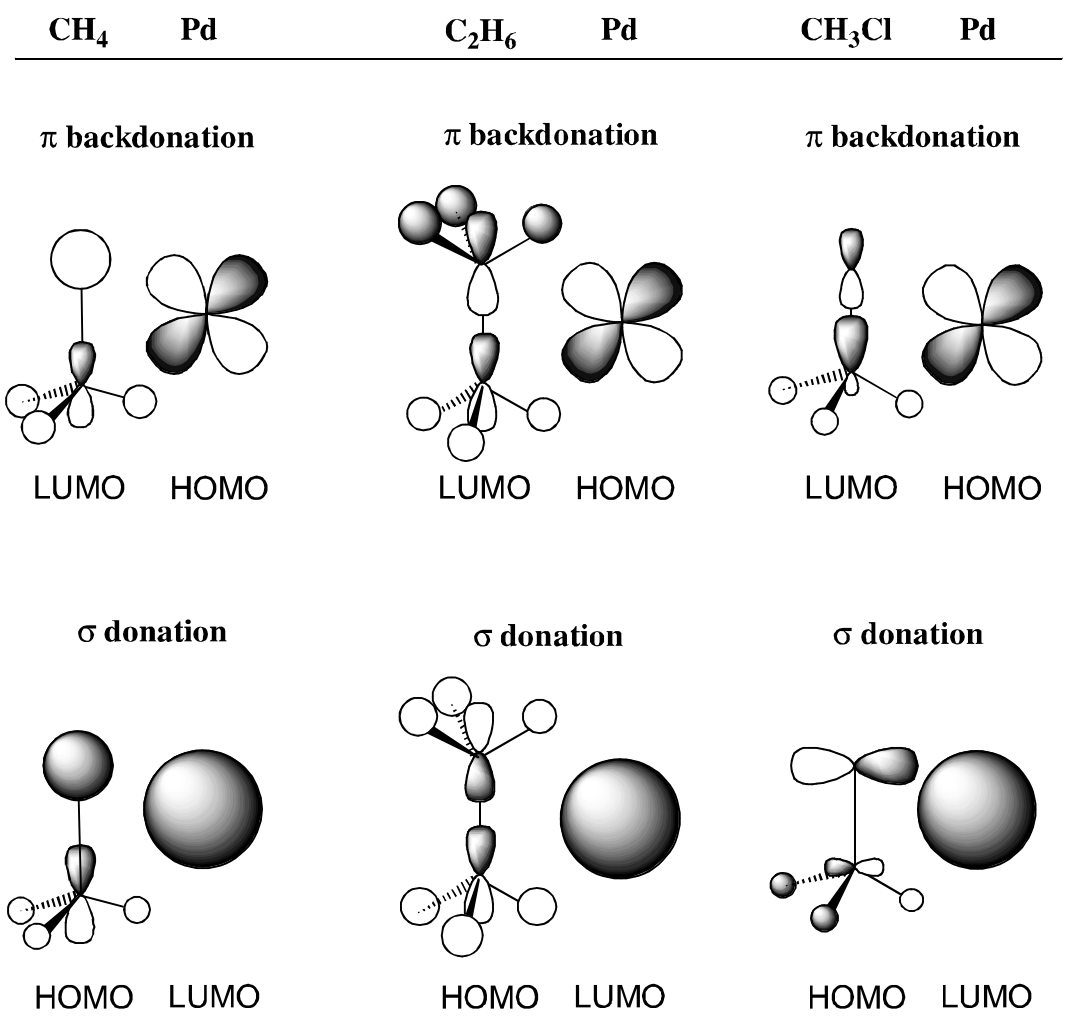

Figure 4. Dominating frontier orbital interactions between Pd and the substrate in the transition states for oxidative insertion into the C–H, C–C and C–Cl bonds of CH_4, C_2H_6 and CH_3Cl emerging from our Kohn-Sham MO analysis of the TS interactions $\Delta E^{\neq}_{\text{int}}$ at nonrelativistic (NR), quasirelativistic (QR) as well as ZORA relativistic BP86/TZ(2)P.

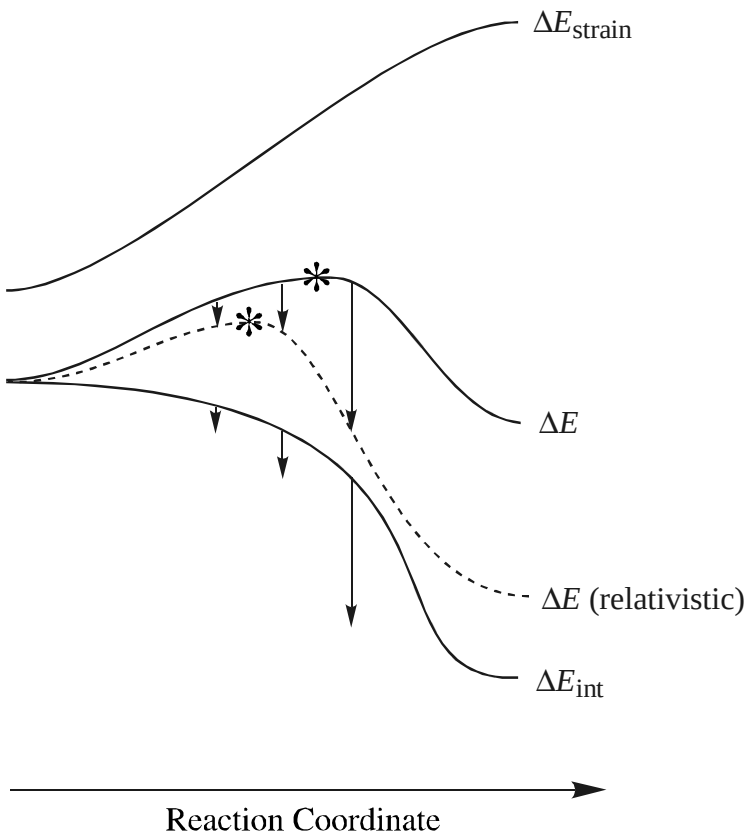

Figure 5. Schematic representation of the nonrelativistic reaction profile provided by the energy ΔE of the reaction system and its decomposition into the strain energy ΔE_{strain} of and interaction energy ΔE_{int} (see eq 6). The relativistic strengthening of ΔE_{int} as well as the concomitant lowering of ΔE are indicated by vertical arrows (the resulting relativistic ΔE profile is shown as dashed line). Note that relativity stabilizes the TS (asterisk) and shifts it along the reaction coordinate toward the reactant complex.

4.4 Conclusions

Relativistic effects are important for an accurate quantum chemical description of the oxidative insertion of the second-row transition metal palladium into C–H, C–C and C–Cl bonds, as follows from our nonlocal DFT study on the model systems CH_4, C_2H_6 and CH_3Cl, respectively, at BP86/TZ(2)P. The effect of relativity in both the quasirelativistic (QR) and, to a slightly lesser extent, in the ZORA approach is that stationary points along the reaction coordinate are stabilized with respect to reactants. This stabilization becomes stronger as the reaction proceeds, i.e., in the order reactant complex (RC) < transition state (TS) < product (P). Consequently, activation enthalpies are reduced by 6 (C–Cl) to 14 kcal/mol (C–H) and reaction enthalpies become more exothermic by 15 (C–Cl) to 20 kcal/mol (C–C). However, the relative order of barrier heights and reaction enthalpies is not affected (the activation barrier decreases in the order C–C > C–H > C–Cl and the reaction becomes more exothermic in the order C–H > C–C > C–Cl). Another effect is that all transition states become more educt-like.

The above-mentioned effects can be understood in terms of the well-known relativistic destabilization of the Pd 4d HOMO and stabilization of the Pd 5s LUMO. These effects make the metal both a better electron donor and acceptor which lead to stronger donor–acceptor interactions between Pd and the substrate. The result is an additional stabilization of transition states and oxidative insertion products relative to the separate reactants.

Finally, the best agreement of our BP86/TZ(2)P results with *ab initio* PCI-80 benchmark values and gas-phase spectroscopic experiments is obtained using the ZORA relativistic approach. For activation energies, discrepancies of 8 - 9 kcal/mol remain which may be ascribed to the combined effect of an underestimation of barriers by DFT and the uncertainty of a few kcal/mol in the PCI-80 results.[7b,8a]

4.5 References

(1) (a) Collman, J. P.; Hegedus, L. S.; Norton, J. R.; Finke, R. G. *Principles and Applications of Organotransition Metal Chemistry*; University Science Books: Mill Valley, CA, 1987. (b) Elschenbroich, Ch.; Salzer, A. *Organometallics. A Concise Indroduction*, 2nd ed.; VCH: Weinheim, Germany 1992. (c) Amatore, C.; Jutand, A. *Acc. Chem. Res.* **2000**, *33*, 314. (d) Yang, H.; Kotz, K. T.; Asplund, M. C.; Wilkens, M. J.; Harris, C. B. *Acc. Chem. Res.* **1999**, *32*, 551. (e) Sen, A. *Acc. Chem. Res.* **1998**, *31*, 550.

(2) Experimental studies on reactions of metal complexes in the condensed phase: (a) Luh, T.-Y.; Leung, M.-k.; Wong, K.-T. *Chem. Rev.* **2000**, *100*, 3187. (b) Stürmer, R. *Angew. Chem.* **1999**, *111*, 3509. (c) Hau, L.-B.; Tanaka, M. *Chem. Comm.* **1999**, *5*, 395. (d) Casado, A. L.; Espinet, P. *Organometallics* **1998**, *17*, 954. (e) Kayser, B.; Missling, C.; Knizek, J.; Noeth, H.; Beck, W. *Eur. J. Inorg. Chem.* **1998**, *3*, 375. (f) Guillevic, M.-A.; Rocaboy, C.; Arif, A. M.; Horvath, I. T.; Gladysz, J. A. *Organometallics* **1998**, *17*, 707. (g) Edelbach, B. L.; Lachicotte, R. J.; Jones, W. D. *J. Am. Chem. Soc.* **1998**, *120*, 2843. (h) Crabtree, R. H. *Chem. Rev.* **1995**, *95*, 987. (i) Grushin, V. V.; Alper, H. *Chem. Rev.* **1994**, *94*, 1047. (j) Ellis, P. R.; Pearson, J. M.; Haynes, A.; Adams, H.; Bailey, N. A.; Maitlis, P. M. *Organometallics* **1994**, *13*, 3215. (k) Wright, M. W.; Smalley, T. L.; Welker, M. E.; Rheingold, A. L. *J. Am. Chem. Soc.* **1994**, *116*, 6777. (l) Sakakaurka, T.; Sodeyama, T.; Sasaki, K.; Wada, K.; Tanaka, M. *J. Am. Chem. Soc.* **1990**, *112*, 7221. (m) Casalnuovo, A. L.; Calabrese, J. C.; Milstein, D. *J. Am. Chem. Soc.* **1988**, *110*, 6738. (n) Janowics, A. H.; Bergman, R. G. *J. Am. Chem. Soc.* **1983**, *105*, 3929. (o) Jones, W. D.; Feher, F. J. *J. Am. Chem. Soc.* **1982**, *104*, 4240. (p) Hickey, C. E.; Maitlis, P. M. *J. Chem. Soc., Chem. Commun.* **1984**, 1609. (q) Forster, D. *Adv. Organomet. Chem.* **1979**, *17*, 255. (r) Forster, D. *J. Am. Chem. Soc.* **1975**, *97*, 951.

(3) (a) Eller, K.; Schwarz, H. *Chem. Rev.* **1991**, *91*, 1121. (b) Armentrout, P. B.; Beauchamp, J. L. *Acc. Chem. Res.* **1989**, *22*, 315.

(4) Experimental studies on reactions of ionic metal atoms and complexes in the gas phase: (a) Brönstrup, M.; Schröder, D.; Schwarz, H. *Organometallics* **1999**, *18*, 1939. (b) Aschi, M.; Brönstrup, M.; Diefenbach, M.; Harvey, J. N.; Schröder, D.; Schwarz, H. *Angew. Chem.* **1998**, *110*, 858. (c) Freiser, B. S. *J. Mass Spectrom.* **1996**, *31*, 703. (d) van Koppen, P. A. M.; Kemper, P. R.; Bushnell, J. E.; Bowers, M. T. *J. Am. Chem. Soc.* **1995**, *117*, 2098. (e) Wesendrup, R.; Schröder, D.; Schwarz, H. *Angew. Chem.* **1994**, *105*, 1232. (f) Chen, Y.-M.; Clemmer, D. E.; Armentrout, P. B. *J. Am . Chem. Soc.* **1994**, *116*, 7815. (g) van den Berg, K. J.;

Ingemann, S.; Nibbering, N. M. M.; Gregor, I. K. *Rapid. Commun. Mass Spectrom.* **1993**, *7*, 769. (h) Chowdhury, A. K.; Wilkins, C. L. *J. Am. Chem. Soc.* **1987**, *109*, 5336. (i) Weil, D. A.; Wilkins, C. L. *J. Am. Chem. Soc.* **1985**, *107*, 7316. (j) Jones, R. W.; Staley, R. H. *J. Phys. Chem.* **1982**, *86*, 1669. (k) Jones, R. W., Staley, R. H. *J. Am. Chem. Soc.* **1980**, *102*, 3794.

(5) Combined experimental and theoretical studies on reactions of ionic metal atoms and complexes in the gas phase: (a) Yi, S. S.; Reichert, E. L.; Holthausen, M. C.; Koch, W.; Weisshaar, J. C. *Chem. Eur. J.* **2000**, *6*, 2232. (b) Blomberg, M.; Yi, S. S.; Noll, R. J.; Weisshaar, J. C. *J. Phys. Chem. A* **1999**, *103*, 7254. (c) Diefenbach, M.; Brönstrup, M.; Aschi, M.; Schröder, D.; Schwarz, H. *J. Am. Chem. Soc.* **1999**, *121*, 10614. (d) Schwarz, J.; Schröder, D.; Schwarz, H.; Heinemann, C.; Hrusák, J. *Helv. Chim. Acta* **1996**, *79*, 1110.

(6) Experimental studies on reactions of neutral metal atoms in the gas phase: (a) Wen, Y.; Porembski, M.; Ferrett, T. A.; Weisshaar, J. C. *J. Phys. Chem. A* **1998**, *102*, 8362. (b) Wen, Y.; Yethiraj, A.; Weisshaar, J. C. *J. Chem. Phys.* **1997**, *106*, 5509. (c) Carroll, J. J.; Weisshaar, J. C. *J. Phys. Chem.* **1996**, *100*, 12355. (d) Chertihin, G. V.; Andrews, L. *J. Am. Chem. Soc.* **1994**, *116*, 8322. (e) Carroll, J. J.; Haug, K. L.; Weisshaar, J. C. *J. Am. Chem. Soc.* **1993**, *115*, 6962. (f) Carroll, J. J.; Weisshaar, J. C. *J. Am. Chem. Soc.* **1993**, *115*, 800. (g) Ritter, D.; Carroll, J. J.; Weisshaar, J. C. *J. Phys. Chem.* **1992**, *96*, *10636*. (h) Mitchell, S. A.; Hackett, P. A. *J. Chem. Phys.* **1990**, *93*, 7822. (i) Ritter, D.; Weisshaar, J. C. *J. Am. Chem. Soc.* **1990**, *112*, 6425. (j) Fayet, P.; Kaldor, A.; Cox, D. M. *J. Chem. Phys.* **1990**, *92*, 254.

(7) Combined experimental and theoretical studies on reactions of neutral metal atoms in the gas phase: (a) Porembski, M.; Weisshaar, J. C. *J. Phys. Chem. A* **2000**, 104, 1524. (b) Carroll, J. J.; Haug, K. L.; Weisshaar, J. C.; Blomberg, M. R. A.; Siegbahn, P. E. M.; Svensson, M. *J. Phys. Chem.* **1995**, *99*, 13955. (c) Carroll, J. J.; Weisshaar, J. C.; Siegbahn, P. E. M.; Wittborn, A. M. C.; Blomberg, M. R. A. *J. Phys. Chem.* **1995**, *99*, 14388. (d) Mitchell, S.; Blitz, M. A.; Siegbahn, P. E. M.; Svenson, M. *J. Chem. Phys.* **1994**, *100*, 423. (e) Weisshaar, J. C. *Acc. Chem. Res.* **1993**, *26*, 213.

(8) Theoretical studies on reactions of metal complexes: (a) Dedieu, A. *Chem. Rev.* **2000**, *100*, 543. (b) Torrent, M.; Solà, M.; Frenking, G. *Chem. Rev.* **2000**, *100*, 439. (c) Griffin, T. R.; Cook, D. B.; Haynes, A.; Pearson, J. M.; Monti, D.; Morris, G. E. *J. Am. Chem. Soc.* **1996**, *118*, 3029. (d) Aullón, G.; Alvarez, S. *Inorg. Chem.* **1996**, *35*, 3137. (e) Ziegler, T. *Chem. Rev.* **1991**, *91*, 651. (f) Koga, N.; Morokuma, K. *Chem. Rev.* **1991**, *91*, 823. (g) Bickelhaupt, F. M.; Baerends, E. J.; Ravenek, W. *Inorg. Chem.* **1990**, *29*, 350. (h) Gritsenko, O. V.; Bagatur'yants, A. A.; Moiseev, I. I.; Kazanskii, V. B. *Russ. Chem. Rev.* **1985**, *54*, 1151.

(9) See also, for example: (a) Lamprecht, D.; Lamprecht, G. J. *J. Comput. Chem.* **2000**, *21*, 692. (b) Minaev, B.; Agren, H. *Int. J. Quantum Chem.* **1999**, *72*, 581. (c) Su, M.-D.; Chu, S.-Y. *J. Am. Chem. Soc.* **1999**, *121*, 1045. (d) Su, M.-D.; Chu, S.-Y. *Inorg. Chem.* **1998**, *37*, 3400. (e) Su, M.-D.; Chu, S.-Y. *Chem. Phys. Lett.* **1998**, *282*, 25. (f) Albert, K.; Gisdakis, P.; Rösch, N. *Organometallics* **1998**, *17*, 1608. (g) Sakaki, S.; Biswas, B.: Sugimoto, M. *Organometallics* **1998**, *17*, 1278. (h) Hill, G. S.; Puddephatt, R. J. *Organometallics* **1998**, *17*, 1478. (i) Sakaki, S.; Ogawa, M.; Kinoshita, M. *J. Phys. Chem.* **1995**, *99*, 9933. (j) Irikura, K. K.; Goddard, W. A., III *J. Am. Chem. Soc.* **1994**, *116*, 8733. (k) Perry, J. K.; Goddard, W. A., III *J. Am. Chem. Soc.* **1994**, *116*, 5013. (l) Sellers, H. *J. Comput. Chem.* **1990**, *11*, 754. (m) Rosi, M.; Bauschlinger Jr., C. W.; Langhoff, S. R.; Partidge, H. *J. Phys. Chem.* **1990**, *94*, 8656. (n) Ziegler, T.; Tschinke, V.; Fan, L.; Becke, A. D. *J. Am. Chem. Soc.* **1989**, *111*, 9177. (o) Low, J. J.; Goddard, W. A., III *J. Am. Chem. Soc.* **1986**, *108*, 6115.

(10) (a) Bickelhaupt, F. M. *J. Comput. Chem.* **1999**, *20*, 114. (b) Bickelhaupt, F. M.; Ziegler, T.; von Ragué Schleyer, P. *Organometallics* **1995**, *14*, 2288.

(11) Theoretical studies on reactions of neutral metal atoms: (a) Wittborn, A. M. C.; Costas, M.; Blomberg, M. R. A.; Siegbahn, P. E. M. *J. Chem. Phys.* **1997**, *107*, 4318. (b) Siegbahn, P. E. M. *J. Am. Chem. Soc.* **1994**, *116*, 7722. (c) Siegbahn, P. E. M. *Organometallics* **1994**, *13*, 2833. (d) Perry, J. K.; Ohanessian, G.; Goddard, W. A., III *Organometallics* **1994**, *13*, 1870. (e) Blomberg, M. R. A.; Siegbahn, P. E. M.; Svensson, M. *Inorg. Chem.* **1993**, *32*, 4218. (f) Siegbahn, P. E. M.; Blomberg, M. R. A.; Svensson, M. *J. Phys. Chem.* **1993**, *97*, 2564. (g) Siegbahn, P. E. M.; Blomberg, M. R. A.; Svensson, M. *J. Am. Chem. Soc.* **1993**, *115*, 1952. (h) Siegbahn, P. E. M.; Blomberg, M. R. A.; Svensson, M. *J. Am. Chem. Soc.* **1993**, *115*, 4191. (i) Siegbahn, P. E. M.; Blomberg, M. R. A. *J. Am. Chem. Soc.* **1992**, *114*, 10548. (j) Blomberg, M. R. A.; Siegbahn, P. E. M.; Svensson, M. *J. Am. Chem. Soc.* **1992**, *114*, 6095. (k) Svensson, M.; Blomberg, M. R. A.; Siegbahn, P. E. M. *J. Am. Chem. Soc.* **1991**, *113*, 7076. (l) Blomberg, M. R. A.; Siegbahn, P. E. M.; Nagashima, U.; Wennerberg, J. *J. Am. Chem. Soc.* **1991**, *113*, 424. (m) Carter, E. A.; Goddard, W. A., III *J. Phys. Chem.* **1988**, *92*, 5679. (n) Low, J. J.; Goddard, W. A., III *Organometallics* **1986**, *5*, 609. (o) Low, J. J.; Goddard, W. A., III *J. Am. Chem. Soc.* **1984**, *106*, 8321.

(12) Relativistic effects: (a) Moss, R. E. *Advanced Molecular Quantum Mechanics*, Chapman and Hall, London, 1973. (b) Pyykkö, P. *Chem. Rev.* **1988**, *88*, 563. See also: (c) Jensen, F. *Introduction to Computational Chemistry*, Wiley, Chichester, 1999.

(13) Density functional theory (DFT): (a) Dreizler, R. M.; Gross, E. K. U. *Density Functional Theory. An approach to the Quantum Many-Body Problem*; Springer: Berlin, 1990. (b) Parr, R. G.; Yang, W. *Density-Functional Theory of Atoms and Molecules*; Oxford University Press: New York, 1989. (c) Gritsenko, O. V.; Ensing, B.; Schipper, P. R. T.; Baerends, E. J. *J. Chem. Phys.*, in press.

(14) Kohn-Sham MO model in DFT: (a) Bickelhaupt, F. M.; Baerends, E. J. In *Reviews in Computational Chemistry*, Vol. 15, Lipkowitz, K. B., Boyd., D. B., Eds.; Wiley-VCH: New York, 2000; Vol. 15, Chapter 1. (b) Baerends, E. J.; Gritsenko, O. V. *J. Phys. Chem. A* **1997**, *101*, 5383.

(15) Diefenbach, A.; Bickelhaupt, F. M., in preparation.

(16) Amsterdam Density Functional (ADF) program: (a) Fonseca Guerra, C.; Visser, O.; Snijders, J. G.; te Velde, G.; Baerends, E. J., *The Parallelization of the Amsterdam Density Functional Program*, In: Methods and Techniques for Computational Chemistry; Clementi, E., Corongiu, G., Eds.; STEF: Cagliari, 1995; p. 305-395. (b) Baerends, E. J.; Ellis, D. E.; Ros, P. *Chem. Phys.* **1973**, *2*, 41. (c) Baerends, E. J.; Ros, P. *Chem. Phys.* **1975**, *8*, 412. (d) Baerends, E. J.; Ros, P. *Int. J. Quantum Chem., Quantum Chem. Symp.* **1978**, *S12*, 169. (e) Fonseca Guerra, C.; Snijders, J. G.; te Velde, G.; Baerends, E. J. *Theor. Chem. Acc.* **1998**, *99*, 391. (f) Boerrigter, P. M.; te Velde, G.; Baerends, E. J. *Int. J. Quantum Chem.* **1988**, *33*, 87. (g) te Velde, G.; Baerends, E. J. *J. Comp. Phys.* **1992**, *99*, 84. (h) Snijders, J. G.; Baerends, E. J.; Vernooijs, P. *At. Nucl. Data Tables* **1982**, *26*, 483. (i) Krijn, J.; Baerends, E. J. *Fit-Functions in the HFS-Method; Internal Report* (in Dutch); Vrije Universiteit: Amsterdam, 1984. (j) Slater, J. C. *Quantum Theory of Molecules and Solids Vol. 4*; McGraw-Hill: New York, 1974. (k) Becke, A. D. *J. Chem. Phys.* **1986**, *84*, 4524. (l) Becke, A. *Phys. Rev. A* **1988**, *38*, 3098. (m) Vosko, S. H.; Wilk, L.; Nusair, M. *Can. J. Phys.* **1980**, *58*, 1200. (n) Perdew, J. P. *Phys. Rev. B* **1986**, *33*, 8822 (Erratum: *Phys. Rev. B* **1986**, *34*, 7406). (o) Fan, L.; Ziegler, T. *J. Chem. Phys.* **1991**, *94*, 6057. (p) Versluis, L.; Ziegler, T. *J. Chem. Phys.* **1988**, *88*, 322. (q) Fan, L.; Versluis, L.; Ziegler, T.; Baerends, E. J.; Ravenek, W. *Int. J. Quantum. Chem., Quantum. Chem. Symp.* **1988**, *S22*, 173. (r) Fan, L.; Ziegler, T. *J. Chem. Phys.* **1990**, *92*, 3645. (s) Banerjee, A.; Adams, N.; Simons, J.; Shepard, R. *J. Phys. Chem.* **1985**, *89*, 52. (t) Baker, J. *J. Comput. Chem.* **1986**, *7*, 385.

(17) Atkins, P. W. *Physical Chemistry*; Oxford University Press: Oxford, 1998.

(18) Quasirelativistic approach: (a) Ziegler, T.; Tschinke, V.; Baerends, E. J.; Snijders, J. G.; Ravenek, W. *J. Phys. Chem.* **1989**, *93*, 3050. See also, for example: (b) Ziegler, T.; Snijders, G. J.; Baerends, E. J. In *The challenge of d and f Electrons*; Salahub, D. R.; Zerner, M. C., Eds.; ACS Symposium Series 395; American

Chemical Society: 1989, p 322. (c) Jacobson, H.; Schreckenbach, G.; Ziegler, T. *J. Phys. Chem.* **1994**, *98*, 11406. (d) Li, J.; Schreckenbach, G.; Ziegler, T. *Inorg. Chem.* **1995**, *34*, 3245.

(19) Pauli Hamiltonian and first-order perturbation approach: (a) Snijders, J. G.; Baerends, E. J. *Mol. Phys.* **1978**, *36*, 1789. (b) Snijders, J. G.; Baerends, E. J.; Ros, P. *Mol. Phys.* **1979**, *38*, 1909. (c) Cowan, R. D.; Griffin, D. C. *J. Opt. Soc. Am.* **1976**, *66*, 1010. (d) Foldy, L. L.; Wouthuysen, S. A. *Phys. Rev.* **1950**, *78*, 29. See also Ref. 12a.

(20) ZORA approach: (a) Chang, C.; Pelissier, M.; Durand, P. *Phys. Scr.* **1986**, *34*, 394. (b) van Lenthe, E.; Baerends, E. J.; Snijders, J. G. *J. Chem. Phys.* **1993**, *99*, 4597. (c) van Lenthe, E.; Snijders, J.; Baerends, E. J. *J. Chem. Phys.* **1996**, *105*, 6505. (d) van Lenthe, E. *Thesis*, Vrije Universiteit, Amsterdam, 1996. (e) van Lenthe, E.; van Leeuwen, R.; Baerends, E. J.; Snijders, J. G. *Int. J. Quantum Chem.* **1996**, *57*, 281.

(21) Bond energy decomposition: (a) Ziegler, T.; Rauk, A. *Inorg. Chem.* **1979**, *18*, 1558. (b) Ziegler, T.; Rauk, A. *Inorg. Chem.* **1979**, *18*, 1755. (c) Ziegler, T.; Rauk, A. *Inorg. Chem.* **1977**, *46*, 1. (d) Bickelhaupt, F.M.; Nibbering, N.M.M.; van Wezenbeek, E.M.; Baerends, E.J. *J. Phys. Chem.* **1992**, *96*, 4864.

(22) Hammond, G. S. *J. Am. Chem. Soc.* **1955**, *77*, 334.

(23) See, for example: (a) Nibbering, N. M. M. *Acc. Chem. Res.* **1990**, *23*, 279. (b) Riveros, J. M.; José, S. M.; Takashima, K. *Adv. Phys. Org. Chem.* **1985**, *21*, 197. (c) Ref. 10a. See also: (d) Bickelhaupt, F.M.; Nibbering, N.M.M.; Baerends, E.J.; Ziegler, T. *J. Am. Chem. Soc.* **1993**, *115*, 9160.

5 Activation of H–H, C–H, C–C and C–Cl Bonds by Pd(0). Insight from the Activation Strain Model

Abstract

To achieve more insight into palladium-catalyzed H–H, C–H, C–C and C–Cl bond activation and the mutual competition between these processes, several mechanistic pathways for oxidative addition of Pd(0) to H_2 (H–H), CH_4 (C–H), C_2H_6 (C–C and C–H) and CH_3Cl (C–Cl) were studied uniformly at the ZORA-BP86/TZ(2)P level of relativistic nonlocal density functional theory (DFT). Oxidative addition is overall exothermic for all model reactions studied, with 298 K reaction enthalpies $\Delta H_{r,298}$ of -35.7 (C–Cl) through -9.7 kcal/mol (C–H in CH_4). The lowest-barrier pathway is the direct oxidative insertion (OxIn) of Pd into the C–X or H–H bond (X = H, CH_3, Cl), with 298 K activation enthalpies $\Delta H^{\neq}_{298}$ that increase in the order H–H (-21.7 kcal/mol) < C–Cl (-6.0 kcal/mol) ≈ C–H (-5.0 and -4.1 kcal/mol for CH_4 and C_2H_6) < C–C (9.6 kcal/mol). The "straight" S_N2 substitution resulting in $PdCH_3^+ + X^-$ or $PdH^+ + H^-$ is highly endothermic (144 - 237 kcal/mol) and thus not competitive. In case of Pd + CH_3Cl, a third pathway is found in which S_N2 substitution occurs in concert with a rearrangement of the Cl^- leaving group from C to Pd (S_N2/Cl-ra) leading, in one step, to CH_3PdCl via an activation barrier $\Delta H^{\neq}_{298}$ of 21.2 kcal/mol. The competition between the various bond activation processes is analyzed using the Activation Strain (or Activation strain-TS interaction, ATS) model in which activation energies $\Delta E^{\neq}$ are decomposed into the activation strain $\Delta E^{\neq}_{strain}$ of and the stabilizing transition state (TS) interaction $\Delta E^{\neq}_{int}$ between the reactants in the activated complex: $\Delta E^{\neq} = \Delta E^{\neq}_{strain} + \Delta E^{\neq}_{int}$. Interestingly, the activation strain $\Delta E^{\neq}_{strain}$ adopts characteristic values for each type of bond and reaction mechanism. The trend in TS interaction $\Delta E^{\neq}_{int}$ turns out to be mainly determined by the donor–acceptor orbital interactions between occupied Pd-4d AOs and the empty $\sigma^*_{C–X}$ (or $\sigma^*_{H–H}$) acceptor orbital associated with the bond to be activated in the substrate.

5.1 Introduction

Oxidative addition (eq 1) is a key step in many catalytic reactions[1] and has thus been intensively investigated both experimentally[2-7] and theoretically.[5,7-12]

$$ML_n + R{-}X \underset{\text{Reductive Elimination}}{\overset{\text{Oxidative Addition}}{\rightleftharpoons}} R{-}ML_n{-}X \qquad (1)$$

The aim of this investigation is to obtain a better understanding of how the electronic structure of a catalyst determines its reactivity toward the archetypical H–H, C–H, C–C and C–Cl bonds in H_2, CH_4, C_2H_6 and CH_3Cl. This is of interest also for industrial chemistry because it enables a more rational design of catalytically active species. One example is the activation and subsequent functionalization of the rather inert alkanes (e.g. CH_4).[13a] Whereas the long-term purpose of our efforts is understanding and directing, in a rational manner, the factors that determine the catalytic activity and selectivity of transition metal *complexes*, the starting point is the investigation of the *intrinsic* reactivity of the transition metal *atom*. Thus, by introducing ligands in a second stage, it can be precisely assessed how they interfere with the metal electronic structure and how they exactly affect the activity and selectivity of the resulting homogeneous catalyst. This modular approach to theoretical homogeneous catalysis is designated Fragment-oriented Design of Catalysts (FDC).

In the present work, a detailed study of the *intrinsic* reactivity of the uncoordinated Pd(0) atom towards H_2, CH_4, C_2H_6 and CH_3Cl has been carried out using relativistic nonlocal density functional theory (DFT) at the ZORA-BP86/TZ(2)P level (see Section 2). Palladium was chosen because this metal is widely used in catalysis[13] and because the atom has a stable closed-shell d^{10} ground state[8a,h,12b] which facilitates comparison with closed-shell Pd(0) complexes in future investigations. Thus,

the potential energy surfaces (PES) of the following model reactions (eq 2) have been explored:

H–H activation	$Pd + H_2 \rightarrow H–Pd–H$	(2a)
C–H activation	$Pd + CH_4 \rightarrow CH_3–Pd–H$	(2b)
	$Pd + C_2H_6 \rightarrow CH_3CH_2–Pd–H$	(2c)
C–C activation	$Pd + C_2H_6 \rightarrow CH_3–Pd–CH_3$	(2d)
C–Cl activation	$Pd + CH_3Cl \rightarrow CH_3–Pd–Cl$	(2e)

For each of the five model reactions of eq 2, the direct oxidative insertion (OxIn) mechanism (eq 3a) and an alternative S_N2 type reaction which overall leads also to oxidative addition (eq 3b) is studied. In this way, a uniform treatment of different reaction mechanisms for the broad spectrum of H–H, C–H, C–C and C–Cl bond activation is achieved. It was shown previously that the ZORA-BP86/TZ(2)P approach yields reliable trends in reactivity.[14]

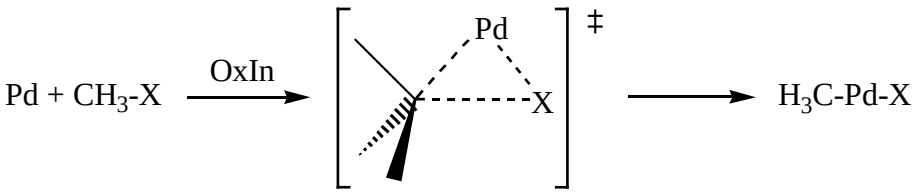

(3a)

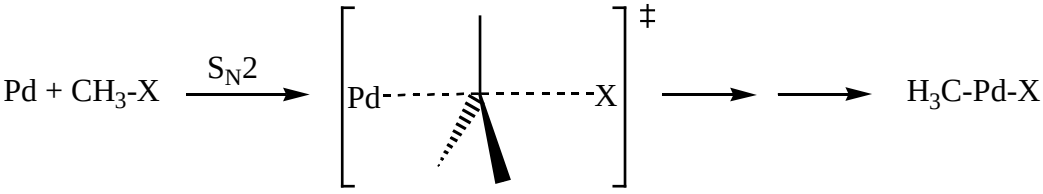

(3b)

Furthermore, the competition between the various bond activation processes and mechanisms is analyzed using the Activation Strain (or Activation strain-TS interaction, ATS) model originally introduced in the context of elementary organic reactions.[10a] In the ATS model, activation energies $\Delta E^{\neq}$ are decomposed into the activation strain $\Delta E^{\neq}_{strain}$ of and the stabilizing transition state (TS) interaction $\Delta E^{\neq}_{int}$

between the reactants in the activated complex: $\Delta E^{\neq} = \Delta E^{\neq}_{strain} + \Delta E^{\neq}_{int}$. At this point, we anticipate that the activation strain $\Delta E^{\neq}_{strain}$ turns out to adopt characteristic values for each type of bond and reaction mechanism. Furthermore, the concept of TS interaction $\Delta E^{\neq}_{int}$ provides the necessary basis for understanding how the activity of a catalyst depends on its electronic structure.

This paper is organized as follows. After the description of our quantum chemical method in Section 5.2, it is proceeded in Section 5.3.1 with the exploration of the PES of the various model reactions. Next, in Sections 5.3.2, the Activation Strain model of chemical reactivity is introduced. This model is applied in Section 5.3.3 in which the competition between, i.e., the relative height of activation barriers of the different model bond activation processes is analyzed. The conclusions are given in Section 5.4.

5.2 Methods

All calculations are based on density functional theory (DFT)[15,16] and have been performed using the Amsterdam-Density-Functional (ADF) program,[17] developed by Baerends *et. al.*[17b,c,d] MOs were expanded in a large uncontracted set of Slater-type orbitals (STOs).[17h] For C, H, O and Cl the basis is of triple-ζ quality, augmented with a 2p and 3d polarization function. The palladium atom is represented by a triple-ζ type basis set augmented with one 5p polarization function. The core shells of carbon (1s), oxygen (1s), chlorine (1s2s2p) and palladium (1s2s2p3s3p3d) were treated by the frozen-core approximation.[17b] An auxiliary set of s, p, d, f and g STOs was used to fit the molecular density and to represent the Coulomb and exchange potentials accurately in each SCF cycle.[17i]

Geometries and energies were calculated using the local density approximation (LDA) with nonlocal corrections (NL). Exchange is described by Slaters Xα potential,[17j] with nonlocal corrections due to Becke.[17k,l] Correlation is treated in the

Vosko-Wilk-Nusair (VWN) parameterization using formula V,[17m] with nonlocal corrections due to Perdew.[17n] Relativistic effects were taken into account by the zeroth-order regular approximation (ZORA).[18] Prior investigations showed that relativistic effects are significant for our systems, and that the ZORA formalism is well suited for describing them.[14]

All energy minima and transition state[17r] structures were verified by frequency calculations:[17q] for minima all normal modes have real frequencies, whereas transition states have one normal mode with an imaginary frequency. The character of the normal mode associated with the imaginary frequency was analyzed to ensure that the correct transition state was found.

Bond enthalpies at 298.15 K and 1 atmosphere (ΔH_{298}) were calculated from 0 K electronic bond energies (ΔE) according to eq 6, assuming an ideal gas.[19]

$$\Delta H_{298} = \Delta E + \Delta E_{\mathrm{trans},298} + \Delta E_{\mathrm{rot},298} + \Delta E_{\mathrm{vib},0} + \Delta(\Delta E_{\mathrm{vib},0})_{298} + \Delta(pV) \qquad (6)$$

Here, $\Delta E_{\mathrm{trans},298}$, $\Delta E_{\mathrm{rot},298}$ and $\Delta E_{\mathrm{vib},0}$ are the differences between products and reactants in translational, rotational and zero point vibrational energy, respectively; $\Delta(\Delta E_{\mathrm{vib}})_{298}$ is the change in the vibrational energy difference as one goes from 0 to 298.15 K. The vibrational energy corrections are based on the frequency calculations. The molar work term $\Delta(pV)$ is $(\Delta n)RT$; Δn = -1 for two reactants (Pd and CH_3X) combining to one species. Thermal corrections for the electronic energy are neglected.

5.3 Results and Discussion

5.3.1 Reaction Profiles and Geometries

In this section, the Potential Energy Surfaces (PES) of the various oxidative insertion and S_N2 reactions are discussed. The results are summarized in Figures 1 and 2 (geometries) and Table 1 (energies). First, the direct oxidative insertion (OxIn) reactions are presented. For all substrates, they proceed from a reactant complex via a TS to a product, see Figure 1.

The oxidative insertion of Pd + H_2 comes along with a relatively flat PES, see Table 1. The activation barrier is -21.7 kcal/mol.[20] relative to the reactants. In the transition state, the H–H bond distance has been stretched by 0.634 Å (85%) and amounts to 1.383 Å. There is essentially no reverse barrier; only a slight barrier of 0.5 kcal/mol on the zero-K electronic energy surface.

The C–H activation is investigated using two different substrates, CH_4 (**2a**) and C_2H_6 (**3a**). Thus, we can reveal if, e.g., the activation strain (see Section 5.3.3) adopts characteristic values for a particular type of bond (i.e. the C–H bond) in different substrates. Geometries for both reactions are shown in Figure 1, structures **2a-d** and **3a-d**. Again, one finds a relatively stable reactant complex. Such a high stability is confirmed by gas-phase experiments where corresponding long-range complexes could be found for some alkanes.[7b] For CH_4, eq 2b, the activation enthalpy is -5.0 kcal/mol relative to the reactants. In the TS, the C–H bond has been stretched by 0.517 Å (47%) and amounts to 1.613 Å. The C–H activation in C_2H_6, eq 2c, proceeds via a transition state **3c** at -4.1 kcal/mol relative to the reactants, to a product **3d**. The C–H bond of the TS is lengthened by 0.530 Å (48%) and amounts to 1.629 Å. This is very similar to the C–H activation of CH_4. The reaction may further proceed from **3d** via a second transition state, corresponding to a rotation of the $-CH_2CH_3$ rest, to a more stable conformation. The latter is more stable than the reactant complex.

Table 1. Reaction Profiles at BP86/TZ(2)P for the Oxidative Insertion (OxIn), the S_N2 and the S_N2/Leaving Group Rearrangement Reactions of Pd with H_2, CH_4, C_2H_6 and CH_3Cl: 298 K Enthalpies (in kcal/mol) Relative to the Reactants.

Activated Bond	Reactants	Reactant Complex	Transition State	Product
Oxidative Insertion				
H–H	Pd + H_2	–24.4 (–24.1 [a])	–21.7 (–21.7 [a])	–21.1 (–22.2 [a])
C–H	Pd + CH_4	–11.4	–5.0	–9.7
	Pd + C_2H_6	–11.6	–4.1	–11.6 [b]
C–C	Pd + C_2H_6	–11.6	9.6	–14.1
C–Cl	Pd + CH_3Cl	–15.6	–6.0	–35.7
S_N2 Substitution				
H–H	Pd + H_2	–8.8 [c]	d	237.0 [e]
C–H	Pd + CH_4	–11.4	d	228.7 [e]
C–C	Pd + C_2H_6	–11.6	d	228.6 [e]
C–Cl	Pd + CH_3Cl	–10.1	d	143.5 [e]
S_N2/ Cl-rearrangement				
C–Cl	Pd + CH_3Cl	–10.1	21.2	–35.7

[a] Zero Kelvin electronic energies.
[b] Primary product of insertion. Rearrangement via second TS (–11.0 kcal/mol) to final product (–12.0 kcal/mol).
[c] Minimum energy structure in forced $C_{\infty v}$ symmetry, 2 imaginary frequencies.
[d] No reverse activation barrier.
[e] Dissociated products of straight S_N2 reaction.

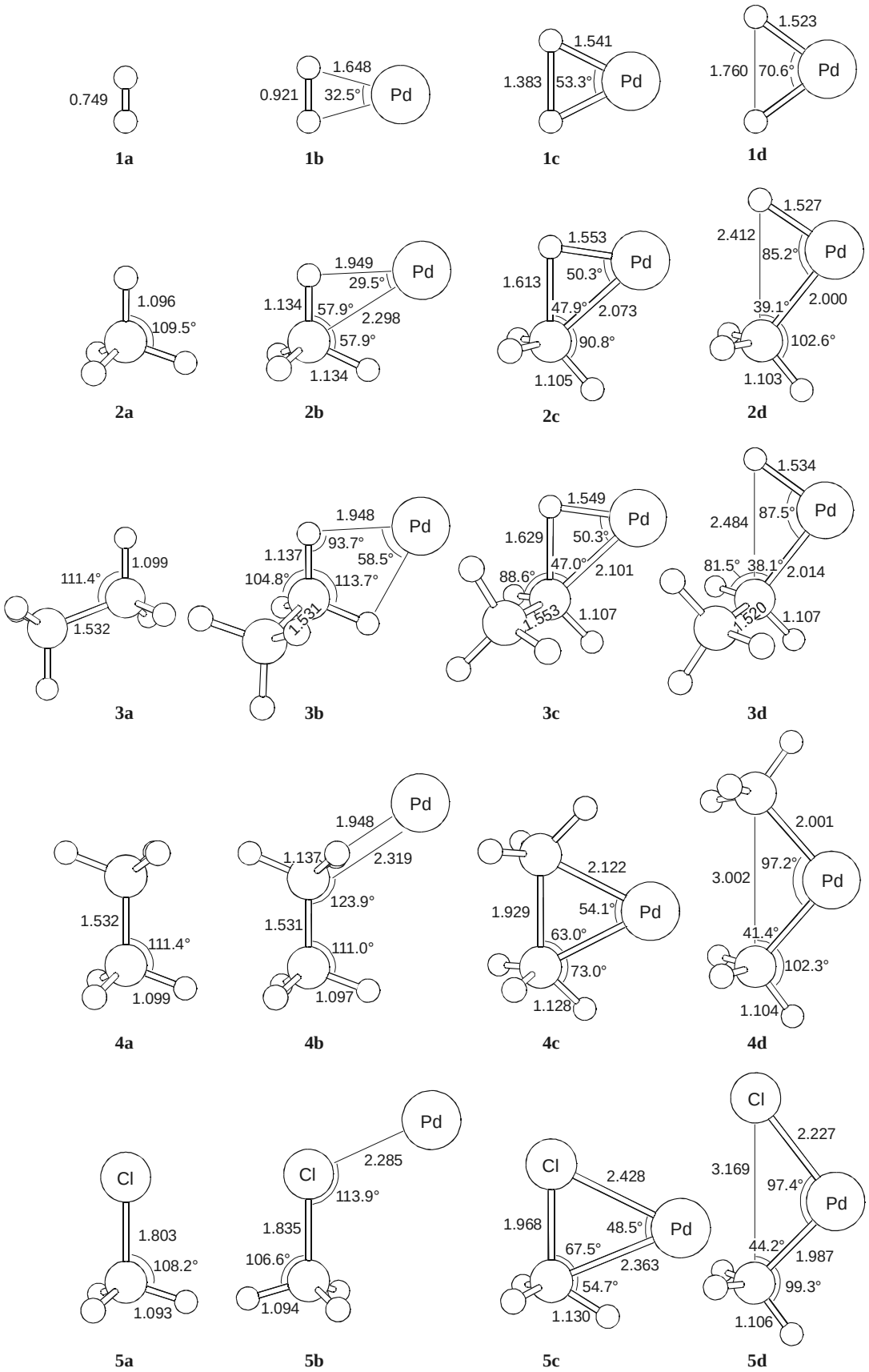

Figure 1. Geometries (in Å, degrees) at ZORA-BP86/TZ(2)P of stationary points along the potential energy surface for oxidative insertion (OxIn) reaction of Pd into: (a) the H–H bond of H_2, (b) the C–H bond of CH_4 (c) the C–H bond of C_2H_6, (d) the C–C bond of C_2H_6, and (e) the C–Cl bond of CH_3Cl.

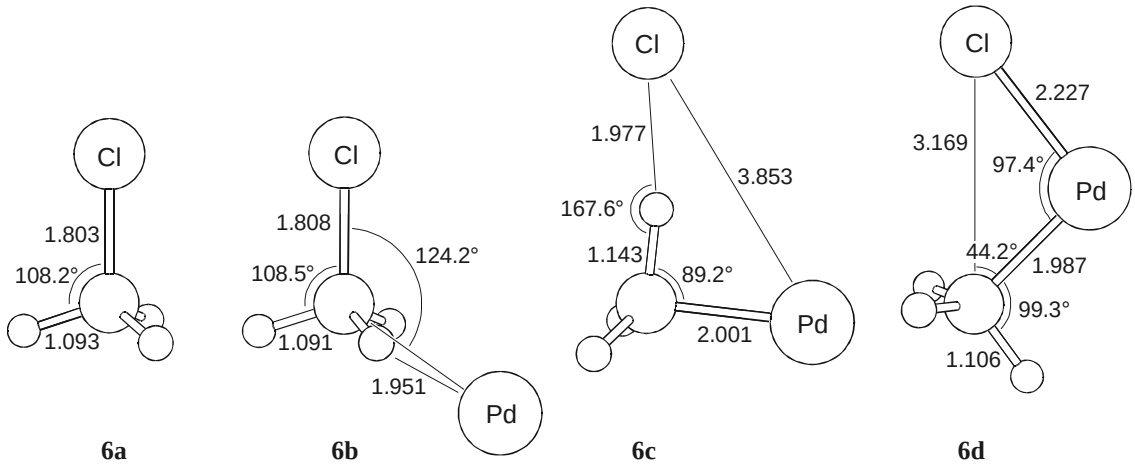

Figure 2. Geometries (in Å, degrees) at ZORA-BP86/TZ(2)P of stationary points along the potential energy surface for the S_N2/Cl^--rearrangement reaction of Pd with CH_3Cl.

The OxIn activation of the C–C bond of ethane (eq 2d) starts from the reactant complex **4b** being identical to structure **3b**. The barrier of the transition state **4c** is with 9.6 kcal/mol significantly higher than in the H–H or C–H activation. Yet, in the TS, the C–C bond is only stretched by 0.397 Å (26%) and amounts to 1.929 Å; the relative stretching is less than in the H–H and C–H activations.

The activation of CH_3Cl **5a** by direct oxidative insertion of Pd is connected with a slight lengthening of the C–Cl bond in the TS: 0.165Å (9%). The bond length is 1.968 Å. The activation barrier of -6.0 kcal/mol is lower than for the C–H and C–C activation; the formation of product **5d** is the most exothermic oxidative addition amongst the model reactions studied.

The activation enthalpies $\Delta H^{\neq}_{298}$ increase in the order H–H < C–Cl ≤ C–H < C–C. Previous explanations concentrate on the directionality of the methyl sp^3 orbital[11n] and on the energy necessary to tilt the methyl groups of CH_4 and C_2H_6 towards the metal:[11i] in C_2H_6, there are two methyl groups to be bend, which leads to a higher barrier. Using the ATS analysis and MO theoretical arguments, we will be able to explain the situation in detail in Section 5.3.3.

Next, the S_N2 type reactions will be discussed. The products of the "straight" S_N2 reaction, i.e., $PdH^+ + H^-$ and $PdCH_3^+ + H^-$, CH_3^- and Cl^-, are highly endothermic due to the charge separation, see Table 1. All S_N2-type reactions occur without reverse activation barrier. In other words, there is no stationary point on the PES associated with a regular S_N2 transition state. However, for reaction 2e, Pd + CH_3Cl, a transition state **6c** could be found which corresponds to an S_N2 substitution occurring in concert with a rearrangement of the leaving group Cl^- (S_N2/Cl-ra), Figure 2. This leads to the oxidative addition product **6d** (which is identical to structure **5d**). For the other substrates, such a TS could not be found. The barrier of the S_N2/Cl-ra pathway of Pd + CH_3Cl, although much lower than for straight S_N2 substitution, is with 21.2 kcal/mol still much higher than the barrier of direct oxidative insertion (-6.0 kcal/mol, Table 1).

5.3.2 Activation-strain TS-interaction Model

The bonding in transition states for oxidative insertion was analyzed in the conceptual framework provided by the Kohn-Sham molecular orbital (KS-MO) model[16] to gain insight into how the activation barriers of the different oxidative insertion reactions arise and how they depend on the electronic structure of catalyst and substrate. This is done using the Activation-strain (or Activation-strain TS-interaction, ATS) model of chemical reactivity (cf. Bickelhaupt[10a]) in which the activation energy $\Delta E^{\neq}$ is decomposed into the activation strain and the transition state interaction $\Delta E^{\neq}_{int}$ (see eq 6 and Figure 3):

$$\Delta E^{\neq} = \Delta E^{\neq}_{strain} + \Delta E^{\neq}_{int} \qquad (6)$$

The activation strain $\Delta E^{\neq}_{strain}$ is the strain energy associated with deforming the reactants from their equilibrium geometry to the geometry they acquire in the activated complex (Figure 3). The TS-interaction $\Delta E^{\neq}_{int}$ is the actual interaction energy between the deformed reactants in the transition state. In the present study, one of the reactants is the Pd-d^{10} atom and the other reactant is one of the substrates H_2, CH_4, C_2H_6, and CH_3Cl.

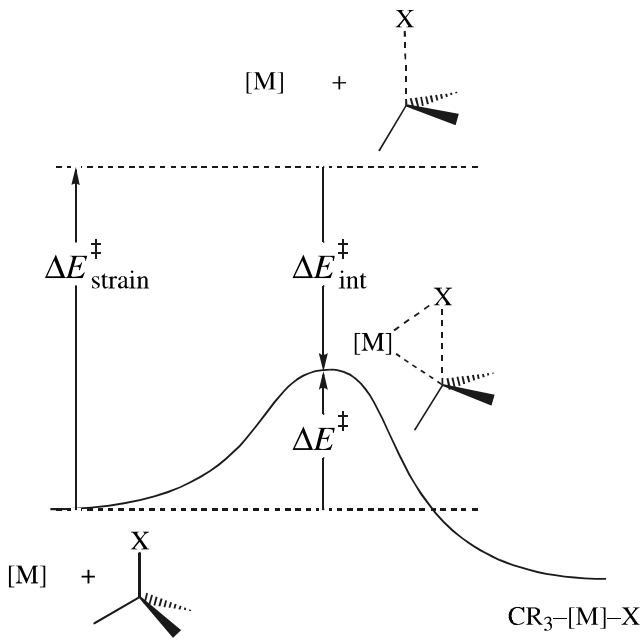

Figure 3. Illustration of the Activation strain-TS interaction (ATS) model in case of C–X bond activation by a transition metal system [M]. The activation energy $\Delta E^{\neq}$ is decomposed into the activation strain $\Delta E^{\neq}_{\text{strain}}$ of and the stabilizing TS interaction $\Delta E^{\neq}_{\text{int}}$ between the reactants in the transition state ($\Delta E^{\neq}_{\text{int}}$ may be further analyzed using, e.g., the ETS method).

The TS interaction $\Delta E^{\neq}_{\text{int}}$ between the strained reactants can be further decomposed into three physically meaningful terms (eq 7) using the extended transition state (ETS) method[21] developed by Ziegler and Rauk.

$$\Delta E^{\neq}_{\text{int}} = \Delta V_{\text{elst}} + \Delta E_{\text{Pauli}} + \Delta E_{\text{oi}} \tag{7}$$

The term ΔV_{elst} corresponds to the classical electrostatic interaction between the unperturbed charge distributions of the deformed reactants and is usually attractive. The Pauli-repulsion ΔE_{Pauli} comprises the destabilizing interactions between occupied orbitals and is responsible for the steric repulsion. The orbital interaction ΔE_{oi} accounts for charge transfer (interaction between occupied orbitals on one moiety with

unoccupied orbitals of the other, including the HOMO–LUMO interactions) and polarization (empty–occupied orbital mixing on one fragment due to the presence of another fragment). As pointed out before, the three terms ΔV_{elst}, ΔE_{Pauli} and ΔE_{oi} should be considered separately.[22]

5.3.3 Analysis of the Activation Barriers for Bond Activation

The results of the ATS analysis are listed in Table 2. It is clear that $\Delta E^{\neq}$ is different for different types of activated bonds whereas for equal bonds (i.e. C–H activation in CH_4, C_2H_6 and, not shown here, CH_3Cl) it is quite similar, independent of the substrate. As will become clear in the following, also the activation strain $\Delta E^{\neq}_{strain}$ adopts specific values for particular bonds to be activated and can therefore be conceived as a characteristic of a particular type of bond.

Importantly, whereas no correlation between the activation energy and the bond strengths or between the activation barrier and the relative bond stretching could be found (*vide supra*), we now see that the stronger the bond, the higher the activation strain, and the higher the bond stretching, the higher the activation strain. As a reminder, the typical strengths and lengths of the bonds under investigation are given: H–H: 104, C–H: 99, C–C: 83, C–Cl: 78 kcal/mol; H–H: ~0.7, C–H: ~1.1, C–C: ~1.5, C–Cl ~1.8 Å.[23] Remembering the relative bond stretching observed in the TS (cmp. Section 5.3.1), i.e. H–H 85%, C–H 47-48%, C–C 26%, C–Cl 9%, one can see that the stronger the bond to be activated, the higher its relative stretching in the TS.

Whereas the activation strain $\Delta E^{\neq}_{strain}$ appears to depend in a straightforward manner on the strength and length of the activated bond, the overall activation barrier $\Delta E^{\neq}$ shows, as already mentioned above, a more complex behavior. This is due to the interplay of $\Delta E^{\neq}_{strain}$ and $\Delta E^{\neq}_{int}$. To understand the TS interaction $\Delta E^{\neq}_{int}$, it is analyzed by decomposing it into electrostatic attraction ΔV_{elst}, Pauli repulsion ΔE_{Pauli} and orbital

Table 2. Analysis of the Activation Energies for the Oxidative Insertion of Pd into the Indicated Bonds of H_2, CH_4, C_2H_6 and CH_3Cl in Terms of the Activation Strain Model.

Substrate	H_2	CH_4	C_2H_6	C_2H_6	CH_3Cl
Activated Bond	H–H	C–H	C–H	C–C	C–Cl
energy decomposition / (kcal/mol)					
$\Delta E^{\neq}$	–21.7	–1.6	–0.7	12.6	–4.3
$\Delta E^{\neq}_{\text{strain}}$	55.6	53.5	54.7	39.4	8.8
$\Delta E^{\neq}_{\text{int}}$	–77.3	–55.1	–55.4	–26.8	–13.1
ΔE_{Pauli}	208.7	211.1	209.8	192.6	112.3
ΔV_{elst}	–183.7	–170.4	–171.9	–139.5	–76.7
ΔE_{oi}	–102.3	–95.8	–93.3	–79.9	–48.7
fragment orbital overlap ⟨ Pd | substrate ⟩					
⟨4d | LUMO⟩	0.300	0.327	0.450	0.129	0.082
⟨5s | HOMO⟩	0.566	0.401	0.359	0.213	0.144
fragment orbital population / *e*					
Pd 5s	0.43	0.38	0.38	0.22	0.18
Pd 4d	9.28	9.32	9.31	9.42	9.59
substrate LUMO	0.45	0.36	0.36	0.25	0.17
substrate HOMO	1.73	1.71	1.74	1.83	1.91
fragment orbital energy / eV					
Pd 5s	–3.423	–3.423	–3.423	–3.423	–3.423
Pd 4d	–4.193	–4.193	–4.193	–4.193	–4.193
substrate LUMO	–2.854	–1.625	–1.597	–0.306	–2.066
substrate HOMO	–8.438	–7.435	–6.806	–7.142	–7.303

interactions ΔE_{oi}.[21] First, electrostatic attraction and Pauli repulsion are inspected. The electrostatic attraction ΔV_{elst} clearly depends on the catalyst-substrate distance. It becomes weaker as the catalyst-substrate distance increases, i.e. in the order H–H > C–H > C–C > C–Cl. Also the Pauli repulsion apparently correlates with the Pd-substrate distance.

Next, the orbital interaction energy ΔE_{oi} will be considered. It becomes weaker in the line H–H > C–H > C–C > C–Cl, see Table 2. It stems from the mixing of the occupied orbitals of one fragment with the unoccupied orbitals of the other fragment, and tightly depends on orbital overlap properties and orbital energies of both the catalyst and the substrate. It is therefore the appropriate term for tuning a catalyst with the help of ligands to optimize it for a specific bond activation process in future application of Fragment-oriented Design of Catalysts (FDC).

Thus, both orbital overlaps and orbital energy matching of the interacting orbitals have to be analyzed in detail to understand the trends in ΔE_{oi}. The analysis of the orbital interactions within the transition states **1c**, **2c**, **3c**, **4c** and **5c** showed that the only important interactions are those between the frontier orbitals, i.e. the donation of the substrate's HOMO into the Pd 5s, and the backdonation from the Pd 4d into the substrate's LUMO. The Pd 5p orbitals do not significantly participate in the interactions. A schematic representation of the frontier orbital interactions in the transition states is given in Figure 4. The LUMOs of the substrates in the TS geometries are the σ^* orbitals of the activated bond. In the following, the orbital interactions are described to obtain insight into the different ΔE_{oi}. First, the overlap properties are considered. Then, the orbital energies are included in the discussion.

Generally, the HOMO-LUMO overlaps depend, of course, on the Pd–substrate distance and, for a given geometry, on the shapes and the nodal structure of the overlapping orbitals. The latter show characteristic differences: The LUMO of H_2, i.e. the $\sigma^*_{H–H}$, possesses one, $\sigma^*_{C–H}$ two, and $\sigma^*_{C–C}$ and $\sigma^*_{C–Cl}$ three nodal planes, see Figure 4. Obviously, if the σ^* orbital has a nodal plane going through one of the atoms

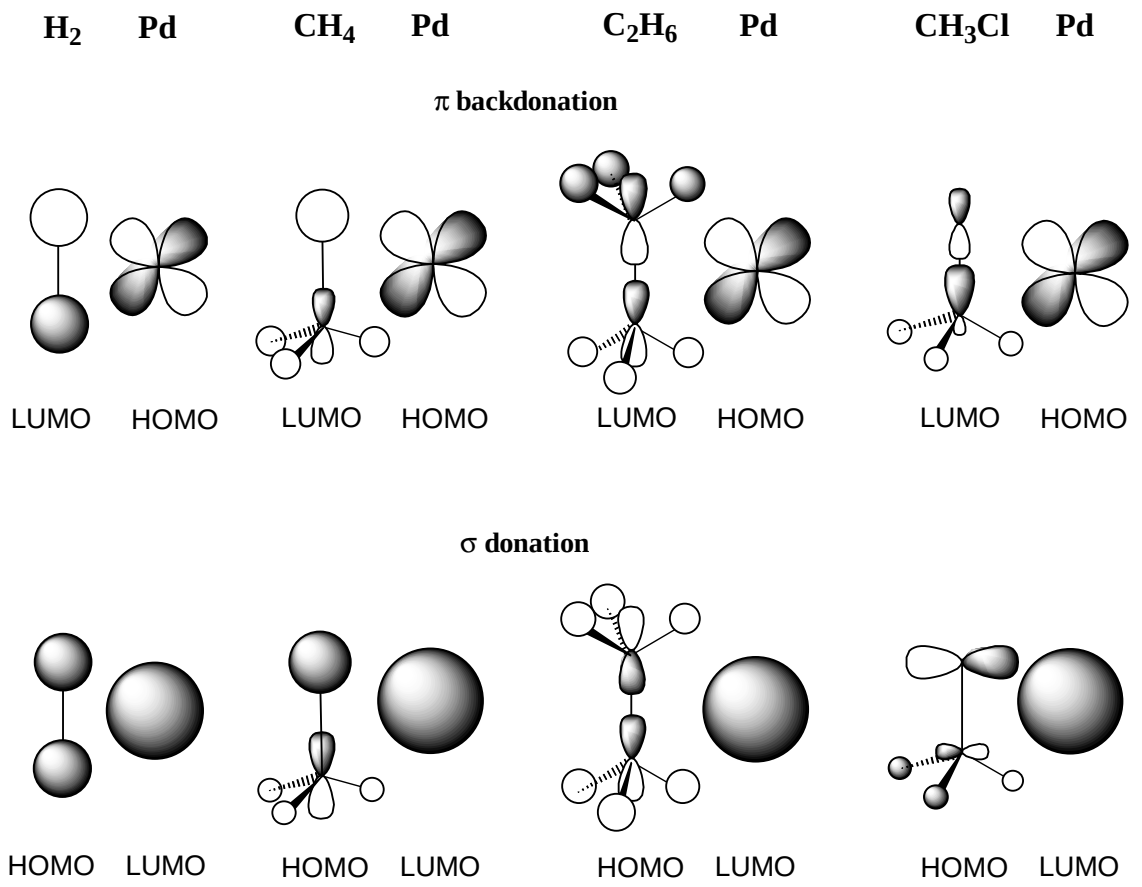

Figure 4. Schematic representation of the frontier orbital interactions between Pd and the substrates H_2, CH_4, C_2H_6 and CH_3Cl in the transition states for oxidative insertion, emerging from the Kohn-Sham MO analyses of the corresponding TS interactions $\Delta E^{\neq}_{\text{int}}$ at ZORA-BP86/TZ(2)P.

belonging to the activated bond (this is the case if there is a p type lobe centered on that atom), the Pd 4d lobe will destructively mix with the orbital part behind this atom. Hence, this atom and the Pd cannot be very close to each other for an optimal $\langle$Pd 4d | $\sigma^*\rangle$ overlap. For the investigated systems, this is nicely demonstrated by the TS of the C–H activation, see Figure 2, structures **2c** and **3c**. Here, the Pd–H distances (1.553 and 1.549 Å) are clearly shorter than the Pd–C distances (2.073 and 2.101 Å).

The ⟨Pd 5s | substrate HOMO⟩ overlaps decrease in the order H–H > C–H > C–C > C–Cl, and nicely correlate with the Pd-catalyst distance. However, this trend is not valid for the ⟨Pd 4d | substrate LUMO⟩ overlaps. As can be seen from Table 2, the ⟨Pd 4d | $\sigma^*_{C–H}$⟩ overlap is higher than ⟨Pd 4d | $\sigma^*_{H–H}$⟩. At first sight, this finding seems to contradict the nodal plane arguments given above, because due to the nodal plane centered on the C atom, the Pd 4d is expected to destructively mix with the p lobe behind the C atom and, therefore, ⟨Pd 4d | $\sigma^*_{C–H}$⟩ should be less than ⟨Pd 4d | $\sigma^*_{H–H}$⟩. However, this trend is masked by the geometrical changes it induces. The Pd–C distance is larger than the Pd–H distance, and, furthermore, the p lobe centered on the C of the C–H bond slightly points toward the Pd atom (for the sake of simplicity, this is not shown in Figure 4). Both factors together allow for the high overlap ⟨Pd 4d | $\sigma^*_{C–H}$⟩. The ⟨Pd 4d | substrate LUMO⟩ overlaps of the C–C and C–Cl activation again correlate with the catalyst-substrate distance, i.e. they become lower with the increase of the catalyst-substrate distance.

The second point to be considered for understanding the orbital interaction energies are the energies of the frontier orbitals, shown in Table 2. Generally, the better the orbital energy matching, the higher the interaction energy. For the backdonation Pd 4d → substrate LUMO, the energy gap becomes larger in the order H–H < C–Cl < C–H < C–C. The differences in the gaps between the Pd 5s and the substrate HOMOs are not that pronounced. The gaps are in the order C–H ≈ C–C ≈ C–Cl < H–H.

With the described overlap and energy matching properties, one is able to understand why the orbital interactions ΔE_{oi} become weaker in the line H–H < C–H < C–C < C–Cl, see Table 2. Starting from the energy matching Pd 4d-substrate LUMO, the order should be H–H < C–Cl < C–H < C–C, see above. Except of the C–Cl, this is the same order as in ΔE_{oi}. However, the overlap of the C–Cl activation is extremely poor and apparently dominates the corresponding interaction. This clarifies why it is the weakest interaction. The increase of the overlap observed in ⟨Pd 4d | substrate LUMO⟩ going from H–H to C–H explains why the difference in ΔE_{oi} is relatively low. The ⟨Pd 5s | substrate HOMO⟩ does not dominate the trend because the energy matching is

much poorer, see Table 2. Apart from providing insight into the bond activation processes as such our analyses illustrate the use of the activation strain model for studying and understanding problems of catalysis and reactivity in general.

5.4 Conclusions

Pd(0)-catalyzed activation of the prototypical H–H, C–H, C–C and C–Cl bonds in H_2, CH_4, C_2H_6 and CH_3Cl, i.e., oxidative addition to a Pd-d^{10} atom is exothermic and occurs via direct oxidative insertion (OxIn) of the metal atom. Activation enthalpies $\Delta H^{\neq}_{298}$ increase in the order H–H < C–Cl ≈ C–H < C–C, as follows from the ZORA-BP86/TZ(2)P investigation. The "straight" S_N2 substitution resulting in $PdCH_3^+ + X^-$ or $PdH^+ + H^-$ is highly endothermic and thus not a competitive alternative for oxidative addition. However, for Pd + CH_3Cl, we find a third mechanism in which S_N2 substitution occurs in concert with a rearrangement of the Cl^- leaving group from C to Pd (S_N2/Cl-ra) leading, in one step, to the oxidative addition product CH_3PdCl via a more moderate activation barrier.

The various bond activation processes have been analyzed using the Activation Strain (or Activation strain-TS interaction, ATS) model in which the activation energy $\Delta E^{\neq}$ is decomposed into the activation strain $\Delta E^{\neq}_{strain}$ of and the stabilizing transition state (TS) interaction $\Delta E^{\neq}_{int}$ between the reactants in the activated complex: $\Delta E^{\neq} = \Delta E^{\neq}_{strain} + \Delta E^{\neq}_{int}$. Interestingly, it turns out that the activation strain $\Delta E^{\neq}_{strain}$ adopts a characteristic value for a particular type of bond and reaction mechanism. In case of the direct oxidative insertion (OxIn) reaction, the activation strain $\Delta E^{\neq}_{strain}$ decreases in the order H–H ≈ C–H < C–C < C–Cl. This trend is determined by two factors: the activation strain $\Delta E^{\neq}_{strain}$ becomes higher (i) if the *strength* of the activated bond increases, and (ii) if the *elongation* of this bond, in terms of percentage, in the TS relative to the isolated substrate increases.

The TS interaction $\Delta E^{\neq}_{int}$ becomes less stabilizing in the order H–H > C–H > C–C > C–Cl. This trend turns out to be mainly determined by the donor–acceptor orbital interactions between occupied Pd 4d AOs and the empty $\sigma^{*}_{C–X}$ (or $\sigma^{*}_{H–H}$) acceptor orbital associated with the bond to be activated in the substrate. The orbital interactions decrease along H–H, C–H and C–C because the σ^{*} acceptor orbital of the substrate goes up in energy leading to a larger HOMO–LUMO gap with the Pd 4d AOs. They further decrease from C–C to C–Cl because of a relatively small Pd 4d–CH_3Cl $\sigma^{*}_{C–Cl}$ overlap.

5.5 References

(1) (a) Collman, J. P.; Hegedus, L. S.; Norton, J. R.; Finke, R. G. *Principles and Applications of Organotransition Metal Chemistry*; University Science Books: Mill Valley, CA, 1987. (b) Elschenbroich, Ch.; Salzer, A. *Organometallics. A Concise Indroduction*, 2nd ed.; VCH: Weinheim, Germany 1992. (c) Amatore, C.; Jutand, A. *Acc. Chem. Res.* **2000**, *33*, 314. (d) Yang, H.; Kotz, K. T.; Asplund, M. C.; Wilkens, M. J.; Harris, C. B. *Acc. Chem. Res.* **1999**, *32*, 551. (e) Sen, A. *Acc. Chem. Res.* **1998**, *31*, 550.

(2) Experimental studies on reactions of metal complexes in the condensed phase: (a) Luh, T.-Y.; Leung, M.-k.; Wong, K.-T. *Chem. Rev.* **2000**, *100*, 3187. (b) Stürmer, R. *Angew. Chem.* **1999**, *111*, 3509. (c) Hau, L.-B.; Tanaka, M. *Chem. Comm.* **1999**, *5*, 395. (d) Casado, A. L.; Espinet, P. *Organometallics* **1998**, *17*, 954. (e) Kayser, B.; Missling, C.; Knizek, J.; Noeth, H.; Beck, W. *Eur. J. Inorg. Chem.* **1998**, *3*, 375. (f) Guillevic, M.-A.; Rocaboy, C.; Arif, A. M.; Horvath, I. T.; Gladysz, J. A. *Organometallics* **1998**, *17*, 707. (g) Edelbach, B. L.; Lachicotte, R. J.; Jones, W. D. *J. Am. Chem. Soc.* **1998**, *120*, 2843. (h) Crabtree, R. H. *Chem. Rev.* **1995**, *95*, 987. (i) Grushin, V. V.; Alper, H. *Chem. Rev.* **1994**, *94*, 1047. (j) Ellis, P. R.; Pearson, J. M.; Haynes, A.; Adams, H.; Bailey, N. A.; Maitlis, P. M. *Organometallics* **1994**, *13*, 3215. (k) Wright, M. W.; Smalley, T. L.; Welker, M. E.; Rheingold, A. L. *J. Am. Chem. Soc.* **1994**, *116*, 6777. (l) Sakakaurka, T.; Sodeyama, T.; Sasaki, K.; Wada, K.; Tanaka, M. *J. Am. Chem. Soc.* **1990**, *112*, 7221. (m) Casalnuovo, A. L.; Calabrese, J. C.; Milstein, D. *J. Am. Chem. Soc.* **1988**, *110*, 6738. (n) Janowics, A. H.; Bergman, R. G. *J. Am. Chem. Soc.* **1983**, *105*, 3929. (o) Jones, W. D.; Feher, F. J. *J. Am. Chem. Soc.* **1982**, *104*, 4240. (p) Hickey, C. E.; Maitlis, P. M. *J. Chem. Soc., Chem. Commun.* **1984**, 1609. (q) Forster, D. *Adv. Organomet. Chem.* **1979**, *17*, 255. (r) Forster, D. *J. Am. Chem. Soc.* **1975**, *97*, 951.

(3) (a) Eller, K.; Schwarz, H. *Chem. Rev.* **1991**, *91*, 1121. (b) Armentrout, P. B.; Beauchamp, J. L. *Acc. Chem. Res.* **1989**, *22*, 315.

(4) Experimental studies on reactions of ionic metal atoms and complexes in the gas phase: (a) Brönstrup, M.; Schröder, D.; Schwarz, H. *Organometallics* **1999**, *18*, 1939. (b) Aschi, M.; Brönstrup, M.; Diefenbach, M.; Harvey, J. N.; Schröder, D.; Schwarz, H. *Angew. Chem.* **1998**, *110*, 858. (c) Freiser, B. S. *J. Mass Spectrom.* **1996**, *31*, 703. (d) van Koppen, P. A. M.; Kemper, P. R.; Bushnell, J. E.; Bowers, M. T. *J. Am. Chem. Soc.* **1995**, *117*, 2098. (e) Wesendrup, R.; Schröder, D.; Schwarz, H. *Angew. Chem.* **1994**, *105*, 1232. (f) Chen, Y.-M.; Clemmer, D. E.; Armentrout, P. B. *J. Am . Chem. Soc.* **1994**, *116*, 7815. (g) van den Berg, K. J.;

Ingemann, S.; Nibbering, N. M. M.; Gregor, I. K. *Rapid. Commun. Mass Spectrom.* **1993**, *7*, 769. (h) Chowdhury, A. K.; Wilkins, C. L. *J. Am. Chem. Soc.* **1987**, *109*, 5336. (i) Weil, D. A.; Wilkins, C. L. *J. Am. Chem. Soc.* **1985**, *107*, 7316. (j) Jones, R. W.; Staley, R. H. *J. Phys. Chem.* **1982**, *86*, 1669. (k) Jones, R. W., Staley, R. H. *J. Am. Chem. Soc.* **1980**, *102*, 3794.

(5) Combined experimental and theoretical studies on reactions of ionic metal atoms and complexes in the gas phase: (a) Yi, S. S.; Reichert, E. L.; Holthausen, M. C.; Koch, W.; Weisshaar, J. C. *Chem. Eur. J.* **2000**, *6*, 2232. (b) Blomberg, M.; Yi, S. S.; Noll, R. J.; Weisshaar, J. C. *J. Phys. Chem. A* **1999**, *103*, 7254. (c) Diefenbach, M.; Brönstrup, M.; Aschi, M.; Schröder, D.; Schwarz, H. *J. Am. Chem. Soc.* **1999**, *121*, 10614. (d) Schwarz, J.; Schröder, D.; Schwarz, H.; Heinemann, C.; Hrusák, J. *Helv. Chim. Acta* **1996**, *79*, 1110.

(6) Experimental studies on reactions of neutral metal atoms in the gas phase: (a) Wen Y.; Porembski, M.; Ferrett, T. A.; Weisshaar, J. C. *J. Phys. Chem. A* **1998**, *102*, 8362. (b) Wen, Y.; Yethiraj, A.; Weisshaar, J. C. *J. Chem. Phys.* **1997**, *106*, 5509. (c) Carroll, J. J.; Weisshaar, J. C. *J. Phys. Chem.* **1996**, *100*, 12355. (d) Chertihin, G. V.; Andrews, L. *J. Am. Chem. Soc.* **1994**, *116*, 8322. (e) Carroll, J. J.; Haug, K. L.; Weisshaar, J. C. *J. Am. Chem. Soc.* **1993**, *115*, 6962. (f) Carroll, J. J.; Weisshaar, J. C. *J. Am. Chem. Soc.* **1993**, *115*, 800. (g) Ritter, D.; Carroll, J. J.; Weisshaar, J. C. *J. Phys. Chem.* **1992**, *96*, *10636*. (h) Mitchell, S. A.; Hackett, P. A. *J. Chem. Phys.* **1990**, *93*, 7822. (i) Ritter, D.; Weisshaar, J. C. *J. Am. Chem. Soc.* **1990**, *112*, 6425. (j) Fayet, P.; Kaldor, A.; Cox, D. M. *J. Chem. Phys.* **1990**, *92*, 254.

(7) Combined experimental and theoretical studies on reactions of neutral metal atoms in the gas phase: (a) Porembski, M.; Weisshaar, J. C. *J. Phys. Chem. A* **2000**, 104, 1524. (b) Carroll, J. J.; Haug, K. L.; Weisshaar, J. C.; Blomberg, M. R. A.; Siegbahn, P. E. M.; Svensson, M. *J. Phys. Chem.* **1995**, *99*, 13955. (c) Carroll, J. J.; Weisshaar, J. C.; Siegbahn, P. E. M.; Wittborn, A. M. C.; Blomberg, M. R. A. *J. Phys. Chem.* **1995**, *99*, 14388. (d) Mitchell, S.; Blitz, M. A.; Siegbahn, P. E. M.; Svenson, M. *J. Chem. Phys.* **1994**, *100*, 423. (e) Weisshaar, J. C. *Acc. Chem. Res.* **1993**, *26*, 213.

(8) Theoretical studies on reactions of metal complexes: (a) Dedieu, A. *Chem. Rev.* **2000**, *100*, 543. (b) Torrent, M.; Solà, M.; Frenking, G. *Chem. Rev.* **2000**, *100*, 439. (c) Griffin, T. R.; Cook, D. B.; Haynes, A.; Pearson, J. M.; Monti, D.; Morris, G. E. *J. Am. Chem. Soc.* **1996**, *118*, 3029. (d) Aullón, G.; Alvarez, S. *Inorg. Chem.* **1996**, *35*, 3137. (e) Ziegler, T. *Chem. Rev.* **1991**, *91*, 651. (f) Koga, N.; Morokuma, K. *Chem. Rev.* **1991**, *91*, 823. (g) Bickelhaupt, F. M.; Baerends, E. J.; Ravenek, W. *Inorg. Chem.* **1990**, *29*, 350. (h) Gritsenko, O. V.; Bagatur'yants, A. A.; Moiseev, I. I.; Kazanskii, V. B. *Russ. Chem. Rev.* **1985**, *54*, 1151.

(9) See also, for example: (a) Lamprecht, D.; Lamprecht, G. J. *J. Comput. Chem.* **2000**, *21*, 692. (b) Minaev, B.; Agren, H. *Int. J. Quantum Chem.* **1999**, *72*, 581. (c) Su, M.-D.; Chu, S.-Y. *J. Am. Chem. Soc.* **1999**, *121*, 1045. (d) Su, M.-D-; Chu, S.-Y. *Inorg. Chem.* **1998**, *37*, 3400. (e) Su, M.-D-; Chu, S.-Y. *Chem. Phys. Lett.* **1998**, *282*, 25. (f) Albert, K.; Gisdakis, P.; Rösch, N. *Organometallics* **1998**, *17*, 1608. (g) Sakaki, S.; Biswas, B.: Sugimoto, M. *Organometallics* **1998**, *17*, 1278. (h) Hill, G. S.; Puddephatt, R. J. *Organometallics* **1998**, *17*, 1478. (i) Sakaki, S.; Ogawa, M.; Kinoshita, M. *J. Phys. Chem.* **1995**, *99*, 9933. (j) Irikura, K. K.; Goddard, W. A., III *J. Am. Chem. Soc.* **1994**, *116*, 8733. (k) Perry, J. K.; Goddard, W. A., III *J. Am. Chem. Soc.* **1994**, *116*, 5013. (l) Sellers, H. *J. Comput. Chem.* **1990**, *11*, 754. (m) Rosi, M.; Bauschlinger Jr., C. W.; Langhoff, S. R.; Partidge, H. *J. Phys. Chem.* **1990**, *94*, 8656. (n) Ziegler, T.; Tschinke, V.; Fan, L.; Becke, A. D. *J. Am. Chem. Soc.* **1989**, *111*, 9177. (o) Low, J. J.; Goddard, W. A., III *J. Am. Chem. Soc.* **1986**, *108*, 6115.

(10) (a) Bickelhaupt, F. M. *J. Comput. Chem.* **1999**, *20*, 114. (b) Bickelhaupt, F. M.; Ziegler, T.; von Ragué Schleyer, P. *Organometallics* **1995**, *14*, 2288.

(11) Theoretical studies on reactions of neutral metal atoms: (a) Maseras, F.; Lledós, A.; Clot, E.; Eisenstein, O. *Chem. Rev.* **2000**, *100*, 601. (b) Cui, Q.; Musaev, D. G.; Morokuma, K. *J. Chem. Phys.* **1998**, *108*, 8418. (c) Wittborn, A. M. C.; Costas, M.; Blomberg, M. R. A.; Siegbahn, P. E. M. *J. Chem. Phys.* **1997**, *107*, 4318. (d) Siegbahn, P. E. M. *J. Am. Chem. Soc.* **1994**, *116*, 7722. (e) Siegbahn, P. E. M. *Organometallics* **1994**, *13*, 2833. (f) Perry, J. K.; Ohanessian, G.; Goddard, W. A., III *Organometallics* **1994**, *13*, 1870. (g) Blomberg, M. R. A.; Siegbahn, P. E. M.; Svensson, M. *Inorg. Chem.* **1993**, *32*, 4218. (h) Siegbahn, P. E. M.; Blomberg, M. R. A.; Svensson, M. *J. Phys. Chem.* **1993**, *97*, 2564. (i) Siegbahn, P. E. M.; Blomberg, M. R. A.; Svensson, M. *J. Am. Chem. Soc.* **1993**, *115*, 1952. (j) Siegbahn, P. E. M.; Blomberg, M. R. A.; Svensson, M. *J. Am. Chem. Soc.* **1993**, *115*, 4191. (k) Siegbahn, P. E. M.; Blomberg, M. R. A. *J. Am. Chem. Soc.* **1992**, *114*, 10548. (l) Blomberg, M. R. A.; Siegbahn, P. E. M.; Svensson, M. *J. Am. Chem. Soc.* **1992**, *114*, 6095. (m) Svensson, M.; Blomberg, M. R. A.; Siegbahn, P. E. M. *J. Am. Chem. Soc.* **1991**, *113*, 7076. (n) Novaro, O.; Jarque, C. *Theor. Chim. Acta* **1991**, *80*, 19. (o) Blomberg, M. R. A.; Siegbahn, P. E. M.; Nagashima, U.; Wennerberg, J. *J. Am. Chem. Soc.* **1991**, *113*, 424. (p) Carter, E. A.; Goddard, W. A., III *J. Phys. Chem.* **1988**, *92*, 5679. (q) Nakatsuji, H.; Hada, M.; Yonezawa, T. *J. Am. Chem. Soc.* **1987**, *109*, 1902. (r) Low, J. J.; Goddard, W. A., III *Organometallics* **1986**, *5*, 609. (s) Koga, N.; Obara, S.; Kitaura, K.; Morokuma, K. *J. Am. Chem. Soc.* **1985**, *107*, 7109. (t) Low, J. J.; Goddard, W. A., III *J. Am. Chem. Soc.* **1984**, *106*, 8321.

(12) Relativistic effects: (a) Moss, R. E. *Advanced Molecular Quantum Mechanics*, Chapman and Hall, London, 1973. (b) Pyykkö, P. *Chem. Rev.* **1988**, *88*, 563. See also: (c) Jensen, F. *Introduction to Computational Chemistry*, Wiley, Chichester, 1999.

(13) (a) Basile, A.; Fasson, S.; Vitulli, G.; Drioli, E. *Stud. Surf. Sci. Catal.* **1998**, *119*, 453. (b) Malleron, J.-L.; Fiaud, J.-C.; Legros, J.-Y. *Handbook of Palladium Catalyzed Organic Reactions*; Academic Press, 1997. (c) Cornils, R.; Herrmann, W. A. *Applied Homogenous Catalysis with Organometallic Compounds. Vol. 1;* VCH: Weinheim, 1996, p. 394.

(14) Diefenbach, A.; Bickelhaupt, F. M., in preparation.

(15) Density functional theory (DFT): (a) Dreizler, R. M.; Gross, E. K. U. *Density Functional Theory. An approach to the Quantum Many-Body Problem*; Springer: Berlin, 1990. (b) Parr, R. G.; Yang, W. *Density-Functional Theory of Atoms and Molecules*; Oxford University Press: New York, 1989. (c) Gritsenko, O. V.; Ensing, B.; Schipper, P. R. T.; Baerends, E. J. *J. Chem. Phys.*, in press.

(16) Kohn-Sham MO model in DFT: (a) Bickelhaupt, F. M.; Baerends, E. J. In *Reviews in Computational Chemistry*, Vol. 15, Lipkowitz, K. B., Boyd., D. B., Eds.; Wiley-VCH: New York, 2000; Vol. 15, Chapter 1. (b) Baerends, E. J.; Gritsenko, O. V. *J. Phys. Chem. A* **1997**, *101*, 5383.

(17) Amsterdam Density Functional (ADF) program: (a) Fonseca Guerra, C.; Visser, O.; Snijders, J. G.; te Velde, G.; Baerends, E. J., *The Parallelization of the Amsterdam Density Functional Program*, In: Methods and Techniques for Computational Chemistry; Clementi, E., Corongiu, G., Eds.; STEF: Cagliari, 1995; p. 305-395. (b) Baerends, E. J.; Ellis, D. E.; Ros, P. *Chem. Phys.* **1973**, *2*, 41. (c) Baerends, E. J.; Ros, P. *Chem. Phys.* **1975**, *8*, 412. (d) Baerends, E. J.; Ros, P. *Int. J. Quantum Chem., Quantum Chem. Symp.* **1978**, *S12*, 169. (e) Fonseca Guerra, C.; Snijders, J. G.; te Velde, G.; Baerends, E. J. *Theor. Chem. Acc.* **1998**, *99*, 391. (f) Boerrigter, P. M.; te Velde, G.; Baerends, E. J. *Int. J. Quantum Chem.* **1988**, *33*, 87. (g) te Velde, G.; Baerends, E. J. *J. Comp. Phys.* **1992**, *99*, 84. (h) Snijders, J. G.; Baerends, E. J.; Vernooijs, P. *At. Nucl. Data Tables* **1982**, *26*, 483. (i) Krijn, J.; Baerends, E. J. *Fit-Functions in the HFS-Method; Internal Report* (in Dutch); Vrije Universiteit: Amsterdam, 1984. (j) Slater, J. C. *Quantum Theory of Molecules and Solids Vol. 4*; McGraw-Hill: New York, 1974. (k) Becke, A. D. *J. Chem. Phys.* **1986**, *84*, 4524. (l) Becke, A. *Phys. Rev. A* **1988**, *38*, 3098. (m) Vosko, S. H.; Wilk, L.; Nusair, M. *Can. J. Phys.* **1980**, *58*, 1200. (n) Perdew, J. P. *Phys. Rev. B* **1986**, *33*, 8822 (Erratum: *Phys. Rev. B* **1986**, *34*, 7406). (o) Fan, L.; Ziegler, T. *J. Chem. Phys.* **1991**, *94*, 6057. (p) Versluis, L.; Ziegler, T. *J. Chem. Phys.* **1988**, *88*, 322. (q) Fan, L.; Versluis, L.; Ziegler, T.; Baerends, E. J.;

Ravenek, W. *Int. J. Quantum. Chem., Quantum. Chem. Symp.* **1988**, *S22*, 173. (r) Fan, L.; Ziegler, T. *J. Chem. Phys.* **1990**, *92*, 3645. (s) Banerjee, A.; Adams, N.; Simons, J.; Shepard, R. *J. Phys. Chem.* **1985**, *89*, 52. (t) Baker, J. *J. Comput. Chem.* **1986**, *7*, 385.

(18) ZORA approach: (a) Chang, C.; Pelissier, M.; Durand, P. *Phys. Scr.* **1986**, *34*, 394. (b) van Lenthe, E.; Baerends, E. J.; Snijders, J. G. *J. Chem. Phys.* **1993**, *99*, 4597. (c) van Lenthe, E.; Baerends, E. J.; Snijders, J. G. *J. Chem. Phys.* **1994**, *101*, 9783. (d) van Lenthe, E.; Snijders, J.; Baerends, E. J. *J. Chem. Phys.* **1996**, *105*, 6505. (e) van Lenthe, E. *Thesis*, Vrije Universiteit, Amsterdam, 1996. (f) van Lenthe, E.; van Leeuwen, R.; Baerends, E. J.; Snijders, J. G. *Int. J. Quantum Chem.* **1996**, *57*, 281.

(19) Atkins, P. W. *Physical Chemistry*; Oxford University Press: Oxford, 1998.

(20) A negative activation energy does not imply the complete absence of any barrier. The reaction is still hampered by a statistical or entropic bottleneck that is associated with the decrease in the number of available quantum states (e.g., of translation, rotation, and vibration) as one goes from the separate, unbound reactants to the tightly bound transition state.

(21) Bond energy decomposition: (a) Ziegler, T.; Rauk, A. *Inorg. Chem.* **1979**, *18*, 1558. (b) Ziegler, T.; Rauk, A. *Inorg. Chem.* **1979**, *18*, 1755. (c) Ziegler, T.; Rauk, A. *Inorg. Chem.* **1977**, *46*, 1. (d) Bickelhaupt, F.M.; Nibbering, N.M.M.; van Wezenbeek, E.M.; Baerends, E.J. *J. Phys. Chem.* **1992**, *96*, 4864.

(22) For the importance of considering ΔV_{elst} and $\Delta E_{\mathrm{Pauli}}$ as separate terms, see: (a) Ref. 16a. See also, for example: (b) Diefenbach, A.; Bickelhaupt, F. M.; Frenking, G. *J. Am. Chem. Soc.* **2000**, *122*, 6449. (c) Fonseca Guerra, C.; Bickelhaupt, F.M. *Angew. Chem.* **1999**, *111*, 3120; *Angew. Chem. Int. Ed.* **1999**, *38*, 2942. (d) Fonseca Guerra, C.; Bickelhaupt, F. M.; Snijders, J. G.; Baerends, E. J. *Chem. Eur. J.* **1999**, *5*, 3581. (e) Bickelhaupt, F. M.; Diefenbach, A.; de Visser, S. V.; de Koning, L. J.; Nibbering, N. M. M. *J. Phys. Chem. A* **1998**, *102*, 9549. (f) Bickelhaupt, F. M.; van Eikema Hommes, N. J. R.; Fonseca Guerra, C.; Baerends, E. J. *Organometallics* **1996**, *15*, 2923. (g) Bickelhaupt, F. M.; Nibbering, N. M. M.; Baerends, E. J.; Ziegler, T. *J. Am. Chem. Soc.* **1993**, *115*, 9160.

(23) Holleman, A. F.; Wiberg, N. *Lehrbuch der Anorganischen Chemie*; de Gruyter: Berlin, 1985.

6 Activation of H–H, C–H, C–C and C–Cl Bonds by Pd and $PdCl^-$

The Mechanism of Anion Assistance in Terms of the Activation Strain Model

Abstract

To understand the mechanism of anion assistance in palladium-catalyzed H–H, C–H, C–C and C–Cl bond activation, several mechanistic pathways for oxidative addition of Pd and $PdCl^-$ to H_2 (H–H), CH_4 (C–H), C_2H_6 (C–C and C–H) and CH_3Cl (C–Cl) were studied uniformly at the ZORA-BP86/TZ(2)P level of relativistic nonlocal density functional theory (DFT). Oxidative addition of the neutral, uncoordinated Pd atom proceeds via direct oxidative insertion ($\Delta H^{\neq}_{298}$ is –22 to 10 kcal/mol) whereas the straight S_N2 substitution is highly endothermic (144 - 237 kcal/mol) and thus not competitive. Anion assistance (i.e. going from Pd to $PdCl^-$) lowers activation barriers and increases the exothermicity of all model reactions studied. The effect is selective as it favors the highly endothermic S_N2 mechanism over direct oxidative insertion (OxIn). Activation enthalpies $\Delta H^{\neq}_{298}$ for oxidative insertion of $PdCl^-$ increase along H–H (–36.0 kcal/mol) < C–H (–14.0 and –13.5 for CH_4 and C_2H_6 kcal/mol) ≈ C–Cl (–11.2 kcal/ mol) < C–C (6.4 kcal/mol), i.e., essentially in the same order as for neutral Pd. Interestingly, in case of $PdCl^-$ + CH_3Cl, the two-step mechanism of S_N2 substitution followed by leaving-group rearrangement becomes the preferred mechanism for oxidative addition. The highest overall barrier of this pathway (–20.2 kcal/mol) drops below the barrier for direct oxidative insertion (–11.2 kcal/mol). The effect of anion assistance is analyzed using the Activation Strain (or Activation strain-TS interaction, ATS) model in which activation energies $\Delta E^{\neq}$ are decomposed into the activation strain $\Delta E^{\neq}_{strain}$ of and the stabilizing transition state (TS) interaction $\Delta E^{\neq}_{int}$ between the reactants in the activated complex: $\Delta E^{\neq} = \Delta E^{\neq}_{strain} + \Delta E^{\neq}_{int}$. For each type of activated bond and reaction mechanism, the activation strain $\Delta E^{\neq}_{strain}$ adopts characteristic values which differ only slightly for corresponding reactions of Pd and $PdCl^-$. The lowering of activation barriers through anion assistance is caused by a stronger, more stabilizing TS interaction $\Delta E^{\neq}_{int}$.

6.1 Introduction

Modern synthetic and industrial chemistry strongly depend on catalysis. Oxidative addition and reductive elimination (eq 1) are key steps in many catalytic reactions[1] and have thus been intensively investigated both experimentally[2-7] and theoretically.[5,7-12]

$$ML_n + R{-}X \underset{\text{Reductive Elimination}}{\overset{\text{Oxidative Addition}}{\rightleftharpoons}} R{-}ML_n{-}X \qquad (1)$$

These studies can basically be divided into two groups associated with two different approaches: (i) the experimental or theoretical investigation of particular transition metal complexes (with more or less realistic model systems in the latter case),[1-5,8,9] and (ii) the investigation of the intrinsic reactivity of metal ions or atoms in the absence of ligands or solvent molecules.[4-7,10,11] Experimentally, the latter is realized by mass spectrometric (metal ions)[3-5] and spectroscopic (neutral metal atoms)[6-7] techniques. Theoretical studies[10,11] play a key role in this approach because they allow for examining model reactions that are experimentally difficult to realize (or even inaccessible) and yet essential for unraveling a particular problem and achieving profound understanding.

Here, an attempt is made to obtain a better understanding of how anion assistance, i.e. the introduction of an additional, negatively charged ligand, influences a catalyst's electronic structure and how this affects its reactivity toward the archetypical H–H, C–H, C–C and C–Cl bonds in H_2, CH_4, C_2H_6 and CH_3Cl. This is of interest also for industrial chemistry because it enables a more rational design of catalytically active species. One example is the activation and subsequent functionalization of the rather inert alkanes (e.g. CH_4).[13] Whereas the long-term purpose of these efforts is understanding and directing, in a rational manner, the factors that determine the catalytic activity and selectivity of transition metal *complexes*, a beginning is made with the investigation of the *intrinsic* reactivity of the transition metal *atom*. Thus, by

introducing ligands in a second stage, one can precisely assess how they interfere with the metal electronic structure and how they exactly affect the activity and selectivity of the resulting homogeneous catalyst. The present study focuses on introducing a single ligand. This modular approach to theoretical homogeneous catalysis is designated Fragment-oriented Design of Catalysts (FDC).

In the present work, a detailed study of the reactivity of $PdCl^-$ toward H_2, CH_4, C_2H_6 and CH_3Cl has been carried out using relativistic nonlocal density functional theory (DFT) at the ZORA-BP86/TZ(2)P level (see Section 2). The reactivity of the monocoordinated $PdCl^-$ complex is then compared with that of the uncoordinated neutral Pd atom studied in Chapter 5. Thus, all together, the potential energy surfaces (PES) of the following model reactions (eq 2) were explored:

H–H activation	$Pd + H_2 \rightarrow H–Pd–H$	(2a)
	$PdCl^- + H_2 \rightarrow H–PdCl–H^-$	(2b)
C–H activation	$Pd + CH_4 \rightarrow CH_3–Pd–H$	(3a)
	$PdCl^- + CH_4 \rightarrow CH_3–PdCl–H^-$	(3b)
	$Pd + C_2H_6 \rightarrow CH_3CH_2–Pd–H$	(4a)
	$PdCl^- + C_2H_6 \rightarrow CH_3CH_2–PdCl–H^-$	(4b)
C–C activation	$Pd + C_2H_6 \rightarrow CH_3–Pd–CH_3$	(5a)
	$PdCl^- + C_2H_6 \rightarrow CH_3–PdCl–CH_3^-$	(5b)
C–Cl activation	$Pd + CH_3Cl \rightarrow CH_3–Pd–Cl$	(6a)
	$PdCl^- + CH_3Cl \rightarrow CH_3–PdCl–Cl^-$	(6b)

For each of the ten model reactions of eq 2, the direct oxidative insertion (OxIn) mechanism (eq 7) and an alternative S_N2 type reaction which overall leads also to oxidative addition (eq 8) is studied. In this way, one achieves a uniform treatment of different reaction mechanisms for the broad spectrum of H–H, C–H, C–C and C–Cl bond activation. It was previously shown that the ZORA-BP86/TZ(2)P approach yields reliable trends in reactivity.[14]

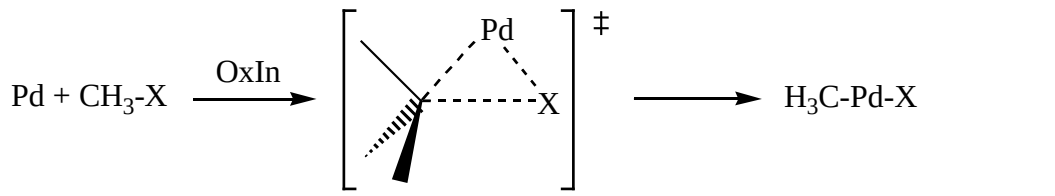

(7)

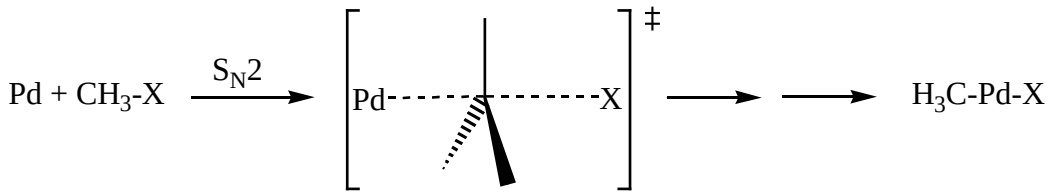

(8)

Furthermore, the effect of anion assistance on the competition between the various bond activation processes and mechanisms is analyzed using the Activation Strain (or Activation strain-TS interaction, ATS) model originally introduced in the context of elementary organic reactions.[10a] In the ATS model, activation energies $\Delta E^{\neq}$ are decomposed into the activation strain $\Delta E^{\neq}_{\text{strain}}$ of and the stabilizing transition state (TS) interaction $\Delta E^{\neq}_{\text{int}}$ between the reactants in the activated complex: $\Delta E^{\neq} = \Delta E^{\neq}_{\text{strain}} + \Delta E^{\neq}_{\text{int}}$. In the course of this work, the interpretative strength of the Activation Strain model will be evaluated.

This chapter is organized as follows. Section 6.2 describes the quantum chemical method, and Section 6.3.1 proceeds with the exploration of the PES of the various model reactions. Next, in Sections 6.3.2, the Activation Strain model of chemical reactivity is introduced. This model is applied in Section 6.3.3 in which the effect of anion assistance on the competition between, i.e., the relative height of activation barriers of the different model bond activation processes is analyzed. The conclusions are given in Section 6.4.

6.2 Methods

All calculations are based on density functional theory (DFT)[15,16] and have been performed using the Amsterdam Density Functional (ADF) program,[17] developed by Baerends and others.[17b-d] MOs were expanded in a large uncontracted set of Slater-type orbitals (STOs).[17h] For C, H, O and Cl the basis is of triple-ζ quality, augmented with a 2p and 3d polarization function. The palladium atom is represented by a triple-ζ type basis set augmented with one 5p polarization function. The core shells of carbon (1s), oxygen (1s), chlorine (1s2s2p) and palladium (1s2s2p3s3p3d) were treated by the frozen-core approximation.[17b] An auxiliary set of s, p, d, f and g STOs was used to fit the molecular density and to represent the Coulomb and exchange potentials accurately in each SCF cycle.[17i]

Geometries and energies were calculated using the local density approximation (LDA) with nonlocal corrections (NL). Exchange is described by Slaters Xα potential[17j] nonlocal corrections owing to Becke.[17k,l] Correlation is treated in the Vosko-Wilk-Nusair (VWN) parameterization (formula V)[17m] with nonlocal corrections due to Perdew.[17n] Relativistic effects were taken into account by the zeroth-order regular approximation (ZORA).[18] Prior investigations showed that relativistic effects are significant for our systems, and that the ZORA formalism is well suited for describing them.[14]

All energy minima and transition state[17r] structures were verified by frequency calculations:[17q] for minima all normal modes have real frequencies, whereas transition states have one normal mode with an imaginary frequency. The character of the normal mode associated with the imaginary frequency was analyzed to ensure that the correct transition state was found.

Bond enthalpies at 298.15 K and 1 atmosphere (ΔH_{298}) were calculated from 0 K electronic bond energies (ΔE) according to eq 9, assuming an ideal gas.[19]

$$\Delta H_{298} = \Delta E + \Delta E_{\mathrm{trans},298} + \Delta E_{\mathrm{rot},298} + \Delta E_{\mathrm{vib},0} + \Delta(\Delta E_{\mathrm{vib},0})_{298} + \Delta(pV) \qquad (9)$$

Here, $\Delta E_{trans,298}$, $\Delta E_{rot,298}$ and $\Delta E_{vib,0}$ are the differences between products and reactants in translational, rotational and zero point vibrational energy, respectively; $\Delta(\Delta E_{vib})_{298}$ is the change in the vibrational energy difference as one goes from 0 to 298.15 K. The vibrational energy corrections are based on the frequency calculations. The molar work term $\Delta(pV)$ is $(\Delta n)RT$; Δn = -1 for two reactants (Pd and CH_3X) combining to one species. Thermal corrections for the electronic energy are neglected.

6.3 Results and Discussion

6.3.1 Reaction Profiles and Geometries

The results are summarized in Figures 1 and 2 (geometries) and Tables 1 (enthalpies), 2 (TS analyses of direct oxidative insertion), 3 and 4 (ATS analyses). For all substrates, the direct oxidative insertion reaction could be completely identified, i.e. stationary points for the reactant complex, the transition state and the product were found on the PES, see Figures 1. On the other hand, all S_N2-type reactions, except for the one of $PdCl^-$ + CH_3Cl, occur without reverse activation barrier (vide infra). The products of the "straight" S_N2 reaction, i.e., $PdClCH_3$ + H^-, CH_3^- and Cl^-, are endothermic although only slightly so for $PdCl^-$ + CH_3Cl. The reaction $PdCl^-$ + CH_3Cl is special in that a genuin transition state **6bCl** (i.e. a first-order saddle point) exists on the PES for S_N2 substitution, and that, proceeding from the S_N2 product complex **6cCl**, the leaving group can rearrange via transition state **6dCl** to form the overall oxidative addition product **6eCl**, see Figure 2.

First, the direct oxidative insertion (OxIn) of Pd into the various bonds is briefly described. For a thorough analysis of the neutral reactions see Ref. 14 and Chapter 5 of this thesis. Then, the effect of anion assistance on the OxIn process will be analyzed. Afterwards, the S_N2 reactions of the neutral and charged systems will be presented.

Table 1. Reaction Profiles at BP86/TZ(2)P for the Oxidative Insertion (OxIn), S_N2 Substitution and S_N2/Cl-rearrangement reactions of Pd with H_2, CH_4, C_2H_6 and CH_3Cl, respectively: 298 K Enthalpies (in kcal/mol) Relative to Reactants.

Activated Bond	**Reactants**	RC [a]	TS [a]	P [a]
		oxidative insertion		
H–H	Pd + H_2	–24.4 (–24.1 [b])	–21.7 (–21.7 [b])	–21.1[c] (–22.2[b])
	$PdCl^-$ + H_2	–36.3 (–36.9 [b])	–36.0 (–35.4 [b])	–36.0[c] (–35.4[b,d])
C–H	Pd + CH_4	–11.4	–5.0	–9.7
	$PdCl^-$ + CH_4	–17.5	–14.0	–15.5
	Pd + C_2H_6	–11.6	–4.1	–11.6 [e]
	$PdCl^-$ + C_2H_6	–17.7	–13.5	–16.1 [f]
C–C	Pd + C_2H_6	–11.6	9.6	–14.1
	$PdCl^-$ + C_2H_6	–17.7	6.4	–16.0
C–Cl	Pd + CH_3Cl	–15.6	–6.0	–35.7
	$PdCl^-$ + CH_3Cl	–20.7	–11.2	–58.7
		S_N2 substitution		
H–H	Pd + H_2	–8.8 [g]	h	237.0 [i]
	$PdCl^-$ + H_2	–12.6 [g]	h	78.5 [i]
C–H	Pd + CH_4	–11.4	h	228.7 [i]
	$PdCl^-$ + CH_4	–17.5	h	88.2 [i]
C–C	Pd + C_2H_6	–11.6	h	228.6 [i]
	$PdCl^-$ + C_2H_6	–16.5	h	88.1 [i]
C–Cl	Pd + CH_3Cl	–10.1	h	143.5 [i]
	$PdCl^-$ + CH_3Cl	–23.9	–22.8 [j]	(–24.1)[k] 3.0 [i]
		S_N2/Cl-rearrangement		
C–Cl	Pd + CH_3Cl	–10.1	21.2	–35.7
	$PdCl^-$ + CH_3Cl	–23.9	–22.8 [j]	(–24.1)[k]
			–20.2 [l]	–58.7 [m]

[a] RC = reactant complex, TS = transition state, P = product (see Figures 2a-e).
[b] Zero-Kelvin electronic energies. – [c] No reverse activation enthalpy.
[d] Essentially no reverse activation energy.
[e] Primary product (P) of insertion. Rearrangement via second TS (–11.0 kcal/mol) to more stable conformation (–12.0 kcal/mol).
[f] Primary product (P) of insertion. Rearrangement via second TS (–15.6 kcal/mol) to more stable conformation (–16.3 kcal/mol).
[g] Minimum energy structure in enforced C_∞ symmetry (2 imaginary frequencies).
[h] No reverse activation barrier. – [i] Products (P) of straight S_N2 substitution.
[j] TS of straight S_N2 substitution. – [k] Product complex (PC) of straight S_N2 substitution.
[l] TS of leaving group rearrangement, proceeding from PC of straight S_N2 reaction of $PdCl^-$ + CH_3Cl (see footnote i).
[m] Oxidative addition product.

Table 2. Stretching of the Activated Bond in the TS for Oxidative Insertion (OxIn) at ZORA-BP86/TZ(2)P.

Activated Bond	Reactants	Length in Substr (Å)	Length in TS (Å)		Stretching in TS (in Å)		Stretching in TS (in %)	
			Pd	$PdCl^-$	Pd	$PdCl^-$	Pd	$PdCl^-$
H–H	Pd + H_2	0.749	1.383	1.354	0.634	0.605	85	81
C–H	Pd + CH_4	1.096	1.613	1.575	0.517	0.479	47	44
	Pd + C_2H_6	1.099	1.629	1.660	0.530	0.561	48	51
C–C	Pd + C_2H_6	1.532	1.929	1.894	0.397	0.362	26	24
C–Cl	Pd + CH_3Cl	1.803	1.968	2.043	0.165	0.240	9	13

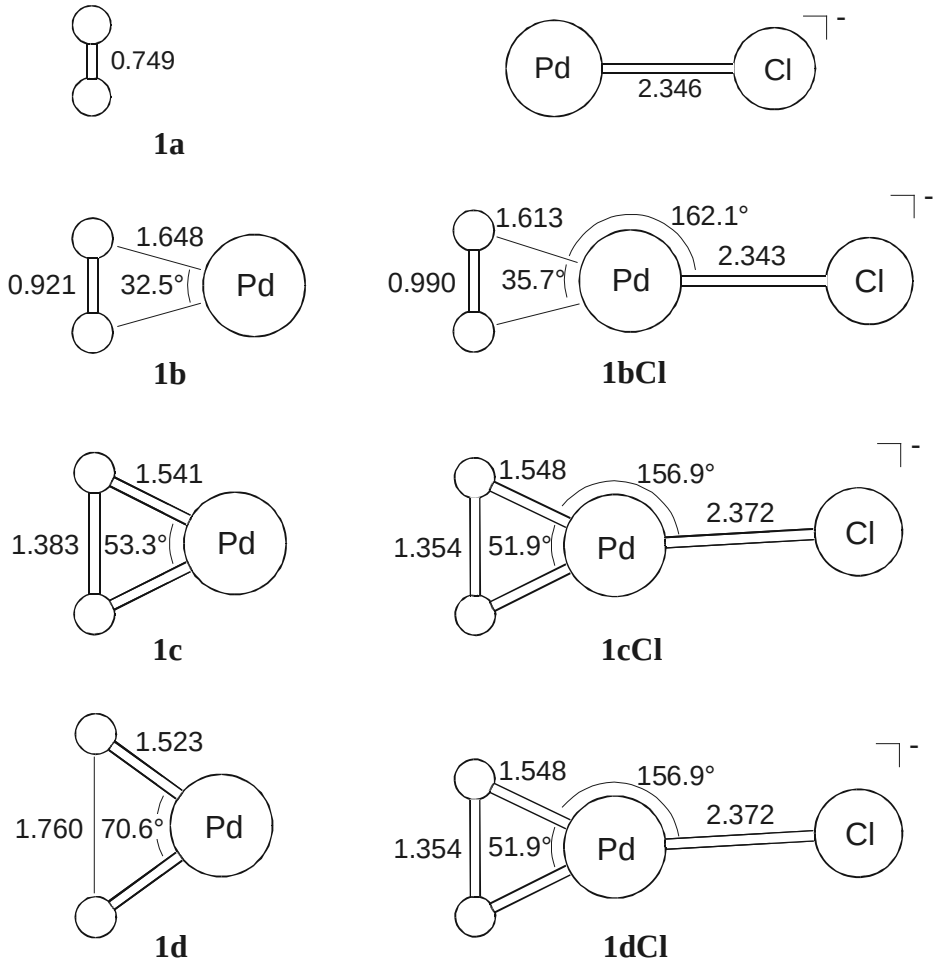

Figure 1a. Geometries (in Å, degrees) at ZORA-BP86/TZ(2)P of stationary points along the potential energy surface for oxidative insertion (OxIn) reaction of Pd and $PdCl^-$ into the H–H bond of H_2.

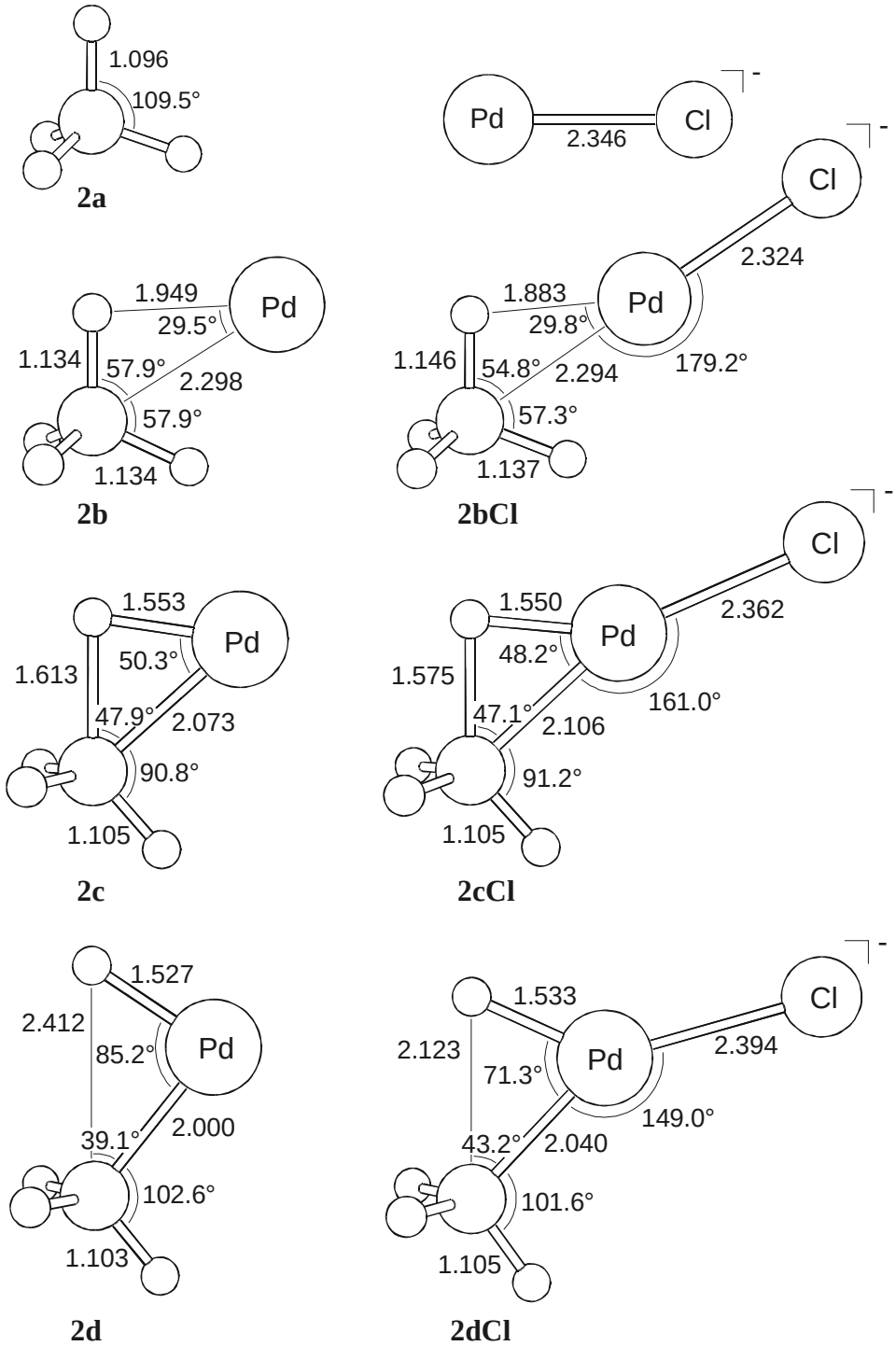

Figure 1b. Geometries (in Å, degrees) at ZORA-BP86/TZ(2)P of stationary points along the potential energy surface for oxidative insertion (OxIn) reaction of Pd and $PdCl^-$ into the C–H bond of CH_4.

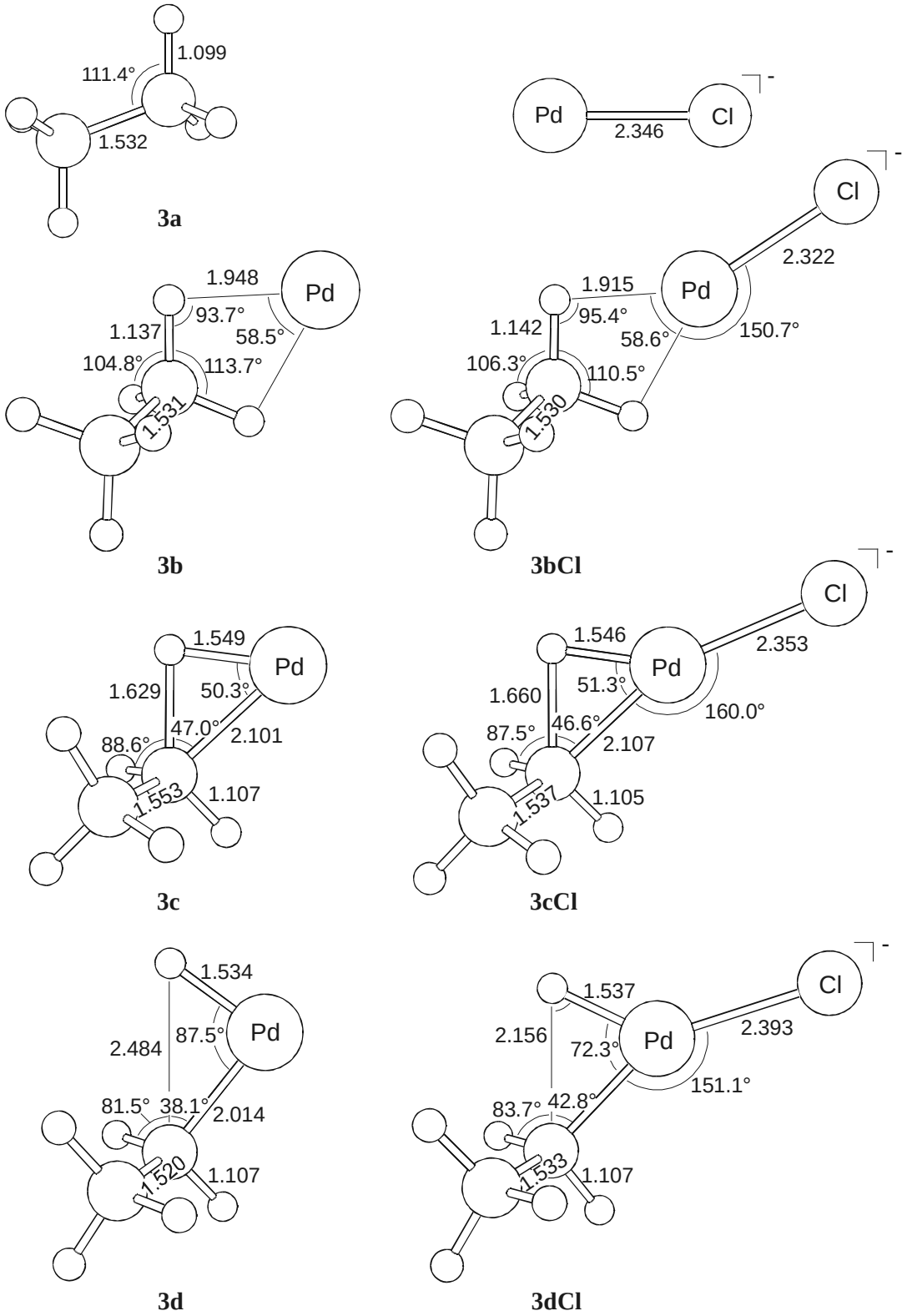

Figure 1c. Geometries (in Å, degrees) at ZORA-BP86/TZ(2)P of stationary points along the potential energy surface for oxidative insertion (OxIn) reaction of Pd and $PdCl^-$ into the C–H bond of C_2H_6.

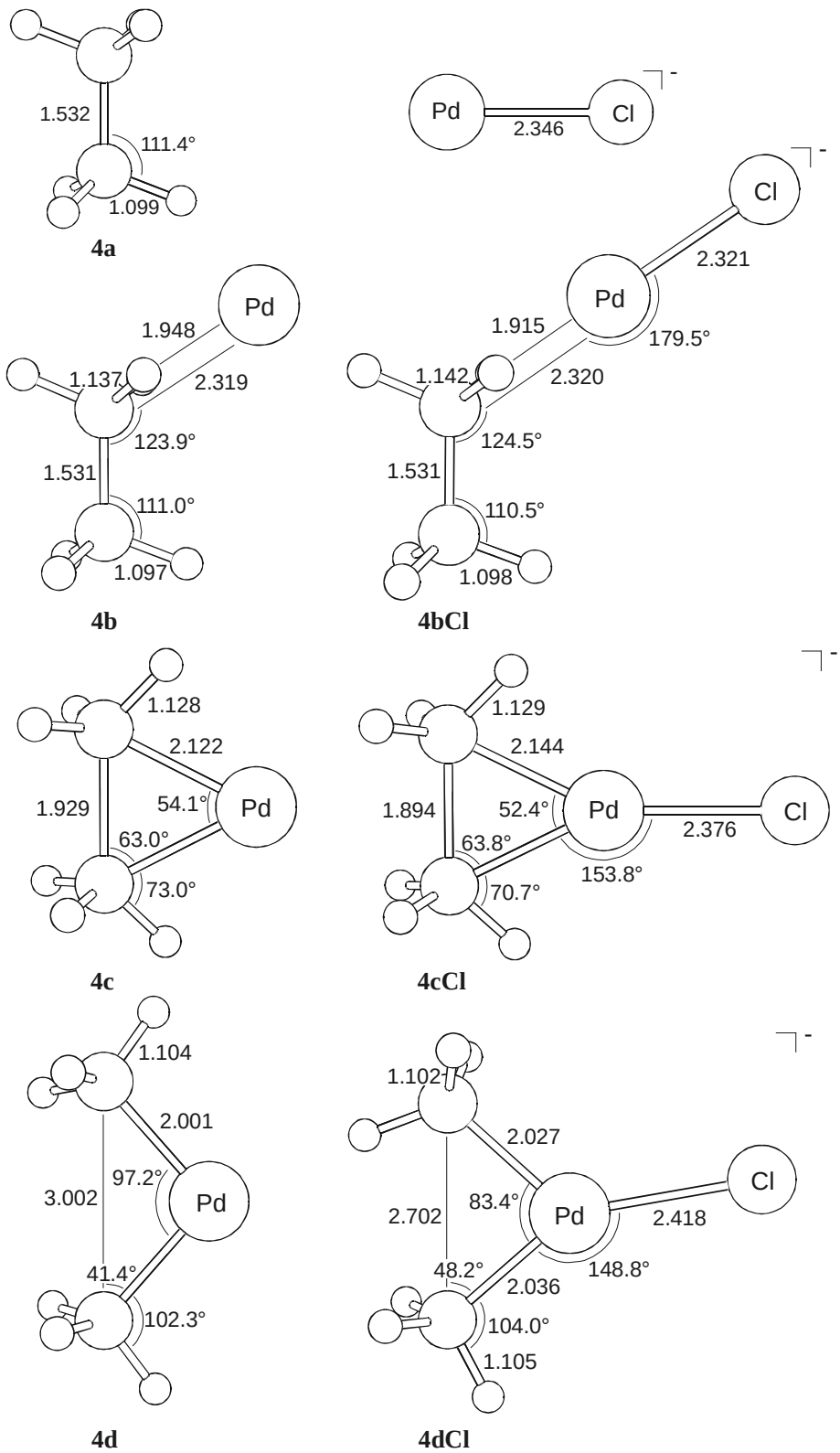

Figure 1d. Geometries (in Å, degrees) at ZORA-BP86/TZ(2)P of stationary points along the potential energy surface for oxidative insertion (OxIn) reaction of Pd and $PdCl^-$ into the C–C bond of C_2H_6.

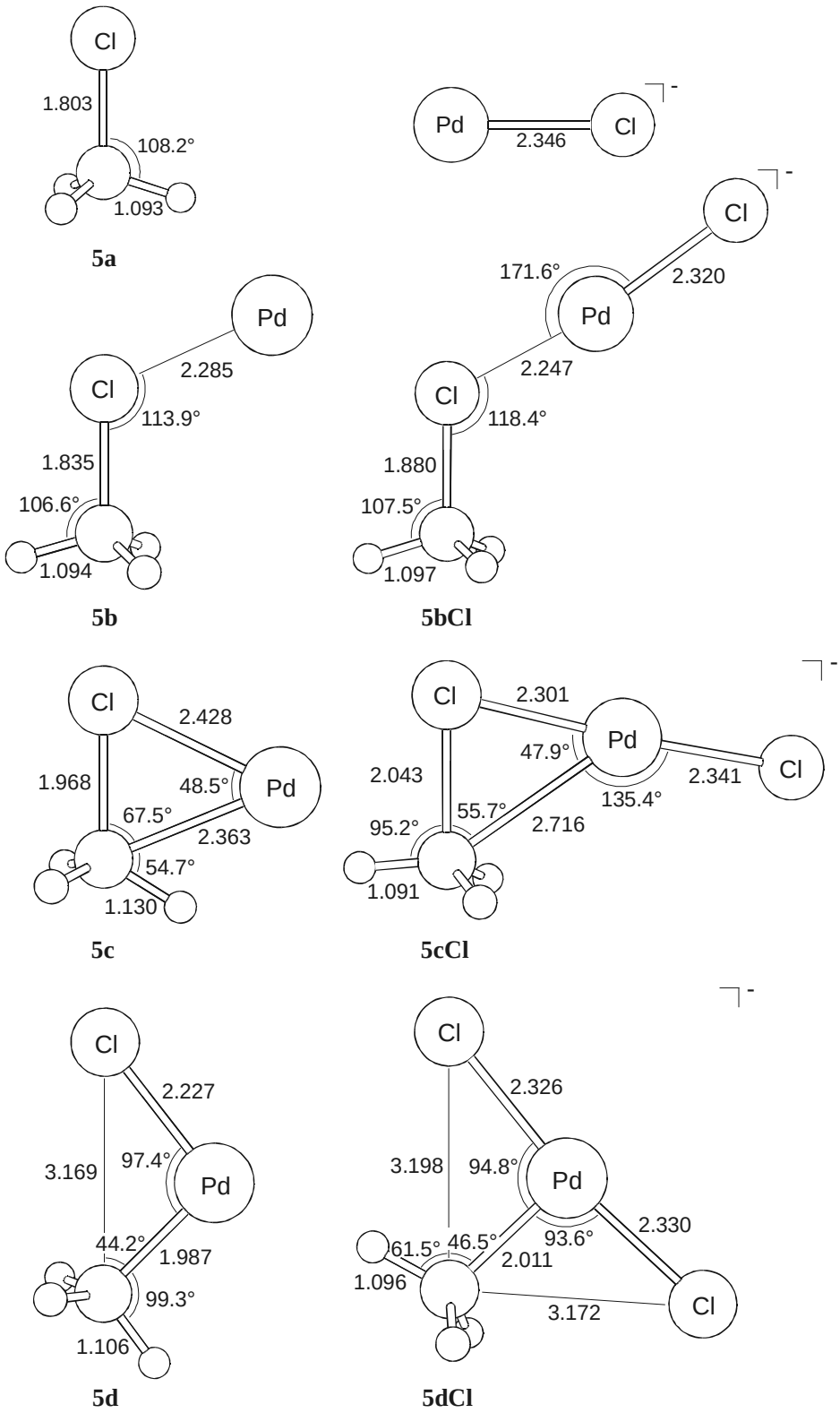

Figure 1e. Geometries (in Å, degrees) at ZORA-BP86/TZ(2)P of stationary points along the potential energy surface for oxidative insertion (OxIn) reaction of Pd and $PdCl^-$ into the C–Cl bond of CH_3Cl.

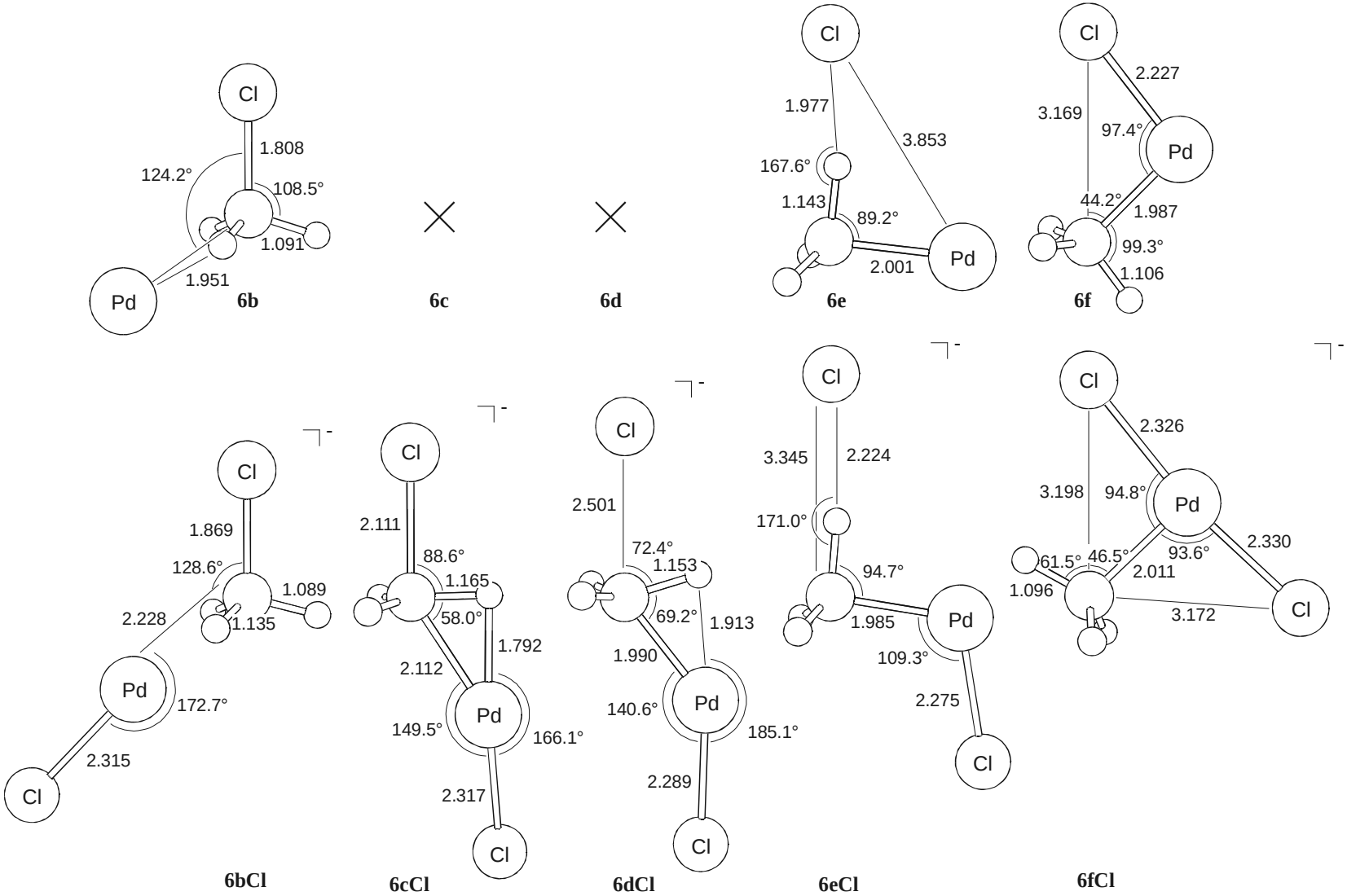

Figure 2. Geometries (in Å, degrees) at ZORA-BP86/TZ(2)P of stationary points along the potential energy surface for the S_N2/Cl^--rearrangement reaction of Pd and $PdCl^-$ with CH_3Cl.

In gas-phase experiments, an insertion of the neutral Pd atom into C–H or C–C bonds of alkanes has not been observed.[7b] However, for alkanes larger than CH_4, collisionally stabilized reactant complexes could be detected by Weisshaar and co-workers.[7b] This is in accordance with the present calculations where relatively stable reactant complexes for each reaction were found, see Table 1. With respect to the free reactants, the 298 K activation enthalpies for oxidative insertion increase in the order H–H (-21.7 kcal/mol) < C–Cl (-6.0 kcal/mol) ≈ C–H (-5.0 and -4.1 kcal/mol for CH_4 and C_2H_6) < C–C (9.6 kcal/mol).[20] For the H–H activation, there is essentially no reverse barrier (only on the zero-K electronic energy surface, there is a slight reverse barrier of 0.5 kcal/mol). All reactions are exothermic. The product **3d** of the Pd insertion into the C_2H_6 C–H bond may be further transformed via a second transition state, corresponding to a rotation of the $-CH_2CH_3$ rest, to a more stable conformation.

An interesting observation can be made in Table 2 for the bond lengths in the Pd catalyzed transition states:[14] the stronger the bond and the more endothermic the reaction, the larger the relative stretching of the activated bond with respect to the free substrates. In particular, the H–H bond (ΔH_{bond} is 104 kcal/mol[21]) has been stretched by 0.634 Å (85%) and amounts to 1.383 Å, the C–H bond (99 kcal/mol) in CH_4 has been stretched by 0.517 Å (47%) to reach 1.613 Å, C–H bond in C_2H_6 has been lengthened by 0.530 Å (48%) and amounts to 1.629 Å, the C–C bond (83 kcal/mol) is stretched by only 0.397 Å (26%) and amounts to 1.929 Å, and, finally, the C–Cl bond (78 kcal/mol) is lengthened by 0.165Å (9%) and amounts to 1.968 Å (see Table 2).

The effect of introducing the anionic chloride ligand on the direct oxidative insertion processes is a stabilization of all stationary points on the PES (i.e. reactant complexes, transition states and products) with respect to the reactants. This means, that the activation barriers are lowered (anion “assistance”) and the overall reactions become more exothermic. The reasons for the stabilization in the TS will be analyzed in Section 6.3.2. Going from Pd to $PdCl^-$, the 298 K activation barriers for oxidative insertion are reduced by 14.3 (H–H) through 3.2 kcal/mol (C–C), and increase along H–H (-36.0 kcal/mol) < C–H (-14.0 and -13.5 kcal/mol for CH_4 and C_2H_6) ≈ C–Cl

(-11.2 kcal/mol) < C–C (6.4 kcal/mol), that is, essentially in the same order as for Pd. Similar to the situation for Pd, essentially no reverse barrier was found for oxidative insertion of $PdCl^-$ into the H–H bond.

As for the Pd catalyzed species, the stretching of the $PdCl^-$ activated bonds in the TSs **1cCl** - **6cCl** increases with increasing bond strength and endothermicity of the reaction (see Table 2): the H–H bond is stretched by 0.605 Å (81%) and amounts to 1.345 Å, the C–H bond in CH_4 is stretched by 0.479 Å (44%) and amounts to 1.575 Å, the C–H in C_2H_6 is stretched by 0.561 Å (51%) and amounts to 1.660 Å, the C–C bond is stretched by 0.362 Å (24%) and amounts to 1.894 Å, and the C–Cl bond is stretched by 0.240 Å (13%) and amounts to 2.043 Å. It can be seen that the percentage of the bond stretching is in the same order for Pd and $PdCl^-$ and is primarily determined by the bond type.

Next, the S_N2-type reactions will be described. The products of the straight S_N2 reactions of Pd with the various substrates are $PdH^+ + H^-$ and $PdCH_3^+ + X^-$ (X = H, CH_3, Cl), in which a charge separation has occurred. All of these products are very endothermic, e.g. 228.6 kcal/mol for the C–C activation, see Table 1. If one goes to $PdCl^-$ as model catalyst, there is no longer a charge separation and, therefore, the endothermicity is strongly reduced, e.g. down to 88.1 kcal/mol for the C–C activation, see Table 1. Still, the S_N2 reaction proceed without reverse barrier in all cases except for the reaction of $PdCl^- + CH_3Cl$.

As pointed out above, for $PdCl^- + CH_3Cl$, a regular S_N2 transition state **6cCl** was found that separates the reactant complex **6bCl** from a product complex **6dCl**, [PdCl-CH_3, Cl^-], Figure 2. Dissociation of this complex leads to the products of the straight S_N2 substitution at 3.0 kcal/mol relative to reactants (Table 1). However, a second transition state **6eCl** was found which corresponds to a rearrangement of the leaving group Cl^- (S_N2/Cl-ra) yielding the net oxidative addition product **6fCl** being identical with **5dCl**. We recall that for Pd + CH_3Cl a similar TS was found, **6e**, but there the S_N2

substitution and Cl^- rearrangement take place in a concerted fashion, i.e., in one elementary step without a separate TS or product complex for the substitution process.

It is interesting to compare the energies of the S_N2/Cl-rearrangement reactions, see Table 1. The effect of the additional charge on the catalyst is a lowering of the barrier of the rearrangement from 21.2 kcal/mol in the case of **6e** to -20.2 kcal/mol in the case of **6eCl**. Thus, whereas for Pd + CH_3Cl the overall barrier for the pathway of S_N2 substitution followed by Cl^- rearrangement (21.2 kcal/mol) is much higher than that for oxidative insertion (-4.8 kcal/mol), it drops in case of $PdCl^-$ + CH_3Cl to -20.2 kcal/mol, i.e., well below the oxidative insertion barrier of -11.2 kcal/mol. Hence, for $PdCl^-$ + CH_3Cl, the two-step S_N2/Cl-ra mechanism becomes the lower barrier pathway for oxidative addition. This, and the reduced endothermicity of the straight S_N2 substitutions show that anion assistance favors the S_N2 pathway over direct oxidative insertion. The origin of this effect is analyzed in Section 6.3.3 using the Activation Strain model, which will be introduced in the following section.

6.3.2 Activation Strain-TS Interaction Model

The bonding in transition states for oxidative insertion was analyzed in the conceptual framework provided by the Kohn-Sham molecular orbital (KS-MO) model[16] to gain insight into how the activation barriers of the different oxidative insertion reactions arise and how they depend on the electronic structure of catalyst and substrate. This is done using the Activation strain (or Activation strain-TS interaction, ATS) model of chemical reactivity (cf. Bickelhaupt[10a]) in which the activation energy $\Delta E^{\neq}$ is decomposed into the activation strain and the transition state interaction $\Delta E^{\neq}_{int}$ (see eq 6 and Figure 3):

$$\Delta E^{\neq} = \Delta E^{\neq}_{strain} + \Delta E^{\neq}_{int} \qquad (6)$$

The activation strain $\Delta E^{\neq}_{strain}$ is the strain energy associated with deforming the reactants from their equilibrium geometry to the geometry they acquire in the activated complex (Figure 3). The TS interaction $\Delta E^{\neq}_{int}$ is the actual interaction energy between the deformed reactants in the transition state. In the present study, one of the reactants

is either the neutral, uncoordinated Pd-d^{10} atom or the anionic model complex $PdCl^-$ and the other reactant is one of the substrates H_2, CH_4, C_2H_6, or CH_3Cl.

The TS interaction $\Delta E^{\neq}_{int}$ between the strained reactants can be further decomposed into three physically meaningful terms (eq 7) using the extended transition state (ETS) method[22] developed by Ziegler and Rauk

$$\Delta E^{\neq}_{int} = \Delta V_{elst} + \Delta E_{Pauli} + \Delta E_{oi} \quad (7)$$

The term ΔV_{elst} corresponds to the classical electrostatic interaction between the unperturbed charge distributions of the deformed reactants and is usually attractive. The Pauli-repulsion ΔE_{Pauli} comprises the destabilizing interactions between occupied orbitals and is responsible for the steric repulsion. The orbital interaction ΔE_{oi} accounts for charge transfer (interaction between occupied orbitals on one moiety with unoccupied orbitals of the other, including the HOMO–LUMO interactions) and polarization (empty–occupied orbital mixing on one fragment due to the presence of another fragment). As pointed out before, the three terms ΔV_{elst}, ΔE_{Pauli} and ΔE_{oi} should be considered separately.[23]

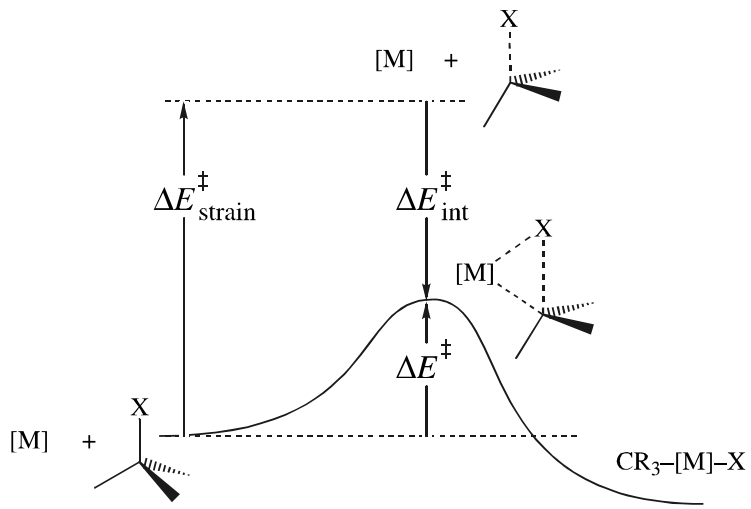

Figure 3. Illustration of the Activation strain-TS interaction (ATS) model in case of C–X bond activation by a transition metal system [M]. The activation energy $\Delta E^{\neq}$ is decomposed into the activation strain $\Delta E^{\neq}_{strain}$ of and the stabilizing TS interaction $\Delta E^{\neq}_{int}$ between the reactants in the transition state ($\Delta E^{\neq}_{int}$ may be further analyzed using, e.g., the ETS method).

Table 3. Analysis of the Activation Energies for the Oxidative Insertion of Pd and $PdCl^-$ into the Indicated Bonds of H_2, CH_4, C_2H_6 and CH_3Cl in Terms of the Activation Strain Model.

Substrate (Bond)	**H_2 (H–H)**		**CH_4 (C–H)**		**C_2H_6 (C–H)**		**C_2H_6 (C–C)**		**CH_3Cl (C–Cl)**	
Catalyst	**Pd**	**$PdCl^-$**	**Pd**	**$PdCl^-$**	**Pd**	**$PdCl^-$**	**Pd**	**$PdCl^-$**	**Pd**	**$PdCl^-$**
energy decomposition / (kcal/mol)										
$\Delta E^{\neq}$	–21.7	–35.4	–1.6	–11.1	–0.7	–10.3	12.6	9.1	–4.3	–10.3
$\Delta E^{\neq}_{\text{strain}}$	55.6	53.3	53.5	49.7	54.7	58.1	39.4	36.3	8.8	9.6
$\Delta E^{\neq}_{\text{int}}$	–77.3	–88.7	–55.1	–60.8	–55.4	–68.4	–26.8	–27.2	–13.1	–19.9
ΔE_{Pauli}	208.7	171.2	211.1	169.4	209.8	184.1	192.6	180.7	112.3	89.3
ΔV_{elst}	–183.7	–168.2	–170.4	–143.3	–171.9	–159.2	–139.5	–126.1	–76.7	–66.9
ΔE_{oi}	–102.3	–91.7	–95.8	–86.9	–93.3	–93.3	–79.9	–81.8	–48.7	–42.3
fragment orbital overlap ⟨ catalyst | substrate ⟩										
⟨HOMO | LUMO⟩	0.300	0.378	0.327	0.263	0.450	0.539	0.129	0.093	0.082	0.042
⟨LUMO | HOMO⟩	0.566	0.706	0.401	0.425	0.359	0.396	0.213	0.212	0.144	0.229
fragment orbital population / *e*										
catalyst LUMO	0.43	0.20	0.38	0.10	0.38	0.11	0.22	0.04	0.18	0.11
catalyst HOMO	9.28	9.32	9.32	9.34	9.31	9.27	9.42	9.32	9.59	9.57
substrate LUMO	0.45	0.55	0.36	0.46	0.36	0.51	0.25	0.31	0.17	0.31
substrate HOMO	1.73	1.89	1.71	1.85	1.74	1.86	1.83	1.89	1.91	1.90
fragment orbital energy / eV										
catalyst LUMO	–3.423	1.789	–3.423	1.800	–3.423	1.810	–3.423	1.785	–3.423	1.823
catalyst HOMO	–4.193	0.813	–4.193	0.814	–4.193	0.814	–4.193	0.812	–4.193	0.804
substrate LUMO	–2.854	–2.708	–1.625	–1.412	–1.597	–1.757	–0.306	–0.164	–2.066	–2.437
substrate HOMO	–8.438	–8.496	–7.435	–7.598	–6.806	–6.835	–7.142	–7.472	–7.303	–7.097

6.3.3 Analysis of the Activation Barriers

The purpose of this section is to understand how the activation barrier of the various model bond activation processes arise and to clarify the origin of the effect of anion assistance. The analyses are based on the Activation strain-TS interaction model described in Section 6.3.2. The results of the analyses are summarized in Tables 3 (direct oxidative insertion) and 4 (S_N2 reactions). The investigations start with the ATS analyses of the direct oxidative insertion processes in Section 6.3.3.1 and the S_N2 pathways in Section 6.3.3.2.

6.3.3.1 Analysis of the Direct Oxidative Insertion Transition States

The analyses of the activation barrier $\Delta E^{\neq}$ in terms of the activation strain $\Delta E^{\neq}_{\text{strain}}$ and the TS interaction $\Delta E^{\neq}_{\text{int}}$ show that the lowering of the activation barriers through anion assistance is caused by a stronger, more stabilizing TS interaction $\Delta E^{\neq}_{\text{int}}$ (see Table 3). The activation strain, on the other hand, adopts a specific value which differs only marginally for the corresponding Pd and $PdCl^-$ induced reactions. For example, with the additional Cl^-, the barrier of the H–H activation is reduced from –21.7 kcal/mol to –35.4 kcal/mol, the activation strain remains in the same order, i.e. ~54 kcal/mol, and the strength of the TS interaction increases from –77.3 kcal/mol to –88.7 kcal/mol. To understand the reasons for the increase of the TS interaction, it can be further analyzed by separating it into the Pauli repulsion ΔE_{Pauli}, the electrostatic attraction ΔV_{elst} and the attractive orbital interactions ΔE_{oi} and by considering the underlying features in the electronic structure, see Table 3.

Later on, it will be necessary to refer to the electronic structures of Pd and $PdCl^-$. Hence, a short description is given now. The ground state configuration of Palladium(0) is $4d^{10}5s^0$. In terms of the Dewar-Chatt-Duncanson (DCD) model,[24] the Pd 5s AO is the acceptor orbital for substrate→metal donation and the 4d AOs are the donor orbitals which serve for substrate←metal backdonation. The process of bond activation is

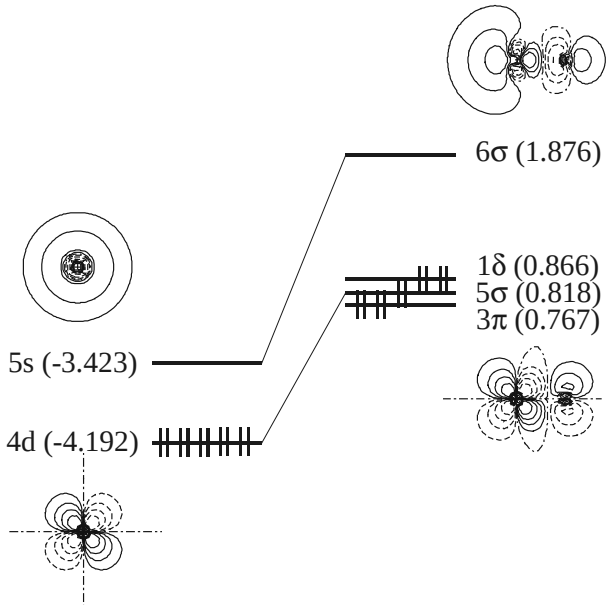

Figure 4. Energy and Shapes of Frontier Orbitals of Pd and $PdCl^-$ (scanvalues: 0.0, ±0.02, ±0.05, ±0.1, ±0.2, ±0.5).

primarily caused by backdonation due to which the antibonding $\sigma^*_{C–X}$ or $\sigma^*_{H–H}$ acceptor orbitals of the substrates get populated. Adding a Cl^- to Pd results in one major effect: the frontier orbital energies rise in energy, see Figure 4, and the formerly degenerate Pd 4d orbitals have been split into the 3π, 5σ and 1δ metal–ligand hybrid orbitals of $PdCl^-$. Furthermore, the orbital shapes are subject to a change.

Next, the decomposition of the TS interaction is considered. The electrostatic attraction ΔV_{elst} becomes weaker as the catalyst–substrate distance in the TS increases, i.e. in the order H–H > C–H > C–C > C–Cl. This is valid for both the Pd and $PdCl^-$ catalyzed systems. There is a striking decrease in Pauli repulsion ΔE_{Pauli} if one goes from Pd to $PdCl^-$ which even compensates for the loss in bonding caused by the weakening in ΔV_{elst}. The explanation for this phenomenon can be found in the

electronic structure of Pd and $PdCl^-$. The rise of the occupied orbitals of the metal system caused by introducing the anionic chloride ligand (see Figure 4) increases the energy difference with the occupied orbitals of the substrates, in particular the substrate HOMO. The larger HOMO–HOMO energy gap translates in a reduced Pauli repulsion.

The orbital interaction energy ΔE_{oi} becomes weaker along H–H ≈ C–H > C–C > C–Cl for both Pd and $PdCl^-$, see Table 3. The orbital interaction energy stems from the mixing of the occupied orbitals of one fragment with the unoccupied orbitals of the other fragment, and tightly depends on orbital overlap properties and orbital energies of both the catalyst and the substrate. The analyses of the attractive orbital interactions showed that only the frontier orbital interactions, i.e. the catalyst HOMO–substrate LUMO and catalyst LUMO–substrate HOMO interactions, are significant. For a discussion of the orbital interactions within the reactions Pd + H_2, CH_4, C_2H_6 and CH_3Cl, the reader is referred to Chapter 5 of this thesis. The orbital interaction of Pd and $PdCl^-$ with one type of bond will be compared in Section 6.3.3.2 to learn about the background of anion assistance.

6.3.3.2 Analysis of the S_N2 Transition States

As pointed out above, for $PdCl^-$ + CH_3Cl, an S_N2 reaction pathway was found that leads via two steps to the net oxidative addition product **5dCl** = **6fCl** and is competitive with oxidative insertion. The first step is the straight S_N2 substitution which occurs with a barrier of –22.8 kcal/mol. In the second step, which proceeds from the S_N2 product complex **6dCl**, the Cl^- leaving group undergoes a rearrangement via transition state **6eCl** at –20.2 kcal/mol relative to reactants ($PdCl^-$ + CH_3Cl) which leads to the oxidative addition product **5dCl** = **6fCl** of the direct oxidative insertion. For the neutral species Pd + CH_3Cl, the corresponding process proceeds via a single TS which has the character of Cl^- rearrangement (a regular S_N2 transition state does not exist) and which

Table 4. Analysis of the Activation Energies for the Straight S_N2 Substitution and Oxidative Insertion Reactions of Pd and $PdCl^-$ with CH_3Cl in Terms of the Activation Strain Model.

	S_N2		**OxIn**	
	Pd [a]	**$PdCl^-$**	**Pd**	**$PdCl^-$**
energy decomposition / (kcal/mol)				
$\Delta E^{\neq}$	0.4	–21.1	–4.3	–10.3
$\Delta E^{\neq}_{strain}$	18.9	18.9	8.8	9.6
$\Delta E^{\neq}_{int}$	–18.5	–40.0	–13.1	–19.9
ΔE_{Pauli}	111.1	98.7	112.3	89.3
ΔV_{elst}	–73.3	–74.9	–76.7	–66.9
ΔE_{oi}	–56.3	–63.9	–48.7	–42.3
fragment orbital overlap ⟨ catalyst | substrate ⟩ [b]				
⟨HOMO | LUMO⟩	0.148	0.307	0.082	0.042
⟨LUMO | HOMO⟩	0.032	0.172	0.144	0.229
fragment orbital population / *e* [b]				
catalyst LUMO	0.19	0.06	0.18	0.11
catalyst HOMO	9.56	9.45	9.59	9.57
substrate LUMO	0.16	0.32	0.17	0.31
substrate HOMO	1.98	1.95	1.91	1.90
fragment orbital energy / eV [b]				
catalyst LUMO	–3.423	1.849	–3.423	1.823
catalyst HOMO	–4.193	0.764, 0.814, 0.869 [c]	–4.193	0.760, 0.814, 0.871 [c]
substrate LUMO	–2.798	–2.798	–2.066	–2.437
substrate HOMO	–6.883	–6.883	–7.303	–7.097

[a] The straight S_N2 substitution with neutral Pd proceeds without reverse activation barrier, i.e., without a saddle point on the PES corresponding to a TS. To nevertheless enable a consistent comparison, the ATS analysis is applied to a fictitious TS with the structure of the TS for straight S_N2 substitution involving $PdCl^-$ with the Cl^- ligand removed from the metal.

[b] For Pd, HOMO refers to the five degenerated 4d AOs and their combined overlaps, populations or their orbital energies. For $PdCl^-$, HOMO refers to the 5σ, two 3π and two 1δ orbitals and their combined overlaps, populations or their orbital energies. The Pd LUMO is the 5s, the $PdCl^-$ LUMO is the 6σ (see also Figure 4).

[c] Energies of $PdCl^-$ 3π, 5σ and 1δ orbitals, respectively.

is *higher* (21.2 kcal/mol) than the TS for oxidative insertion (–6.0 kcal/mol). To trace the origin of these differences, the S_N2 transition state **6cCl** of $PdCl^-$ + CH_3Cl and a fictitious one for Pd + CH_3Cl which derives from the former by removing the Cl^- ligand and keeping the geometry frozen are analyzed with the ATS model. The results are summarized in Table 4.

Comparing the transition state of $PdCl^-$ + CH_3Cl with the fictitious S_N2 transition state of Pd + CH_3Cl, one notices that the activation energy $\Delta E^{\neq}$ of the former is 20 kcal/mol lower than that of the latter. This is in line with the formerly mentioned effect of the lowering of activation barriers by anion assistance (see Section 6.3.1). Note that the addition stabilization in $\Delta E^{\neq}_{int}$ caused by anion assistance is roughly three times larger for S_N2 than for OxIn. In the (fictitious) S_N2 transition state, CH_3Cl fragment is more deformed (i.e., the C–Cl bond is more expanded) than in the OxIn transition state. Consequently, the $\sigma^*_{C–Cl}$ orbital is lower in energy and interacts more strongly with the metal HOMO. Also because of this smaller energy gap, this interaction is more sensitive to changes in the energy of the metal HOMO as one goes from Pd to $PdCl^-$.

6.4 Conclusions

Anion assistance lowers activation barriers and increases the exothermicity of palladium-catalyzed H–H, C–H, C–C and C–Cl bond activation as follows from the ZORA-BP86/TZ(2)P study on the oxidative addition of Pd and $PdCl^-$ to H_2 (H–H), CH_4 (C–H), C_2H_6 (C–C and C–H) and CH_3Cl (C–Cl). Activation enthalpies $\Delta H^{\neq}_{298}$ for oxidative insertion of $PdCl^-$ into the various types of bonds are lower than but increase essentially in the same order as for Pd, that is, along H–H < C–H ≈ C–Cl < C–C.

The effect of anion assistance is selective. It favors the highly endothermic S_N2 mechanism over direct oxidative insertion (OxIn). Interestingly, in case of $PdCl^-$ + CH_3Cl, this leads to the two-step mechanism of S_N2 substitution followed by leaving-group rearrangement (S_N2/Cl-ra) becoming the preferred mechanism for oxidative addition. The highest overall barrier of this pathway (–20.2 kcal/mol) drops below the barrier for direct oxidative insertion (–11.2 kcal/mol). For all other bond activation

processes of $PdCl^-$ (i.e. H–H, C–H, C–C), oxidative insertion remains the lowest-barrier pathway.

The mechanism through which anion assistance works has been analyzed using the Activation Strain (or Activation strain-TS interaction, ATS) model in which activation energies $\Delta E^{\neq}$ are decomposed into the activation strain $\Delta E^{\neq}_{strain}$ of and the stabilizing transition state (TS) interaction $\Delta E^{\neq}_{int}$ between the reactants in the activated complex: $\Delta E^{\neq} = \Delta E^{\neq}_{strain} + \Delta E^{\neq}_{int}$. It is found that, for each particular bond and reaction mechanism, the activation strain $\Delta E^{\neq}_{strain}$ adopts a specific value which differs only marginally for corresponding Pd and $PdCl^-$ induced reactions. Thus, the activation strain can be conceived as a characteristic of the bond and the mechanism of its activation, in line with previous findings for elementary organic E2 and S_N2 reactions.[10a]

The lowering of activation barriers through anion assistance is caused by a stronger, more stabilizing TS interaction $\Delta E^{\neq}_{int}$. This increase in $\Delta E^{\neq}_{int}$ can be ascribed to the raise in Pd-4d derived orbitals in $PdCl^-$ which translates, amongst others, into a more binding donor–acceptor orbital interaction between the metal and the substrate.

6.5 References

(1) (a) Collman, J. P.; Hegedus, L. S.; Norton, J. R.; Finke, R. G. *Principles and Applications of Organotransition Metal Chemistry*; University Science Books: Mill Valley, CA, 1987. (b) Elschenbroich, Ch.; Salzer, A. *Organometallics. A Concise Indroduction*, 2nd ed.; VCH: Weinheim, Germany 1992. (c) Amatore, C.; Jutand, A. *Acc. Chem. Res.* **2000**, *33*, 314. (d) Yang, H.; Kotz, K. T.; Asplund, M. C.; Wilkens, M. J.; Harris, C. B. *Acc. Chem. Res.* **1999**, *32*, 551.

(2) Experimental studies on reactions of metal complexes in the condensed phase: (a) Luh, T.-Y.; Leung, M.-k.; Wong, K.-T. *Chem. Rev.* **2000**, *100*, 3187. (b) Stürmer, R. *Angew. Chem.* **1999**, *111*, 3509. (c) Hau, L.-B.; Tanaka, M. *Chem. Comm.* **1999**, *5*, 395. (d) Casado, A. L.; Espinet, P. *Organometallics* **1998**, *17*, 954. (e) Kayser, B.; Missling, C.; Knizek, J.; Noeth, H.; Beck, W. *Eur. J. Inorg. Chem.* **1998**, *3*, 375. (f) Guillevic, M.-A.; Rocaboy, C.; Arif, A. M.; Horvath, I. T.; Gladysz, J. A. *Organometallics* **1998**, *17*, 707. (g) Edelbach, B. L.; Lachicotte, R.

J.; Jones, W. D. *J. Am. Chem. Soc.* **1998**, *120*, 2843. (h) Crabtree, R. H. *Chem. Rev.* **1995**, *95*, 987. (i) Grushin, V. V.; Alper, H. *Chem. Rev.* **1994**, *94*, 1047. (j) Ellis, P. R.; Pearson, J. M.; Haynes, A.; Adams, H.; Bailey, N. A.; Maitlis, P. M. *Organometallics* **1994**, *13*, 3215. (k) Wright, M. W.; Smalley, T. L.; Welker, M. E.; Rheingold, A. L. *J. Am. Chem. Soc.* **1994**, *116*, 6777. (l) Sakakaurka, T.; Sodeyama, T.; Sasaki, K.; Wada, K.; Tanaka, M. *J. Am. Chem. Soc.* **1990**, *112*, 7221. (m) Casalnuovo, A. L.; Calabrese, J. C.; Milstein, D. *J. Am. Chem. Soc.* **1988**, *110*, 6738. (n) Janowics, A. H.; Bergman, R. G. *J. Am. Chem. Soc.* **1983**, *105*, 3929. (o) Jones, W. D.; Feher, F. J. *J. Am. Chem. Soc.* **1982**, *104*, 4240. (p) Hickey, C. E.; Maitlis, P. M. *J. Chem. Soc., Chem. Commun.* **1984**, 1609. (q) Forster, D. *Adv. Organomet. Chem.* **1979**, *17*, 255. (r) Forster, D. *J. Am. Chem. Soc.* **1975**, *97*, 951.

(3) (a) Eller, K.; Schwarz, H. *Chem. Rev.* **1991**, *91*, 1121. (b) Armentrout, P. B.; Beauchamp, J. L. *Acc. Chem. Res.* **1989**, *22*, 315.

(4) Experimental studies on reactions of ionic metal atoms and complexes in the gas phase: (a) Brönstrup, M.; Schröder, D.; Schwarz, H. *Organometallics* **1999**, *18*, 1939. (b) Aschi, M.; Brönstrup, M.; Diefenbach, M.; Harvey, J. N.; Schröder, D.; Schwarz, H. *Angew. Chem.* **1998**, *110*, 858. (c) Freiser, B. S. *J. Mass Spectrom.* **1996**, *31*, 703. (d) van Koppen, P. A. M.; Kemper, P. R.; Bushnell, J. E.; Bowers, M. T. *J. Am. Chem. Soc.* **1995**, *117*, 2098. (e) Wesendrup, R.; Schröder, D.; Schwarz, H. *Angew. Chem.* **1994**, *105*, 1232. (f) Chen, Y.-M.; Clemmer, D. E.; Armentrout, P. B. *J. Am . Chem. Soc.* **1994**, *116*, 7815. (g) van den Berg, K. J.; Ingemann, S.; Nibbering, N. M. M.; Gregor, I. K. *Rapid. Commun. Mass Spectrom.* **1993**, *7*, 769. (h) Chowdhury, A. K.; Wilkins, C. L. *J. Am. Chem. Soc.* **1987**, *109*, 5336. (i) Weil, D. A.; Wilkins, C. L. *J. Am. Chem. Soc.* **1985**, *107*, 7316. (j) Jones, R. W.; Staley, R. H. *J. Phys. Chem.* **1982**, *86*, 1669. (k) Jones, R. W., Staley, R. H. *J. Am. Chem. Soc.* **1980**, *102*, 3794.

(5) Combined experimental and theoretical studies on reactions of ionic metal atoms and complexes in the gas phase: (a) Yi, S. S.; Reichert, E. L.; Holthausen, M. C.; Koch, W.; Weisshaar, J. C. *Chem. Eur. J.* **2000**, *6*, 2232. (b) Blomberg, M.; Yi, S. S.; Noll, R. J.; Weisshaar, J. C. *J. Phys. Chem. A* **1999**, *103*, 7254. (c) Diefenbach, M.; Brönstrup, M.; Aschi, M.; Schröder, D.; Schwarz, H. *J. Am. Chem. Soc.* **1999**, *121*, 10614. (d) Schwarz, J.; Schröder, D.; Schwarz, H.; Heinemann, C.; Hrusák, J. *Helv. Chim. Acta* **1996**, *79*, 1110.

(6) Experimental studies on reactions of neutral metal atoms in the gas phase: (a) Wen Y.; Porembski, M.; Ferrett, T. A.; Weisshaar, J. C. *J. Phys. Chem. A* **1998**, *102*, 8362. (b) Wen, Y.; Yethiraj, A.; Weisshaar, J. C. *J. Chem. Phys.* **1997**, *106*, 5509. (c) Carroll, J. J.; Weisshaar, J. C. *J. Phys. Chem.* **1996**, *100*, 12355. (d) Chertihin, G. V.; Andrews, L. *J. Am. Chem. Soc.* **1994**, *116*, 8322. (e) Carroll, J.

J.; Haug, K. L.; Weisshaar, J. C. *J. Am. Chem. Soc.* **1993**, *115*, 6962. (f) Carroll, J. J.; Weisshaar, J. C. *J. Am. Chem. Soc.* **1993**, *115*, 800. (g) Ritter, D.; Carroll, J. J.; Weisshaar, J. C. *J. Phys. Chem.* **1992**, *96*, *10636*. (h) Mitchell, S. A.; Hackett, P. A. *J. Chem. Phys.* **1990**, *93*, 7822. (i) Ritter, D.; Weisshaar, J. C. *J. Am. Chem. Soc.* **1990**, *112*, 6425. (j) Fayet, P.; Kaldor, A.; Cox, D. M. *J. Chem. Phys.* **1990**, *92*, 254.

(7) Combined experimental and theoretical studies on reactions of neutral metal atoms in the gas phase: (a) Porembski, M.; Weisshaar, J. C. *J. Phys. Chem. A* **2000**, 104, 1524. (b) Carroll, J. J.; Haug, K. L.; Weisshaar, J. C.; Blomberg, M. R. A.; Siegbahn, P. E. M.; Svensson, M. *J. Phys. Chem.* **1995**, *99*, 13955. (c) Carroll, J. J.; Weisshaar, J. C.; Siegbahn, P. E. M.; Wittborn, A. M. C.; Blomberg, M. R. A. *J. Phys. Chem.* **1995**, *99*, 14388. (d) Mitchell, S.; Blitz, M. A.; Siegbahn, P. E. M.; Svenson, M. *J. Chem. Phys.* **1994**, *100*, 423. (e) Weisshaar, J. C. *Acc. Chem. Res.* **1993**, *26*, 213.

(8) Theoretical studies on reactions of metal complexes: (a) Dedieu, A. *Chem. Rev.* **2000**, *100*, 543. (b) Torrent, M.; Solà, M.; Frenking, G. *Chem. Rev.* **2000**, *100*, 439. (c) Griffin, T. R.; Cook, D. B.; Haynes, A.; Pearson, J. M.; Monti, D.; Morris, G. E. *J. Am. Chem. Soc.* **1996**, *118*, 3029. (d) Aullón, G.; Alvarez, S. *Inorg. Chem.* **1996**, *35*, 3137. (e) Ziegler, T. *Chem. Rev.* **1991**, *91*, 651. (f) Koga, N.; Morokuma, K. *Chem. Rev.* **1991**, *91*, 823. (g) Bickelhaupt, F. M.; Baerends, E. J.; Ravenek, W. *Inorg. Chem.* **1990**, *29*, 350. (h) Gritsenko, O. V.; Bagatur'yants, A. A.; Moiseev, I. I.; Kazanskii, V. B. *Russ. Chem. Rev.* **1985**, *54*, 1151.

(9) See also, for example: (a) Lamprecht, D.; Lamprecht, G. J. *J. Comput. Chem.* **2000**, *21*, 692. (b) Minaev, B.; Agren, H. *Int. J. Quantum Chem.* **1999**, *72*, 581. (c) Su, M.-D.; Chu, S.-Y. *J. Am. Chem. Soc.* **1999**, *121*, 1045. (d) Su, M.-D-; Chu, S.-Y. *Inorg. Chem.* **1998**, *37*, 3400. (e) Su, M.-D-; Chu, S.-Y. *Chem. Phys. Lett.* **1998**, *282*, 25. (f) Albert, K.; Gisdakis, P.; Rösch, N. *Organometallics* **1998**, *17*, 1608. (g) Sakaki, S.; Biswas, B.: Sugimoto, M. *Organometallics* **1998**, *17*, 1278. (h) Hill, G. S.; Puddephatt, R. J. *Organometallics* **1998**, *17*, 1478. (i) Sakaki, S.; Ogawa, M.; Kinoshita, M. *J. Phys. Chem.* **1995**, *99*, 9933. (j) Irikura, K. K.; Goddard, W. A., III *J. Am. Chem. Soc.* **1994**, *116*, 8733. (k) Perry, J. K.; Goddard, W. A., III *J. Am. Chem. Soc.* **1994**, *116*, 5013. (l) Sellers, H. *J. Comput. Chem.* **1990**, *11*, 754. (m) Rosi, M.; Bauschlinger Jr., C. W.; Langhoff, S. R.; Partidge, H. *J. Phys. Chem.* **1990**, *94*, 8656. (n) Ziegler, T.; Tschinke, V.; Fan, L.; Becke, A. D. *J. Am. Chem. Soc.* **1989**, *111*, 9177. (o) Low, J. J.; Goddard, W. A., III *J. Am. Chem. Soc.* **1986**, *108*, 6115.

(10) (a) Bickelhaupt, F. M. *J. Comput. Chem.* **1999**, *20*, 114. (b) Bickelhaupt, F. M.; Ziegler, T.; von Ragué Schleyer, P. *Organometallics* **1995**, *14*, 2288.

(11) Theoretical studies on reactions of neutral metal atoms: (a) Maseras, F.; Lledós, A.; Clot, E.; Eisenstein, O. *Chem. Rev.* **2000**, *100*, 601. (b) Cui, Q.; Musaev, D. G.; Morokuma, K. *J. Chem. Phys.* **1998**, *108*, 8418. (c) Wittborn, A. M. C.; Costas, M.; Blomberg, M. R. A.; Siegbahn, P. E. M. *J. Chem. Phys.* **1997**, *107*, 4318. (d) Siegbahn, P. E. M. *J. Am. Chem. Soc.* **1994**, *116*, 7722. (e) Siegbahn, P. E. M. *Organometallics* **1994**, *13*, 2833. (f) Perry, J. K.; Ohanessian, G.; Goddard, W. A., III *Organometallics* **1994**, *13*, 1870. (g) Blomberg, M. R. A.; Siegbahn, P. E. M.; Svensson, M. *Inorg. Chem.* **1993**, *32*, 4218. (h) Siegbahn, P. E. M.; Blomberg, M. R. A.; Svensson, M. *J. Phys. Chem.* **1993**, *97*, 2564. (i) Siegbahn, P. E. M.; Blomberg, M. R. A.; Svensson, M. *J. Am. Chem. Soc.* **1993**, *115*, 1952. (j) Siegbahn, P. E. M.; Blomberg, M. R. A.; Svensson, M. *J. Am. Chem. Soc.* **1993**, *115*, 4191. (k) Siegbahn, P. E. M.; Blomberg, M. R. A. *J. Am. Chem. Soc.* **1992**, *114*, 10548. (l) Blomberg, M. R. A.; Siegbahn, P. E. M.; Svensson, M. *J. Am. Chem. Soc.* **1992**, *114*, 6095. (m) Svensson, M.; Blomberg, M. R. A.; Siegbahn, P. E. M. *J. Am. Chem. Soc.* **1991**, *113*, 7076. (n) Novaro, O.; Jarque, C. *Theor. Chim. Acta* **1991**, *80*, 19. (o) Blomberg, M. R. A.; Siegbahn, P. E. M.; Nagashima, U.; Wennerberg, J. *J. Am. Chem. Soc.* **1991**, *113*, 424. (p) Carter, E. A.; Goddard, W. A., III *J. Phys. Chem.* **1988**, *92*, 5679. (q) Nakatsuji, H.; Hada, M.; Yonezawa, T. *J. Am. Chem. Soc.* **1987**, *109*, 1902. (r) Low, J. J.; Goddard, W. A., III *Organometallics* **1986**, *5*, 609. (s) Koga, N.; Obara, S.; Kitaura, K.; Morokuma, K. *J. Am. Chem. Soc.* **1985**, *107*, 7109. (t) Low, J. J.; Goddard, W. A., III *J. Am. Chem. Soc.* **1984**, *106*, 8321.

(12) Relativistic effects: (a) Moss, R. E. *Advanced Molecular Quantum Mechanics*, Chapman and Hall, London, 1973. (b) Pyykkö, P. *Chem. Rev.* **1988**, *88*, 563. See also: (c) Jensen, F. *Introduction to Computational Chemistry*, Wiley, Chichester, 1999.

(13) (a) Basile, A.; Fasson, S.; Vitulli, G.; Drioli, E. *Stud. Surf. Sci. Catal.* **1998**, *119*, 453. (b) Malleron, J.-L.; Fiaud, J.-C.; Legros, J.-Y. *Handbook of Palladium Catalyzed Organic Reactions*; Academic Press, 1997. (c) Cornils, R.; Herrmann, W. A. *Applied Homogenous Catalysis with Organometallic Compounds. Vol. 1;* VCH: Weinheim, 1996, p394.

(14) Diefenbach, A.; Bickelhaupt, F. M., in preparation.

(15) Density functional theory (DFT): (a) Dreizler, R. M.; Gross, E. K. U. *Density Functional Theory. An approach to the Quantum Many-Body Problem*; Springer: Berlin, 1990. (b) Parr, R. G.; Yang, W. *Density-Functional Theory of Atoms and Molecules*; Oxford University Press: New York, 1989. (c) Gritsenko, O. V.; Ensing, B.; Schipper, P. R. T.; Baerends, E. J. *J. Chem. Phys.*, in press.

(16) Kohn-Sham MO model in DFT: (a) Bickelhaupt, F. M.; Baerends, E. J. In *Reviews in Computational Chemistry*, Vol. 15, Lipkowitz, K. B., Boyd., D. B., Eds.; Wiley-VCH: New York, 2000; Vol. 15, Chapter 1. (b) Baerends, E. J.; Gritsenko, O. V. *J. Phys. Chem. A* **1997**, *101*, 5383.

(17) Amsterdam Density Functional (ADF) program: (a) Fonseca Guerra, C.; Visser, O.; Snijders, J. G.; te Velde, G.; Baerends, E. J., *The Parallelization of the Amsterdam Density Functional Program*, In: Methods and Techniques for Computational Chemistry; Clementi, E., Corongiu, G., Eds.; STEF: Cagliari, 1995; p. 305-395. (b) Baerends, E. J.; Ellis, D. E.; Ros, P. *Chem. Phys.* **1973**, *2*, 41. (c) Baerends, E. J.; Ros, P. *Chem. Phys.* **1975**, *8*, 412. (d) Baerends, E. J.; Ros, P. *Int. J. Quantum Chem., Quantum Chem. Symp.* **1978**, *S12*, 169. (e) Fonseca Guerra, C.; Snijders, J. G.; te Velde, G.; Baerends, E. J. *Theor. Chem. Acc.* **1998**, *99*, 391. (f) Boerrigter, P. M.; te Velde, G.; Baerends, E. J. *Int. J. Quantum Chem.* **1988**, *33*, 87. (g) te Velde, G.; Baerends, E. J. *J. Comp. Phys.* **1992**, *99*, 84. (h) Snijders, J. G.; Baerends, E. J.; Vernooijs, P. *At. Nucl. Data Tables* **1982**, *26*, 483. (i) Krijn, J.; Baerends, E. J. *Fit-Functions in the HFS-Method; Internal Report* (in Dutch); Vrije Universiteit: Amsterdam, 1984. (j) Slater, J. C. *Quantum Theory of Molecules and Solids Vol. 4*; McGraw-Hill: New York, 1974. (k) Becke, A. D. *J. Chem. Phys.* **1986**, *84*, 4524. (l) Becke, A. *Phys. Rev. A* **1988**, *38*, 3098. (m) Vosko, S. H.; Wilk, L.; Nusair, M. *Can. J. Phys.* **1980**, *58*, 1200. (n) Perdew, J. P. *Phys. Rev. B* **1986**, *33*, 8822 (Erratum: *Phys. Rev. B* **1986**, *34*, 7406). (o) Fan, L.; Ziegler, T. *J. Chem. Phys.* **1991**, *94*, 6057. (p) Versluis, L.; Ziegler, T. *J. Chem. Phys.* **1988**, *88*, 322. (q) Fan, L.; Versluis, L.; Ziegler, T.; Baerends, E. J.; Ravenek, W. *Int. J. Quantum. Chem., Quantum. Chem. Symp.* **1988**, *S22*, 173. (r) Fan, L.; Ziegler, T. *J. Chem. Phys.* **1990**, *92*, 3645. (s) Banerjee, A.; Adams, N.; Simons, J.; Shepard, R. *J. Phys. Chem.* **1985**, *89*, 52. (t) Baker, J. *J. Comput. Chem.* **1986**, *7*, 385.

(18) ZORA approach: (a) Chang, C.; Pelissier, M.; Durand, P. *Phys. Scr.* **1986**, *34*, 394. (b) van Lenthe, E.; Baerends, E. J.; Snijders, J. G. *J. Chem. Phys.* **1993**, *99*, 4597. (c) van Lenthe, E.; Baerends, E. J.; Snijders, J. G. *J. Chem. Phys.* **1994**, *101*, 9783. (d) van Lenthe, E.; Snijders, J.; Baerends, E. J. *J. Chem. Phys.* **1996**, *105*, 6505. (e) van Lenthe, E. *Thesis*, Vrije Universiteit, Amsterdam, 1996. (f) van Lenthe, E.; van Leeuwen, R.; Baerends, E. J.; Snijders, J. G. *Int. J. Quantum Chem.* **1996**, *57*, 281.

(19) Atkins, P. W. Physical *Chemistry*; Oxford University Press: Oxford, 1998.

(20) A negative activation energy does not imply the complete absence of any barrier. The reaction is still hampered by a statistical or entropic bottleneck that is associated with the decrease in the number of available quantum states (e.g., of

translation, rotation, and vibration) as one goes from the separate, unbound reactants to the tightly bound transition state.

(21) Holleman, A. F.; Wiberg, N. *Lehrbuch der Anorganischen Chemie*; de Gruyter: Berlin, 1985.

(22) Bond energy decomposition: (a) Ziegler, T.; Rauk, A. *Inorg. Chem.* **1979**, *18*, 1558. (b) Ziegler, T.; Rauk, A. *Inorg. Chem.* **1979**, *18*, 1755. (c) Ziegler, T.; Rauk, A. *Inorg. Chem.* **1977**, *46*, 1. (d) Bickelhaupt, F.M.; Nibbering, N.M.M.; van Wezenbeek, E.M.; Baerends, E.J. *J. Phys. Chem.* **1992**, *96*, 4864.

(23) For the importance of considering ΔV_{elst} and $\Delta E_{\mathrm{Pauli}}$ as separate terms, see: (a) Ref. 16a. See also, for example: (b) Diefenbach, A.; Bickelhaupt, F. M.; Frenking, G. *J. Am. Chem. Soc.* **2000**, *122*, 6449. (c) Fonseca Guerra, C.; Bickelhaupt, F. M. *Angew. Chem.* **1999**, *111*, 3120; *Angew. Chem. Int. Ed.* **1999**, *38*, 2942. (d) Fonseca Guerra, C.; Bickelhaupt, F. M.; Snijders, J. G.; Baerends, E. J. *Chem. Eur. J.* **1999**, *5*, 3581. (e) Bickelhaupt, F. M.; Diefenbach, A.; de Visser, S. V.; de Koning, L. J.; Nibbering, N. M. M. *J. Phys. Chem. A* **1998**, *102*, 9549. (f) Bickelhaupt, F. M.; van Eikema Hommes, N. J. R.; Fonseca Guerra, C.; Baerends, E. J. *Organometallics* **1996**, *15*, 2923. (g) Bickelhaupt, F. M.; Nibbering, N. M. M.; Baerends, E. J.; Ziegler, T. *J. Am. Chem. Soc.* **1993**, *115*, 9160.

(24) (a) Dewar, M. J. S. *Bull. Soc. Chim. Fr.* **1951**, *18*, C79. (b) Chatt, J.; Duncanson, L. A. *J. Chem. Soc.* **1953**, 2929.

7 Toward Fragment-Oriented Design of Catalysts

Abstract

To learn how ligands direct the palladium-catalyzed activation of C–H, C–C and C–I bonds, the oxidative addition of Pd and *cis*-$Pd(CO)_2I_2$ to CH_4 (C–H), C_2H_6 (C–C and C–H) and CH_3I (C–I) have been explored at the ZORA-BP86/TZ(2)P level of density functional theory (DFT). The purpose of the present study is a rough exploration of how the mechanism of bond activation changes if one goes from an uncoordinated metal atom to a metal complex as model catalyst. For both Pd and *cis*-$Pd(CO)_2I_2$, direct oxidative insertion (OxIn) is the lowest-barrier pathway whereas nucleophilic substitution (S_N2) is highly endothermic, and therefore not competitive. The effect of introducing ligands if one goes from Pd to *cis*-$Pd(CO)_2I_2$ is an increase of the activation enthalpy for oxidative insertion by 50 - 60 kcal/mol. For example, $\Delta H^{\neq}_{298}$ is -5.0 kcal/mol for Pd + CH_4 and 48.9 kcal/mol for *cis*-$Pd(CO)_2I_2$ + CH_4. The overall reactions are exothermic by -10 (C–H in CH_4) through -45 kcal/mol (C–I) for Pd, and endothermic by 21 (C–I) through 47 kcal/mol (C–C) for *cis*-$Pd(CO)_2I_2$. Obviously, the latter complex would be a poor catalyst. Yet, the exploration of its reactivity reveals interesting features that are not present in the reactions of uncoordinated Pd. First, in the TS for oxidative insertion, the C–X bond (X = H, C, I) to be activated can have, in principle, different orientations with respect to the square-planar *cis*-$Pd(CO)_2I_2$ complex, e.g.,
C–X or X–C along an I–Pd–CO axis, or in between two I–Pd–CO axes. Second, at variance to the uncoordinated metal, the metal complex may be deformed in the TS. This can be monitored by and leads to an extension of the Activation Strain (or Activation strain-TS interaction, ATS) model of chemical reactivity.

7.1 Introduction

Oxidative addition and reductive elimination (1) are ubiquitous in homogeneous catalysis[1] and, therefore, have been intensively studied both experimentally[2-7] and theoretically.[7-12]

$$ML_n + R{-}X \underset{\text{Reductive Elimination}}{\overset{\text{Oxidative Addition}}{\rightleftharpoons}} R{-}ML_n{-}X \qquad (1)$$

In the previous chapters of this thesis, the reactions of uncoordinated Pd(0) and $PdCl^-$ toward H–H, C–H, C–C and C–X (X = Cl) bonds were investigated. Palladium was chosen because this metal is widely used in catalysis[13] and because the atom has a stable closed-shell d^{10} ground state which facilitates comparison with closed-shell Pd(0) complexes. In this chapter, the next step toward a Fragment-oriented Design of Catalysts is taken by introducing the prototypical ligands CO and I^- into the model catalyst, that is, the reactivities of Pd and *cis*-$Pd(CO)_2I_2$ are compared. In analogy to the previous chapters, the activation of prototypical C–H, C–C and C–I bonds is investigated by exploring and analyzing the reactions of both Pd and *cis*-$Pd(CO)_2I_2$ with CH_4, C_2H_6 and CH_3I (eq 2):

C-H activation	$Pd + CH_4$	$\rightarrow$	$Pd(CH_3)H$	(2a)
	$Pd(CO)_2I_2 + CH_4$	$\rightarrow$	$Pd(CH_3)H(CO)_2I_2$	(2b)
	$Pd + C_2H_6$	$\rightarrow$	$Pd(C_2H_5)H$	(2c)
	$Pd(CO)_2I_2 + C_2H_6$	$\rightarrow$	$Pd(C_2H_5)H(CO)_2I_2$	(2d)
C-C activation	$Pd + C_2H_6$	$\rightarrow$	$Pd(CH_3)_2$	(2e)
	$Pd(CO)_2I_2 + C_2H_6$	$\rightarrow$	$Pd(CH_3)_2(CO)_2I_2$	(2f)
C-I activation	$Pd + CH_3I$	$\rightarrow$	$Pd(CH_3)I$	(2g)
	$Pd(CO)_2I_2 + CH_3I$	$\rightarrow$	$Pd(CH_3)(CO)_2I_3$	(2h)

Note that *cis*-$Pd(CO)_2I_2$ is not a "real-world" catalyst in the sense that, as will be seen later on, it does not speed up and even retards the bond activation processes relative to the uncoordinated Pd atom. However, by exploring the reactivity of the *cis*-$Pd(CO)_2I_2$ model catalyst, one can reveal and learn about interesting features that can occur only for catalytically active transition metal complexes and not for uncoordinated Pd. For example, in the TS for oxidative insertion, the C–X bond (X = H, C, I) to be activated can have, in principle, different orientations with respect to the square-planar *cis*-$Pd(CO)_2I_2$ complex, e.g., C–X or X–C along an I–Pd–CO axis, or in between two I–Pd–CO axes. Furthermore, at variance to the uncoordinated metal, the metal complex may be deformed in the TS. These effects have been analyzed using the Activation Strain (or Activation strain-TS interaction, ATS) model of chemical reactivity introduced in chapter 5 of this thesis. The new features encountered in the reactions of the *cis*-$Pd(CO)_2I_2$ complex lead to an extension of the ATS model that is presented in Section 7.3.2.

The organization of this chapter is as follows. Section 7.2 describes the computational methods used. The results of the calculations and analyses are presented and discussed in Section 7.3. The conclusions are summarized in Section 7.4. References are given in Section 7.5.

7.2 Methods

The present study is based on density functional theory (DFT).[10a,15,16] All calculations have been performed using the Amsterdam Density Functional (ADF) program,[17] developed by Baerends *et. al.*[17b,c,d] MOs were expanded in a large uncontracted set of Slater-type orbitals (STOs).[17h] For C, H, O and I, the basis is of triple-ζ quality, augmented with two polarization functions: 2p and 3d for H, 3d and 4f for C and O, and 4d and 4f for I. The palladium atom is represented by a triple-ζ type basis set augmented with one 5p polarization function. The core shells of carbon (1s),

oxygen (1s), iodine (1s2s2p3s3p3d4s4p) and palladium (1s2s2p3s3p3d) were treated by the frozen-core approximation.[17b] An auxiliary set of s, p, d, f and g STOs was used to fit the molecular density and to represent the Coulomb and exchange potentials accurately in each SCF cycle.[17i]

Geometries and energies were calculated using the Local Density Approximation (LDA) with nonlocal corrections (NL). Exchange is described by Slaters Xα potential,[17j] corrected by the non-local exchange potential of Becke.[17k,l] Correlation is treated in the Vosko-Wilk-Nusair (VWN) parameterization[17m] using formula V, corrected for nonlocal effects due to Perdew.[17n] Relativistic effects were taken into account by the zeroth-order regular approximation (ZORA).[18]

All energy minima and transition state[17r] structures were verified by frequency calculations:[17q] for minima all normal modes have real frequencies, transition states have one normal mode with an imaginary frequency. The character of the normal mode associated with the imaginary frequency was analyzed to ensure that the correct transition state was found.

Bond enthalpies at 298.15 K and 1 atmosphere (ΔH_{298}) were calculated from 0 K electronic bond energies (ΔE) according to eq 3, assuming an ideal gas.[19]

$$\Delta H_{298} = \Delta E + \Delta E_{\mathrm{trans},298} + \Delta E_{\mathrm{rot},298} + \Delta E_{\mathrm{vib},0} + \Delta(\Delta E_{\mathrm{vib},0})_{298} + \Delta(pV) \qquad (3)$$

Here, $\Delta E_{\mathrm{trans},298}$, $\Delta E_{\mathrm{rot},298}$ and $\Delta E_{\mathrm{vib},0}$ are the differences between products and reactants in translational, rotational and zero point vibrational energy, respectively; $\Delta(\Delta E_{\mathrm{vib}})_{298}$ is the change in the vibrational energy difference as one goes from 0 to 298.15 K. The vibrational energy corrections are based on our frequency calculations. The molar work term $\Delta(pV)$ is $(\Delta n)RT$; Δn = -1 for two reactants (Pd and CH_3X) combining to one species. Thermal corrections for the electronic energy are neglected.

7.3 Results and Discussion

This section is organized as follows. In Section 7.3.1, the Potential Energy Surfaces (PES) of the investigated reactions are discussed. Then, in Section 7.3.2, the Activation Strain (or Activation strain-TS interaction, ATS) model of chemical reactivity is presented and an extension is proposed which will be used in Section 7.3.3 for analyzing the activation barriers for the oxidative addition reactions of the *cis*-$Pd(CO)_2I_2$ model catalyst.

7.3.1 Potential Energy Surfaces of Direct Oxidative Insertion and S_N2 Substitution

In this section, the Potential Energy Surfaces (PES) of the various oxidative insertion (OxIn) and S_N2 reactions (eq 2a-h) are discussed. Results are summarized in Table 1 (enthalpies) and Figure 1 (geometries). The straight S_N2 reactions are highly endothermic and occur without reverse barrier because of the charge separation that occurs in the product $PdCH_3^+ + X^-$ and $Pd(CO)_2I_2(CH_3)^+ + X^-$ (X = H, CH_3, I). In case of Pd + CH_4, for example, the reaction is endothermic by 228.7 kcal/mol. The endothermicity further increases for all reactions by some 30 kcal/mol if one goes from Pd to the model complex *cis*-$Pd(CO)_2I_2$.

The OxIn pathway has been explored for both model catalysts and all substrates. Each of the reactions with the uncoordinated Pd atom proceeds via a reactant complex, whereas for *cis*-$Pd(CO)_2I_2$, stable reactant complexes could not be identified. The reactions proceed via a TS to the products, and are exothermic for the Pd. However, for *cis*-$Pd(CO)_2I_2$, they become endothermic.

At variance with the situation for the uncoordinated Pd atom, the activated bond can in principle adopt several orientations with respect to the *cis*-$Pd(CO)_2I_2$ model catalyst. A number of basic orientations are shown in Scheme 1, but of course also intermediate situations, say, in between **O-1** and **O-2** are conceivable.

– Scheme 1 –

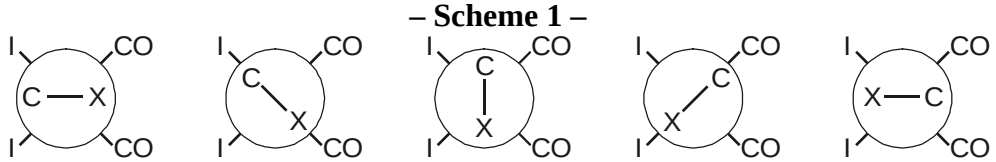

O-1 **O-2** **O-3** **O-4** **O-5**

For the activation of C–H bonds in CH_4 and C_2H_6, two distinct transition states, i.e., **1b** and **1c** (CH_4) and **2b** and **2c** (C_2H_6, see Figure 1) were found. They correspond to orientation **O-2** and **O-4** respectively, and are very close in energy. For the C–C and C–I activation, only one TS could be determined with an orientation between **O-1** and **O-2** for C–C, and orientation **O-1** for C–I, see Figure 1. The transition states and products using Pd as catalyst are 50 - 60 kcal more stable with respect to reactants than those using *cis*-$Pd(CO)_2I_2$; the overall TS stability pattern stays approximately the same, that is, activation enthalpies increase in the order C–I $\approx$ C–H < C–C. Obviously, *cis*-$Pd(CO)_2I_2$ is a very poor catalyst. However, it is expected that these barriers can significantly be reduced by introducing an additional I^- to *cis*-$Pd(CO)_2I_2$, see Chapter 6. Note that $Pd(CO)_2I_3^-$ will only allow for an S_N2 mechanism because it lacks enough vacant coordination space.

Comparing the TS structures that involved uncoordinated Pd with those involving the *cis*-$Pd(CO)_2I_2$ complex, one sees that the activated bond in the latter systems has been stretched more. For example, the C–H bond of CH_4 is stretched by 0.517 Å (47%) and amounts to 1.613 Å in the TS when activated by Pd. Using *cis*-$Pd(CO)_2I_2$, it is stretched by 0.680 Å (62%) and amounts to 1.776 Å in transition state **1b**. Regarding the higher endothermicity of the *cis*-$Pd(CO)_2I_2$ catalyzed reactions (see Table 1), this is in line with the Hammond postulate.

Note that also the *cis*-$Pd(CO)_2I_2$ complex is more strongly distorted if the strength of the bonds to be activated and the endothermicity of the reaction increase (ΔH_{bond} is 99 (C–H), 83 (C–C) and 51 (C–I) kcal/mol[20]). This means that if one wishes to activate a strong bond associated with a rather endothermic oxidative addition, the catalytically active complex must me either flexible (i.e., it should take only little energy to deform it appropriately) or the appropriate distortion must be already “built in”, e.g., by using bidental ligands with short bridges. Also, anion assistance can be invoked to further reduce the barrier and, in particular, to relieve the endothermicity of the activation process (see Chapter 6).

Table 1. Reaction Profiles at ZORA-BP86/TZ(2P) for the Oxidative Insertion of Pd and $Pd(CO)_2I_2$ into the C–H, C–C and C–I Bonds of CH_4, C_2H_6 and CH_3I, respectively. 298K Enthalpies (in kcal/mol) relative to free Reactants.

Activated Bond	Reactants	Reactant Complex	Transition State	Product
Direct Oxidative Insertion				
C–H	Pd + CH_4	–11.4	–5.0	–9.7
	$Pd(CO)_2I_2$ + CH_4 [a]	–	48.9	45.1
	$Pd(CO)_2I_2$ + CH_4 [b]	–	49.3	44.6
	Pd + C_2H_6	–11.6	–4.1	–11.6 [c]
	$Pd(CO)_2I_2$ + C_2H_6 [d]	–	47.6	42.7
	$Pd(CO)_2I_2$ + C_2H_6 [e]	–	47.8	42.1
C–C	Pd + C_2H_6	–11.6	9.6	–14.1
	$Pd(CO)_2I_2$ + C_2H_6	–	70.9	46.7
C–I	Pd + CH_3I	–23.2	–14.9	–44.0
	$Pd(CO)_2I_2$ + CH_3I	0.2	48.8	20.9
S_N2 Reaction				
C–H	Pd + CH_4	–11.4	f	228.7 [g]
	$Pd(CO)_2I_2$ + CH_4	–	f	259.7 [g]
C–C	Pd + C_2H_6	–11.6	f	228.6 [g]
	$Pd(CO)_2I_2$ + C_2H_6	–	f	259.6 [g]
C–I	Pd + CH_3I	–	f	127.0 [g]
	$Pd(CO)_2I_2$ + CH_3I	0.2	f	158.6 [g]

[a] Orientation of catalyst corresponds to structure **1b**, Figure 1. Scheme 1: **O-2**.

[b] Orientation of catalyst corresponds to structure **1c** Figure 1. Scheme 1: **O-4.**

[c] Primary product of insertion. Rearrangement via second TS (-11.0 kcal/mol) to final product (-12.0 kcal/mol).

[d] Orientation of catalyst corresponds to structure **2b**, Figure 1. Scheme 1: **O-2**.

[e] Orientation of catalyst corresponds to structure **2c**, Figure 1. Scheme 1: **O-4**.

[f] No reverse activation barrier.

[g] Dissociated products of straight S_N2 reaction.

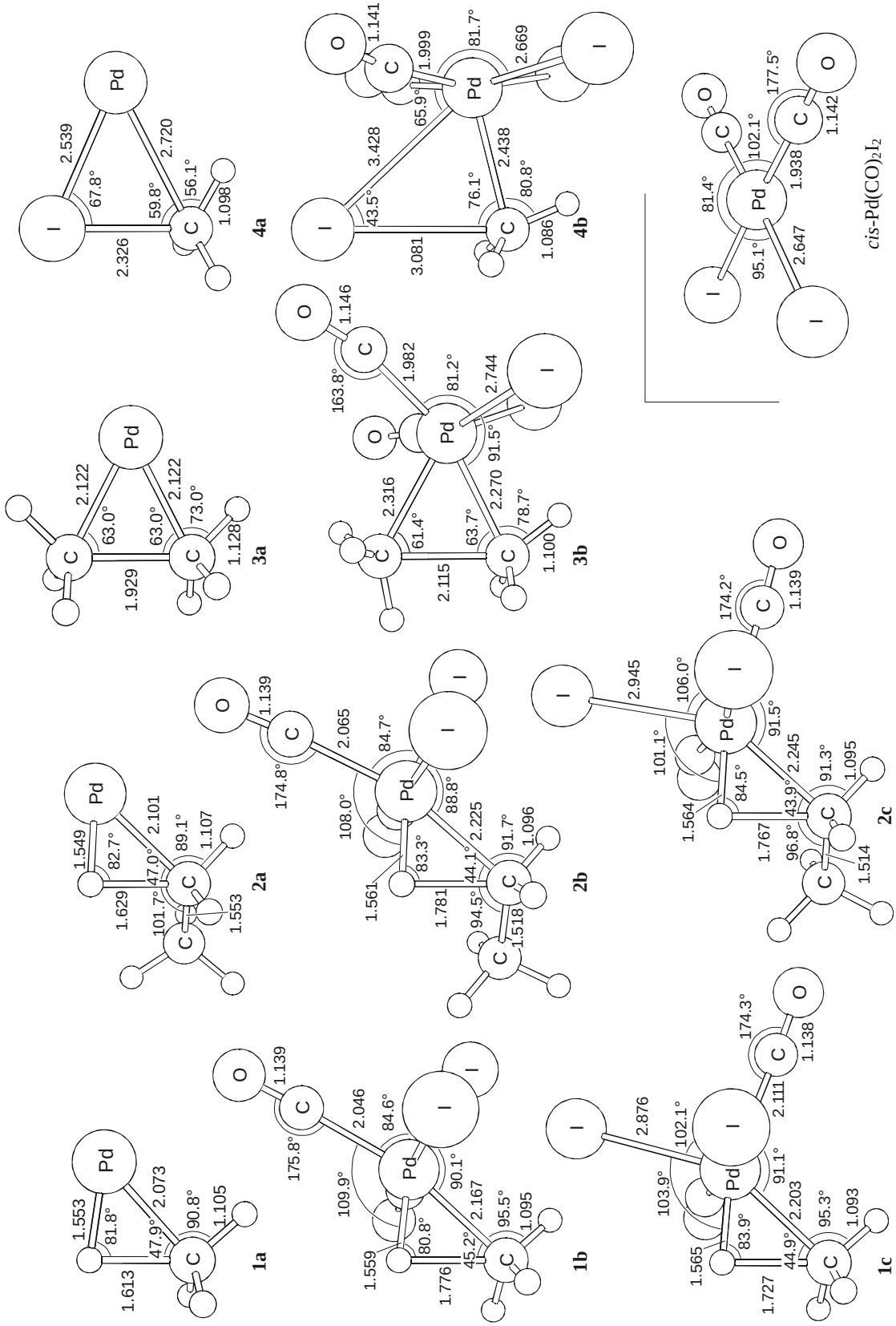

Figure 1. Structures of transition states of the various direct oxidative insertion reactions and equilibrium geometry of *cis*-$Pd(CO)_2I_2$ at ZORA-BP86/TZ(2)P. Bond lengths are given in Å.

7.3.2 The Activation Strain-Transition State Interaction (ATS) Model

The Activation Strain (or Activation strain-TS interaction, ATS) model of chemical reactivity provides the basis for the investigations carried out in this thesis. It was introduced in Chapter 5. Here, its basic ideas are repeated and an extension is presented which will be used in the following section.

The ATS model separates the TS structure into the former catalyst and substrate. The activation barrier $\Delta E^{\neq}$ is then analyzed by dividing it into two distinct terms.

$$\Delta E^{\neq} = \Delta E^{\neq}_{\text{strain}} + \Delta E^{\neq}_{\text{int}} \tag{5}$$

The activation strain $\Delta E^{\neq}_{\text{strain}}$ is the energy needed for geometrical distortion of the free catalyst and substrate to the geometry they possess in the TS. The TS interaction $\Delta E^{\neq}_{\text{int}}$ represents the energy obtained by the interaction of the so-prepared fragments.

While for the Pd atom as catalyst, $\Delta E^{\neq}_{\text{strain}}$ gives only the energy connected with the geometrical distortion of the substrate, in the systems with *cis*-$Pd(CO)_2I_2$ it contains in addition a contribution from the catalyst which can now, in principle, be distorted. Consequently, the activation strain $\Delta E^{\neq}_{\text{strain}}$ is decomposed into a part belonging to the catalyst, $\Delta E^{\neq}_{\text{strain,cat}}$, and a part representing the substrate, $\Delta E^{\neq}_{\text{strain,sub}}$, see eq 6. A schematic sketch of the ATS model is given in figure 3.

$$\Delta E^{\neq} = \Delta E^{\neq}_{\text{strain,cat}} + \Delta E^{\neq}_{\text{strain,sub}} + \Delta E^{\neq}_{\text{int}} \tag{6}$$

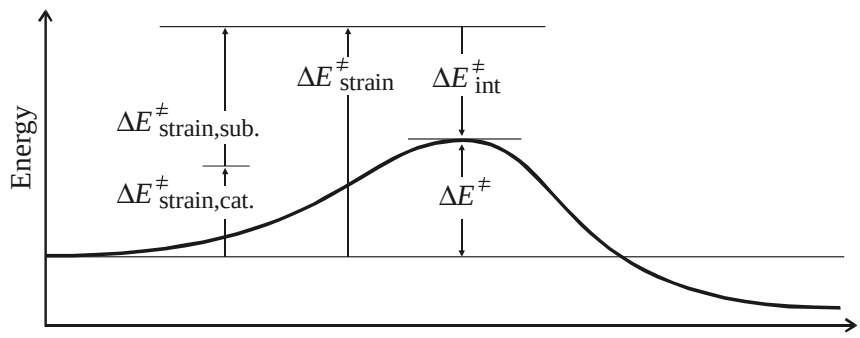

Figure 3. The Activation strain-TS interaction (ATS) model of chemical reactivity. The activation barrier $\Delta E^{\neq}$ is analyzed in terms of interaction energy $\Delta E^{\neq}_{\text{int}}$ and activation-strain $\Delta E^{\neq}_{\text{strain}}$. The latter can be divided into distinct parts for the substrate, $\Delta E^{\neq}_{\text{strain,sub}}$, and the catalyst, $\Delta E^{\neq}_{\text{strain,cat}}$.

7.3.3 The Calibration Process of Catalyst and Substrate

The purpose of this section is to further analyze how the activation barriers of the *cis*-$Pd(CO)_2I_2$-induced reactions arise by applying the extended ATS model introduced in Section 7.3.2. The results are summarized in Table 2.

The activation of a bond is inherently connected with a geometrical change of the substrate, that is, an elongation of the bond to be activated and, possibly, a tilting or further deformation of the fragments that it holds together. This gives rise to activation strain $\Delta E^{\neq}_{strain}$. In the previous chapters, it was shown that the activation strain adopts a characteristic value for a particular type of bond and that this value changes only marginally between Pd and $PdCl^-$ model catalysts. The situation may change, however, if the model catalyst is modified in a more drastic manner, e.g., by going from Pd to *cis*-$Pd(CO)_2I_2$ where the metal center has been oxidized from d^{10} to d^8 and the available coordination space has been practically saturated with four ligands. Now, also the catalyst may be deformed in a fashion that depends on its flexibility and sterical demands but also, of course, on the substrate or bond to be activated. This deformation affects in turn the electronic structure the catalyst effectively posses in the TS and, thus, also the bond elongation in the substrate. Thus, one has to deal with a process of mutual adjustment of the catalyst and the substrate in the TS. This process is designated calibration.

One may expect that the calibration of a more complex catalyst, such as *cis*-$Pd(CO)_2I_2$, and the substrate induces changes in the overall activation strain $\Delta E^{\neq}_{strain}$, but also in the activation strain stemming specifically from the substrate $\Delta E^{\neq}_{strain,sub}$. In addition, the TS interaction $\Delta E^{\neq}_{int}$ is affected both by the change in the catalyst's electronic structure and the way in which the substrate reacts to this. These expectations, borne out of qualitative considerations and our experience obtained so far with Pd- and $PdCl^-$- induced bond activation (see Chapters 4 - 6) is confirmed by the ATS analyses of the *cis*-$Pd(CO)_2I_2$-catalyzed processes (see Table 2). It was already mentioned in Section 7.3.1 that the barriers of the Pd-catalyzed reactions are lower than those induced by the *cis*-$Pd(CO)_2I_2$ complex. This trend turns out to be caused primarily by a substantial increase in activation strain and is further reinforced by a concomitant

reduction of the stabilizing TS interaction, especially for C–C and C–I activation. For example, the activation strain of the C–H activation in C_2H_6 is 55 kcal/mol for Pd, and some 103 kcal/mol for *cis*-$Pd(CO)_2I_2$, whereas the strength of the TS interaction decreases only slightly from –55 kcal/mol for Pd to ca –53 kcal/mol for the *cis*-$Pd(CO)_2I_2$. Note that as expected the activation strain $\Delta E^{\neq}_{strain}$ changes if one goes from Pd to *cis*-$Pd(CO)_2I_2$, Note however also that it adopts again characteristic values for each type of bond, e.g. 100 - 105 kcal/mol for C–H, 91 for C–C and 59 for C–I activation. A more detailed inspection reveals that the more endothermic oxidative insertion reactions of the stronger C–H and C–C bonds is associated with a substantial contribution $\Delta E^{\neq}_{strain,cat}$ of 32 - 35 kcal/mol from the catalyst to the overall activation strain $\Delta E^{\neq}_{strain}$, in line with the higher degree of geometrical distortion mentioned before (see Figure 1). The activation strain $\Delta E^{\neq}_{strain,sub}$ associated with the substrate also increases if one goes from Pd to *cis*-$Pd(CO)_2I_2$, especially for C–I activation (Table 2). This is in line with the more pronounced stretching of the activated bonds in the TS of the more endothermic $Pd(CO)_2I_2$-induced reactions. Tracing how the process of calibration is exactly determined by the interplay of $\Delta E^{\neq}_{strain,sub}$, $\Delta E^{\neq}_{strain,cat}$ and $\Delta E^{\neq}_{int}$ will be the subject of future investigations.

Finally, an important consequence of the phenomenon of calibration is that, for designing and tuning the electronic structure of the catalyst for a particular bond with the help of ligands, one must consider its structure in the TS (i.e. after calibration) which is not necessarily the same as the equilibrium geometry. It is the catalyst's structure that counts because in this geometry and with the associated electronic structure the catalyst enters into the TS interaction.

Table 2. Analysis of the Activation Energies (in kcal/mol) for the Direct Oxidative Insertion of Pd and *cis*-$Pd(CO)_2I_2$ into C–H, C–C and C–I Bonds by the Extended Activation-Strain Transition-State Interaction (ATS) Model.

Catalyst	No.	Activation Barrier $\Delta E^{\neq}$	Interaction Energy $\Delta E^{\neq}_{int}$	Activation Strain $\Delta E^{\neq}_{strain}$	Catalyst Strain $\Delta E^{\neq}_{strain,cat.}$	Substrate Strain $\Delta E^{\neq}_{strain,sub.}$
C–H Bond Activation in CH_4						
Pd	**1a**	–1.6	–55.1	53.5	–	53.5
$Pd(CO)_2I_2$	**1b**	50.5	–54.7	105.2	34.9	70.3
$Pd(CO)_2I_2$	**1c**	51.0	–48.5	99.5	33.6	65.9
C–H Bond Activation in C_2H_6						
Pd	**2a**	–0.7	–55.4	54.7	–	54.7
$Pd(CO)_2I_2$	**2b**	49.7	–53.0	102.7	35.0	67.7
$Pd(CO)_2I_2$	**2c**	49.8	–50.9	100.7	34.4	66.3
C–C Bond Activation in C_2H_6						
Pd	**3a**	12.6	–26.8	39.4	–	39.4
$Pd(CO)_2I_2$	**3b**	72.6	–18.8	91.4	31.9	59.5
C–I Bond Activation in CH_3I						
Pd	**4a**	–15.2	–19.3	4.1	–	4.1
$Pd(CO)_2I_2$	**4b**	49.7	–9.5	59.2	4.0	55.2

7.4 Conclusion

The introduction of ligands, if one goes from uncoordinated Pd to the *cis*-$Pd(CO)_2I_2$ model catalyst, has a number of substantial effects on palladium-catalyzed activation of C–H, C–C and C–I bonds, as follows from the ZORA-BP86/TZ(2)P exploration of the oxidative addition of Pd and *cis*-$Pd(CO)_2I_2$ to CH_4 (C–H), C_2H_6 (C–C and C–H) and CH_3I (C–I). For Pd and *cis*-$Pd(CO)_2I_2$, direct oxidative insertion (OxIn) is the lowest-barrier pathway. Nucleophilic substitution (S_N2) is highly endothermic and therefore not competitive because of the charge separation in the products $PdCH_3^+ + X^-$ and $Pd(CO)_2I_2(CH_3)^+ + X^-$ (X = H, CH_3, I). The effect of introducing ligands, i.e. going from Pd to *cis*-$Pd(CO)_2I_2$, is a substantial increase of the activation enthalpy for oxidative insertion by 50 - 60 kcal/mol. Activation energies for oxidative insertion increase in the order C–I $\lessapprox$ C–H < C–C for both Pd and *cis*-$Pd(CO)_2I_2$ (with higher absolute values for the latter). Overall oxidative addition is exothermic by -10 (C–H in CH_4) through -45 kcal/mol (C–I) for Pd, and endothermic by 21 (C–I) through 47 kcal/mol (C–C) for *cis*-$Pd(CO)_2I_2$.

Obviously, the *cis*-$Pd(CO)_2I_2$ complex would be a poor catalyst. Yet, the exploration of its reactivity has uncovered interesting features that are not present in the reactions of uncoordinated Pd. First, in the TS for oxidative insertion, the C–X bond (X = H, C, I) that is to be activated can have, in principle, different orientations with respect to the square-planar *cis*-$Pd(CO)_2I_2$ complex, e.g., C–X (**O-1**) or X–C (**O-4**) along an I–Pd–CO axis, or in between two I–Pd–CO axes (**O-1**, **O-3**, **O-5**; see Scheme 1). It was found that oxidative insertion of *cis*-$Pd(CO)_2I_2$ into the C–H bonds can occur via two different transition states, corresponding to orientation **O-2** and **O-4**, at approximately the same energy. For oxidative insertion of *cis*-$Pd(CO)_2I_2$ into each, C–C and C–I bonds, it was found only one TS corresponding to an orientation between **O-1** and **O-2** (C–C) and **O-1** (C–I).

A second point is that, at variance to the uncoordinated metal, the metal complex may be deformed in the TS. This leads to the phenomenon of calibration or adjustment of the catalyst to the substrate in the TS. To quantitatively monitor the calibration

process, the Activation Strain (or Activation strain-TS interaction, ATS) model has been extended in that the activation strain $\Delta E^{\neq}_{\text{strain}}$ is separated into distinct terms for substrate and catalyst. Both terms prove to be characteristic for each type of activated bond. However, the drastic change in the character of the pathway associated with going from Pd (or $PdCl^{-}$, see Chapter 6) to the sterically more demanding and flexible *cis*-$Pd(CO)_2I_2$ complex leads to a change in all activation strain values. Furthermore, it was found that the stronger the bond and the more endothermic the reaction, the higher the activation strain of both the substrate and the *cis*-$Pd(CO)_2I_2$ model catalyst. An important consequence of the phenomenon of calibration is that, for designing and tuning the electronic structure of the catalyst for a particular bond with the help of ligands, one must consider its structure in the TS (i.e. after calibration). This is the geometry that counts because it is the one in which the catalyst has the TS interaction with the substrate. Note, that the catalyst's structure in the TS can and does in a number of cases differ from its own equilibrium geometry.

7.5 References

(1) (a) Collman, J. P.; Hegedus, L. S.; Norton, J. R.; Finke, R. G. *Principles and Applications of Organotransition Metal Chemistry*; University Science Books: Mill Valley, CA, 1987. (b) Elschenbroich, Ch.; Salzer, A. *Organometallics. A Concise Indroduction*, 2nd ed.; VCH: Weinheim, Germany 1992. (c) Amatore, C.; Jutand, A. *Acc. Chem. Res.* **2000**, *33*, 314. (d) Yang, H.; Kotz, K. T.; Asplund, M. C.; Wilkens, M. J.; Harris, C. B. *Acc. Chem. Res.* **1999**, *32*, 551. (e) Sen, A. *Acc. Chem. Res.* **1998**, *31*, 550.

(2) Experimental studies on reactions of metal complexes in the condensed phase: (a) Luh, T.-Y.; Leung, M.-k.; Wong, K.-T. *Chem. Rev.* **2000**, *100*, 3187. (b) Stürmer, R. *Angew. Chem.* **1999**, *111*, 3509. (c) Hau, L.-B.; Tanaka, M. *Chem. Comm.* **1999**, *5*, 395. (d) Casado, A. L.; Espinet, P. *Organometallics* **1998**, *17*, 954. (e) Kayser, B.; Missling, C.; Knizek, J.; Noeth, H.; Beck, W. *Eur. J. Inorg. Chem.* **1998**, *3*, 375. (f) Guillevic, M.-A.; Rocaboy, C.; Arif, A. M.; Horvath, I. T.; Gladysz, J. A. *Organometallics* **1998**, *17*, 707. (g) Edelbach, B. L.; Lachicotte, R. J.; Jones, W. D. *J. Am. Chem. Soc.* **1998**, *120*, 2843. (h) Crabtree, R. H. *Chem. Rev.* **1995**, *95*, 987. (i) Grushin, V. V.; Alper, H. *Chem. Rev.* **1994**, *94*, 1047. (j) Ellis, P. R.; Pearson, J. M.; Haynes, A.; Adams, H.; Bailey, N. A.; Maitlis, P. M. *Organometallics* **1994**, *13*, 3215. (k) Wright, M. W.; Smalley, T. L.; Welker, M. E.; Rheingold, A. L. *J. Am. Chem. Soc.* **1994**, *116*, 6777. (l) Sakakaurka, T.; Sodeyama, T.; Sasaki, K.; Wada, K.; Tanaka, M. *J. Am. Chem. Soc.* **1990**, *112*, 7221. (m) Casalnuovo, A. L.; Calabrese, J. C.; Milstein, D. *J. Am. Chem. Soc.* **1988**, *110*, 6738. (n) Janowics, A. H.; Bergman, R. G. *J. Am. Chem. Soc.* **1983**, *105*, 3929. (o) Jones, W. D.; Feher, F. J. *J. Am. Chem. Soc.* **1982**, *104*, 4240. (p) Hickey, C. E.; Maitlis, P. M. *J. Chem. Soc., Chem. Commun.* **1984**, 1609. (q) Forster, D. *Adv. Organomet. Chem.* **1979**, *17*, 255. (r) Forster, D. *J. Am. Chem. Soc.* **1975**, *97*, 951.

(3) (a) Eller, K.; Schwarz, H. *Chem. Rev.* **1991**, *91*, 1121. (b) Armentrout, P. B.; Beauchamp, J. L. *Acc. Chem. Res.* **1989**, *22*, 315.

(4) Experimental studies on reactions of ionic metal atoms and complexes in the gas phase: (a) Brönstrup, M.; Schröder, D.; Schwarz, H. *Organometallics* **1999**, *18*, 1939. (b) Aschi, M.; Brönstrup, M.; Diefenbach, M.; Harvey, J. N.; Schröder, D.; Schwarz, H. *Angew. Chem.* **1998**, *110*, 858. (c) Freiser, B. S. *J. Mass Spectrom.* **1996**, *31*, 703. (d) van Koppen, P. A. M.; Kemper, P. R.; Bushnell, J. E.; Bowers, M. T. *J. Am. Chem. Soc.* **1995**, *117*, 2098. (e) Wesendrup, R.; Schröder, D.; Schwarz, H. *Angew. Chem.* **1994**, *105*, 1232. (f) Chen, Y.-M.; Clemmer, D. E.; Armentrout, P. B. *J. Am . Chem. Soc.* **1994**, *116*, 7815. (g) van den Berg, K. J.; Ingemann, S.; Nibbering, N. M. M.; Gregor, I. K. *Rapid. Commun. Mass*

Spectrom. **1993**, *7*, 769. (h) Chowdhury, A. K.; Wilkins, C. L. *J. Am. Chem. Soc.* **1987**, *109*, 5336. (i) Weil, D. A.; Wilkins, C. L. *J. Am. Chem. Soc.* **1985**, *107*, 7316. (j) Jones, R. W.; Staley, R. H. *J. Phys. Chem.* **1982**, *86*, 1669. (k) Jones, R. W., Staley, R. H. *J. Am. Chem. Soc.* **1980**, *102*, 3794.

(5) Combined experimental and theoretical studies on reactions of ionic metal atoms and complexes in the gas phase: (a) Yi, S. S.; Reichert, E. L.; Holthausen, M. C.; Koch, W.; Weisshaar, J. C. *Chem. Eur. J.* **2000**, *6*, 2232. (b) Blomberg, M.; Yi, S. S.; Noll, R. J.; Weisshaar, J. C. *J. Phys. Chem. A* **1999**, *103*, 7254. (c) Diefenbach, M.; Brönstrup, M.; Aschi, M.; Schröder, D.; Schwarz, H. *J. Am. Chem. Soc.* **1999**, *121*, 10614. (d) Schwarz, J.; Schröder, D.; Schwarz, H.; Heinemann, C.; Hrusák, J. *Helv. Chim. Acta* **1996**, *79*, 1110.

(6) Experimental studies on reactions of neutral metal atoms in the gas phase: (a) Wen Y.; Porembski, M.; Ferrett, T. A.; Weisshaar, J. C. *J. Phys. Chem. A* **1998**, *102*, 8362. (b) Wen, Y.; Yethiraj, A.; Weisshaar, J. C. *J. Chem. Phys.* **1997**, *106*, 5509. (c) Carroll, J. J.; Weisshaar, J. C. *J. Phys. Chem.* **1996**, *100*, 12355. (d) Chertihin, G. V.; Andrews, L. *J. Am. Chem. Soc.* **1994**, *116*, 8322. (e) Carroll, J. J.; Haug, K. L.; Weisshaar, J. C. *J. Am. Chem. Soc.* **1993**, *115*, 6962. (f) Carroll, J. J.; Weisshaar, J. C. *J. Am. Chem. Soc.* **1993**, *115*, 800. (g) Ritter, D.; Carroll, J. J.; Weisshaar, J. C. *J. Phys. Chem.* **1992**, *96*, *10636*. (h) Mitchell, S. A.; Hackett, P. A. *J. Chem. Phys.* **1990**, *93*, 7822. (i) Ritter, D.; Weisshaar, J. C. *J. Am. Chem. Soc.* **1990**, *112*, 6425. (j) Fayet, P.; Kaldor, A.; Cox, D. M. *J. Chem. Phys.* **1990**, *92*, 254.

(7) Combined experimental and theoretical studies on reactions of neutral metal atoms in the gas phase: (a) Porembski, M.; Weisshaar, J. C. *J. Phys. Chem. A* **2000**, 104, 1524. (b) Carroll, J. J.; Haug, K. L.; Weisshaar, J. C.; Blomberg, M. R. A.; Siegbahn, P. E. M.; Svensson, M. *J. Phys. Chem.* **1995**, *99*, 13955. (c) Carroll, J. J.; Weisshaar, J. C.; Siegbahn, P. E. M.; Wittborn, A. M. C.; Blomberg, M. R. A. *J. Phys. Chem.* **1995**, *99*, 14388. (d) Mitchell, S.; Blitz, M. A.; Siegbahn, P. E. M.; Svenson, M. *J. Chem. Phys.* **1994**, *100*, 423. (e) Weisshaar, J. C. *Acc. Chem. Res.* **1993**, *26*, 213.

(8) Theoretical studies on reactions of metal complexes: (a) Dedieu, A. *Chem. Rev.* **2000**, *100*, 543. (b) Torrent, M.; Solà, M.; Frenking, G. *Chem. Rev.* **2000**, *100*, 439. (c) Griffin, T. R. *J. Am. Chem. Soc.* **1996**, *118*, 3029. (d) Aullón, G.; Alvarez, S. *Inorg. Chem.* **1996**, *35*, 3137. (e) Ziegler, T. *Chem. Rev.* **1991**, *91*, 651. (f) Koga, N.; Morokuma, K. *Chem. Rev.* **1991**, *91*, 823. (g) Bickelhaupt, F. M.; Baerends, E. J.; Ravenek, W. *Inorg. Chem.* **1990**, *29*, 350. (h) Gritsenko, O. V.; Bagatur'yants, A. A.; Moiseev, I. I.; Kazanskii, V. B. *Russ. Chem. Rev.* **1985**, *54*, 1151.

(9) See also, for example: (a) Lamprecht, D.; Lamprecht, G. J. *J. Comput. Chem.* **2000**, *21*, 692. (b) Minaev, B.; Agren, H. *Int. J. Quantum Chem.* **1999**, *72*, 581. (c) Su, M.-D.; Chu, S.-Y. *J. Am. Chem. Soc.* **1999**, *121*, 1045. (d) Su, M.-D-; Chu, S.-Y. *Inorg. Chem.* **1998**, *37*, 3400. (e) Su, M.-D-; Chu, S.-Y. *Chem. Phys. Lett.* **1998**, *282*, 25. (f) Albert, K.; Gisdakis, P.; Rösch, N. *Organometallics* **1998**, *17*, 1608. (g) Sakaki, S.; Biswas, B.: Sugimoto, M. *Organometallics* **1998**, *17*, 1278. (h) Hill, G. S.; Puddephatt, R. J. *Organometallics* **1998**, *17*, 1478. (i) Sakaki, S.; Ogawa, M.; Kinoshita, M. *J. Phys. Chem.* **1995**, *99*, 9933. (j) Irikura, K. K.; Goddard, W. A., III *J. Am. Chem. Soc.* **1994**, *116*, 8733. (k) Perry, J. K.; Goddard, W. A., III *J. Am. Chem. Soc.* **1994**, *116*, 5013. (l) Sellers, H. *J. Comput. Chem.* **1990**, *11*, 754. (m) Rosi, M.; Bauschlinger Jr., C. W.; Langhoff, S. R.; Partidge, H. *J. Phys. Chem.* **1990**, *94*, 8656. (n) Ziegler, T.; Tschinke, V.; Fan, L.; Becke, A. D. *J. Am. Chem. Soc.* **1989**, *111*, 9177. (o) Low, J. J.; Goddard, W. A., III *J. Am. Chem. Soc.* **1986**, *108*, 6115.

(10) (a) Bickelhaupt, F. M. *J. Comput. Chem.* **1999**, *20*, 114. (b) Bickelhaupt, F. M.; Ziegler, T.; von Ragué Schleyer, P. *Organometallics* **1995**, *14*, 2288.

(11) Theoretical studies on reactions of neutral metal atoms: (a) Maseras, F.; Lledós, A.; Clot, E.; Eisenstein, O. *Chem. Rev.* **2000**, *100*, 601. (b) Cui, Q.; Musaev, D. G.; Morokuma, K. *J. Chem. Phys.* **1998**, *108*(20), 8418. (c) Wittborn, A. M. C.; Costas, M.; Blomberg, M. R. A.; Siegbahn, P. E. M. *J. Chem. Phys.* **1997**, *107*, 4318. (d) Siegbahn, P. E. M. *J. Am. Chem. Soc.* **1994**, *116*, 7722. (e) Siegbahn, P. E. M. *Organometallics* **1994**, *13*, 2833. (f) Perry, J. K.; Ohanessian, G.; Goddard, W. A., III *Organometallics* **1994**, *13*, 1870. (g) Blomberg, M. R. A.; Siegbahn, P. E. M.; Svensson, M. *Inorg. Chem.* **1993**, *32*, 4218. (h) Siegbahn, P. E. M.; Blomberg, M. R. A.; Svensson, M. *J. Phys. Chem*. **1993**, *97*, 2564. (i) Siegbahn, P. E. M.; Blomberg, M. R. A.; Svensson, M. *J. Am. Chem. Soc.* **1993**, *115*, 1952. (j) Siegbahn, P. E. M.; Blomberg, M. R. A.; Svensson, M. *J. Am. Chem. Soc.* **1993**, *115*, 4191. (k) Siegbahn, P. E. M.; Blomberg, M. R. A. *J. Am. Chem. Soc.* **1992**, *114*, 10548. (l) Blomberg, M. R. A.; Siegbahn, P. E. M.; Svensson, M. *J. Am. Chem. Soc.* **1992**, *114*, 6095. (m) Svensson, M.; Blomberg, M. R. A.; Siegbahn, P. E. M. *J. Am. Chem. Soc.* **1991**, *113*, 7076. (n) Novaro, O.; Jarque, C. *Theor. Chim. Acta* **1991**, *80*, 19. (o) Blomberg, M. R. A.; Siegbahn, P. E. M.; Nagashima, U.; Wennerberg, J. *J. Am. Chem. Soc.* **1991**, *113*, 424. (p) Carter, E. A.; Goddard, W. A., III *J. Phys. Chem.* **1988**, *92*, 5679. (q) Nakatsuji, H.; Hada, M.; Yonezawa, T. *J. Am. Chem. Soc.* **1987**, *109*, 1902. (r) Low, J. J.; Goddard, W. A., III *Organometallics* **1986**, *5*, 609. (s) Koga, N.; Obara, S.; Kitaura, K.; Morokuma, K. *J. Am. Chem. Soc.* **1985**, *107*, 7109. (t) Low, J. J.; Goddard, W. A., III *J. Am. Chem. Soc.* **1984**, *106*, 8321. (u) Blomberg, M.; Brandemark, U.; Petterson, L.; Siegbahn, P. *Int. J. Quantum Chem.* **1983**, *23*, 855.

(12) Theoretical studies on ML_n: (a) Vedernikov, A. N.; Shamov, G. A.; Solomonov, B. N. *Russ. J. Gen. Chem.***1998**, *68*(5), 667. (b) Vedernikov, A. N.; Shamov, G. A.; Solomonov, B. N. *Russ. J. Gen. Chem.***1998**, *68*(5), 675. (c) Sakaki, S.; Biswas, B.; Sugimoto, M. *J. Chem. Soc., Dalton Trans.* **1997**, 803. (d) Shamov, G. A.; Vedernikov, A. N.; Solomonov, B. N. *Russ. J. Gen. Chem.* **1997**, *67*(7), 999. (e) Ziegler, T. *Inorg. Chem.* **1985**, *24*, 1547.

(13) Palladium as catalyst: Malleron, J.-L.; Fiaud, J.-C.; Legros, J.-Y. *Handbook of Palladium Catalyzed Organic Reactions*; Academic Press, 1997. (c) Cornils, R.; Herrmann, W. A. *Applied Homogenous Catalysis with Organometallic Compounds. Vol. 1;* VCH: Weinheim, 1996, p394.

(14) Diefenbach, A.; Bickelhaupt, F. M., in preparation. Compare the chapters of this thesis.

(15) Density functional theory (DFT): (a) Dreizler, R. M.; Gross, E. K. U. *Density Functional Theory. An approach to the Quantum Many-Body Problem*; Springer: Berlin, 1990. (b) Parr, R. G.; Yang, W. *Density-Functional Theory of Atoms and Molecules*; Oxford University Press: New York, 1989. (c) Gritsenko, O. V.; Ensing, B.; Schipper, P. R. T.; Baerends, E. J. *J. Chem. Phys.*, in press.

(16) Kohn-Sham MO model in DFT: (a) Bickelhaupt, F. M.; Baerends, E. J. In *Reviews in Computational Chemistry*, Vol. 15, Lipkowitz, K. B., Boyd., D. B., Eds.; Wiley-VCH: New York, 2000; Vol. 15, Chapter 1. (b) Baerends, E. J.; Gritsenko, O. V. *J. Phys. Chem. A* **1997**, *101*, 5383.

(17) Amsterdam Density Functional (ADF) program: (a) Fonseca Guerra, C.; Visser, O.; Snijders, J. G.; te Velde, G.; Baerends, E. J., *The Parallelization of the Amsterdam Density Functional Program*, In: Methods and Techniques for Computational Chemistry; Clementi, E., Corongiu, G., Eds.; STEF: Cagliari, 1995; p. 305-395. (b) Baerends, E. J.; Ellis, D. E.; Ros, P. *Chem. Phys.* **1973**, *2*, 41. (c) Baerends, E. J.; Ros, P. *Chem. Phys.* **1975**, *8*, 412. (d) Baerends, E. J.; Ros, P. *Int. J. Quantum Chem., Quantum Chem. Symp.* **1978**, *S12*, 169. (e) Fonseca Guerra, C.; Snijders, J. G.; te Velde, G.; Baerends, E. J. *Theor. Chem. Acc.* **1998**, *99*, 391. (f) Boerrigter, P. M.; te Velde, G.; Baerends, E. J. *Int. J. Quantum Chem.* **1988**, *33*, 87. (g) te Velde, G.; Baerends, E. J. *J. Comp. Phys.* **1992**, *99*, 84. (h) Snijders, J. G.; Baerends, E. J.; Vernooijs, P. *At. Nucl. Data Tables* **1982**, *26*, 483. (i) Krijn, J.; Baerends, E. J. *Fit-Functions in the HFS-Method; Internal Report* (in Dutch); Vrije Universiteit: Amsterdam, 1984. (j) Slater, J. C. *Quantum Theory of Molecules and Solids Vol. 4*; McGraw-Hill: New York, 1974. (k) Becke, A. D. *J. Chem. Phys.* **1986**, *84*, 4524. (l) Becke, A. *Phys. Rev. A* **1988**, *38*, 3098. (m) Vosko, S. H.; Wilk, L.; Nusair, M. *Can. J. Phys.* **1980**, *58*, 1200. (n) Perdew, J. P. *Phys. Rev. B* **1986**, *33*, 8822 (Erratum: *Phys. Rev. B* **1986**, *34*, 7406). (o) Fan, L.;

Ziegler, T. *J. Chem. Phys.* **1991**, *94*, 6057. (p) Versluis, L.; Ziegler, T. *J. Chem. Phys.* **1988**, *88*, 322. (q) Fan, L.; Versluis, L.; Ziegler, T.; Baerends, E. J.; Ravenek, W. *Int. J. Quantum. Chem., Quantum. Chem. Symp.* **1988**, *S22*, 173. (r) Fan, L.; Ziegler, T. *J. Chem. Phys.* **1990**, *92*, 3645. (s) Banerjee, A.; Adams, N.; Simons, J.; Shepard, R. *J. Phys. Chem.* **1985**, *89*, 52. (t) Baker, J. *J. Comput. Chem.* **1986**, *7*, 385.

(18) ZORA approach: (a) Chang, C.; Pelissier, M.; Durand, P. *Phys. Scr.* **1986**, *34*, 394. (b) van Lenthe, E.; Baerends, E. J.; Snijders, J. G. *J. Chem. Phys.* **1993**, *99*, 4597. (c) van Lenthe, E.; Baerends, E. J.; Snijders, J. G. *J. Chem. Phys.* **1994**, *101*, 9783. (d) van Lenthe, E.; Snijders, J.; Baerends, E. J. *J. Chem. Phys.* **1996**, *105*, 6505. (e) van Lenthe, E. *Thesis*, Vrije Universiteit, Amsterdam, 1996. (f) van Lenthe, E.; van Leeuwen, R.; Baerends, E. J.; Snijders, J. G. *Int. J. Quantum Chem.* **1996**, *57*, 281.

(19) Atkins, P. W. *Physical Chemistry*; Oxford University Press: Oxford, 1998.

(20) Holleman, A. F.; Wiberg, N. *Lehrbuch der Anorganischen Chemie*; de Gruyter: Berlin, 1985.

8 Summary

This thesis presents the results of a density functional theoretical (DFT) study of palladium-catalyzed C–X bond activation, an elementary organometallic processes that is ubiquitous in homogeneous catalysis (see general introduction, chapter 1). In particular, the oxidative addition of C–H, C–C, C–Cl and C–I bonds as well as, for comparison, the H–H bond to both the uncoordinated palladium atom and palladium–ligand complexes is investigated at the BP86/TZ(2)P level of theory taking relativistic effects into account through the ZORA approach (see methods, chapter 2). The purpose is to introduce the concept of and provide a foundation for Fragment-oriented Design of Catalysts (FDC). This is a new approach for rationally designing catalytically active and selective transition metal systems. The basic idea is to reveal the actual influence of the ligands by first studying the intrinsic reactivity of the uncoordinated metal atom and adding the ligands stepwise in a second stage. A key role in this approach is played by the Activation strain-TS interaction (ATS) model of chemical reactivity in which activation energies $\Delta E^{\neq}$ are decomposed into and interpreted in terms of: (i) the activation strain $\Delta E^{\neq}_{\text{strain}}$ associated with deforming the reactants (e.g. catalyst and substrate) from their equilibrium structure to the geometry they adopt in the activated complex, and (ii) the TS interaction $\Delta E^{\neq}_{\text{int}}$, that is, the actual interaction between these strained reactants in the transition state ($\Delta E^{\neq} = \Delta E^{\neq}_{\text{strain}} + \Delta E^{\neq}_{\text{int}}$).

After the general introduction in chapter 1 and an overview of theoretical methods in chapter 2, the investigation starts with a detailed analysis of the nature of the transition metal–carbonyl bond in a series of neutral and ionic hexacarbonyl complexes in chapter 3. This serves a better understanding, which comes in helpful in the later chapters on FDC, of how ligands interact with and affect the electronic structure at the metal center of a catalyst. The model systems considered are the isoelectronic hexacarbonyls $Ir(CO)_6^{3+}$, $Os(CO)_6^{2+}$, $Re(CO)_6^{+}$, $W(CO)_6$, $Ta(CO)_6^{-}$ and $Hf(CO)_6^{2-}$ The transition metal–carbonyl interaction in each of these complexes is analyzed in two different, complementary fashions: (i) as the interaction between a (neutral or charged)

$M(CO)_5^q$ fragment and one CO ligand, and (ii) as the interaction between a (neutral or charged) transition metal atom M^q and a cage of six CO ligands, $(CO)_6$. Both approaches reveal that the net charge significantly influences the relative importance of σ donation (from the CO 5σ orbital) and π backdonation (into the CO $1\pi^*$ orbital). Whereas σ donation and π backdonation are more or less in balance for the neutral tungsten and the singly positive rhenium complexes, σ donation becomes dominant for the more strongly positively charges systems and π backdonation prevails in the negatively charged complexes. An important finding is that the p AOs of the transition metals studied are strongly involved in the coordination bond and can certainly be conceived as valence orbitals.

Next, in chapter 4, the importance of relativistic effects for the DFT calculations on palladium-catalyzed C–X bond activation is assessed and the overall performance of the ZORA-BP86/TZ(2)P approach for computing reliable trends in reactivity is evaluated. This is done by systematically studying the oxidative addition reactions of Pd(0) with CH_4, C_2H_6 and CH_3Cl using nonrelativistic (NR), quasirelativistic (QR), and zeroth-order regular approximated (ZORA) relativistic density functional theory (DFT) at the BP86/TZ(2)P level. It turns out that relativistic effects are indeed important for an accurate quantum chemical description of the oxidative insertion of the second-row transition metal palladium into C–H, C–C and C–Cl bonds of the model systems CH_4, C_2H_6 and CH_3Cl, respectively, at BP86/TZ(2)P. The effect of relativity in both the quasirelativistic (QR) and, to a slightly lesser extent, in the ZORA approach is that stationary points along the reaction coordinate are stabilized with respect to reactants. This stabilization becomes stronger as the reaction proceeds, i.e., in the order reactant complex (RC) < transition state (TS) < product (P). Consequently, activation enthalpies are reduced by 6 (C–Cl) to 14 kcal/mol (C–H) and reaction enthalpies become more exothermic by 15 (C–Cl) up to 20 kcal/mol (C–C). However, the relative order of barrier heights and reaction enthalpies is not affected. In all three approaches, i.e. NR, QR and ZORA, the activation barrier decreases in the order C–C > C–H > C–Cl and the reaction becomes more exothermic in the order C–H > C–C > C–Cl. At ZORA-

BP86/TZ(2)P one obtains, for example, 298 K activation enthalpies $\Delta H^{\neq}_{298}$ of –5.0 (C–H), 9.6 (C–C) and –6.0 kcal/mol (C–Cl). Another relativistic effect is that all transition states become more educt-like. These effects can be understood in terms of the well-known relativistic destabilization of the Pd 4d HOMO and stabilization of the Pd 5s LUMO. This makes the metal both a better electron donor and acceptor which leads to stronger donor–acceptor interactions between Pd and the substrate. The result is an additional stabilization of transition states and oxidative insertion products relative to the separate reactants.

Best agreement of the BP86/TZ(2)P results with *ab initio* PCI-80 benchmark values and gas-phase spectroscopic experiments is obtained using the ZORA relativistic approach. In accordance with gas-phase experiments by Weisshaar and others on reactions of Pd with alkanes, reaction profiles are obtained with pronounced potential wells for reactant complexes bound by –11.4 (CH_4), –11.6 (C_2H_6) and –15.6 kcal/mol (CH_3Cl). In the experiments, such complexes have been collisionally stabilized and observed for alkanes larger than CH_4. However, while ZORA-BP86/TZ(2)P and PCI-80 yield the same trends for reactivity, discrepancies of 8 - 9 kcal/mol remain for absolute values in activation energies. This may be ascribed to the combined effect of an underestimation of barriers by DFT and the uncertainty of a few kcal/mol in the PCI-80 results of Siegbahn, Blomberg and coworkers.

Thereafter, in chapters 5 and 6, the approach of Fragment-oriented Design of Catalysts (FDC) is introduced and developed. To achieve a better understanding of palladium-catalyzed H–H, C–H, C–C and C–Cl bond activation and the mutual competition between these processes, in chapter 5 several mechanistic pathways for oxidative addition of Pd(0) to H_2 (H–H), CH_4 (C–H), C_2H_6 (C–C and C–H) and CH_3Cl (C–Cl) are investigated uniformly at the ZORA-BP86/TZ(2)P level of relativistic nonlocal density functional theory (DFT). Pd(0)-catalyzed activation of the prototypical H–H, C–H, C–C and C–Cl bonds in H_2, CH_4, C_2H_6 and CH_3Cl, i.e., oxidative addition to a Pd-d^{10} atom is exothermic and occurs via direct oxidative insertion (OxIn) of the metal atom. Activation enthalpies $\Delta H^{\neq}_{298}$ increase from –21.7 to +9.6 kcal/mol in the

order H–H < C–Cl ≈ C–H < C–C. The "straight" S_N2 substitution resulting in $PdCH_3^+$ + X^- or PdH^+ + H^- is highly endothermic (144 - 237 kcal/mol) and thus not a competitive alternative for oxidative addition. However, for Pd + CH_3Cl, a third mechanism is found in which S_N2 substitution occurs in concert with a rearrangement of the Cl^- leaving group from C to Pd (S_N2/Cl-ra) leading, in one step, to the oxidative addition product CH_3PdCl via a more moderate activation barrier $\Delta H^{\neq}_{298}$ of 19.3 kcal/mol.

The various bond activation processes have been analyzed using the Activation Strain (or Activation strain-TS interaction, ATS) model in which the activation energy $\Delta E^{\neq}$ is decomposed into the activation strain $\Delta E^{\neq}_{strain}$ of and the stabilizing transition state (TS) interaction $\Delta E^{\neq}_{int}$ between the reactants in the activated complex: $\Delta E^{\neq} = \Delta E^{\neq}_{strain} + \Delta E^{\neq}_{int}$. Interestingly, it turns out that the activation strain $\Delta E^{\neq}_{strain}$ adopts a characteristic value for a particular type of bond and reaction mechanism. In case of the direct oxidative insertion (OxIn) reaction, the activation strain $\Delta E^{\neq}_{strain}$ decreases in the order H–H ≈ C–H < C–C < C–Cl. This trend in $\Delta E^{\neq}_{strain}$ is determined by (i) the *strength* of the activated bond, and (ii) the *elongation* of this bond, in terms of percentage, in the TS relative to the isolated substrate. The TS interaction $\Delta E^{\neq}_{int}$ becomes less stabilizing in the order H–H > C–H > C–C > C–Cl. This trend turns out to be mainly determined by the donor–acceptor orbital interactions between occupied Pd 4d AOs and the empty $\sigma^*_{C–X}$ (or $\sigma^*_{H–H}$) acceptor orbital associated with the bond to be activated in the substrate.

In chapter 6, the mechanism of anion assistance in palladium-catalyzed H–H, C–H, C–C and C–Cl bond activation is to be unraveled and understood by studying several mechanistic pathways for oxidative addition of Pd and $PdCl^-$ to H_2 (H–H), CH_4 (C–H), C_2H_6 (C–C and C–H) and CH_3Cl (C–Cl). Anion assistance turns out to lower activation barriers and to increase the exothermicity of the various bond activation processes. Activation enthalpies $\Delta H^{\neq}_{298}$ for oxidative insertion of $PdCl^-$ into the various types of bonds are lower than but increase essentially in the same order as for Pd, that is, along H–H < C–H ≈ C–Cl < C–C. The effect of anion assistance is selective. It favors the highly endothermic S_N2 mechanism over direct oxidative insertion (OxIn). Interestingly, in case of $PdCl^-$ + CH_3Cl, this leads to the two-step mechanism of S_N2

substitution followed by leaving-group rearrangement (S_N2/Cl-ra) becoming the preferred mechanism for oxidative addition. The highest overall barrier of this pathway (–20.2 kcal/mol) drops below the barrier for direct oxidative insertion (–11.2 kcal/mol). For all other bond activation processes of $PdCl^-$ (i.e. H–H, C–H, C–C), oxidative insertion remains the lowest-barrier pathway.

The mechanism through which anion assistance works has been analyzed using again the Activation Strain model. It was found that, for each particular bond and reaction mechanism, the activation strain $\Delta E^{\neq}_{strain}$ adopts a specific value which differs only marginally for corresponding Pd and $PdCl^-$ induced reactions. Thus, the activation strain can be conceived as a characteristic of the bond and the mechanism of its activation. The lowering of activation barriers through anion assistance is caused by a stronger, more stabilizing TS interaction $\Delta E^{\neq}_{int}$. This increase in $\Delta E^{\neq}_{int}$ can be ascribed to the raise in Pd-4d derived orbitals in $PdCl^-$ which translates, amongst others, into a more binding donor–acceptor orbital interaction between the metal and the substrate.

Finally, to learn how ligands direct the palladium-catalyzed activation of C–H, C–C and C–I bonds, the oxidative addition of Pd and *cis*-$Pd(CO)_2I_2$ to CH_4 (C–H), C_2H_6 (C–C and C–H) and CH_3I (C–I) were explored at the ZORA-BP86/TZ(2)P level of density functional theory (DFT) in chapter 7. The purpose is a rough exploration of how the mechanism of bond activation changes if one goes from an uncoordinated metal atom to a metal complex as model catalyst. The introduction of ligands if one goes from uncoordinated Pd to the *cis*-$Pd(CO)_2I_2$ model catalyst turns out to have a number of substantial effects on palladium-catalyzed activation of C–H, C–C and C–I bonds. For both Pd and *cis*-$Pd(CO)_2I_2$, direct oxidative insertion (OxIn) is the lowest-barrier pathway whereas nucleophilic substitution (S_N2) is highly endothermic and therefore not competitive. The effect of introducing ligands is a substantial increase of the activation enthalpy for oxidative insertion by 50 - 60 kcal/mol. Activation enthalpies for oxidative insertion increase in the order C–I $\lesssim$ C–H < C–C for both Pd and *cis*-$Pd(CO)_2I_2$ (with higher absolute values for the latter). Overall oxidative addition is

exothermic by –10 (C–H in CH_4) through –45 kcal/mol (C–I) for Pd, and endothermic by 21 (C–I) through 47 kcal/mol (C–C) for *cis*-$Pd(CO)_2I_2$.

Obviously, the *cis*-$Pd(CO)_2I_2$ complex would be a poor catalyst. Yet, the exploration of its reactivity has uncovered interesting features that are not present in the reactions of uncoordinated Pd. First, in the TS for oxidative insertion, the C–X bond (X = H, C, I) that is to be activated can have, in principle, different orientations with respect to the square-planar *cis*-$Pd(CO)_2I_2$ complex, e.g., C–X (**O-1**) or X–C (**O-4**) along an I–Pd–CO axis, or in between two I–Pd–CO axes (**O-1**, **O-3**, **O-5**; see also Scheme 1 in Chapter 7). It was found that oxidative insertion of *cis*-$Pd(CO)_2I_2$ into the C–H bonds can occur via two different transition states, corresponding to two orientations of the C–H bond along an I–Pd–CO axis, i.e. **O-2** and **O-4**, at approximately the same energy. For oxidative insertion of *cis*-$Pd(CO)_2I_2$ into each, C–C and C–I bonds, only one TS was found corresponding to an orientation of the activated in between two I–Pd–CO axes (i.e., between **O-1** and **O-2** for C–C, and **O-1** for C–I). Furthermore, at variance to the uncoordinated metal, the metal complex may be deformed in the TS. This leads to the phenomenon of calibration or adjustment of the catalyst to the substrate in the TS. To quantitatively monitor the calibration process, the Activation Strain (or Activation strain-TS interaction, ATS) model has been extended in that the activation strain $\Delta E^{\neq}_{\text{strain}}$ is separated into distinct terms for substrate and catalyst. Both terms prove to be characteristic for each type of activated bond. However, the drastic change in the character of the pathway associated with going from Pd to the sterically more demanding and flexible *cis*-$Pd(CO)_2I_2$ complex leads to a change in all activation strain values. Furthermore, it was found that the stronger the bond and the more endothermic the reaction, the higher the activation strain of both the substrate and the *cis*-$Pd(CO)_2I_2$ model catalyst. An important consequence of the phenomenon of calibration is that, for designing and tuning the electronic structure of the catalyst for a particular bond with the help of ligands, one must consider its structure in the TS (i.e. after calibration). This is the geometry that counts because it is the one in which the

catalyst has the TS interaction with the substrate. Note, that the catalyst's structure in the TS can and does in a number of cases differ from its own equilibrium geometry.

In conclusion, the investigations have shown that elementary organometallic reactions that play a role in catalysis can be understood in detail on the basis of the Activation Strain (or Activation strain-TS interaction, ATS) model. It is now possible to characterize an activation barrier in terms of the activation strain, a characteristic of the bond to be activated (but also of the catalytically active metal complex), and the TS interaction. The latter provides the necessary basis for understanding how the activity of a catalyst depends on its electronic structure. Still, much work remains to be done. In the first place, one will have to explore the possibilities of tuning the catalyst's electronic structure, through a clever choice of ligands, such that the TS interaction is selectively optimized (i.e. maximized) for one particular bond. On the other hand, it will also be important to apply and test the performance of a new generation of highly accurate density functionals, i.e., the meta-GGAs (which contain the kinetic energy density or the Laplacian of the density *in addition* to the density and its gradient) that are just beginning to become available. Finally, the insights obtained in the investigations on simple models for catalytic processes provide a basis for and may be considered as a first step toward a genuine Fragment-oriented Design of Catalysts (FDC) in which highly selective catalysts can be designed modularly and in a rational manner.

Zusammenfassung

In der Organometallchemie stellen C–X Bindungsaktivierungen einen elementaren Schritt dar, der bei der homogenen Katalyse häufig angetroffen wird (vgl. allgemeine Einleitung, Kapitel 1). Ein umfassendes theoretisches Verständnis dieses Schrittes ist daher außerordentlich wichtig. Mit dieser Dissertation wird hierzu ein Beitrag geliefert, der auf einem neuartigen Konzept basiert: dem „Fragment-orientierten Katalysatordesign“ (vgl. Kapitel 5).

Die vorgelegte Arbeit basiert auf ZORA-BP86/TZ(2)P Dichtefunktionaltheorie-Rechnungen von Palladium-katalysierten C–X Bindungsaktivierungen. Untersucht wurde die oxidative Addition von H–H, C–H, C–C, C–Cl und C–I Bindungen an ein unkoordiniertes Palladiumatom und an Palladium-Komplexe. Mit diesen Untersuchungen wurde das Konzept des Fragment-orientierten Katalysatordesigns (*fragment-oriented design of catalysts*, FDC) eingeführt. FDC ist ein neuartiger Ansatz zur rationalen Entwicklung katalytisch aktiver und selektiver Systeme. Der Grundgedanke ist, durch einen schrittweisen Aufbau eines Katalysators die Einflüsse der Liganden offen zu legen und zu erkennen. Hierzu wird mit der Erforschung der intrinsischen Reaktivität eines unkoordinierten Übergangsmetallatoms begonnen. In folgenden Schritten werden zum Metallatom nach und nach Liganden hinzugefügt und die Änderungen der Katalysatorreaktivität beobachtet. Hierbei spielt das Aktivierungsspannungs-Modell der chemischen Reaktivität (*Activation Strain* oder auch *Activation strain-Transition State interaction model*, ATS) eine Schlüsselrolle. In ihm wird zu Interpretationszwecken die Übergangszustandsstruktur in diejenigen Fragmente eingeteilt, die dem ursprünglichen Substrat bzw. Katalysator zuzuordnen sind. Die Aktivierungsbarriere $\Delta E^{\neq}$ wird dann in die Aktivierungsspannung $\Delta E^{\neq}_{\text{strain}}$ und die Wechselwirkungsenergie $\Delta E^{\neq}_{\text{int}}$ zerlegt: $\Delta E^{\neq} = \Delta E^{\neq}_{\text{strain}} + \Delta E^{\neq}_{\text{int}}$. Erste gibt an, wie viel Energie nötig ist, um Substrat und Katalysator, ausgehend von ihren Gleichgewichtsgeometrien, in die Geometrie des Übergangszustandes zu bringen. Die Energie, die bei der Wechselwirkung der beiden so vorbereiteten Fragmente frei wird, ist in $\Delta E^{\neq}_{\text{int}}$ subsummiert.

Nach einer allgemeinen Einführung in Kapitel 1 und einem Überblick über die verwendeten theoretischen Methoden in Kapitel 2, werden in Kapitel 3 die Untersuchungen mit einer detaillierten Analyse der Natur der Übergangsmetall-Carbonyl Bindung in einer Serie von neutralen bzw. geladenen, isoelektronischen Hexacarbonylkomplexen begonnen: $Ir(CO)_6^{3+}$, $Os(CO)_6^{2+}$, $Re(CO)_6^{+}$, $W(CO)_6$, $Ta(CO)_6^{-}$ und $Hf(CO)_6^{2-}$. Hierdurch wird ein tieferes Verständnis der Metall–Ligand Wechselwirkung erlangt, das in späteren Stadien des FDC Ansatzes nützlich ist. Die Übergangsmetall–Carbonyl Wechselwirkungen in diesen Komplexen werden in zwei unterschiedlichen, sich ergänzenden Weisen untersucht: (1) Als Wechselwirkung zwischen einem neutralen bzw. geladenen Fragment $M(CO)_5^q$ und einem CO, sowie (2) als Wechselwirkung zwischen dem neutralen bzw. geladenen Metallatom M^q und dem kompletten $(CO)_6$ Käfig. Beide Ansätze zeigen, dass die Ladung q die relative Bedeutungen der σ Donierung vom CO 5σ Orbital in unbesetzte Metallorbitale und der π Rückdonierung von besetzten Metallorbitalen in das CO $1\pi^*$ signifikant beeinflusst. Wohingegen die σ Donierung und π Rückdonierung in den neutralen und einfach geladenen Spezies mehr oder weniger ausgeglichen ist, dominiert in den höher positiv geladenen Komplexen die σ Donierung, und in den stark negativ geladenen Komplexen die π Rückdonierung. Die Studie zeigt, dass die p Atomorbitale der untersuchten Übergangsmetalle stark an den Bindungen zu den koordinierten Liganden beteiligt sind, und daher als Valenzorbitale aufgefasst werden können.

In Kapitel 4 wird die Bedeutung von relativistischen Effekten auf die Dichtefunktionalberechnungen der Palladium-katalysierten C–X Bindungsaktivierungen untersucht, sowie die Tauglichkeit der ZORA-BP86/TZ(2)P Rechnungen zur Bestimmung verlässlicher Trends geprüft (ZORA = *zeroth-order regular approximation*). Hierzu wird die oxidative Addition von Pd^0 und CH_4, C_2H_6 und CH_3Cl auf der Basis nichtrelativistischer, quasirelativistischer und ZORA-relativistischer Dichtefunktionaltheorie des Niveaus BP86/TZ(2)P berechnet. Die Ergebnisse zeigen, dass relativistische Effekte für eine akkurate Beschreibung der untersuchten Systeme

essentiell wichtig sind. Bei der Berücksichtigung relativistischer Effekt werden stationäre Punkte, d.h. Reaktand-Komplexe (*reactant complex*, RC), Übergangszustände (*transition state*, TS) und Produkte (*product*, P), entlang der Reaktionskoordinate in Bezug auf die freien Reaktanden, d.h. Pd^0 und das jeweilige freie Substrat, stabilisiert. Die Stabilisierung ist umso stärker, je weiter die Reaktion fortschreitet, d.h. in der Reihenfolge RC < TS < P. Entsprechend werden die Aktivierungsbarrieren reduziert (die Erniedrigung liegt zwischen 6 (C–Cl) und 14 kcal/mol (C–H)) und die Reaktionen werden exothermer (zwischen 15 (C–Cl) und 20 kcal/mol (C–C)). Die relative Ordnung der Barrierenhöhen und Reaktionsenthalpien bleibt bestehen. In allen drei Ansätzen, d.h. im nichtrelativistischen, quasirelativistischen und ZORA-relativistischen, nehmen die Aktivierungsbarrieren in der Reihenfolge C–C > C–H > C–Cl ab, und die Reaktionen werden in der Reihenfolge C–H < C–C < C–Cl exothermer. So betragen zum Beispiel die 298 K Aktivierungsenthalpien $\Delta H^{\neq}_{298}$ auf dem ZORA-BP86/TZ(2)P Niveau –5.0 (C–H), 9.6 (C–C) und –6.0 kcal/mol (C–Cl) im Bezug auf die freien Reaktanden. Ein weiterer relativistischer Effekt ist, dass die Übergangszustände den Edukten ähnlicher werden. Im allgemeinen fallen die Effekte, die nach der ZORA Methode berechnet wurden, etwas moderater aus als diejenigen, die mit dem quasirelativistischen Ansatz bestimmt wurden.

Die beobachteten Effekte lassen sich auf die bekannte relativistische Destabilisierung der besetzten Pd 4d Orbitale und der Stabilisierung und Kontraktion des Pd 5s Orbitals zurückführen: die Donierungs- und Akzeptorfähigkeit des Palladiums nehmen hierdurch zu. Daher werden die Donor-Akzeptor Wechselwirkungen zwischen Pd und den Substraten gestärkt. Als Ergebnis findet sich eine Stabilisierung der Übergangszustände und der Reaktionsprodukte relativ zu den getrennten Edukten.

Die beste Übereinstimmung zwischen den BP86/TZ(2)P Rechnungen und Benchmark *ab initio* PCI-80 Berechnungen, sowie in Bezug auf spektroskopische Experimente in der Gasphase, finden sich mit der ZORA Methode. In Übereinstimmung mit experimentellen Untersuchungen (durchgeführt von Weisshaar und anderen) der

Gasphasenreaktionen von Pd mit Alkanen wurden stabile Reaktand-Komplexe gefunden: –11.4 (CH_4), –11.6 (C_2H_6) und –15.6 kcal/mol (CH_3Cl) auf ZORA-BP86/TZ(2)P. Im Experimenten wurden diese Komplexe durch Kollisionen mit dem Puffergas stabilisiert und konnten für Alkane nachgewiesen werden, die größer als CH_4 sind. Obgleich die ZORA-BP86/TZ(2)P und PCI-80 Berechnungen die gleichen Trends für die Reaktivität liefern, bleiben in den absoluten Werten Unterschiede von 8 - 9 kcal/mol bestehen. Diese Diskrepanz ist zu verstehen, da zum einen Aktivierungsbarrieren durch DFT Rechnungen im allgemeinen unterschätzt werden, und zum anderen in den PCI-80 Rechnungen von Siegbahn, Blomberg *et. al.* eine Restunsicherheit von einigen kcal/mol vorhanden ist.

In den Kapiteln 5 und 6 wird der Ansatz des Fragment-orientierten Katalysatordesigns (*fragment-oriented design of catalysts*, FDC) eingeführt und weiter entwickelt. Um ein eingehendes Verständnis der Palladium-katalysierten H–H, C–H, C–C und C–Cl Bindungsaktivierungen sowie deren gegenseitige Konkurrenz zu erhalten, werden in Kapitel 5 verschiedene Reaktionsmechanismen der oxidativen Addition von Pd^0 und H_2 (H–H), CH_4 (C–H), C_2H_6 (C–H und C–C) und CH_3Cl (C–Cl) mit ZORA-BP86/TZ(2)P Dichtefunktionalberechnungen untersucht. Die untersuchten Pd^0-katalysierten Aktivierungen sind exotherm und verlaufen über eine direkte oxidative Insertion (OxIn) des Metallatoms in die entsprechende Bindung. Die Aktivierungsenthalpien $\Delta H^{\neq}_{298}$ liegen zwischen –21.7 und 9.6 kcal/mol, und nehmen in der Reihenfolge H–H < C–Cl ≈ C–H < C–C zu. Eine prinzipielle Alternative zur direkten oxidativen Insertion ist die S_N2 Substitution mit den dissoziierten Spezies $PdCH_3^+ + X^-$ bzw. $PdH^+ + H^-$ als Produkt. Aufgrund der Ladungstrennung sind diese sehr endotherm (144 - 237 kcal/mol). Daher stellt der S_N2 Mechanismus keinen echten Konkurrenzmechanismus dar. Für das System Pd + CH_3Cl wurde ein dritter Reaktionspfad gefunden, in dem sich direkt im Anschluss einer S_N2 Substitution die Abgangsgruppe Cl^- vom C zum Pd umlagert (S_N2/Cl-ra Reaktion) und sich so das Produkt der direkten oxidativen Insertion, CH_3PdCl, bildet. Die Aktivierungsbarriere dieser Reaktion ist 21.2 kcal/mol.

Die verschiedenen Bindungsaktivierungsprozesse wurden mit dem Aktivierungsspannungs-Modell der chemischen Reaktivität (*Activation Strain* oder auch *Activation strain-Transition State interaction model*, ATS) untersucht, in dem die Aktivierungsenergie $\Delta E^{\neq}$ in die Aktivierungsspannung $\Delta E^{\neq}_{\text{strain}}$ und die stabilisierende Übergangszustandswechselwirkungsenergie $\Delta E^{\neq}_{\text{int}}$ aufgeteilt wird: $\Delta E^{\neq} = \Delta E^{\neq}_{\text{strain}} + \Delta E^{\neq}_{\text{int}}$ (vgl. auch Beginn der Zusammenfassung). Interessanterweise wird festgestellt, dass die Aktivierungsspannung $\Delta E^{\neq}_{\text{strain}}$ sowohl für die Art einer Bindung als auch für den Reaktionspfad charakteristische Werte annimmt. Im Falle der direkten oxidativen Insertion (OxIn) nimmt die Aktivierungsspannung $\Delta E^{\neq}_{\text{strain}}$ in der Reihenfolge H–H ≈ C–H > C–C > C–Cl ab. Dieser Trend wird durch die Stärke der aktivierten Bindung und durch ihre prozentuelle Verlängerung relativ zur entsprechenden Länge im freien Substrat bestimmt. Die Stabilisierung der Übergangszustandswechselwirkungsenergie nimmt in der Reihenfolge H–H > C–H > C–C > C–Cl ab. Hier spielt die Donor-Akzeptor Orbitalwechselwirkung zwischen den besetzten Pd 4d und den unbesetzten $\sigma^*_{\text{C–X}}$ (bzw. $\sigma^*_{\text{H–H}}$) der jeweiligen aktivierten Bindung in den Substraten die ausschlaggebende Rolle.

Im 6. Kapitel wird der Einfluss einer negativen Ladung („Anionen-Assistenz“) auf Palladium-katalysierte H–H, C–H, C–C und C–Cl Bindungsaktivierungen untersucht. Hierzu werden mehrerer Reaktionsmechanismen der oxidativen Addition von Pd und $PdCl^-$ an H_2 (H–H), CH_4 (C–H), C_2H_6 (C–C und C–H) und CH_3Cl (C–Cl) studiert. Durch die Anionen-Assistenz werden die Aktivierungsbarrieren erniedrigt und die Reaktionen exothermer. Wohingegen die Aktivierungsenthalpien $\Delta H^{\neq}_{298}$ der direkten oxidativen Insertion von $PdCl^-$ in die unterschiedlichen Bindungen niedriger ist als diejenigen von Pd, so nimmt die relative Stabilität in beiden Fällen in der gleichen Ordnung zu: H–H < C–H ≈ C–Cl < C–C. Die Anionen-Assistenz wirkt selektiv und bevorzugt den endothermen S_N2 Mechanismus gegenüber der direkten oxidativen Insertion (OxIn). Interessanterweise wird für die Reaktion $PdCl^- + CH_3Cl$ ein Zwei-Schritt Mechanismus erhalten, bei dem der Übergangszustand der S_N2 Substitution gefolgt wird von einer Umlagerung der Abgangsgruppe Cl^- (S_N2/Cl-ra Mechanismus).

Dieser Zwei-Schritt Mechanismus ist energetisch günstiger als die direkte oxidative Insertion! Die höchste Barriere dieser Reaktion liegt mit –20.2 kcal/mol deutlich unter derjenigen der direkten oxidativen Insertion (–11.2 kcal/mol). Für alle anderen Bindungsaktivierungen mit $PdCl^-$ bleibt die direkte oxidative Insertion der bevorzugte Reaktionsweg.

Der der Anionen-Assistenz zugrundeliegende Mechanismus wurde mit Hilfe des Aktivierungsspannungs-Modells (ATS) untersucht. Dabei wurde festgestellt, dass für jeden Bindungstyp und für jeden Reaktionsweg die Aktivierungsspannung $\Delta E^{\neq}_{strain}$ spezifische Werte annimmt, die sich für die beiden Katalysatoren Pd und $PdCl^-$ nur marginal unterscheiden. Daher kann die Aktivierungsspannung $\Delta E^{\neq}_{strain}$ als Charakteristikum der zu aktivierenden Bindung und des verfolgten Reaktionspfades aufgefasst werden. Die Erniedrigung der Aktivierungsbarrieren durch Anionen-Assistenz wird hervorgerufen durch eine stärkere Übergangszustandswechselwirkung $\Delta E^{\neq}_{int}$. Diese Stärkung basiert auf der höheren Energie der $PdCl^-$ HOMOs im Vergleich zu den Pd 4d Orbitalen. Hierdurch wird die Donor-Akzeptor Orbitalwechselwirkung zwischen Katalysator und Substrat gestärkt.

Um die Einflussnahme von Liganden auf Palladium-katalysierte C–H, C–C und C–I Bindungsaktivierungen zu erforschen, wurde abschließend in Kapitel 7 die oxidative Addition von Pd und *cis*-$Pd(CO)_2I_2$ an CH_4 (C–H), C_2H_6 (C–H und C–C) und CH_3I (C–I) mit Hilfe von Dichtefunktionaltheorieberechnungen (ZORA-BP86/TZ(2)P) untersucht. Es sollte dabei festgestellt werden, inwiefern sich der Mechanismus der Bindungsaktivierung ändert, wenn statt des unkoordinierten Palladiumatoms ein Palladiumkomplex als Modellkatalysator verwendet wird. Für beide Katalysatoren ist die direkte oxidative Insertion (OxIn) der günstigste Reaktionsweg. Die nucleophile S_N2 Substitution ist jeweils stark endotherm und damit klar benachteiligt. Die Einführung von Liganden, d.h. der Übergang von Pd zu *cis*-$Pd(CO)_2I_2$, hat mehrere substantielle Änderungen bei der Aktivierung der C–H, C–C und C–I Bindungen zur Folge. So wird die Aktivierungsenthalpie der oxidativen Insertion erheblich angehoben, nämlich um 50 - 60 kcal/mol. Die Aktivierungsenthalpien nehmen in der Ordnung C–I $\lessapprox$ C–H <

C–C für beide Katalysatoren zu (wobei die Absolutwerte für den Palladiumkomplex größer sind als für das unkoordinierte Pd). Die Gesamtreaktion ist für das unkoordinierte Pd exotherm, für den Palladiumkomplex jedoch endotherm. Im ersten Falle liegen die Enthalpien im Bereich von –10 (C–H in CH_4) bis –45 kcal/mol (C–I), im zweiten zwischen 21 (C–I) und 47 kcal/mol (C–C).

Offensichtlich wäre der Komplex *cis*-$Pd(CO)_2I_2$ ein schlechter Katalysator. Nichtsdestotrotz wurden durch die Untersuchung seiner Aktivierungseigenschaften interessante Merkmale aufgedeckt, die nicht in den Reaktionen mit dem unkoordinierten Pd vorhanden sind. So kann im Übergangszustand der direkten oxidativen Insertion das planare *cis*-$Pd(CO)_2I_2$ prinzipiell unterschiedliche Orientierungen gegenüber den zu aktivierenden Bindungen einnehmen. Zum Beispiel können diese entlang einer I–Pd–CO Achse liegen, oder aber sich zwischen den beiden I–Pd–CO Achsen befinden (vgl. hierzu das Schema 1 in Kapitel 7). Für die C–H Aktivierungen in CH_4 und C_2H_6 wurden zwei unterschiedliche Übergangszustände mit sehr ähnlichem Energieinhalt gefunden, bei denen sich die C–H Bindung jeweils entlag einer I–Pd–CO Achse befindet (Orientierungen **O-2** und **O-4**, siehe Schema 1 in Kapitel 7). Für die oxidative Insertion in die C–C und C–I Bindung wurde jeweils nur ein Übergangszustand identifiziert (C–C Aktivierung: Orientierung zwischen **O-1** und **O-2**; C–I Aktivierung: Orientierung **O-1**). Abgesehen von den unterschiedlichen Orientierungsmöglichkeiten ist ein weiterer Unterschied, dass sich im Gegensatz zum unkoordinierten Pd der Komplex *cis*-$Pd(CO)_2I_2$ geometrisch verzerren kann. Dies führt zum Phänomen der Kalibrierung (oder Angleichung) von Katalysator und Substrat im Übergangszustand. Um diesen Prozess quantitativ zu verfolgen wurde das Aktivierungsspannungs-Modell (ATS) erweitert indem die Aktivierungsspannung $\Delta E^{\neq}_{strain}$ aufgeteilt wird in separate Anteile für Substrat und Katalysator. Die Untersuchungen zeigen, dass beide Terme für den Typ der zu aktivierenden Bindung charakteristisch sind. Der große Unterschied zwischen dem unkoordinierten Pd und dem sterisch anspruchsvolleren, flexiblen *cis*-$Pd(CO)_2I_2$ führt jedoch dazu, dass sich auch die Werte der Aktivierungsspannungen ändern. Es wurde weiterhin gezeigt, dass je stärker die Bindung und je endothermer die Reaktion

ist, desto höher ist die Aktivierungsspannung. Dies gilt sowohl für das unkoordinierte Pd als auch für *cis*-$Pd(CO)_2I_2$. Das Phänomen der Kalibrierung von Substrat und Katalysator demonstriert, dass es für das Design und die Optimierung der elektronischen Struktur des Katalysators in Hinsicht auf eine bestimmte Bindung (z.B. durch die Verwendung von Liganden) notwendig ist, die Katalysatorstruktur im Übergangszustand zu berücksichtigen, da sich diese oftmals von der Gleichgewichtsgeometrie unterscheidet.

Die im Rahmen dieser Dissertation vorgestellten Ergebnisse zeigen, dass elementare organometallische Reaktionen, die eine wichtige Rolle in katalytischen Prozessen spielen, auf der Basis des Aktivierungsspannungs-Modells (*Activation Strain* oder auch *Activation strain-TS interaction*, ATS) im Detail verstanden werden können. Es ist möglich, eine vorhandene Aktivierungsbarriere anhand der Aktivierungs-spannung, einer charakteristischen Größe der zu aktivierenden Bindung und des katalytisch aktiven Metallkomplexes, und anhand der Übergangszustands-wechselwirkung (*TS interaction*) zu interpretieren. Letztere liefert eine Grundlage, auf der die Abhängigkeit der Aktivität eines Katalysators von seiner elektronischen Struktur verstanden werden kann. Nach wie vor existieren viele weitere Aufgaben, deren Untersuchung ein umfassenderes Verständnis der ATS Modellgrößen liefern kann. An erster Stelle sei hier die Frage genannt, inwiefern durch einen gezielten Einsatz von Liganden die elektronische Struktur des Katalysators so maßgeschneidert werden kann, dass diese im Übergangszustand selektiv die Wechselwirkung mit dem Substrat maximiert. Des weiteren wäre es wichtig, neuere Dichtefunktionale (wie z.B. die gerade aufkommenden meta-GGAs) anzuwenden und ihre Leistung zu testen. Abschließend soll festgestellt werden, dass die Einsichten, die durch die Untersuchungen katalytischer Prozesse anhand einfacher Modellsysteme erzielt werden konnten, eine Basis und einen ersten Schritt des fragmentorientierte Katalysatordesign (*Fragment-oriented Design of Catalysts*, FDC) darstellen, mit dessen Hilfe hochselektive Katalysatoren schrittweise und rational entwickelt werden können.